UNIVERSITY OF SOUTHAMPTON

PERMEABILITY IDENTIFICATION OF POROUS MEDIA IN RESIN TRANSFER MOULDING

by

Jun Xing

Faculty of Engineering and Applied Science,
School of Engineering Sciences, Ship Science,
University of Southampton,
Highfield, Southampton, SO17 1BJ,
United Kingdom.

June, 2001

UNIVERSITY OF SOUTHAMPTON

ABSTRACT

FACULTY OF ENGINEERING AND APPLIED SCIENCE
SCHOOL OF ENGINEERING SCIENCES, SHIP SCIENCE

Doctor of Philosophy

PERMEABILITY IDENTIFICATION OF POROUS MEDIA IN RESIN TRANSFER MOULDING

by Jun Xing

The aim of this thesis is to investigate permeability identification methods of porous media in Resin Transfer Moulding (RTM)by means of experimental measurements.

Fundamental research areas concerning Resin Transfer Moulding (RTM) are categorized in three main topics: *Permeability identification*, *Flow analysis* and *Injection pressure predication*. Some fundamental problems on permeability identification which is considered as a base of RTM researches are theoretically and experimentally examined. Under generalised boundary conditions of injection pressures or flow rates considered as time functions, several analytical solutions for both channel flows and radial flows through isotropic or anisotropic fiber preforms are developed. The gravitational effect is also considered, while these solutions are derived. By using these solutions in permeability identification measurements, it is no longer required that injection pressures or flow rates are to be constants as reported in current references. It is demonstrated that the effect of gravitation on two- or three-dimensional radial flows is to produce a translation of the wetted domain of medium. A moving coordinate system fixed at the centre of wetted area is proposed to avoid the gravitational effect on experiment measurements.

Eighty seven practical identification experiments are completed to validate these fundamental results and the proposed experiment methods. Further research problems into the theoretical results and experimental work are described.

Contents

List of Tables

List of Figures

Acknowledgments

This PhD was only possible with the support and help of many people.

First and foremost, I would like to thank my supervisors Prof. R A Shenoi and Mr. P A Wilson for their faith and patience and for their guidance throughout the course of my Ph.D.

Valuable advice and suggestion given by Dr. S S J Moy and Prof. J T Xing were most helpful for the development of the ideas presented in this thesis.

I would like to thank Prof. W G Price, Head of School of Engineering Sciences, Ship Science, for his kind support and constant encouragement as well as making the departmental facilities available to me. Thanks to Mr. P A Wilson and Dr. M Y Tan for giving continuous help regarding the computer problems.

I am especially grateful to my parents for their support, patience and *love*. Without them this work would never have come into existence (literally).

Finally, I wish to thank my colleagues in Lightweight Structure Research Group for their stimulating supports and suggestions towards my research. Also, I express my thanks to the technicians in the Transport Systems Research Laboratory of the School of Engineering Sciences, the University of Southampton for their help during my experiments.

Nomenclature

Indices and coordinate systems

i, j, k	small English letter subscripts $(= 1, 2, 3)$, obeying the summation convention
$()_{,i}$	$= \partial()/\partial x_i$ or $= \partial()/\partial X_i$, etc.
$()_{,t}$	$= \partial()/\partial t$
$()^{(i)}$	a quantity related to the principal direction X_i, no obeying the summation convention
$()^T$	transpose of a matrix or tensor $()$
$()^0$	a quantity related to flow injection gate
$()^f$	a quantity related to flow front
$\overline{()}$	a quantity related to two-dimensional or three-dimensional quasi-isotropic radial flows

$O - x_1x_2x_3$	spatial Cartesian coordinate system
$O - x'_1x'_2x'_3$	another spatial Cartesian coordinate system
$O - X_1X_2X_3$	principal coordinate system of a permeability tensor
$O - y_1y_2y_3$	a measurement coordinate system
$O - y'_1y'_2y'_3$	another measurement coordinate system
x_i	spatial coordinates under the $O - x_1x_2x_3$ system
X_i	spatial coordinates under the $O - X_1X_2X_3$ system
y_i	spatial coordinates under the $O - y_1y_2y_3$ system
y'_i	spatial coordinates under the $O - y'_1y'_2y'_3$ system

$\boldsymbol{e}_i$	unit vector along the x_i or y_i direction
$\boldsymbol{n}^{(i)}$	unit vector along the X_i direction
$n_i^{(r)}$	unit vector along the X_r direction
$\boldsymbol{e}'_i$	unit vector along the x'_i or y'_i direction

Letters

a	a radius of an ellipse or ellipsoid
A	horizontal section area of Darcy's homogeneous filter bed
A_n	a cross-sectional area of the mould
b	a radius of an ellipse or ellipsoid
c	a radius of an ellipse or ellipsoid
e_{ijk}	permutation symbol
g	gravity acceleration
h	height of Darcy's homogeneous filter bed
h_1	liquid height in the manometer tube at outflow end of Darcy's filter bed
h_2	liquid height in the manometer tube at inflow end of Darcy's filter bed
H	thickness of the cavity
$\boldsymbol{I}$	unit matrix
I_1, I_2, I_3	three scalar invariants of permeability tensor k_{ij}
$\boldsymbol{J}$	generalized pressure gradient vector
J_i	generalized pressure gradient vector
k	permeability constant for isotropic media
$k^{(i)}$	principal permeability coefficient along the i-th direction
k_{ij}	permeability tensor
$\tilde{k}_{11}$	effective permeability along x_1 direction
$\tilde{k}_{22}$	effective permeability along x_2 direction
$\tilde{k}_{33}$	effective permeability along x_3 direction
$\tilde{k}_{ij}$	effective permeability in two-dimensional flows
k_J	directional permeability along the pressure gradient $\boldsymbol{J}$
k_q	directional permeability along the flow vector $\boldsymbol{q}$
k^r	permeability along radial direction r
$\boldsymbol{k}$	permeability tensor under a coordinate system $O - x_1x_2x_3$

$\boldsymbol{k}'$	permeability tensor under another coordinate system $O - x_1'x_2'x_3'$
K	a constant in original Darcy's law
$\tilde{K}$	a new constant in original Darcy's law
$\overline{k}$	permeability of quasi-isotropic system
$\boldsymbol{N}$	principal direction matrix $(= [\boldsymbol{n}^{(1)}\boldsymbol{n}^{(2)}\boldsymbol{n}^{(3)}])$
N	number of fibre layers
p	fluid pressure at a point
p^0	injection pressure
p^f	flow front pressure
P	resin injection pressure impulse
Δp	pressure difference between inlet and outlet
q	seepage velocity in Darcy's experiment
q_i	flow velocity vector
q_i^0	flow injection velocity vector
q_r	radial flow velocity for radial flows
$\boldsymbol{q}$	flow velocity vector
q_i^g	flow rate caused by gravitation force
$\boldsymbol{q}^g$	flow rate vector caused by gravitation force
$\overline{q}_i$	quasi-isotropic flow velocity vector
$\overline{q}^0$	quasi-isotropic flow injection velocity vector
$\overline{q}_r$	quasi-isotropic radial flow velocity
Q	volume flow rate
$\overline{Q}$	quasi-isotropic volume flow rate
r	radial coordinate for radial flows
r^0	coordinate of radial flow injection end
r^f	coordinate of radial flow front
$\overline{r}$	radial coordinate for quasi-isotropic radial flows
$\overline{r}^0$	radial coordinate of quasi-isotropic radial flow injection end
$\overline{r}^f$	radial coordinate of quasi-isotropic radial flow front

v_f	fibre volume fraction
W	mass per square meter of fibre mat
x^0	coordinate of one-dimensional flow injection end
x^f	coordinate of one-dimensional flow front
$\overline{x}_i$	coordinates for quasi-isotropic flows

Greek symbols

α_i	angle between $\boldsymbol{J}$ and $\boldsymbol{n}^{(i)}$
$\boldsymbol{\beta}$	coordinate transformation matrix with elements β_{ij}
β_{ij}	direction cosine, $= \boldsymbol{e}_i' \dot{\boldsymbol{e}}_j = \cos(\boldsymbol{e}_i', \boldsymbol{e}_j$
β_i^g	direction cosine of the vertical direction under the principal coordinate system
$\beta_{\overline{r}i}$	direction cosine of $\overline{r}$ direction under the principal coordinate system
γ	angle between the negative direction of gravitation and the r direction
$\gamma_1, \gamma_3, \gamma_3$	three Euler angles
δ_{ij}	Kronecker delta
ε	effective porosity
θ	angle between $\boldsymbol{q}$ and $\boldsymbol{J}$
$\theta_1, \theta_3, \theta_3$	three Euler angles
$\boldsymbol{\Lambda}$	principal permeability matrix
μ	viscosity of a liquid
ρ	density of a liquid
ρ_f	density of a fibre material
ρ_b	bulk density of a porous medium
ϕ_i	three direction angles between $\boldsymbol{q}$ and $\boldsymbol{n}^{(i)}$
φ	the orientation of principal

Chapter 1

Introduction

1.1 Resin transfer moulding (RTM)

Composite materials have fully established themselves as workable engineering materials and are now relatively commonplace around the world, particularly for structural purposes (Cai 1987). In various composite materials, fibre reinforced plastics (FRP) with different polymer matrices have took a very important position in engineering applications (Brittles 1994). Today, the aircraft, automobile, electronic and medical industries are dependant upon FRP.

Early military applications of FRP were during World War II, especially in the marine industry. As described (Smith 1990), FRP were first used by the US Navy in the 1940's to build boats. It soon became the most popular building material for pleasure craft. In 1955 4% of all small boats where built from FRP compared to more than 80% in 1972. It has remained at that level since. The main reason to use FRP in boat building is that the raw materials are easily obtainable at short notice with consistent material properties. Beside this, semi-skilled labour is needed to process the materials and build the boats. For larger production runs this offers significant benefits over other materials, such as wood and steel. FRP also allows the building of complex shapes which may be required by hydrodynamic or structural reasons.

The traditional moulding techniques used to produce these boats are hand lay-up and spray-up techniques. However, economic pressure and environmental requirements on styrene emission (Williams et al 1996) make these techniques less acceptable. Instead of these tradition moulding techniques, RTM has become increasingly popular for the production of high quality FRP composites. Now it is a widely used manufacturing method for making large FRP structures of all shapes, sizes and degrees of complexity, in many fields. The main advantages of RTM are that it is a closed moulding process and produces high quality components with smooth surfaces on both sides. Because of the low injection pressure the tooling is quite cheap. It also has potential for a high degree of automation and a considerable cost advantage (Foley 1991). RTM has become a standard process in the automobile industry to produce high quality body panels of sports cars and utility vehicles (Rudd et al 1997.) RTM also offers advantages to aerospace end users such as relatively low tooling costs and component integration with the potential to mould complex structures in a single shot. In the new book, Liquid moulding technologies, written by Rudd et al (Rudd et al 1997), more successful application examples of RTM technologies in various industry production processes are presented.

RTM is also known as resin injection, which is that a positive/negative pressure is used to drive/to attract a liquid resin into a mould cavity containing a dry fibre preform (see, for example, Hayward et al 1989, 1990; Williams et al 1996; Rudd et al 1997). A typical RTM process cycle is shown in Figure 1.1 (Weitzenböck 1996). The first step is preform preparation where the fibre mats are cut to size, then these preforms are placed in a mould and after this the resin is injected into the cavity and then is left to cure, finally the cured component is moved.

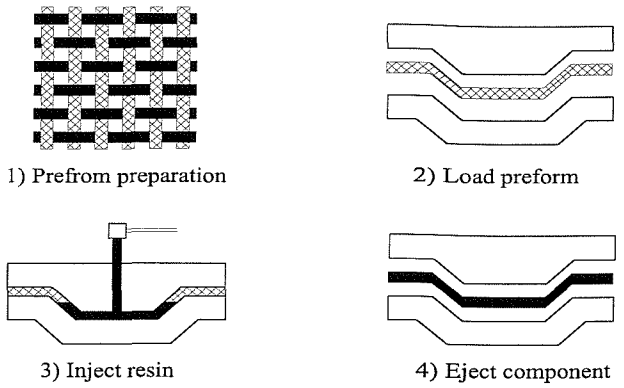

Figure 1.1: A typical RTM process cycle.

1.2 The position of permeability measurement in RTM

In the typical RTM process cycle shown in Figure 1.1, step 3, the resin injection, is the most important thing of the total RTM process, which directly affects the quality of RTM products. Therefore, to improve the quality of RTM products, the key element is to control the process of resin injection flow. For this purpose, it is necessary to built a mathematical model of resin injection flows, which can be used to investigate the resin injection flow process by numerical methods and computer simulation for its optimizing. Up to now, it has been widely accepted that this process can be described by flow in porous media (Scheidegger 1960, 1963a and 1963b), in which fibre materials and liquid resins are treated as porous media and viscous fluids, respectively. In principle, a flow in porous media can be solved by using the fundamental laws of continuum mechanics, such as momentum balance and the law of mass conservation (Fung, 1977). However, since a porous medium generally is an very complicated network of channels and obstructions, it is not possible directly to solve these fundamental equations defined in a porous medium and it has to be described statistically and in some average sense. To this end, Darcy's law (Darcy 1856), describing flow rate as a function of potential drop is used to calculate flow in porous media. Darcy's law is an experimental law and is mainly based on a very important parameter, perme-

ability $\boldsymbol{k}$, which provides a statistical description of the characteristics of porous media in RTM. The fundamentals of the resin injection process in RTM may be represented in Figure 1.2. In this figure, the p, $\boldsymbol{k}$ and $\boldsymbol{q}$ represent the injection pressure, the permeability of the porous media and the resin flow vector, respectively. Investigation topics concerning the resin injection process in RTM may be categorized in the following three kinds.

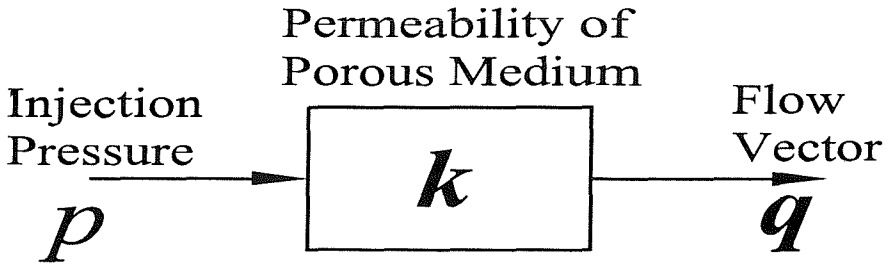

Figure 1.2: A relative diagram of p, $\boldsymbol{k}$ and $\boldsymbol{q}$.

Permeability identification: The purpose of this kind of investigations is to determine the permeability $\boldsymbol{k}$ of a porous medium in resin injection process in RTM. It has not found any reports to obtain the permeability of a porous medium or a fibre material by using microscopic or macroscopic analytical methods. The permeability of a fibre material treated as a porous medium has to be determined by experimental methods. In this problem, the resin injection pressure p is prescribed and the resin flow $\boldsymbol{q}$ is measured, and then the characteristics of the porous media, the permeability parameters $\boldsymbol{k}$ are to be determined. This kind of problem will be designated as the *permeability identification.*

Flow analysis: In this kind of investigation problem, the injection pressure p is prescribed and the porous media are given, which means that the permeabil-

ity parameters $\boldsymbol{k}$ of those media are known, the resin flow $\boldsymbol{q}$ is required to be determined. This kind of problem can be solved by numerical methods or experimental approaches. This will be designated as the *Flow analysis* in resin injection processes.

Injection pressure prediction: This is a reverse of the problem of flow analysis. For a given porous medium of which the permeability $\boldsymbol{k}$ is known, a pre-designed flow $\boldsymbol{q}$ is given and the injection pressure p to produce this designed flow is required to be determined. Obviously, this is a very useful topic to control resin injection flows. This will be designated as the problem of *Injection pressure prediction.*

From the above discussion, it can be concluded that the permeability identification is a key problem in RTM research and it is a base to study the flow analysis and injection pressure prediction in RTM process (see, for example Rudd et al 1996a). This thesis intends to give a further theoretical and experimental investigation to this key problem.

These points are certainly a fundamental study of permeability identification methods in RTM process. The present work attempts to address these problems by using theoretical analysis and experimental demonstration.

Chapter 2

Literature review

2.1 Fluid flow in porous media

2.1.1 Definition of porous media

In order to study the resin flow through fibre materials, which are treated as porous media, it is first of all necessary to clarify what is understood by the term porous media. A porous medium is a solid containing holes or pores in it. Usually the number of holes or pores is sufficiently large that a volume average is needed to calculate pertinent properties. Pores which occupy some definite fraction of the bulk volume form a complex network of voids. Furthermore, the pores must be small compared with the external dimensions of the material. The pores may be interconnected or non-interconnected.

In this research, a mould cavity containing a dry fibre preform in RTM process is considered as a porous medium. Obviously, the fibre perform forms affect the properties of this porous medium. When properties of porous media are concerned, the following terms are needed to be distinguished.

(i) *Homogeneity*: Homogeneity is also called *uniformity*, which means that the properties of the material at different points are same. In other words, the pa-

rameters describing the properties of the material are not dependent upon the point within the material. Ideally, a mould cavity containing a dry fibre upon the preform in RTM process or a composite should be homogeneous, or uniform, but this is difficult to achieve.

(ii) *Isotropy* and *anisotropy*: At a point in the space occupied by a porous medium, directions may affect the properties of the medium. If the properties of the medium are independent of direction, this medium is said to be *isotropic*, otherwise *anisotropic*. The orientation of the reinforcement within the matrix affects the isotropy of the system.

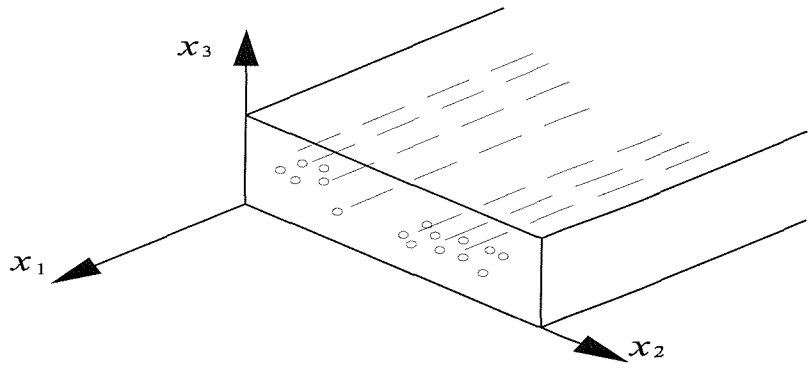

Figure 2.1: A unidirectional medium.

(iii) *Transversely isotropy*: When calculating the properties of porous media it is convenient to start by considering a porous medium in which all the fibres aligned in one direction (i.e., a unidirectional medium), as shown in Figure 2.1. In a unidirectional medium the fibre distribution implies that the behaviour is essential isotropic in a cross-section perpendicular to the fibres. In other words, if a test is conducted by applying a material strip in the direction x_2 or in the direction x_3 (both normal to the fibre axes), the same property constants would be obtained from each test. The material is classified as *transversely isotropic* (see, for example, Matthews and Rawlings, 1994). Clearly the properties in the longitudinal direction x_1 are very different from those in the other two directions.

These materials are called *orthotropic.*

In describing flow phenomena in porous media interests focussed on interconnected pores since these are the ones that affect flow. Unconnected pores do not affect flow directly but may affect the compressibility of the matrix. If flow within the porous medium is to be possible, at least part of the pore space must be interconnected. The pore space which is interconnected is termed the effective pore space of the porous medium. Porosity and permeability are the two main properties in description of RTM flow process.

2.1.2 Porosity

The preform of a porous medium is the material in which the holes or pores are embedded. The manner in which the holes are embedded, how they are interconnected, and the description of their location, size, shape, and interconnection characterize the porous medium. The porosity is a quantitative property that describes the fraction of the medium that is voids. When a flow is concerned, the pores or fraction of the medium that contributes to flow constitutes the *effective porosity.* Recognizing that in defining porosity the complex network of voids is replaced with a single number that represents an average property. A porous medium of a given porosity can be extremely different from another porous medium that has same porosity.

The porosity is defined as the ratio of void volume to bulk volume of the porous media. The absolute porosity is the ratio of total void volume to bulk volume. The effective porosity represented by ε is the ratio of effective pore space to bulk volume, i.e.

$$\varepsilon = \frac{\text{Effective pore space}}{\text{Bulk volume}}. \tag{2.1}$$

The most popular method of obtaining porosity is the gas expansion method (see, for example, Scheidegger, 1960, 1963b). In this method, a medium of known bulk volume and a given amount of air or gas are placed in a container of known volume

under pressure. This container is then connected with an evacuated container of known volume. The new pressure of the system is read, and this allows one to calculate from the gas laws the volume of gas that was originally in the porous medium.

If the density ρ_f of the fibre materials making up the porous medium is known, then the bulk density ρ_b of the latter is related to the porosity ε as follows:

$$\varepsilon = 1 - \frac{\rho_b}{\rho_f}, \tag{2.2}$$

or

$$\varepsilon = 1 - v_f, \tag{2.3}$$

where v_f is Fibre Volume Fraction, it is calculated by using the following formula

$$v_f = \frac{NW}{H\rho_f}, \tag{2.4}$$

where N, W, H, and ρ_f represent the number of fibre layers, the mass per square metre of fibre mat, the thickness of the cavity, and the density of the fibre material, respectively. This method is used to obtain the porosity ε in this research.

2.2 Darcy's law

The modern theory of flow through porous media finds its basis in a simple experiment first performed by Darcy (Darcy, 1856) which is, in essence, a large-scale filtration experiment. A homogeneous filter bed of height $h = Z_2 - Z_1$, bounded by horizontal plane areas of size A, is being percolate by an incompressible liquid as shown in Figure 2.2. If open manometer tubes are attached at the upper (no.2) and lower (no.1) boundaries of the filter bed, the liquid rises to the heights h_2 and h_1 above a certain (arbitrary) datum level, respectively. By varying the various parameters involved, Darcy deduced heuristically the following relation between the variables and the total volume Q of fluid percolating in unit time,

$$Q = -KA(h_2 - h_1)/h, \tag{2.5}$$

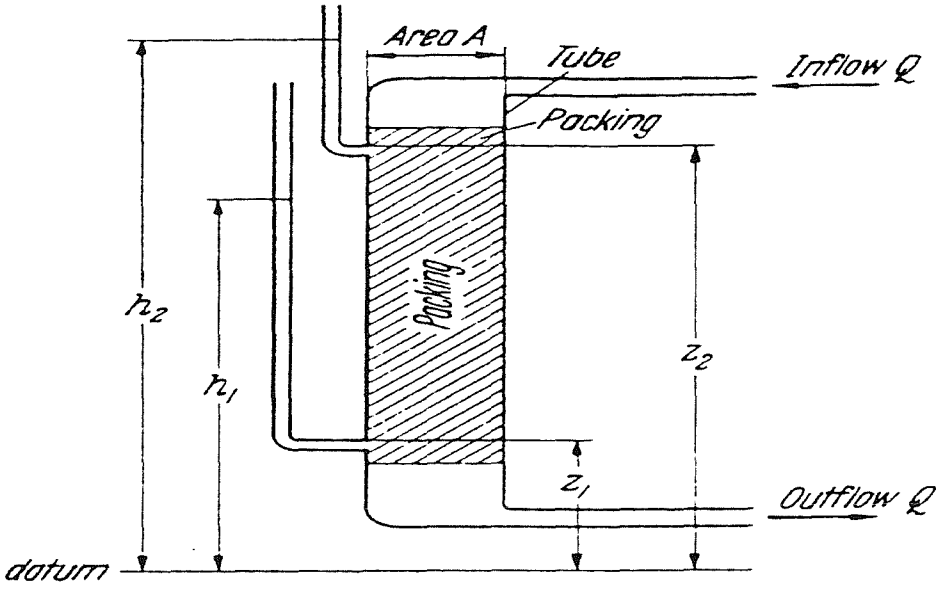

Figure 2.2: Schematic drawing of Darcy's experiment.

where K is a constant depending on properties of both fluid and solid. This relationship has subsequently been shown valid as a reasonable approximation for a wide variety of cases (see, for example, Scheidegger, 1963b).

Darcy's law can be restated in terms of the pressure p and the density ρ of the liquid. By introducing of a new constant $\tilde{K}$, one then can write,

$$Q = -\tilde{K}A(p_2 - p_1 + \rho g h)/h, \tag{2.6}$$

which is equivalent to equation (2.5).

Darcy's law as stated in equation (2.6) is rather restricted in its applicability. As indicated above for K, the new constant $\tilde{K}$, too, must be expected to depend on the properties of both the fluid and the porous medium. Nutting (Nutting, 1930) showed by experimentation that to a reasonable approximation,

$$\tilde{K} = k/\mu, \tag{2.7}$$

where μ is the viscosity of the liquid and k a constant depending only on the properties of the porous medium. This constant is called the *permeability* of the porous medium, which has its unit m^2.

Darcy's law, as developed so far, may now be written as follows:

$$q = Q/A = -(k/\mu)(p_2 - p_1 + \rho g h)/h, \tag{2.8}$$

which further been expressed as a differential equation by letting h become infinitesimal, i.e.

$$q = Q/A = -(k/\mu)(\frac{\partial p}{\partial x_3} + \rho g), \tag{2.9}$$

where x_3 represents a coordinate pointing vertically upward, and q is called *local seepage velocity.*

As indicated above, the permeability k of a porous medium depends only on the properties of the porous medium. These include both of the geometrical and physical properties, such as the size of the pores, tortuous paths, capillaries, interfacial force due to constructions, fibre compressibility and etc. in the medium. It is very difficult to determine the permeability of a porous medium by an analytical method and this important parameter has to be obtained by the experimental methods

2.2.1 Generalization of Darcy's law

Darcy's law is an empirically determined relation for a one-dimensional single-fluid flow in a homogeneous medium. How should Darcy's law be written if the medium is complex? As it has known that the permeability used in Darcy's law is a property of porous media. Therefore, for a different porous medium, there is a different permeability and the corresponding form of Darcy's law.

Isotropic media

The first possible generalization of equation (2.9) obtained from one dimensional

flows is to extend it to flows in isotropic porous media in the three-dimensional space. This can be done by representing equation (2.9) in a vector form

$$q_i = -(k/\mu)(p_{,i} + \rho g \delta_{i3}), \tag{2.10}$$

where q_i represents the velocity vector of the flow; $p_{,i}$ is the pressure gradient vector; k is the permeability constant; g is the magnitude of gravity acceleration pointing vertically downward, i.e. along the negative direction of the coordinate x_3. If a generalized pressure gradient vector J_i is defined as

$$J_i = p_{,i} + \rho g \delta_{i3}, \tag{2.11}$$

it gives,

$$q_i = -\frac{k}{\mu} J_i. \tag{2.12}$$

Anisotropic media

A further generalization of Darcy's law can be attempted in anisotropic porous media are considered. The form in equations (2.10) and (2.12) immediately suggests that in anisotropic media the permeability constant k should be replaced by a symmetric tensor k_{ij} (see, for example, Scheidegger, 1963b; Bear 1972) and the corresponding Darcy's law takes the form

$$q_i = -\frac{k_{ij}}{\mu} J_j. \tag{2.13}$$

The permeability tensor k_{ij} and Darcy's law described in equation (2.13) can be rewritten in the matrix form as follows:

$$\boldsymbol{k} = \begin{bmatrix} k_{11} & k_{12} & k_{13} \\ k_{21} & k_{22} & k_{23} \\ k_{31} & k_{32} & k_{33} \end{bmatrix}, \tag{2.14}$$

$$\begin{bmatrix} q_1 \\ q_2 \\ q_3 \end{bmatrix} = -\frac{1}{\mu} \begin{bmatrix} k_{11} & k_{12} & k_{13} \\ k_{21} & k_{22} & k_{23} \\ k_{31} & k_{32} & k_{33} \end{bmatrix} \begin{bmatrix} J_1 \\ J_2 \\ J_3 \end{bmatrix}. \tag{2.15}$$

This generalization implies the following consequences:

(i) The scalar permeability constant k is extended to a permeability tensor k_{ij} which is a symmetric tensor and there are 6 constants in it. Physically, a coefficient in the permeability tensor k_{ij}, such as k_{12}, represents the seepage velocity component q_1 (multiplied by $-\mu$) produced by a unit generalized pressure gradient component J_2.

(ii) In general, the generalized pressure gradient J_i and the seepage velocity vector q_i are not parallel. This represents that a generalized pressure gradient J_i will produces the flows in both the tangent and normal directions to its direction.

(iii) For a permeability tensor k_{ij}, there are three orthogonal axes (principal axes, see Chapter 3) in space along which the generalized pressure gradient J_i and the seepage velocity vector q_i do have an opposite direction.

Transversely anisotropic media

For transversely isotropic media in which the longitudinal direction represents by x_1(see Figure 2.1), therefore, $k_{12} = k_{13}$, $k_{22} = k_{33}$ and $k_{23} = 0$ and then there are only 3 constants in the permeability tensor k_{ij}. The permeability tensor k_{ij} reduces to the following form

$$\boldsymbol{k} = \begin{bmatrix} k_{11} & k_{12} & k_{12} \\ k_{21} & k_{22} & 0 \\ k_{21} & 0 & k_{22} \end{bmatrix}. \tag{2.16}$$

2.2.2 The statistical characteristics of Darcy's law

As mentioned in the introduction, in principle, this same flow in porous media can also be solved by using the fundamental laws in continuum mechanics, such as the momentum balance and the law of mass conservation. Therefore, there definitely exists a relation between Darcy's law and the fundamental laws in continuum

mechanics. To further understand the essential aspect of Darcy's law and its restrictions to applications, it is necessary to study this relation. DeWiest (1969) showed that Darcy's law is the empirical equivalent of the momentum balance equation in continuum mechanics. He demonstrated that statistical averages of the momentum equations and neglecting the inertial terms result in Darcy's law. Therefore, as same as the porosity, the permeability is also an average property of porous media. When the medium is replaced with its average properties, some information concerning the microscopic description are lost, but consider its statistical bulk description.

2.3 Measurement of permeability

Following Darcy's original experiment (Darcy 1856), there have been a lot of references to discuss the methods to identify permeabilities of porous media by experiment measurements. The earliest references on this topic are mainly in connection with the exploitation of oil fields and the most important contributions are probably those of Miller, Dyes and Hutchinson (1950), Horner (1951), and Hazebrook, Rainbow and Matthews (1958). The details of these earliest researches can been found in Scheidegger's famous books (Scheidegger 1960, 1963b).

As composite materials are widely used in various engineering areas, liquid moulding technologies including RTM are more and more attractive. As result of this, a great number of papers and reports appeared in which improvements and generalizations of the underlying theories were discussed. The most relevant of these are those that follows. It seems that the fundamental theories and some special flow solutions through porous media, which are used in permeability identification references can be found in the historical books written by Scheidegger 1960, 1963b; Bear 1972; Greenkorn 1983. As far as RTM is concerned, a more excellent new book written by Rudd et al (1997) contributed more details on test fluids, test techniques, test process, a comparison of test methods and the two

flowcharts for calculation of principal permeabilities from radial flow tests with constant pressure rate (Hirt et al 1987) and constant flow volume rate (Chick et al 1996). A comprehensive review on the experimental approach for this topic in RTM process is given in the Ph.D thesis (Weitzenböck 1996).

In principle, all the methods used in permeability identification measurements may be divided into two general categories: those employing rectilinear or channel flow, as described by Gauvin et al. (1986, 1990, 1994), Gebart et al. (1991, 1992, 1996), Parnas et al. (1993) and Ferland et al. (1996), and those using radial flow as described in detail by Adams et al. (1986, 1987,1988, 1991a and 1991b), Chan et al. (1991, 1993) and Chick (1996). Either method may employ constant injection pressure or constant injection flow rate or volume flow rate.

2.3.1 Channel flow

Rectilinear tests (channel flow tests) are made by introducing the fluid into the reinforcement using an edge gate and constraining it to advance along a parallel sided cavity towards an edge vent. The advantages of using rectilinear flow include simplicity of data analysis and when constant injection pressures are used, there is a particular advantage in being able to take an averaged velocity of the advancing flow front. The main disadvantages are that more than one test is required to characterize the permeability for anisotropic media. Table 2.1 list some selected methods of permeability measurement by using channel flow. In this table, the CFR and CIP are constant flow rate and constant injection pressure, respectively, and UD is unidirectional fabric.

The channel flow tests was employed mainly to characterize isotropic preforms by Gauvin et al 1986 and 1996, Fracchia et al 1989, Bruschke et al 1990, Kim et al 1991, Gebart et al 1991, 1992 and 1996 and Perry et al 1992. In these cases, only one measurement is needed.

For constant injection pressure, the permeability of isotropic media is calculated as follows (Gebart et al 1991, 1992 and 1996)

$$k = -\frac{\mu \varepsilon x_f^2}{2\Delta p t}, \tag{2.17}$$

where x^f is the position of the flow front, Δp is the pressure difference between inlet (p^0) and outlet (p^f), that is $\Delta p = p^f - p^0$ and p^0 is a constant in this equation, μ is the viscosity of liquid, ε is effective porosity and t is time of flow process.

The permeability of isotropic media with constant flow rate can be obtained as follows (Gauvin et al 1986 and 1996),

$$k = \frac{\mu Q}{A_n} \frac{x^f}{p^0}, \tag{2.18}$$

where Q is the flow rate, it is constant, A_n is the cross-sectional area of the mould and p^0 is the pressure at inlet.

The equations (2.17) and (2.18) are basic formulae for measuring permeability under constant injection pressure and constant flow rate condition, respectively. Although there exists only a small difference in the equations to be used in calculation of the permeabilities in most of references published, the fundamental equation is same as these two equations.

Table 2.1: Some selected methods of permeability measurement by using channel flow

Author(s)	Method	Formulae	Reinforcement	Comment
Gauvin et al. (1986)	CFR	$k = \frac{\mu Q}{A}\frac{x^f}{p^0}$ or $k = \frac{\mu Q}{A}\frac{(x_2-x_1)}{(p_1-p_2)}$	Random fabric.	A basic formula to measure permeability under CFR.
Gauvin et al. (1996)	CFR CIP	$k = \frac{v\mu}{\Delta p}$	Random fabric.	This equation can be used to calculate the permeability of both CFR and CIP experiments.
Ferland, et al. (1996)	CFR and CIP	$k = \frac{\mu {x^f}^2 v}{P^0}$ and $k = \frac{{x^f}^2\mu}{2\int_0^t P^0(t)dt}$	Random fabrics.	Both of these two equations can be used in CIP and CFR. The inlet pressure is time-varying in CIP.
Gebart, (1992)	CIP	$k = \frac{\mu(1-V_f){x^f}^2}{2\Delta pt}$	UD	A general case for permeability measurement.
Weitzenböck et al. (1996, 1999 c)	CIP	$k^{(1)} = k_I\frac{(A-D)}{(A-\frac{D}{\cos 2\theta})}$ $k_2 = k_{III}\frac{(A+D)}{(A+\frac{D}{\cos 2\theta})}$ $\theta = \frac{1}{2}\tan^{-1}C$ $C = \frac{A}{D} - \frac{A^2-D^2}{k_{II}D}$ $A = \frac{k_I+k_{III}}{2}$ $D = \frac{k_I-k_{III}}{2}$	Anisotropic fabric .	The principal permeability and orientation were calculated by channel flow test in these paper.

These two equations also can be used in calculation of the permeabilities of anisotropic media. In this case the above equations are the effective permeability along the measurement direction. To calculate the principal permeability and orientation, at least three times experiments should be done, in the other word, three effective permeabilities along three different directions should be obtained firstly. Several investigations, as reported by Ferland et al 1996, Martin 1986, Fracchia et al 1989, Fracchia 1990, Chibani 1990 and Weitzenböck 1996 and 1999, used this simple technique to measure successively the preform permeabilities along its two principal directions for a two-dimensional case by means of a unidirectional flow inside a rectangular cavity. The principal permeability and orientation can be calculated from (Weitzenböck 1996 and 1999c):

$$\begin{aligned} k^{(1)} &= k_I \frac{(A-D)}{(A-D/\cos 2\varphi)}, \\ k^{(2)} &= k_{III} \frac{(A+D)}{(A+D/\cos 2\varphi)}, \\ \varphi &= \frac{1}{2}\tan^{-1}\left\{\frac{A}{D} - \frac{A^2-D^2}{k_{II}D}\right\}, \\ A &= \frac{k_I + k_{III}}{2}, \\ D &= \frac{k_I - k_{III}}{2}. \end{aligned} \tag{2.19}$$

Where $k^{(1)}$ and $k^{(2)}$ are the principal permeabilities, k_I, k_{II} and k_{III} are the effective permeabilities measured in directions I, II and III, which can be obtained from equations (2.17) or (2.18) and φ is the orientation of principal.

A new method for measurement of the in-plane permeability tensor has been proposed by Gebart et al in 1996, the new method combines the simplicity of the radial flow method with the small mould deflection of the channel flow method.

As shown in Figure 2.3 (Gebart, 1996), the new method is to connect four parallel flow mould cavities to a common inlet. The mould cavities are loaded with the test material oriented in the 0^o, 45^o and 90^o directions. The fourth mould cavity is loaded with a reference material with known permeability. This method has a

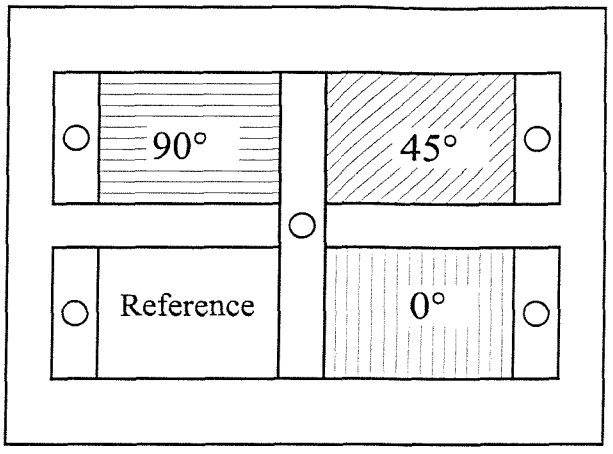

Figure 2.3: Definition sketch for the multiparallel flow method for permeability measurement.

number of additional advantage in that the number of experimental parameters that must be measured is reduced and in that the permeability of the test material is related directly to a reference material. But it seems that this method did not widely use in the permeability measurement.

2.3.2 Radial flow

Radial tests are performed using a centre gate to produce a diverging flow in a mould cavity which is vented at the periphery. Tests rigs often consist of one or both plates manufactured from Perspex or glass to allow visualisation of the filling stage. The permeability for a two-dimensional case is usually defined by two principal values measured in the plane of the reinforcement. Comparing with the channel flow tests, it can be found that the radial flow methods require more complex analysis of experimental data, but have the advantage that principal permeability values can be determined in a single experiment. It is therefore widely used by researchers (Adams et al. 1986, 1987,1988, 1991a and 1991b, Chan et al 1991, 1993, Chick 1996, Gauvin 1996, Gebart et al 1996, Rudd 1995, Weitzenböck 1996, 1999a and 1999b). The glass or acrylic cover are often used in this kind of experiment, this limits the fluid flow rate and pressure to at least

an order of magnitude lower than those typically of industrial structural reaction injection moulding (SRIM) (Adams, 1988). Table 2.2 list some selected methods of permeability measurement by using radial flow.

The permeability measurement of isotropic media are very simple, in the constant inlet pressure experiments, normally, for isotropic materials the permeability is defined as,

$$k = -[r^{f2}(2\ln\frac{r^f}{r^0} - 1) + r^{02}]\frac{\varepsilon\mu}{4(p^f - p^0)t}. \tag{2.20}$$

Where r^f is the position of the flow front at time t, r^0 is the radius of inlet, p^f is pressure at flow front and p^0 is a constant injection pressure. This formulation were used in great number of references (Adams et al. 1986, 1987,1988, 1991a and 1991b, Weitzenböck 1996, 1999a and 1999b). The paper published by Adams et al in 1986 was the first to propose the radial flow technique for permeability measurement in RTM.

For permeabilities of anisotropic materials, the analysis of the experimental data are more complex. Both the principal permeability values and their orientation of anisotropic media can be obtained by following equations (Weitzenböck 1996):

$$\begin{aligned}
k^{(1)} &= F_I\frac{(A-D)}{(A-D/\cos 2\varphi)}C, \\
k^{(2)} &= F_{III}\frac{(A+D)}{(A+D/\cos 2\varphi)}C, \\
\varphi &= \frac{1}{2}\tan^{-1}\left\{\frac{A}{D} - \frac{A^2-D^2}{F_{II}D}\right\}, \\
F_i &= \left\{r_i^{f2}[2\ln(\frac{r_i^f}{r_i^0}) - 1] + r_i^{02}\right\}\frac{1}{t_i}, \quad (i = I, II, III), \\
A &= \frac{F_I + F_{III}}{2}, \\
D &= \frac{F_I - F_{III}}{2}, \\
C &= \frac{\mu\varepsilon}{4\Delta p}.
\end{aligned} \tag{2.21}$$

Table 2.2: Some selected methods of permeability measurement by using radial flow

Author(s)	Method	Formulae	Reinforcement	Comment
Adams et al. (1986, 1987, 1991 a and b)	CIP	$k = \frac{m\varepsilon\mu}{2\Delta p}$ $m = \frac{d(r^{f^2})\ln\frac{r^f}{r^0}}{dt}$	Continuous strand mats, random fabrics.	This is the first paper to propose the radial flow technique of permeability measurement.
Adams et al. (1988)	CIP	Isotropic preform $k = -[r^{f^2}(2\ln\frac{r^f}{r^0} - 1) + r^{0^2}]\frac{\varepsilon\mu}{4(p^f - p^0)t}$.	Isotropic media and anisotropic media.	This equation is a fundamental equation for isotropic media.
Gauvin et al. (1996)	CIP	Isotropic preform $k = \frac{F\varepsilon\mu}{4\Delta pt}$, $F = r^{0^2}\{(\frac{r^f}{r^0})^2[2\ln(\frac{r^f}{r^0}) - 1] + 1\}$. Anisotropic preform $\overline{k} = \frac{F_a\varepsilon\mu}{4\Delta pt}$, $F_a = \overline{r}^{0^2}\{(\frac{\overline{r}^f}{\overline{r}^0})^2[2\ln(\frac{\overline{r}^f}{\overline{r}^0}) - 1] + 1\}$,	Isotropic media and anisotropic media.	$\overline{k}$ is the quasi-isotropic permeability. The first step to calculate the principal permeability of anisotropic media.

Weitzenböck et al. (1996, 1999 a & b)	CIP	Isotropic preform $k = -[{r^f}^2(2\ln\frac{r^f}{r^0} - 1) + {r^0}^2]\frac{\varepsilon\mu}{4(p^f - p^0)t}$. Anisotropic preform $k^{(1)} = F_I\frac{(A-D)}{(A-\frac{D}{\cos 2\theta})}\frac{\mu\varepsilon}{4\Delta p}$, $k^{(2)} = F_{III}\frac{(A+D)}{(A+\frac{D}{\cos 2\theta})}\frac{\mu\varepsilon}{4\Delta p}$, $\theta = \frac{1}{2}\tan^{-1}\left\{\frac{A}{D} - \frac{A^2-D^2}{F_{II}D}\right\}$, $F_i = \left\{{r_i^f}^2[2\ln(\frac{r_i^f}{r_i^0}) - 1] + {r_i^0}^2\right\}\frac{1}{t_i}$, $(i = I, II, III)$, $A = \frac{F_I+F_{III}}{2}$, $D = \frac{F_I-F_{III}}{2}$.	Random fabric, Twill fabric, Unidirectional material.	The principal permeability and orientation were calculated in these paper. These equations are unified, they can be used in calculate both of isotropic and anisotropic preform in constant inlet pressure experiments.
Gauvin et al. (1996)	CFR	Isotropic preform $k = \frac{Q\mu}{2\pi hp^0}\ln\frac{r^f}{r^0}$, Anisotropic preform $\overline{k} = \frac{Q\mu}{2\pi hm}$, $m = \frac{p^0}{\ln\overline{r}^f}$,	Isotropic media and Anisotropic media.	$\overline{k}$ the quasi-isotropic permeability.

Chan et al. (1993)	CFR	Isotropic preform $k = \frac{Q\mu}{2\pi hp^0} \ln \frac{r^f}{r^0}$, Orthotropic preform $\overline{k} = \frac{Q\mu}{2\pi hp^0} \ln \overline{r}^f$, $k^{(1)} = \frac{\overline{k}}{m_1}$, $k^{(2)} = \overline{k} m_1$, $m_1 = \frac{r^y}{r^x}$. Anisotropic preform $k_{11} = \frac{k^{(1)}+k^{(2)}}{2} + \frac{k^{(1)}-k^{(2)}}{2} \cos 2\theta$ $k_{12} = k_{21} = \frac{k^{(1)}-k^{(2)}}{2} \sin 2\theta$ $k_{22} = \frac{k^{(1)}+k^{(2)}}{2} - \frac{k^{(1)}-k^{(2)}}{2} \cos 2\theta$	Isotropic media, Orthotropic media and Anisotropic media.	These equations are often used to calculate the permeability of porous media.

2.3.3 Measurement of three-dimensional permeability

The most common method to measure the through thickness permeability is to use the one-dimensional channel flow test (Trevino et al 1991, Wu et al 1994). Equation (2.18) is also be used to calculate the through thickness permeability. The in-plane permeabilities are determined from a two-dimensional flow (radial flow) experiments.

Ahn et al (1995) firstly presented an experimental technique to measure simultaneously the three principal permeabilities of fibre preforms . Two kinds of transversely orthotropic preforms were examined, one was woven glass fabric and the other was glass fibre chopped strand mat. The technique utilizes embedded optical fibre sensors for detecting the position of the liquid front inside the preform. The formulae used to calculate the three principal permeabilities are as shown as follows:

$$\begin{aligned} k^{(1)} &= \frac{\mu(1-v_f)a^2}{6(p^0-p^f)t}[2(\frac{{X_1}^f}{a})^3 - 3(\frac{{X_1}^f}{a})^2 + 1], \\ k^{(2)} &= \frac{\mu(1-v_f)b^2}{6(p^0-p^f)t}[2(\frac{{X_2}^f}{b})^3 - 3(\frac{{X_2}^f}{b})^2 + 1], \\ k^{(3)} &= \frac{\mu(1-v_f)c^2}{6(p^0-p^f)t}[2(\frac{{X_3}^f}{c})^3 - 3(\frac{{X_3}^f}{c})^2 + 1]. \end{aligned} \tag{2.22}$$

where $a = b = c \cong r^0$.

Weitzenböck et al in 1998 also reported their finding of a similar experiment to measure a three-dimensional permeability by using radial flow test. In these tests, the through thickness direction also is one principal direction, the heated thermistor sensors were used to measure the flow front through this direction.

As described in above, in the three-dimensional permeability measurement, one principal direction always has known before experiment. However when we do not know any principal direction of three-dimensional permeability is, how can it be measured?

2.3.4 The measurement techniques in permeability identification

As far as measurement techniques are concerned, two main aspects should be mentioned. The first one is the technique of measuring the pressure drop in the flow process. The pressure transducer is the most important facility in this measurement technique. Usually, at least there must be one pressure transducer to be used to measure the inlet pressure. Several investigators have used two or more pressure transducers. For example, Chick et al (1996) used at least four pressure transducers to measure the pressure drop. The signal obtained from the pressure transducer will be recorded by computer and then be used to calculate permeability.

Another important technique is to measure flow front positions. Observation of the resin flow front progression was considered first by Adams et al (1986). A liquid of known viscosity is injected at the centre of the top plate and the inlet pressure is kept constant. The position of the flow front is observed through the transparent bottom plate. Usually, a transparent cover is used to permit observation of the progression of the flow front, this enables the recording of the flow front progression with a video camera which can be connected to image processing software to obtain the coordinates of the flow front at a given time step. A important consideration is the cover which must be sufficiently stiff or properly reinforced to avoid excessive defection, which could considerably perturbate the measured values. For this reason glass is preferred to acrylic. Trevino et al. (1991) proposed an edge flow mould to observe flow in the out of plane direction. It consisted of a L-shaped acrylic base plate with inlet gate and outlet located closed to the edge to make the flow as one dimensional as possible. In 1994, Gauvin et al. used photodiodes to measure the flow front for channel flow. These photodiodes were positioned underneath the rectangular transparent cavity measure the light intensity variation which occurs when the advancing flow front over

the photodiods. This light intensity variation is translated into a voltage variation which can be recorded to obtain the flow front speed and position.

The flow visualisation technique is suitable for measuring the principal permeabilities of isotropic and transversely orthotropic preforms. However, they are not applicable to more complex preforms. The magnitudes and directions of the principal permeabilities of preforms with more complex fibre arrangement can be measured by the use of intrusive sensors. Trochu et al. (1993) applied successfully heated thermistors to measure the flow front of resin through a multilayer fibrous reinforcement. In order to detect the shape of the flow front, thermistors had been inserted between the layers of preform in vertical positions of each ply. The wires of the thermistors were laid so as to minimize perturbation of the flow. The signal from the thermistors is transmitted to a computer. When the resin, which has been heated just before experiment, comes in contact with the thermistors, a rapid change in voltage occurs which permits to detect accurately the progression of the resin flow. A similar approach was used by Diallo et al (1995) where thin electrical wires (0.35mm diameter) were placed at various location within the mould cavity of a channel flow mould. Optical fibre sensors are used to monitor the flow of the resin through a preform by Ahn et al (1995). The optical fibre containing several such 'bare spots' was embedded inside the preform. Laser light is transmitted through the optical fibre, and the light intensity at the end of the optical fibre was recorded. When the fluid reached these 'bare spots', there was a significant and sudden drop in the transmitted light intensity. From these observed changes, the rate of flow front can be deduced.

2.3.5 Discussion

Both of the channel flow measurement and the radial flow measurement are based on the corresponding analytical solutions for which the injection pressure or the injection flow rate/volume rate required as a constant (see, Rudd et al 1997), although Ferland (1996) presented a formulation with a variable pressure.

As can be seen from the references (Adams et al 1986, 1987, 1991, Gebart 1992, Gebart et al 1996, Gauvin 1996, Weitzenböck 1996, 1999a, 1999b, 1999c), these formulae for computation of permeability are all under constant injection pressure boundary conditions. In all these experiments, the value of these injection pressure are at a lower level, such as, 0.067 - 0.67 bar used by Adams in 1986 and 0.5 - 0.7 bar by Gauvin in 1996. Although a little higher injection pressure (2 - 3 bar) was used by Gebart (1992, 1996) and Weitzenböck (1996, 1999a, 1999b), they are also more lower if it is compared with industrial liquid moulding. Under this low pressure conditions, the injection pressure may possibly be kept as a constant. But if a higher injection pressure is used, to keep it as constant is more difficult. In this experiment when the pressure source is 1 bar, the inlet pressure is approximately a constant, but when the pressure source is 3 bar, the pressure measured at inlet is not a constant at all, it is variable.

Practically, in most experiment rig it is need to arrange a flow tube between the pressure source and the injection gate to supply the fluid. In this tube, the flow must be governed by Bernoulli's equation (Douglas et al 1995) and therefore the summation of the dynamic pressure and the static pressure at the injection gate is equal to the static pressure at the pressure source. As the fluid in the tube flows, the injection pressure at the injection gate will change with the variation of the flow speed. Theoretically, RTM flow process is a flow with a moving flow front boundary for which the position of the flow front is not prescribed and wetted domain is increasing with time. It has been observed that the speed of the flow front is slower and slower when the wetted domain increases in the experiments. From the continuous condition of the flow, the inlet flow speed will also be slower. As result of these, it is difficult to control a constant injection pressure or a constant injection flow velocity at a higher inject pressure. Although as Darcy's original experiment, if injection flow process is required to be so slow that it can be considered as a 'statical' process, the condition of the constant injection pres-

sure or the constant injection velocity may be approximately satisfied, but it is better to develop some solutions under a condition of variable injection pressure or velocity to support practical permeability identification experiments.

There is another problem should be noted. For a two-dimensional flow experiment, the test plane can always be chosen in the horizontal plane in which the gravitational effect can be neglected. However, for a three-dimensional flow experiment, the gravitational effect along the vertical direction has to be considered. Although in Darcy's original experiment, the gravitational effect was considered, but this effect has been neglected in the references. From practical viewpoint during the production process of a big composite structure, some parts of the total structure have to be located in the vertical direction. Therefore, the gravitational effect can not be avoided. For a more generalized purpose, the gravitational effect should be considered as Darcy's original experiment.

2.4 The present investigation

Having briefly examined and discussed the literature on permeability identification methods of porous media, some comments could be made. Namely,
(1) Both of the channel flow measurement and the radial flow measurement are based on the corresponding analytical solutions for which the injection pressure or the injection flow rate/volume rate required as a constant (see, Rudd et al 1997). But as described in above, it is difficult to control a constant injection pressure or a constant injection flow velocity. Although in Darcy's original experiment, if injection flow process is required to be so slow that it can be considered as a 'statical' process, the condition of the constant injection pressure or the constant injection velocity may be approximately satisfied, but it is better to develop some solutions under a condition of variable injection pressure or velocity to support practical permeability identification experiments.

(2) For a two-dimensional flow experiment, the test plane can always be chosen in a horizontal plane in which the gravitational effect can be avoided. However, for a three-dimensional flow experiment, the gravitational effect along the vertical direction has to be considered. Although in Darcy's original experiment as shown in Figure 2.2 and equation (2.5), the gravitational effect was considered, but this effect is always neglected in reference reports. The reason may be because researches for a three-dimensional cases are not common. For a more generalized purpose, the gravitational effect should be considered as Darcy's original experiment.

(3) Since RTM molded parts are, most of the time, thin shells, the transverse permeability along the direction normal to the shell surface is usually neglected and only planar permeabilities need to be evaluated. Therefore, references on permeability measurement problems are mainly concentrated into a two-dimensional cases. It has been accepted that for a two-dimensional anisotropic materials, at least 3 channel flow measurements in-plane need to be done to determine the two principal permeability and their directions. For the discussion on the three-dimensional cases are relatively much less than the two-dimensional cases. Woerdeman et al (1995) and Weitzenböck (1996 and 1998) discussed a three-dimensional permeability measurements for RTM modeling and they concluded that six experimental flow orientation measurements need to determine three principal permeabilities and their directions. In order to do so the six measurement directions have to be independent of each other, which needs to be checked by a suitable method.

Chapter 3

The permeability tensor k_{ij}

A conclusion from the literature survey is drawn that the permeability for general anisotropic media can be represented by a symmetrical tensor k_{ij} of second-order. The characteristics of this tensor are discussed as follows.

3.1 Coordinate transformation

If a Cartesian coordinate system $O - x_1x_2x_3$ is fixed at a point O in a porous medium consisting of the fibre material in RTM, as shown in Figure 3.1, the corresponding base vectors of this reference system are represented by $\boldsymbol{e}_1$, $\boldsymbol{e}_2$ and $\boldsymbol{e}_3$, respectively. Under this coordinate system, the permeability tensor $\boldsymbol{k}$ of this porous medium can be represented as an entity in the form,

$$\boldsymbol{k} = k_{ij}\boldsymbol{e}_i\boldsymbol{e}_j. \tag{3.1}$$

Under another Cartesian coordinate system $O - x_1'x_2'x_3'$ fixed at the same origin O, which has its corresponding base vectors $\boldsymbol{e}_1'$, $\boldsymbol{e}_2'$ and $\boldsymbol{e}_3'$ shown in Figure 3.1, this same permeability tensor $\boldsymbol{k}$ can also be represented as

$$\boldsymbol{k}' = k_{ij}'\boldsymbol{e}_i'\boldsymbol{e}_j'. \tag{3.2}$$

Therefore, as an entity, the permeability tensor $\boldsymbol{k}$ is independent of the coordinate system. However, the same permeability tensor $\boldsymbol{k}$ is characterized by the two

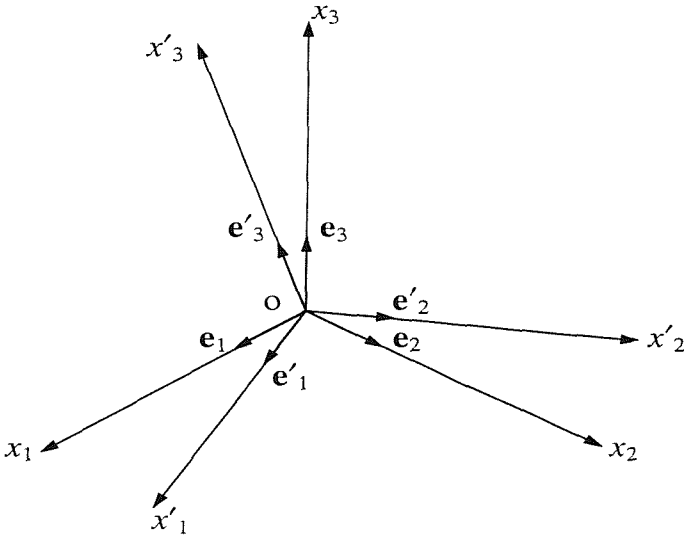

Figure 3.1: Coordinate rotations.

different sets of components k_{ij} and k'_{ij} in two different coordinate systems $O - x_1x_2x_3$ and $O - x'_1x'_2x'_3$ as shown in Figure 3.1. Assume that β_{ij} denotes the direction cosines of the base vectors $\boldsymbol{e}'_i$ under the coordinate system $O - x_1x_2x_3$, that is,

$$\beta_{ij} = \cos(\boldsymbol{e}'_i, \boldsymbol{e}_j) = \boldsymbol{e}'_i \cdot \boldsymbol{e}_j. \tag{3.3}$$

Here, the first index i and the second index j of β_{ij} correspond to the primed coordinate system $O - x'_1x'_2x'_3$ and the un-primed coordinate system $O - x_1x_2x_3$, respectively. Therefore, the β_{ij} is not symmetric with respect to its two indices i and j, i.e.

$$\beta_{ij} \neq \beta_{ji}. \tag{3.4}$$

However, it is valid that,

$$\begin{aligned} \beta_{ir}\beta_{is} &= \delta_{rs}, \\ \beta_{rj}\beta_{sj} &= \delta_{rs}. \end{aligned} \tag{3.5}$$

There exists the following transformation relations between these two different sets of components k_{ij} and k'_{ij},

$$k'_{ij} = \beta_{ir}\beta_{js}k_{rs}, \tag{3.6}$$

$$k_{ij} = \beta_{ri}\beta_{sj}k'_{rs}. \tag{3.7}$$

These two transformation relations can be rewritten in the following matrix forms

$$\begin{aligned} \boldsymbol{k}' &= \boldsymbol{\beta} \cdot \boldsymbol{k} \cdot \boldsymbol{\beta}^T, \\ \boldsymbol{k} &= \boldsymbol{\beta}^T \cdot \boldsymbol{k}' \cdot \boldsymbol{\beta}, \end{aligned} \tag{3.8}$$

respectively, where the superscript T represents a transpose of a matrix and

$$\boldsymbol{\beta} = \begin{bmatrix} \beta_{11} & \beta_{12} & \beta_{13} \\ \beta_{21} & \beta_{22} & \beta_{23} \\ \beta_{31} & \beta_{32} & \beta_{33} \end{bmatrix}. \tag{3.9}$$

3.2 Principal directions and permeabilities

Starting from Darcy's law described in equation (2.10), it can be rewritten in the form,

$$\boldsymbol{q} = -\frac{\boldsymbol{k} \cdot \boldsymbol{J}}{\mu}, \tag{3.10}$$

where the flow vector $\boldsymbol{q}$ and the generalized pressure gradient vector $\boldsymbol{J}$ take the following forms,

$$\boldsymbol{q} = q_j \boldsymbol{e}_j, \tag{3.11}$$

$$\boldsymbol{J} = J_j \boldsymbol{e}_j. \tag{3.12}$$

The Darcy's law described in equation (3.10) represents the scalar product of the permeability tensor $\boldsymbol{k}$ and a prescribed generalized pressure gradient vector $\boldsymbol{J}$ gives a flow vector $\boldsymbol{q}$ in porous media. As mentioned in section 3.4, in the general case, the flow vector $\boldsymbol{q}$ has a different direction relative to the generalized pressure gradient vector $\boldsymbol{J}$, at any point in a porous medium, the generalized

pressure gradient $\boldsymbol{J}$ produces the flow in both directions tangential and normal to the $\boldsymbol{J}$ direction. The following problem can now be posed: Does there exist an orientation $\boldsymbol{n}$ for which the the pressure gradient $\boldsymbol{J}$ along the direction $\boldsymbol{n}$ does not produce any flow normal to the direction of the the generalized pressure gradient $\boldsymbol{J}$? These orientations $\boldsymbol{n}^{(r)}$, $(r = 1, 2, 3)$, satisfying the condition described above are called the principal directions of the permeability tensor $\boldsymbol{k}$ and the corresponding permeability coefficients $k^{(r)}$ along the principal directions $\boldsymbol{n}^{(r)}$ are called the principal permeabilities of the permeability tensor $\boldsymbol{k}$.

3.2.1 The eigenvalue problem

The problem posed above can be represented by the following equation of the eigenvalue problem with the permeability tensor k_{ij}, i.e.

$$(k_{ij} - k\delta_{ij})n_j = 0, \tag{3.13}$$

where k is a scalar principal permeability, a eigenvalue of the permeability tensor k_{ij} and the vector n_j is a eigenvector corresponding to the eigenvalue k. In a matrix form, equation (3.13) becomes,

$$\begin{bmatrix} k_{11} - k & k_{12} & k_{13} \\ k_{21} & k_{22} - k & k_{23} \\ k_{31} & k_{32} & k_{33} - k \end{bmatrix} \begin{bmatrix} n_1 \\ n_2 \\ n_3 \end{bmatrix} = \begin{bmatrix} 0 \\ 0 \\ 0 \end{bmatrix}. \tag{3.14}$$

Because $|\boldsymbol{n}| = 1$,

$$\boldsymbol{n} \cdot \boldsymbol{n} = n_i n_i = 1 \tag{3.15}$$

and it can be inferred that at least one of the components $n_i \neq 0$. Consequently, a solution of equation (3.14) requires that,

$$\begin{vmatrix} k_{11} - k & k_{12} & k_{13} \\ k_{21} & k_{22} - k & k_{23} \\ k_{31} & k_{32} & k_{33} - k \end{vmatrix} = 0. \tag{3.16}$$

Upon expanding equation (3.16),

$$k^3 - I_1 k^2 + I_2 k - I_3 = 0 \tag{3.17}$$

where I_1, I_2 and I_3 are three scalar quantities which are said to be the invariants of the permeability tensor k_{ij}, that is, they will not change as a result of coordinate rotations. The expressions of these three invariants can be derived as follows. Assume that the determinant in equation (3.16) is represented by $a(k)$ which can be represented in the form described in equation (A.11), i.e.

$$\begin{aligned} a(k) &= -(k^3 - I_1 k^2 + I_2 k - I_3) \\ &= e_{ijs}(k_{i1} - k\delta_{i1})(k_{j2} - k\delta_{j2})(k_{s3} - k\delta_{s3}). \end{aligned} \tag{3.18}$$

From this equation, the derivative with respect to k can be obtained,

$$\begin{aligned} \frac{\partial a(k)}{\partial k} &= -(3k^2 - 2I_1 k + I_2) \\ &= -e_{1js}(k_{j2} - k\delta_{j2})(k_{s3} - k\delta_{s3}) - e_{i2s}(k_{i1} - k\delta_{i1})(k_{s3} - k\delta_{s3}) \\ &\quad -e_{ij3}(k_{i1} - k\delta_{i1})(k_{j2} - k\delta_{j2}), \end{aligned} \tag{3.19}$$

$$\begin{aligned} \frac{\partial^2 a(k)}{\partial k^2} &= -(6k - 2I_1) \\ &= 2e_{12s}(k_{s3} - k\delta_{s3}) + 2e_{1j3}(k_{j2} - k\delta_{j2}) + 2e_{i23}(k_{i1} - k\delta_{i1}). \end{aligned} \tag{3.20}$$

A substitution of $k = 0$ into equations (3.18)-(3.20) gives the three invariants as follows

$$\begin{aligned} I_1 &= e_{12s}k_{s3} + e_{1j3}k_{j2} + e_{i23}k_{i1} \\ &= k_{ii}, \\ I_2 &= e_{1js}k_{j2}k_{s3} + e_{i2s}k_{i1}k_{s3} + e_{ij3}k_{i1}k_{j2} \\ &= \begin{vmatrix} k_{22} & k_{23} \\ k_{32} & k_{33} \end{vmatrix} + \begin{vmatrix} k_{11} & k_{13} \\ k_{31} & k_{33} \end{vmatrix} + \begin{vmatrix} k_{11} & k_{12} \\ k_{21} & k_{22} \end{vmatrix}, \\ I_3 &= a(0) \\ &= \begin{vmatrix} k_{11} & k_{12} & k_{13} \\ k_{21} & k_{22} & k_{23} \\ k_{31} & k_{32} & k_{33} \end{vmatrix}. \end{aligned} \tag{3.21}$$

In general, equation (3.14) will have three distinct roots $k^{(r)}$, $r = 1, 2, 3$, and with each root a unit vector can be associated with components $n_i^{(r)}$, $i = 1, 2, 3$. These

unit vectors $\boldsymbol{n}^{(r)}$, $r = 1, 2, 3$ specify the principal directions of the permeability tensor k_{ij}, and they form the orthonormal basis of the associated principal axis system. Along the principal directions $\boldsymbol{n}^{(r)}$, $r = 1, 2, 3$, the principal permeability components are $k^{(r)}$, $r = 1, 2, 3$, respectively. These principal directions $\boldsymbol{n}^{(r)}$, $r = 1, 2, 3$ satisfy the following orthogonality relation.

3.2.2 The orthogonality of the principal directions $n^{(r)}$

It can be demonstrated that any two principal directions $\boldsymbol{n}^{(r)}$ and $\boldsymbol{n}^{(s)}$, which have their corresponding distinct principal permeabilities $k^{(r)}$ and $k^{(s)}$, $k^{(r)} \neq k^{(s)}$, are mutually orthogonal. Because the vector $\boldsymbol{n}^{(r)}$ and the real number $k^{(r)}$ are assumed to be the principal direction and its corresponding principal permeability, they satisfy equation (3.13), that is,

$$k_{ij} n_j^{(r)} = k^{(r)} n_i^{(r)}. \tag{3.22}$$

A scalar multiplication of this equation by the vector $n_i^{(s)}$ gives,

$$n_i^{(s)} k_{ij} n_j^{(r)} = k^{(r)} n_i^{(s)} n_i^{(r)}. \tag{3.23}$$

Similarly,

$$n_i^{(r)} k_{ij} n_j^{(s)} = k^{(s)} n_i^{(r)} n_i^{(s)}. \tag{3.24}$$

Because of the symmetry of the tensor k_{ij} and equation (A.6), if follows that,

$$n_i^{(r)} k_{ij} n_j^{(s)} = n_j^{(r)} k_{ji} n_i^{(s)} = n_i^{(s)} k_{ij} n_j^{(r)}. \tag{3.25}$$

Therefore subtracting (3.23) from (3.24) gives

$$(k^{(r)} - k^{(s)}) n_i^{(r)} n_i^{(s)} = 0. \tag{3.26}$$

Because $k^{(r)} \neq k^{(s)}$, it is obtained that

$$n_i^{(r)} n_i^{(s)} = 0, \tag{3.27}$$

which proves that the two vectors $n_i^{(r)}$ and $n_i^{(s)}$ are orthogonal. In combination with equation (3.15) which represents the case of $\boldsymbol{n}^{(r)} = \boldsymbol{n}^{(s)}$, $r = s$, the orthogonality of the principal directions $\boldsymbol{n}^{(r)}$ of the permeability tensor k_{ij} can be rewritten as,

$$n_i^{(r)} k_{ij} n_j^{(s)} = k^{(r)} \delta_{rs}. \tag{3.28}$$

Now, a principal direction matrix $\boldsymbol{N}$ and a principal permeability matrix $\boldsymbol{\Lambda}$ are introduced as follows,

$$\boldsymbol{N} = \begin{bmatrix} \boldsymbol{n}^{(1)} & \boldsymbol{n}^{(2)} & \boldsymbol{n}^{(3)} \end{bmatrix} = \begin{bmatrix} n_1^{(1)} & n_1^{(2)} & n_1^{(3)} \\ n_2^{(1)} & n_2^{(2)} & n_2^{(3)} \\ n_3^{(1)} & n_3^{(2)} & n_3^{(3)} \end{bmatrix}, \tag{3.29}$$

$$\boldsymbol{\Lambda} = \begin{bmatrix} k^{(1)} & 0 & 0 \\ 0 & k^{(2)} & 0 \\ 0 & 0 & k^{(3)} \end{bmatrix}, \tag{3.30}$$

where $\boldsymbol{n}^{(r)}$, $r = 1, 2, 3$ represents the r-principal direction column vector, that is

$$\boldsymbol{n}^{(r)} = \begin{bmatrix} n_1^{(1)} \\ n_2^{(1)} \\ n_3^{(1)} \end{bmatrix}. \tag{3.31}$$

The equation (3.28) can be represented in the matrix form

$$\boldsymbol{N}^T \boldsymbol{k} \boldsymbol{N} = \boldsymbol{\Lambda}. \tag{3.32}$$

By use of the relation,

$$\boldsymbol{N}^T \boldsymbol{N} = \boldsymbol{N} \boldsymbol{N}^T = \boldsymbol{I}, \tag{3.33}$$

where $\boldsymbol{I}$ is a unit matrix, from equation (3.32) it is obtained that,

$$\boldsymbol{k} = \boldsymbol{N} \boldsymbol{\Lambda} \boldsymbol{N}^T = \boldsymbol{n}^{(1)} k^{(1)} \boldsymbol{n}^{(1)^T} + \boldsymbol{n}^{(2)} k^{(2)} \boldsymbol{n}^{(2)^T} + \boldsymbol{n}^{(3)} k^{(3)} \boldsymbol{n}^{(3)^T}, \tag{3.34}$$

or its equivalent form,

$$\boldsymbol{k} = k^{(1)} \boldsymbol{n}^{(1)} \boldsymbol{n}^{(1)} + k^{(2)} \boldsymbol{n}^{(2)} \boldsymbol{n}^{(2)} + k^{(3)} \boldsymbol{n}^{(3)} \boldsymbol{n}^{(3)}. \tag{3.35}$$

This equation gives an expression of the all permeability coefficients in the permeability tensor $\boldsymbol{k}$ by means of the principal directions $\boldsymbol{n}^{(r)}$ and permeabilities $k^{(r)}$, $r = 1, 2, 3$. This expression has its component form as follows,

$$k_{ij} = k^{(1)} n_i^{(1)} n_j^{(1)} + k^{(2)} n_i^{(2)} n_j^{(2)} + k^{(3)} n_i^{(3)} n_j^{(3)}. \tag{3.36}$$

3.2.3 The principal directions and permeabilities for three kinds of media

According to the number of distinct roots of equation (3.14), there are three cases discussed as follow.

Anisotropic media

This is a general case of anisotropic media, for which there are three distinct roots $k^{(r)}$, $(r = 1, 2, 3)$ of equation (3.14). In association with these three distinct roots, there are three corresponding principal directions $\boldsymbol{n}^{(r)}$, $r = 1, 2, 3$ which are mutually perpendicular. Under this principal axis system, the permeability tensor $\boldsymbol{k}$ takes the form,

$$\boldsymbol{k} = \begin{bmatrix} k^{(1)} & 0 & 0 \\ 0 & k^{(2)} & 0 \\ 0 & 0 & k^{(3)} \end{bmatrix}. \tag{3.37}$$

For this kind of general anisotropic media, to get full information of its permeability, it is necessary to obtain its three principal directions and the corresponding principal permeabilities.

Transversely anisotropic media

For this case of a double root of equation (3.14) can be found. Physically, the longitudinal direction, denoted by x_1(see Figure 2.1), of this kind of media, is a principal direction determined uniquely. On any plane perpendicular to the longitudinal direction, any two mutually perpendicular directions denoted by x_2

and x_3 are other two principal directions with a same principal permeability, which represents that the media are isotropic in the plane $O - x_2x_3$. Therefore, it is not needed to distinguish the directions x_2 and x_3. If the permeability in a plane through the longitudinal direction axis x_1 is obtained, we will have the full permeability information of the media. Under the principal axis system, the permeability tensor reduces to the form,

$$\boldsymbol{k} = \begin{bmatrix} k^{(1)} & 0 \\ 0 & k^{(2)} \end{bmatrix}. \tag{3.38}$$

For this kind of media, the two principal directions have been determined by the structure of the media. If two principal permeabilities can be obtained, it is possible to get full information about the permeability characteristics of the media.

Isotropic media

For this case, a triple root of equation (3.14) can be found and the three orthogonal principal directions can be chosen arbitrarily. The permeability tensor reduces to a three-dimensional isotropic tensor

$$\boldsymbol{k} = \begin{bmatrix} k & 0 & 0 \\ 0 & k & 0 \\ 0 & 0 & k \end{bmatrix}, \tag{3.39}$$

where k is a real number. If this real number k is obtained, the permeability characteristics of the isotropic media is fully known.

3.3 Effective permeability

The Darcy's law described in equation (3.10) can be rewritten as the matrix form as,

$$-\frac{1}{\mu}\begin{bmatrix} k_{11} & k_{12} & k_{13} \\ k_{21} & k_{22} & k_{23} \\ k_{31} & k_{32} & k_{33} \end{bmatrix}\begin{bmatrix} J_1 \\ J_2 \\ J_3 \end{bmatrix} = \begin{bmatrix} q_1 \\ q_2 \\ q_3 \end{bmatrix}, \tag{3.40}$$

which is valid for any coordinate system. Now, assume that $q_2 = 0 = q_3$, what is the relation between the flow q_1 and the pressure gradient J_1? In practice, this flow represents a one-dimensional flow along a tube filled by a porous medium strip which is cut out from a porous medium along its x_1 direction. This question is discussed as follows.

3.3.1 One-dimensional effective permeability

For this case, equation (3.40) takes the form

$$-\frac{1}{\mu}\begin{bmatrix} k_{11} & k_{12} & k_{13} \\ k_{21} & k_{22} & k_{23} \\ k_{31} & k_{32} & k_{33} \end{bmatrix}\begin{bmatrix} J_1 \\ J_2 \\ J_3 \end{bmatrix} = \begin{bmatrix} q_1 \\ 0 \\ 0 \end{bmatrix}, \tag{3.41}$$

which represents that the flow q_1 in x_1 direction is dependent of the permeability parameters on the $O - x_2x_3$ plane perpendicular to the x_1 direction, i.e.

$$q_1 = -\frac{1}{\mu}(k_{11}J_1 + \begin{bmatrix} k_{12} & k_{13} \end{bmatrix}\begin{bmatrix} J_2 \\ J_3 \end{bmatrix}), \tag{3.42}$$

$$-\frac{1}{\mu}(\begin{bmatrix} k_{21} \\ k_{31} \end{bmatrix}J_1 + \begin{bmatrix} k_{22} & k_{23} \\ k_{32} & k_{33} \end{bmatrix}\begin{bmatrix} J_2 \\ J_3 \end{bmatrix}) = \begin{bmatrix} 0 \\ 0 \end{bmatrix}. \tag{3.43}$$

From these two equations, it is obtained that,

$$q_1 = -\frac{1}{\mu}\tilde{k}_{11}J_1, \tag{3.44}$$

where $\tilde{k}_{11}$ denotes the effective permeability along the x_1 direction,

$$\begin{aligned} \tilde{k}_{11} &= k_{11} - \begin{bmatrix} k_{12} & k_{13} \end{bmatrix}\begin{bmatrix} k_{22} & k_{23} \\ k_{32} & k_{33} \end{bmatrix}^{-1}\begin{bmatrix} k_{21} \\ k_{31} \end{bmatrix} \\ &= \frac{I_3}{\begin{vmatrix} k_{22} & k_{23} \\ k_{32} & k_{33} \end{vmatrix}}, \end{aligned} \tag{3.45}$$

where I_3 is the third invariant of the permeability tensor k_{ij} as shown in equation (3.21).

Similarly, to obtain the effective permeabilities and the corresponding Darcy's law equations along x_2 and x_3 directions as follows,

$$\tilde{k}_{22} = \frac{I_3}{\begin{vmatrix} k_{11} & k_{13} \\ k_{31} & k_{33} \end{vmatrix}}, \qquad q_2 = -\frac{1}{\mu}\tilde{k}_{22}J_2, \tag{3.46}$$

$$\tilde{k}_{33} = \frac{I_3}{\begin{vmatrix} k_{11} & k_{12} \\ k_{21} & k_{22} \end{vmatrix}}, \qquad q_3 = -\frac{1}{\mu}\tilde{k}_{33}J_3, \tag{3.47}$$

Concluding these results given in equations (3.45)-(3.47),the following theorem can be obtained.

THEOREM 1: One-dimensional effective permeability theorem. *For an arbitrary chosen Cartesian coordinate system $O - x_1x_2x_3$ fixed in an anisotropic porous medium, the one-dimensional effective permeability $\tilde{k}_{\alpha\alpha}$ along any coordinate direction x_α, $(\alpha = 1, 2, 3)$, is equal to the third invariant I_3 of the permeability tensor k_{ij} of this medium divided by the sub-determinant obtained by deleting the row and column relating to the index α from the determinant I_3.*

From equations (3.21) and (3.45)-(3.47), it follows that,

$$\frac{1}{\tilde{k}_{11}} + \frac{1}{\tilde{k}_{22}} + \frac{1}{\tilde{k}_{33}} = \frac{I_2}{I_3}. \tag{3.48}$$

Since I_3 and I_2 are the invariants of the permeability tensor k_{ij}, their values do not change when the coordinate system changes. Under the principal coordinate system $O - X_1X_2X_3$, the permeability tensor k_{ij} takes its simplest form described by equation (3.30) and I_3 and I_2 can be represented as

$$I_3 = k^{(1)}k^{(2)}k^{(3)}, \tag{3.49}$$

$$I_2 = k^{(1)}k^{(2)} + k^{(2)}k^{(3)} + k^{(1)}k^{(3)}. \tag{3.50}$$

From these two equations and equation (3.48), the following theorem it is concluded.

THEOREM 2: One-dimensional effective permeability invariance theorem. *For an arbitrary anisotropic porous medium, the sum of the reciprocal of their three one-dimensional effective permeabilities along any three Cartesian coordinate directions is an invariant which equal to the sum of the reciprocal of the three principal permeabilities of the medium, that is*

$$\frac{1}{\tilde{k}_{11}} + \frac{1}{\tilde{k}_{22}} + \frac{1}{\tilde{k}_{33}} = \frac{1}{k^{(1)}} + \frac{1}{k^{(2)}} + \frac{1}{k^{(3)}}. \tag{3.51}$$

For a two-dimensional porous media, if a Cartesian coordinate $O - x_1x_2$ is chosen, equations (3.45)-(3.47) described by theorem 1 and equation (3.51) described by theorem 2 are respectively reduced to the forms

$$\tilde{k}_{11} = \frac{I_2}{k_{22}}, \tag{3.52}$$

$$\tilde{k}_{22} = \frac{I_2}{k_{11}}, \tag{3.53}$$

$$\frac{1}{\tilde{k}_{11}} + \frac{1}{\tilde{k}_{22}} = \frac{1}{k^{(1)}} + \frac{1}{k^{(2)}}. \tag{3.54}$$

For a very special case in which the coordinate system $O - x_1x_2x_3$ chosen is exactly the principal coordinate system $O - X_1X_2X_3$, the three effective permeabilities $\tilde{k}_{\alpha\alpha}$ along the principal directions α, $(\alpha = 1, 2, 3)$, are the three principal permeabilities $k^{(\alpha)}$ because of the orthogonality of principal directions described in section 3.2.2. The equations (3.45)-(3.47) and (3.51) correctly represent these practical result, which further demonstrate the two theorems given above.

3.3.2 Two-dimensional effective permeability

If a two-dimensional coordinate system $O - x_1x_2$ is fixed on this plane, the flow velocities q_1 and q_2 and the pressure p are functions of the coordinate x_1 and x_2. These variables are independent of the coordinate x_3 which is perpendicular to the $O - x_1x_2$ plane. The flows between two parallel plates is a typical example

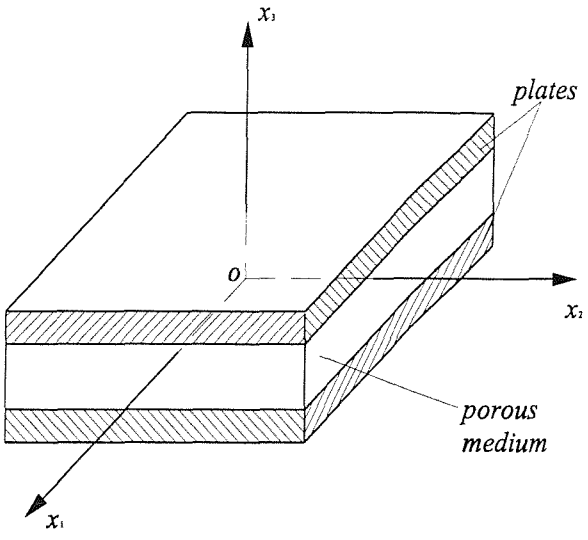

Figure 3.2: A two-dimensional flow between two parallel plates.

of two-dimensional flows, as shown in Figure 3.2. In this case, because the two plates are assumed to be non-permeable, the flow velocity q_3 on the two plate surfaces vanishes. Furthermore, the distance between the two parallel plates is assumed to be such small that the flow along the x_3 direction can be neglected. Substituting the condition $q_3 = 0$ in to Darcy's law in equation (2.13), to obtain,

$$\begin{bmatrix} q_1 \\ q_2 \end{bmatrix} = -\frac{1}{\mu}\left(\begin{bmatrix} k_{11} & k_{12} \\ k_{21} & k_{22} \end{bmatrix} \begin{bmatrix} J_1 \\ J_2 \end{bmatrix} + \begin{bmatrix} k_{13} \\ k_{23} \end{bmatrix} J_3 \right) \tag{3.55}$$

and

$$0 = -\frac{1}{\mu}\left(\begin{bmatrix} k_{31} & k_{32} \end{bmatrix} \begin{bmatrix} J_1 \\ J_2 \end{bmatrix} + k_{33} J_3 \right). \tag{3.56}$$

From these two equations, it follows that,

$$\begin{bmatrix} q_1 \\ q_2 \end{bmatrix} = -\frac{1}{\mu} \begin{bmatrix} \tilde{k}_{11} & \tilde{k}_{12} \\ \tilde{k}_{21} & \tilde{k}_{22} \end{bmatrix} \begin{bmatrix} J_1 \\ J_2 \end{bmatrix}, \tag{3.57}$$

where $\tilde{()}$ represents the effective permeability coefficients,

$$\begin{bmatrix} \tilde{k}_{11} & \tilde{k}_{12} \\ \tilde{k}_{21} & \tilde{k}_{22} \end{bmatrix} = \begin{bmatrix} k_{11} & k_{12} \\ k_{21} & k_{22} \end{bmatrix} - \begin{bmatrix} k_{13} \\ k_{23} \end{bmatrix} \frac{1}{k_{33}} \begin{bmatrix} k_{31} & k_{32} \end{bmatrix}. \tag{3.58}$$

Equation (3.57) provides a generalized relationship between the flows (q_1, q_2) and the pressure gradients (J_1, J_2) for flows between two parallel plates. If the x_3 direction is a principal direction of the medium, that is the $O - x_1x_2$ plane is a principal plane of the medium, then $k_{31} = 0 = k_{32}$ and the effective permeability coefficients in equation (3.58) are equal to the real permeability coefficients of the medium.

3.4 Directional permeability

As shown in Figure 3.3, a point A in the porous media is investigated (see, for example, Bear 1972). The coordinate system $O-X_1X_2X_3$ represents the principal axes of the permeability tensor $\boldsymbol{k}$ at the point A. The angle θ represents the angle between the flow velocity vector $\boldsymbol{q}$ and the pressure gradient vector $\boldsymbol{J}$. In this principal axes, the flow velocity vector $\boldsymbol{q}$, the pressure gradient vector $\boldsymbol{J}$ and the permeability tensor $\boldsymbol{k}$ can be represent as,

$$\boldsymbol{q} = q_1\boldsymbol{n}^{(1)} + q_2\boldsymbol{n}^{(2)} + q_3\boldsymbol{n}^{(3)}, \tag{3.59}$$

$$\boldsymbol{J} = J_1\boldsymbol{n}^{(1)} + J_2\boldsymbol{n}^{(2)} + J_3\boldsymbol{n}^{(3)}, \tag{3.60}$$

$$\boldsymbol{k} = k^{(1)}\boldsymbol{n}^{(1)}\boldsymbol{n}^{(1)} + k^{(2)}\boldsymbol{n}^{(2)}\boldsymbol{n}^{(2)} + k^{(3)}\boldsymbol{n}^{(3)}\boldsymbol{n}^{(3)}, \tag{3.61}$$

where $\boldsymbol{n}^{(r)}, (r = 1, 2, 3)$ denote the unit vectors along the principal axes x_r.

By using the rules for vector operation, equations (3.59)-(3.61) and Darcy's law in equation (3.10), it is obtained that

$$\begin{aligned}
\cos\theta &= \frac{\boldsymbol{q}.\boldsymbol{J}}{qJ} \\
&= -\frac{\boldsymbol{J}.\boldsymbol{k}.\boldsymbol{J}}{\mu qJ} \\
&= -\frac{k^{(1)}J_1^2 + k^{(2)}J_2^2 + k^{(3)}J_3^2}{\mu qJ}, \qquad (3.62)\\
q_1 &= -k^{(1)}J_1/\mu = q\cos\phi_1, \qquad (3.63)\\
q_2 &= -k^{(2)}J_2/\mu = q\cos\phi_2, \qquad (3.64)
\end{aligned}$$

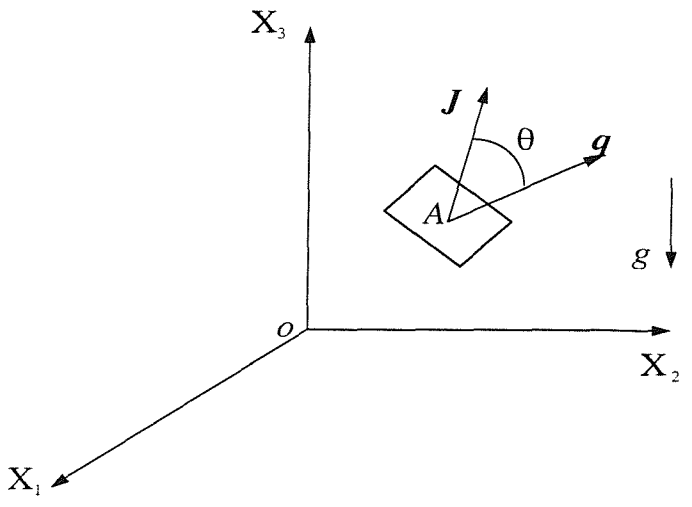

Figure 3.3: A representation of the velocity vector $\boldsymbol{q}$ and the pressure gradient $\boldsymbol{J}$.

$$q_3 = -k^{(3)} J_3/\mu = q\cos\phi_3, \tag{3.65}$$

$$J_1 = J\cos\alpha_1, \tag{3.66}$$

$$J_2 = J\cos\alpha_2, \tag{3.67}$$

$$J_3 = J\cos\alpha_3, \tag{3.68}$$

where q and J represent the amplitudes of the vectors $\boldsymbol{q}$ and $\boldsymbol{J}$, respectively. The angles ϕ_j and α_j, $(j = 1, 2, 3)$ denote the directional angles of the vectors $\boldsymbol{q}$ and $\boldsymbol{J}$ in the principal axes system, respectively. These two angles respectively satisfy the relations,

$$\cos^2\phi_1 + \cos^2\phi_2 + \cos^2\phi_3 = 1, \tag{3.69}$$

$$\cos^2\alpha_1 + \cos^2\alpha_2 + \cos^2\alpha_3 = 1. \tag{3.70}$$

3.4.1 Directional permeability k_J

From Darcy's law, the component q_J of the flow vector $\boldsymbol{q}$ along the pressure gradient vector $\boldsymbol{J}$ can be represented as,

$$q_J = q\cos\theta$$

$$= \frac{\boldsymbol{J}.\boldsymbol{q}}{J}$$
$$= -\frac{\boldsymbol{J}.\boldsymbol{k}.\boldsymbol{J}}{J\mu}. \tag{3.71}$$

If the pressure gradient vector $\boldsymbol{J}$ has the same direction as the first axis of a coordinate system, the pressure gradient vector $\boldsymbol{J}$ and the permeability tensor $\boldsymbol{k}$ can be represented as,

$$\boldsymbol{J} = \begin{bmatrix} J \\ 0 \\ 0 \end{bmatrix}, \tag{3.72}$$

$$\boldsymbol{k} = \begin{bmatrix} k_J & k_{12} & k_{13} \\ k_{21} & k_{22} & k_{23} \\ k_{31} & k_{32} & k_{33} \end{bmatrix}. \tag{3.73}$$

Substituting equations (3.72) and (3.73) into equation (3.71), it gives,

$$q_J = -\frac{1}{\mu} k_J J, \tag{3.74}$$

which gives the directional permeability k_J along the direction of the pressure gradient vector $\boldsymbol{J}$ as,

$$k_J = -\frac{\mu q_J}{J} = -\frac{\mu q \cos\theta}{J}. \tag{3.75}$$

A substitution of equation (3.62) into equation (3.75) give the directional permeability k_J in the form,

$$k_J = \frac{k^{(1)} J_1^2 + k^{(2)} J_2^2 + k^{(3)} J_3^2}{J^2}, \tag{3.76}$$

which from equations (3.66)-(3.68) can be further rewritten as,

$$k_J = k^{(1)} \cos^2\alpha_1 + k^{(2)} \cos^2\alpha_2 + k^{(3)} \cos^2\alpha_3, \tag{3.77}$$

or

$$\frac{1}{1/k_J} = \frac{\cos^2\alpha_1}{1/k^{(1)}} + \frac{\cos^2\alpha_2}{1/k^{(2)}} + \frac{\cos^2\alpha_3}{1/k^{(3)}}. \tag{3.78}$$

In the principal axis system $O - X_1X_2X_3$, a radius vector $\boldsymbol{r}$, which is collinear with $\boldsymbol{J}$, has the components: $X_1 = r\cos\alpha_1$; $X_2 = r\cos\alpha_2$; $X_3 = r\cos\alpha_3$. Hence,

equation (3.78) becomes

$$\frac{r^2}{1/k_J} = \frac{X_1^2}{1/k^{(1)}} + \frac{X_2^2}{1/k^{(2)}} + \frac{X_3^2}{1/k^{(3)}}. \tag{3.79}$$

By drawing a segment of length $r = \sqrt{1/k_J}$ in the direction of $\boldsymbol{J}$, therefore

$$\frac{X_1^2}{1/k^{(1)}} + \frac{X_2^2}{1/k^{(2)}} + \frac{X_3^2}{1/k^{(3)}} = 1, \tag{3.80}$$

which is the canonical equation of an ellipsoid in the $O - X_1X_2X_3$ coordinate systems shown in Figure 3.4. Its semiaxes are $1/\sqrt{k^{(1)}}$, $1/\sqrt{k^{(2)}}$ and $1/\sqrt{k^{(3)}}$ in the X_1, X_2 and X_3 directions, respectively. The vector $\boldsymbol{r}$ in this ellipsoid gives the directional permeability ($k_J = 1/r^2$) in the direction of the pressure gradient $\boldsymbol{J}$.

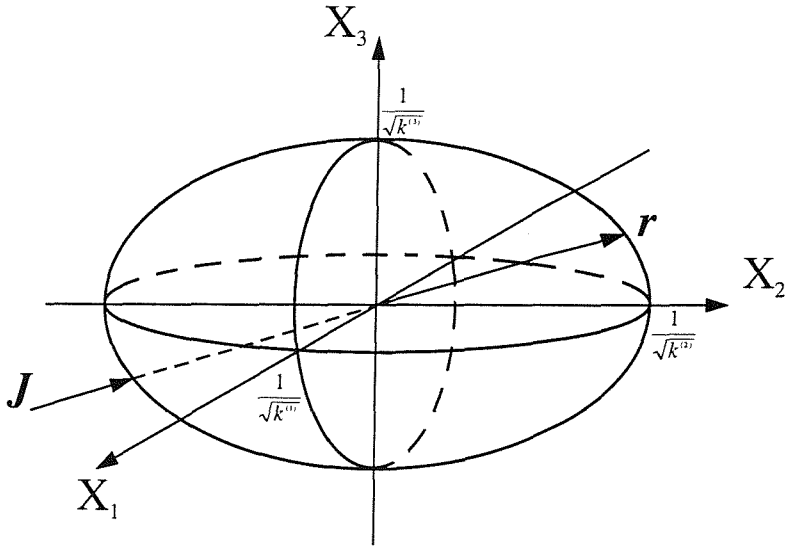

Figure 3.4: The ellipsoid representing the directional permeability k_J in the pressure gradient $\boldsymbol{J}$.

3.4.2 Directional permeability k_q

Similarly, from Darcy's law, the component J_q of the pressure gradient vector $\boldsymbol{J}$ along the flow vector $\boldsymbol{q}$ can be represented as,

$$J_q = J\cos\theta \tag{3.81}$$

If the flow vector $\boldsymbol{q}$ has the same direction as the first axis of a coordinate system, the flow vector $\boldsymbol{q}$ and pressure gradient vector $\boldsymbol{J}$ can be represented as,

$$\boldsymbol{q} = \begin{bmatrix} q \\ 0 \\ 0 \end{bmatrix}, \tag{3.82}$$

$$\boldsymbol{J} = \begin{bmatrix} J_q \\ J_2 \\ J_3 \end{bmatrix}. \tag{3.83}$$

Therefore, Darcy's law for this coordinate system can be written as

$$\begin{bmatrix} q \\ 0 \\ 0 \end{bmatrix} = -\frac{1}{\mu}\begin{bmatrix} k'_{11} & k'_{12} & k'_{13} \\ k'_{21} & k'_{22} & k'_{23} \\ k'_{31} & k'_{32} & k'_{33} \end{bmatrix}\begin{bmatrix} J_q \\ J'_2 \\ J'_3 \end{bmatrix}, \tag{3.84}$$

where $()'$ represent these values for this special chosen coordinate system. In comparison of this equation with equation (3.41), the effective permeability equation (3.44) along the flow vector $\boldsymbol{q}$ direction can be rewritten as,

$$q = -\frac{1}{\mu}k_q J_q, \tag{3.85}$$

where k_q is the effective permeability along the $\boldsymbol{q}$ direction. This special chosen effective permeability k_q is called the directional permeability along the flow vector $\boldsymbol{q}$ direction and it is defined as,

$$k_q = -\frac{\mu q}{J_q}. \tag{3.86}$$

Substituting equations (3.81) and (3.62) into equation (3.86), to give,

$$k_q = \frac{\mu^2 q^2}{k^{(1)}J_1^2 + k^{(2)}J_2^2 + k^{(3)}J_3^2}. \tag{3.87}$$

From equations (3.63)-(3.65), it follows that,

$$k_q = \frac{1}{\frac{\cos^2\phi_1}{k^{(1)}} + \frac{\cos^2\phi_2}{k^{(2)}} + \frac{\cos^2\phi_3}{k^{(2)}}}, \tag{3.88}$$

which can be further rewritten as,

$$\frac{1}{k_q} = \frac{\cos^2\phi_1}{k^{(1)}} + \frac{\cos^2\phi_2}{k^{(2)}} + \frac{\cos^2\phi_3}{k^{(2)}}. \tag{3.89}$$

In the principal axis system $O - X_1X_2X_3$, a radius vector $\boldsymbol{r}$, which is collinear with $\boldsymbol{q}$, has the components: $X_1 = r\cos\phi_1$; $X_2 = r\cos\phi_2$; $X_3 = r\cos\phi_3$. Hence, equation (3.89) becomes,

$$\frac{r^2}{k_q} = \frac{X_1^2}{k^{(1)}} + \frac{X_2^2}{k^{(2)}} + \frac{X_3^2}{k^{(3)}}. \tag{3.90}$$

By drawing a segment of length $r = \sqrt{k_q}$ in the direction of $\boldsymbol{q}$, to obtain from equation (3.90) that,

$$\frac{X_1^2}{k^{(1)}} + \frac{X_2^2}{k^{(2)}} + \frac{X_3^2}{k^{(3)}} = 1, \tag{3.91}$$

which is the canonical equation of an ellipsoid in the $O - X_1X_2X_3$ coordinate systems shown in Figure 3.5. Its semiaxes are $\sqrt{k^{(1)}}$, $\sqrt{k^{(2)}}$ and $\sqrt{k^{(3)}}$ in the X_1, X_2 and X_3 directions, respectively. The vector $\boldsymbol{r}$ in the ellipsoid thus gives directional permeability $k_q = r^2$ in the flow direction.

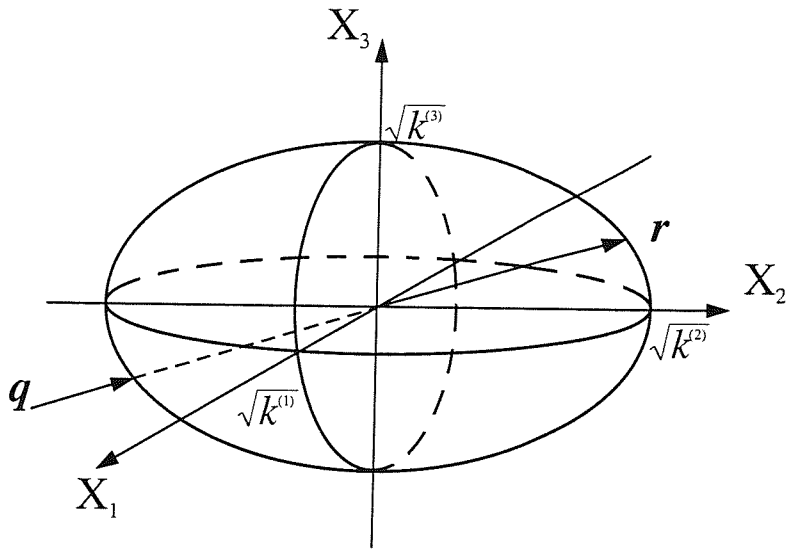

Figure 3.5: The ellipsoid representing the directional permeability k_q in the flow vector $\boldsymbol{q}$.

Chapter 4

Mathematical Description of Resin Injection Flows

As indicated in section 2.2, the generalized Darcy's law described in equation (2.10) only is the statistical average of the momentum balance equation and the constitutive relation in continuum mechanics. Comparing with all governing equations in continuum mechanics, it is necessary to define two further equations, the continuity condition and the state equation, to obtain a complete system of equations to describe resin injection flows in porous media consisting of various fibre reinforcements. These three equations and suitable supplementary boundary conditions provide a mathematical formulation of various resin flows in RTM. All of these governing equations are listed as follows.

4.1 Governing equations

4.1.1 Generalized Darcy's law

The generalized Darcy's law for anisotropic media described in equation (2.10) are repeated herein for a convenience in our discussion of this chapter.

$$q_i = -\frac{k_{ij}}{\mu}(p_{,j} + \rho g \delta_{3j}). \tag{4.1}$$

4.1.2 Continuity equation

In the continuity equation given herein, there exists a coefficient ε before the time derivative $\rho_{,t}$ of the mass density, which is different with the common continuity equation in continuum mechanics. This coefficient ε represents the effective porosity of the media.

$$-\varepsilon\rho_{,t} = (\rho q_j)_{,j}. \tag{4.2}$$

4.1.3 State equation

The state equation gives a relation between the resin density of mass ρ and the flow pressure p, i.e.

$$\rho = \rho(p). \tag{4.3}$$

4.1.4 Boundary conditions

There are two kinds of boundary conditions suitable to equations above, one is the pressure boundary condition and the other is the velocity boundary condition. On each boundary only the pressure or the velocity is needed. For example, on the fixed boundaries, the velocity of flow vanishes, the suitable condition is the velocity condition,

$$q_i = 0, \tag{4.4}$$

and on the flow front boundary, the pressure p^f on the flow front can be assumed to be the atmospheric pressure or a vacuum condition, i.e.

$$p^f = Atmosphericpressure \quad Openflowfrontboundary \tag{4.5}$$

On the resin injection boundary, there are two conditions to be chosen. One is the *resin injection pressure* p^0 and the other is the *resin injection velocity* q_i^0.

That is

$$\begin{array}{ll} p = p^0(t) & \text{Injection pressure is defined} \\ q_i = q_i^0(t) & \text{Injection velocity is defined} \end{array} . \tag{4.6}$$

For general cases, these injection pressure p^0 and velocity q_i^0 may not be constants but time functions, which will be considered in this thesis.

In these equations, there are 5 unknown variables q_i, p and ρ and 5 equations expressed in equations (4.1)-(4.6). The solution of these equations with a suitable initial time condition provides a description of a flow in RTM process. The main difficulty in solving these equations is that the boundary on the output (vacuum) side is a movable boundary, on which the flow front moves as the time goes during resin injection processes. However, for some special cases, analytical solutions may be derived. To this end, it is assumed that the resin discussed is incompressible, and therefore its density ρ is a constant, and $\rho_{,t} = 0 = \rho_{,j}$, which means that equation (4.2) reduces to,

$$q_{j,j} = 0. \tag{4.7}$$

These analytical solutions are described in the following section to provide a basis of applications in related permeability measurements.

4.2 Injection pressure is given

Here some analytical solutions for the case in which the injection pressure $p^0(t)$ is given are developed.

4.2.1 One-dimensional channel flows in isotropic and anisotropic media

As shown in Figure 4.1, a one-dimensional tube is filled by a porous medium strip which is cut out from a porous medium along its x_1 direction, which is assumed to be located in a horizontal plane. The section of the tube perpendicular to the

x_1 direction is parallel to the $O - x_2x_3$ plane of the reference coordinate system fixed in the porous medium to be studied herein. Because the tube section is much smaller than its length, the flow on each section perpendicular to the x_1 axis is neglected, which gives $q_2 = q_3 = 0$. However, because of the viscosity effect of the resin, the pressure on each section perpendicular the x_1 axis may not be constant. As result of this, the pressure gradient components $p_{,2}$ and $p_{,3}$ may not be zero. The following two cases are discussed.

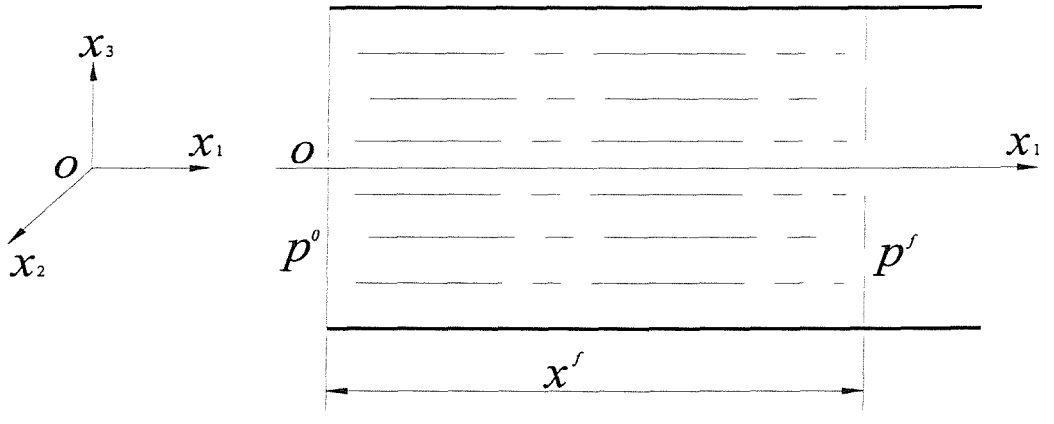

Figure 4.1: One-dimensional flow in a horizontal direction x_1.

The flow along a horizontal direction x_1

(i) x_1 *is a principal direction*

In this case (see Figure 4.1), it is assumed that the x_1 direction is a principal direction of the porous medium. The pressure gradient component $p_{,1}$ will not produce any flow in the section perpendicular to the x_1 axis. The equation (4.1)

takes the form

$$-\frac{1}{\mu}\begin{bmatrix} k_{11} & 0 & 0 \\ 0 & k_{22} & k_{23} \\ 0 & k_{32} & k_{33} \end{bmatrix}\begin{bmatrix} p_{,1} \\ p_{,2} \\ p_{,3}+\rho g \end{bmatrix} = \begin{bmatrix} q_1 \\ 0 \\ 0 \end{bmatrix}, \tag{4.8}$$

which gives that the flow in x_1 direction is independent of the permeability parameters on the $O - x_2x_3$ plane perpendicular to the x_1 direction, i.e.

$$q_1 = -\frac{k_{11}}{\mu}p_{,1}. \tag{4.9}$$

Therefore, equation (4.7) reduces to $p_{,11} = 0$ which combined with the corresponding boundary conditions gives the following equations to describe this one-dimensional resin flow along a principal direction x_1 of the porous medium, i.e.

$$\frac{d^2p}{dx_1^2} = 0, \tag{4.10}$$

$$p = p^0, \qquad x_1 = x^0, \tag{4.11}$$

$$p = p^f, \qquad x_1 = x^f, \tag{4.12}$$

where p^0 and p^f represent the injection pressure at the resin injection end $x_1 = 0$ and the pressure on the flow front $x_1 = x^f$. Both of these two pressures are prescribed time functions. The solution of this problem is,

$$p = \frac{p^f(x_1 - x^0) - p^0(x_1 - x^f)}{x^f - x^0}, \tag{4.13}$$

from which it follows that,

$$\frac{dp}{dx_1} = \frac{p^f - p^0}{x^f - x^0}. \tag{4.14}$$

Substituting this equation into equation (4.9), therefore,

$$q_1 = -\frac{k_{11}}{\mu}\frac{p^f - p^0}{x^f - x^0}. \tag{4.15}$$

Because of the flow velocity $q_1(x^f)$ at the front of flow at $x_1 = x^f$ is,

$$q_1(x^f) = \varepsilon\frac{dx^f}{dt}, \tag{4.16}$$

and therefore,

$$\varepsilon\frac{dx^f}{dt} = -\frac{k_{11}}{\mu}\frac{p^f - p^0}{x^f - x^0}. \tag{4.17}$$

Integrating this equation, to obtain,

$$\frac{\varepsilon(x^f - x^0)^2}{2} = -\frac{k_{11}}{\mu}\int_0^t (p^f - p^0)dt, \tag{4.18}$$

and,

$$k_{11} = -\frac{\varepsilon\mu(x^f - x^0)^2}{2\int_0^t (p^f - p^0)dt}. \tag{4.19}$$

In this solution, the injection pressure p^0 is not required to be a constant as required by current references (for example, Rudd, Long, Kendall and Mangin 1997)

(ii) x_1 *is an arbitrary direction*

In this case, as the direction x_1 is an arbitrary direction, the pressure gradient component $p_{,1}$ will produce flows on the section perpendicular to the x_1 axis and the flow q_1 in x_1 direction is dependent of the permeability parameters on the $O - x_2x_3$ plane perpendicular to the x_1 direction. The relationship between the flow q_1 and the pressure gradient $J_1 = p_{,1}$ takes the form described in equation (3.44) by using the one-dimensional effective permeability, that is

$$q_1 = -\frac{1}{\mu}\tilde{k}_{11}p_{,1}, \tag{4.20}$$

where $\tilde{k}_{11}$ denotes the effective permeability along the x_1 direction given in equation (3.45).

For this case, equations (4.10-14) and (4.16) remain valid. By using a similar way as in the case of the flow along a principal direction x_1 to solve equations (4.10-14), (4.16) and (4.20), to obtain,

$$q_1 = -\frac{\tilde{k}_{11}}{\mu}\frac{p^f - p^0}{x^f - x^0}, \tag{4.21}$$

$$\varepsilon\frac{dx^f}{dt} = -\frac{\tilde{k}_{11}}{\mu}\frac{p^f - p^0}{x^f - x^0}, \tag{4.22}$$

$$\frac{\varepsilon(x^f - x^0)^2}{2} = -\frac{\tilde{k}_{11}}{\mu}\int_0^t (p^f - p^0)dt, \tag{4.23}$$

and

$$\tilde{k}_{11} = -\frac{\varepsilon\mu(x^f - x^0)^2}{2\int_0^t (p^f - p^0)dt}. \tag{4.24}$$

The flow along a vertical direction x_3

As shown in Figure 4.2, for the flow along a vertical direction x_3, the gravitational effect have to be considered. By using the similar mathematical method used in the study of the flow along a horizontal direction x_1 described above, the following results are obtained.

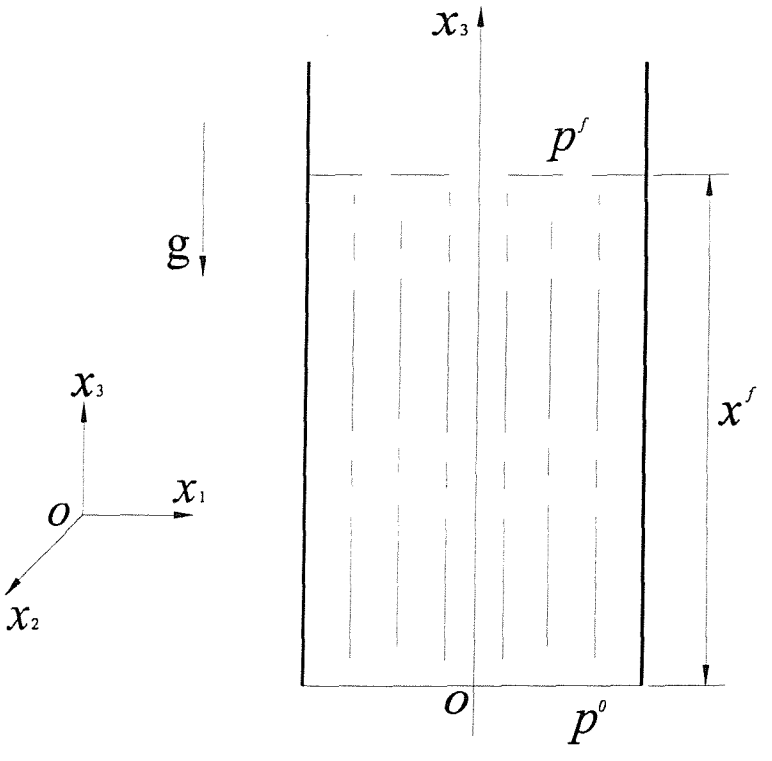

Figure 4.2: One-dimensional flow in a vertical direction x_3.

(i) *x_3 is a principal direction*

In this case, it is assumed that the x_3 direction is a principal direction of the porous medium. The pressure gradient component $p_{,3} + \rho g$ will not produce any flow on the section perpendicular to the x_3 axis. Then equation (4.1) takes the form

$$-\frac{1}{\mu}\begin{bmatrix} k_{11} & k_{12} & 0 \\ k_{21} & k_{22} & 0 \\ 0 & 0 & k_{33} \end{bmatrix}\begin{bmatrix} p_{,1} \\ p_{,2} \\ p_{,3}+\rho g \end{bmatrix} = \begin{bmatrix} 0 \\ 0 \\ q_3 \end{bmatrix}, \tag{4.25}$$

which gives that the flow in x_3 direction independent of the permeability parameters on the $O - x_1x_2$ plane perpendicular to the x_3 direction, i.e.

$$q_3 = -\frac{k_{33}}{\mu}(p_{,3} + \rho g). \tag{4.26}$$

Therefore, equation (4.7) reduces to $p_{,33} = 0$ which combined with the corresponding boundary conditions gives the following equations to describe this one-dimensional resin flow along a vertical principal direction x_3 of the porous medium, i.e.

$$\frac{d^2p}{dx_3^2} = 0, \tag{4.27}$$

$$p = p^0, \qquad x_3 = x^0, \tag{4.28}$$

$$p = p^f, \qquad x_3 = x^f, \tag{4.29}$$

where p^0 and p^f represent the injection pressure at resin injection end $x_3 = x^0$ and the pressure on the flow front $x_3 = x^f$. Both of these two pressures are prescribed time functions. The solution of this problem is,

$$p = \frac{p^f(x_3 - x^0) - p^0(x_3 - x^f)}{x^f - x^0}, \tag{4.30}$$

from which it follows that,

$$\frac{dp}{dx_3} = \frac{p^f - p^0}{x^f - x^0}. \tag{4.31}$$

Substituting this equation into equation (4.26), it is obtained that,

$$q_3 = -\frac{k_{11}}{\mu}(\frac{p^f - p^0}{x^f - x^0} + \rho g). \tag{4.32}$$

Because of the flow velocity $q_3(x^f)$ at the front of flow at $x_3 = x^f$ is,

$$q_3(x^f) = \varepsilon\frac{dx^f}{dt}, \tag{4.33}$$

and therefore

$$\varepsilon\frac{dx^f}{dt} = -\frac{k_{33}}{\mu}(\frac{p^f - p^0}{x^f - x^0} + \rho g). \tag{4.34}$$

Integrating this equation, it gives,

$$\frac{\varepsilon(x^f - x^0)^2}{2} = -\frac{k_{33}}{\mu}\{\int_0^t (p^f - p^0)dt + \int_0^t \rho g[x^f(t) - x^0]dt\}, \tag{4.35}$$

and

$$k_{33} = -\frac{\varepsilon\mu(x^f - x^0)^2}{2[\int_0^t (p^f - p^0)dt + \int_0^t \rho g[x^f(t) - x^0]dt]}. \tag{4.36}$$

Here, the integral $\int_0^t \rho g[x^f(t) - x^0]dt$ in the above equations represents the gravitational effect. Recording the time histories of the injection pressure $p^0(t)$ and the flow front $x^f(t)$ from the $t = 0$ to the final time t of an experiment will give us the permeability k_{33} by using equation (4.36).

(ii) x_3 *is an arbitrary direction*

As the direction x_3 is an arbitrary direction, the pressure gradient component $p_{,3} + \rho g$ will produce flows on the section perpendicular to the x_3 axis and the flow q_3 in x_3 direction is dependent of the permeability parameters on the $O-x_1x_2$ plane perpendicular to the x_3 direction. The Darcy's law in equation (4.26) is replaced by equation (3.47) in association with $J_3 = p_{,3} + \rho g$, i.e.

$$q_3 = -\frac{1}{\mu}\tilde{k}_{33}(p_{,3} + \rho g), \tag{4.37}$$

where $\tilde{k}_{33}$ denotes the effective permeability along the x_3 direction given in equation (3.47).

By using a similar way as in the case of the flow along an arbitrary direction x_1, to give,

$$q_3 = -\frac{\tilde{k}_{33}}{\mu}(\frac{p^f - p^0}{x^f - x^0} + \rho g), \tag{4.38}$$

$$\varepsilon\frac{dx^f}{dt} = -\frac{\tilde{k}_{33}}{\mu}(\frac{p^f - p^0}{x^f - x^0} + \rho g), \tag{4.39}$$

$$\frac{\varepsilon(x^f - x^0)^2}{2} = -\frac{\tilde{k}_{33}}{\mu}\{\int_0^t (p^f - p^0)dt + \int_0^t \rho g[x^f(t) - x^0]dt\}, \tag{4.40}$$

and

$$\tilde{k}_{33} = -\frac{\varepsilon\mu(x^f - x^0)^2}{2\{\int_0^t (p^f - p^0)dt + \int_0^t \rho g[x^f(t) - x^0]dt\}}. \tag{4.41}$$

4.2.2 Two-dimensional radial flows in isotropic and anisotropic media

A two-dimensional flow is a plane flow as shown in Figure 3.2. In this case, because the two plates are assumed to be non-permeable, the flow velocity q_3 on the two plate surfaces vanishes. The two-dimensional effective permeability and the corresponding Darcy's law are represented by equations (3.57) and (3.58).

Here some analytical solutions of the radial flows in both isotropic and anisotropic media are discussed as follows.

Radial flow of isotropic media in a horizontal plane

For an isotropic medium, any direction in it is its principal direction of the permeability tensor of the medium. As result of this, any plane across the medium is a principal plane of the permeability tensor of the medium. Then Darcy's law now takes the form

$$\begin{bmatrix} q_1 \\ q_2 \end{bmatrix} = -\frac{1}{\mu} \begin{bmatrix} k & 0 \\ 0 & k \end{bmatrix} \begin{bmatrix} p_{,1} \\ p_{,2} \end{bmatrix}, \tag{4.42}$$

which is substituted into equation (4.7) gives the two-dimensional Laplace equation,

$$p_{,11} + p_{,22} = 0. \tag{4.43}$$

As shown in Figure 4.3 (a), the two-dimensional radial flow in isotropic media is an two-dimensional center-symmetrical flow, in which the pressure p and the front of flow is a function of the polar coordinate r, and therefore the front of flow is a circle as shown in Figure 4.3 (b). In this polar coordinate system, the Laplace equation given in equation (4.43) and the Darcy's law in equation (4.42) take the form,

$$\frac{1}{r}\frac{d}{dr}(r\frac{dp}{dr}) = 0, \tag{4.44}$$

$$q_r = -\frac{k}{\mu}\frac{dp}{dr}. \tag{4.45}$$

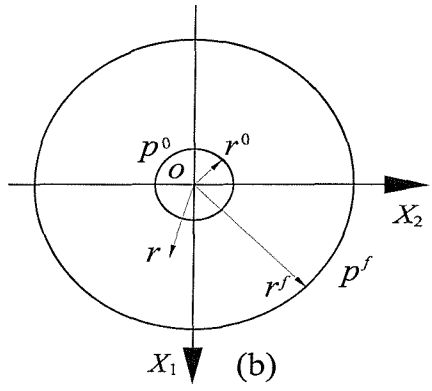

Figure 4.3: A two-dimensional radial flow in a horizontal plane $O - X_1X_2$ filled with isotropic media.

The boundary conditions for this radial flow have the following forms,

$$p = p^0, \qquad r = r^0, \tag{4.46}$$

$$p = p^f, \qquad r = r^f, \tag{4.47}$$

where p^0 and p^f represents the injection pressure and the flow front pressure, respectively. These pressures may be prescribed functions of the time t.

An integration of equation (4.44) and using the boundary conditions describing in equations (4.46) and (4.47) give a solution of this radial flow,

$$p(r) = \frac{p^f - p^0}{\ln \frac{r^f}{r^0}} \ln \frac{r}{r^0} + p^0, \tag{4.48}$$

and from this solution it follows that,

$$\frac{dp}{dr}(r) = \frac{p^f - p^0}{\ln(\frac{r^f}{r^0})} \frac{1}{r}, \tag{4.49}$$

$$\frac{dp}{dr}(r^f) = \frac{p^f - p^0}{\ln(\frac{r^f}{r^0})} \frac{1}{r^f}. \tag{4.50}$$

Substituting this result into equation (4.45), to give,

$$q_r(r^f) = -\frac{k^r}{\mu} \frac{p^f - p^0}{\ln \frac{r^f}{r^0}} \frac{1}{r^f}, \tag{4.51}$$

where $k^r = k$ is introduced for a notation convenience. Because the flow velocity $q_r(r^f)$ at the front of flow at $r = r^f$ is,

$$q_r(r^f) = \varepsilon \frac{dr^f}{dt}, \tag{4.52}$$

and therefore,

$$\varepsilon \frac{dr^f}{dt} = -\frac{k^r}{\mu} \frac{p^f - p^0}{\ln \frac{r^f}{r^0}} \frac{1}{r^f}, \tag{4.53}$$

from which it follows that,

$$r^f \ln \frac{r^f}{r^0} dr^f = -\frac{k^r}{\varepsilon \mu}(p^f - p^0)dt, \tag{4.54}$$

Integrating this equation, to obtain,

$$\int_{r^0}^{r^f} r^f \ln \frac{r^f}{r^0} dr^f = -\frac{k^r}{\varepsilon \mu} \int_0^t (p^f - p^0)dt, \tag{4.55}$$

which gives that

$$k^r = -[{r^f}^2(2 \ln \frac{r^f}{r^0} - 1) + {r^0}^2] \frac{\varepsilon \mu}{4 \int_0^t (p^f - p^0)dt}. \tag{4.56}$$

This equation will be used to calculate the permeabilities in the experiment.

Radial flow of isotropic media in a vertical plane

For a general case considering the gravitational effect, the flow plane is assumed in $O - X_1X_2$ plane (see Figure 4.4). In this case, the Darcy's law takes the form

$$\begin{bmatrix} q_1 \\ q_2 \end{bmatrix} = -\frac{1}{\mu} \begin{bmatrix} k & 0 \\ 0 & k \end{bmatrix} \begin{bmatrix} p_{,1} \\ p_{,2} + \rho g \end{bmatrix}, \tag{4.57}$$

which is substituted into equation (4.7) gives the two-dimensional Laplace equation

$$p_{,11} + p_{,22} = 0. \tag{4.58}$$

Figure 4.4 shows the two-dimensional radial flow in a vertical plane of isotropic media. From equation (4.57), it follows that the flow caused by the gravity is a constant $q_2^g = -\frac{k}{\mu}\rho g$ at every point in the media. The wet area of the media

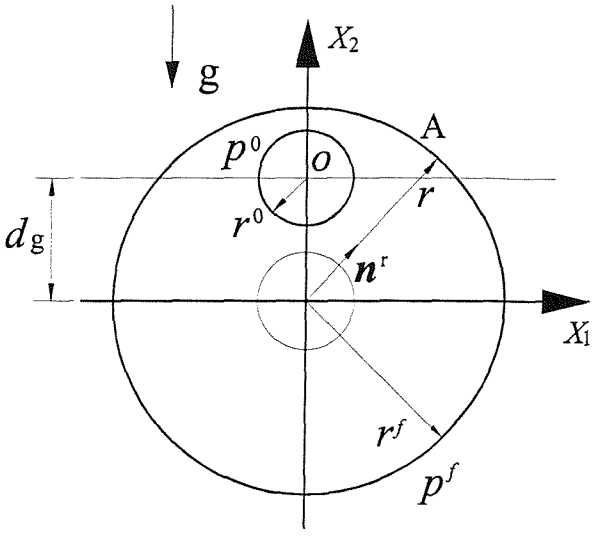

Figure 4.4: A two-dimensional radial flow in a vertical plane $O - X_1X_2$ filled with isotropic media.

moves a distance $d_g = \frac{k}{\varepsilon\mu}\rho g t$. Following the principle of superposition for linear systems, the solution of the radial flow of the isotropic in a vertical plane can be obtained by the summation of the radial flow solution in a horizontal plane produced by the injection pressure p^0 and the flow q_2^g caused by the gravity. The pressure p and the front of flow is a function of the polar coordinate r, and the front of flow is also a circle, but the center of this circle has a translation d_g. If a moving coordinate system $O - X_1X_2$ with the constant velocity is used as shown Figure 4.4, the flow rate at a point A on the flow front equals to,

$$\boldsymbol{q}_A = -\frac{k}{\mu}\frac{dp}{dr}\boldsymbol{n}^r + q_2^g\boldsymbol{n}^{(2)}, \tag{4.59}$$

where $\boldsymbol{n}^{(2)}$ represents a unit vector along X_2 direction. Under this moving system, the radial flow described by equations (4.44) - (4.56) is also valid. Therefore, the gravitational effect on the permeability measurement can be eliminated by using this moving system.

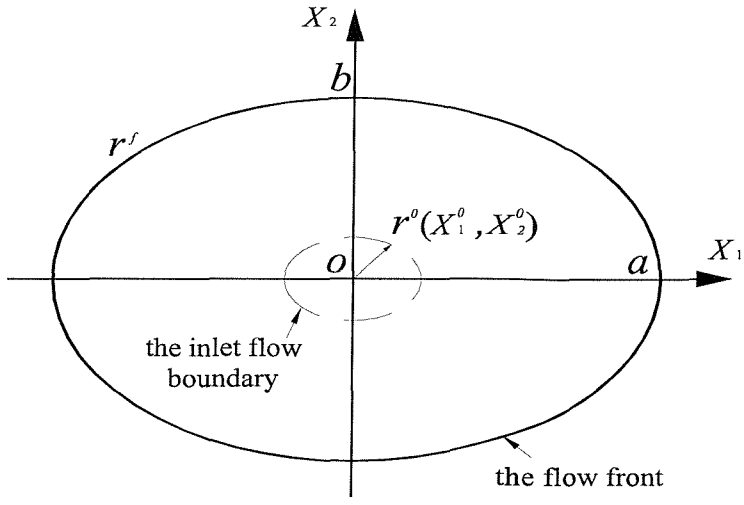

Figure 4.5: The flow front of anisotropic media in horizontal plane $O - X_1X_2$.

Radial flow of anisotropic media in a horizontal plane

As shown in Figure 4.5, it is assumed that the horizontal flow plane $O - X_1X_2$ is a principal plane of an anisotropic medium and the axes X_1 and X_2 are its two principal axes with their principal permeabilities $k^{(1)}$ and $k^{(2)}$, respectively. According to this assumption, Darcy's law takes the form,

$$q_1 = -\frac{k^{(1)}}{\mu}\frac{\partial p}{\partial x_1}, \tag{4.60}$$

$$q_2 = -\frac{k^{(2)}}{\mu}\frac{\partial p}{\partial x_2}, \tag{4.61}$$

which is substituted into equation (4.7) gives the equation,

$$k^{(1)}\frac{\partial^2 p}{\partial x_1^2} + k^{(2)}\frac{\partial^2 p}{\partial x_2^2} = 0. \tag{4.62}$$

In order to transform this equation into a standard Laplace's equation, the following coordinate transformation,

$$\overline{x}_1 = \frac{x_1}{\sqrt{k^{(1)}}} \tag{4.63}$$

$$\overline{x}_2 = \frac{x_2}{\sqrt{k^{(2)}}} \tag{4.64}$$

is introduced. As it is indicated in section 2.2, the dimension of the permeabilities $k^{(1)}$ and $k^{(2)}$ is square meter. Therefore, this transformation represents that the

two different 'rulers', $k^{(1)}$ and $k^{(2)}$, are used to measure the lengths along the x_1 and x_2 direction, respectively. Obviously, both of the coordinates $\overline{x}_1$ and $\overline{x}_2$ are non-dimensional. From this transformation, it follows that,

$$\frac{\partial p}{\partial x_1} = \frac{1}{\sqrt{k^{(1)}}}\frac{\partial p}{\partial \overline{x}_1}, \qquad \frac{\partial^2 p}{\partial x_1^2} = \frac{1}{k^{(1)}}\frac{\partial^2 p}{\partial \overline{x}_1^2}, \tag{4.65}$$

$$\frac{\partial p}{\partial x_2} = \frac{1}{\sqrt{k^{(2)}}}\frac{\partial p}{\partial \overline{x}_2}, \qquad \frac{\partial^2 p}{\partial x_2^2} = \frac{1}{k^{(2)}}\frac{\partial^2 p}{\partial \overline{x}_2^2}. \tag{4.66}$$

A substitution of these equations (4.65) and (4.66) into equations (4.60), (4.61) associated with using the coordinate transformation rule for a vector q_i given in Chapter 3 and (4.62) gives,

$$\overline{q}_1 = \frac{q_1}{\sqrt{k^{(1)}}} = -\frac{1}{\mu}\frac{\partial p}{\partial \overline{x}_1}, \tag{4.67}$$

$$\overline{q}_2 = \frac{q_2}{\sqrt{k^{(2)}}} = -\frac{1}{\mu}\frac{\partial p}{\partial \overline{x}_2}, \tag{4.68}$$

$$\overline{q}_{\overline{r}} = \beta_{\overline{r}i}\overline{q}_i = -\frac{1}{\mu}\frac{\partial p}{\partial \overline{r}}, \tag{4.69}$$

and

$$\frac{\partial^2 p}{\partial \overline{x}_1^2} + \frac{\partial^2 p}{\partial \overline{x}_2^2} = 0 \tag{4.70}$$

which describe a quasi-isotropic system. In this quasi-isotropic system, the flow rate $\overline{q}$ has dimensions of s^{-1} and the permeability $\overline{k}$ is non-dimensional with a constant value 1 for all anisotropic medium. The pressure p has its normal dimension Nm^{-2}.

Under a polar coordinate system, a quasi-isotropic radial flow in anisotropic media can be defined as follows,

$$\frac{1}{\overline{r}}\frac{d}{d\overline{r}}\left(\overline{r}\frac{dp}{d\overline{r}}\right) = 0, \tag{4.71}$$

$$p = p^0, \qquad \overline{r} = \overline{r}^0, \tag{4.72}$$

$$p = p^f, \qquad \overline{r} = \overline{r}^f, \tag{4.73}$$

where

$$\overline{r} = \sqrt{\overline{x}_1^2 + \overline{x}_2^2},$$

$$\begin{aligned} \overline{r}^f &= \sqrt{\overline{x}_1^{f\,2} + \overline{x}_2^{f\,2}}, \\ \overline{r}^0 &= \sqrt{\overline{x}_1^{0\,2} + \overline{x}_2^{0\,2}}. \end{aligned} \tag{4.74}$$

A comparison between equations (4.44), (4.46), (4.47) and (4.71-73) can give the solution of equations (4.71-73) as,

$$p(\overline{r}) = \frac{p^f - p^0}{\ln \frac{\overline{r}^f}{\overline{r}^0}} \ln \frac{\overline{r}}{\overline{r}^0} + p^0. \tag{4.75}$$

Using same mathematical process as for equations (4.51) and (4.56), it gives,

$$\overline{q}_{\overline{r}}(\overline{r}^f) = -\frac{\overline{k}^r}{\mu} \frac{p^f - p^0}{\ln \frac{\overline{r}^f}{\overline{r}^0}} \frac{1}{\overline{r}^f}, \tag{4.76}$$

and

$$\overline{k}^r = -[\overline{r}^{f\,2}(2 \ln \frac{\overline{r}^f}{\overline{r}^0} - 1) + \overline{r}^{0\,2}] \frac{\varepsilon\mu}{4 \int_0^t (p^f - p^0) dt} = \overline{k} = 1, \tag{4.77}$$

in which $\overline{k}^r = 1$ is obtained from equation (4.69). From equation (4.74), it follows that,

$$\overline{r}^f = \sqrt{\overline{x}_1^{f\,2} + \overline{x}_2^{f\,2}}, \tag{4.78}$$

and

$$\overline{r}^0 = \sqrt{\overline{x}_1^{0\,2} + \overline{x}_2^{0\,2}}, \tag{4.79}$$

which can further be rewritten as,

$$\frac{x_1^{f\,2}}{k^{(1)} \overline{r}^{f\,2}} + \frac{x_2^{f\,2}}{k^{(2)} \overline{r}^{f\,2}} = 1 \tag{4.80}$$

and

$$\frac{x_1^{0\,2}}{k^{(1)} \overline{r}^{0\,2}} + \frac{x_2^{0\,2}}{k^{(2)} \overline{r}^{0\,2}} = 1. \tag{4.81}$$

Equation (4.80) represent that the flow front an ellipse with semiaxes $\sqrt{k^{(1)}} \overline{r}^f$ and $\sqrt{k^{(2)}} \overline{r}^f$, as shown in Figure 4.5. The inlet flow boundary is another ellipse with the semiaxes $\sqrt{k^{(1)}} \overline{r}^0$ and $\sqrt{k^{(2)}} \overline{r}^0$ described by equation (4.81).

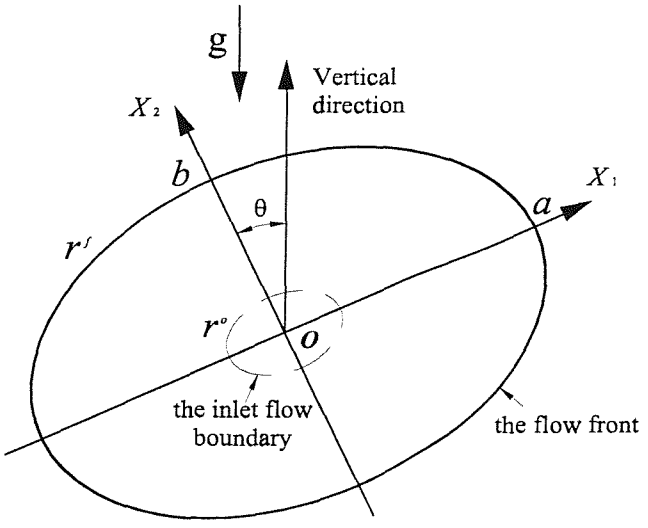

Figure 4.6: The flow front of anisotropic media in vertical plane $O - X_1X_2$.

Radial flow of anisotropic media in a vertical plane

As shown in Figure 4.6, it is assumed that the vertical flow plane $O - X_1X_2$ is a principal plane of an anisotropic medium and the axes X_1 and X_2 are its two principal axes with their principal permeabilities $k^{(1)}$ and $k^{(2)}$, respectively. According to this assumption, Darcy's law takes the form,

$$q_1 = -\frac{k^{(1)}}{\mu}(\frac{\partial p}{\partial x_1} + \rho g \beta_1^g), \tag{4.82}$$

$$q_2 = -\frac{k^{(2)}}{\mu}(\frac{\partial p}{\partial x_2} + \rho g \beta_2^g). \tag{4.83}$$

The flow rate caused by gravity can be represented as

$$\boldsymbol{q}^g = -\frac{k^{(1)}}{\mu}\rho g \beta_1^g \boldsymbol{n}^{(1)} - \frac{k^{(2)}}{\mu}\rho g \beta_2^g \boldsymbol{n}^{(2)}, \tag{4.84}$$

which is a constant vector at every point in the media. Therefore, the wet area in this radial flow of anisotropic media in a vertical plane moves a distance $\boldsymbol{q}^g t/\varepsilon$ along the $\boldsymbol{q}^g$ direction. For anisotropic cases, the $\boldsymbol{q}^g$ may not take the direction of the gravitational acceleration.

In a similar way as in the isotropic case, an application of the moving coordi-

nate system gives a convenience to measure the permeability but avoiding the effect of the gravity.

4.2.3 Three-dimensional radial flows in isotropic and anisotropic media

Substituting equation (4.1) into equation (4.7), the equation satisfied by the pressure in a three-dimensional flow in RTM, is

$$k_{ij}p_{,ji} = 0. \tag{4.85}$$

For isotropic media, $k_{ij} = k\delta_{ij}$, this equation reduces to Laplace's equation in three-dimensional space,

$$p_{,jj} = 0. \tag{4.86}$$

For anisotropic media, if the principal axis reference system is used, the permeability k_{ij} takes its form as shown in equation (3.37) or (3.30). As result of this, under the principal axis system, equation (4.85) takes the following simplest form

$$k^{(1)}p_{,11} + k^{(2)}p_{,22} + k^{(3)}p_{,33} = 0. \tag{4.87}$$

Radial flows in isotropic media

As shown in Figure 4.7, Darcy's law in equation (4.1) can be represented in the form,

$$q_i = -\frac{k^r}{\mu}(\frac{\partial p}{\partial x_i} + \rho g\delta_{i3}), \tag{4.88}$$

$$= -\frac{k^r}{\mu}\frac{\partial p}{\partial x_i} + q_i^g, \tag{4.89}$$

where $q_i^g = -\frac{k}{\mu}\rho g\delta_{i3}$, which represents the flow rates caused by gravity. The flow takes the direction of gravity. The effect of the gravity can be eliminated by considering the translation the wet volume along the gravitational direction,

$$\boldsymbol{q}^g = -\frac{k^r}{\mu}\rho g\boldsymbol{n}^{(3)}. \tag{4.90}$$

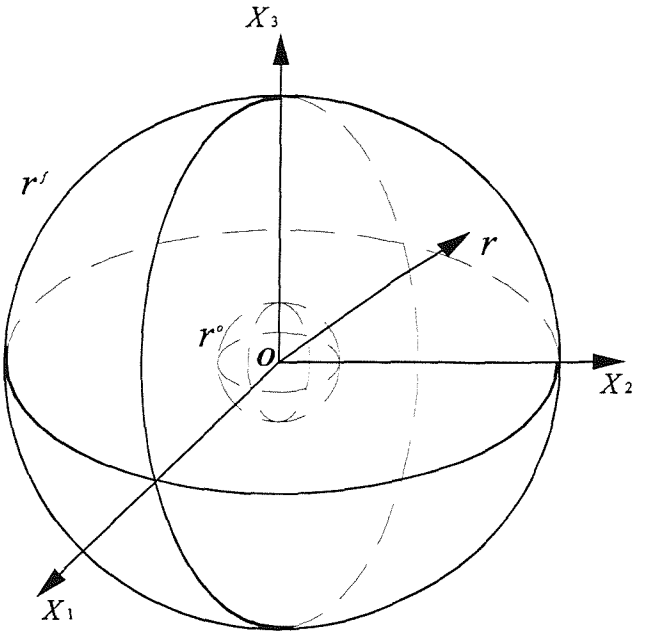

Figure 4.7: Three-dimensional radial flows in isotropic media.

A three-dimensional radial flow without effect of the gravity is a center symmetrical flow in which the pressure p is a function of a spherical polar coordinate r and the front of the flow is a sphere about the injection center. Under the spherical polar coordinate system, equation (4.86) has the form

$$\frac{1}{r^2}\frac{d}{dr}(r^2\frac{dp}{dr}) = 0. \tag{4.91}$$

The boundary conditions for this radial flow are represented by,

$$p = p^0, \qquad r = r^0, \tag{4.92}$$

$$p = p^f, \qquad r = r^f. \tag{4.93}$$

Integrating equations (4.91-93), it gives,

$$p(r) = -\frac{r^0 r^f (p^f - p^0)}{r(r^f - r^0)} + \frac{p^f r^f - p^0 r^0}{r^f - r^0}, \tag{4.94}$$

which gives its derivative with respect to r as

$$\frac{\partial p}{\partial r}(r) = \frac{r^0 r^f (p^f - p^0)}{r^2(r^f - r^0)}, \tag{4.95}$$

and

$$\frac{\partial p}{\partial r}(r^f) = \frac{r^0(p^f - p^0)}{r^f(r^f - r^0)}. \tag{4.96}$$

Substituting this result into Darcy's law for isotropic media represented in equation (4.89) and using the coordinate transformation rule described in section 3.1, to give,

$$\begin{aligned} q_r(r^f) &= \beta_{ri} q_i \\ &= -\frac{k^r}{\mu}\frac{\partial p}{\partial r} \\ &= -\frac{k^r}{\mu}\frac{r^0(p^f - p^0)}{r^f(r^f - r^0)}, \end{aligned} \tag{4.97}$$

where $k^r = k$. For the same reason as in a two-dimensional radial flows, equation (4.52) is valid for a three-dimensional radial flows, and therefore,

$$\varepsilon\frac{dr^f}{dt} = -\frac{k^r}{\mu}\frac{r^0(p^f - p^0)}{r^f(r^f - r^0)}, \tag{4.98}$$

from which it follows that,

$$r^f(r^f - r^0)dr^f = -\frac{k^r}{\mu\varepsilon}r^0(p^f - p^0)dt. \tag{4.99}$$

Integrating this equation, to obtain

$$\int_{r_0}^{r^f} r^f(r^f - r^0)dr^f = -\frac{k^r}{\mu\varepsilon}\int_0^t r^0(p^f - p^0)dt, \tag{4.100}$$

which gives,

$$k^r = -\frac{\mu\varepsilon(\frac{1}{3}r^{f3} - \frac{1}{2}r^0 r^{f2} + \frac{1}{6}r^{03})}{r^0\int_0^t(p^f - p^0)dt}. \tag{4.101}$$

Radial flows in anisotropic media

For this case, as shown in Figure 4.8, it is convenient to use the principal axis system under which the permeability tensor takes a simpler form as described in equation (3.37). The Darcy's law can be represented as,

$$q_i = -\frac{k^{(i)}}{\mu}(\frac{\partial p}{\partial x_i} + \rho g\beta_i^g), \tag{4.102}$$

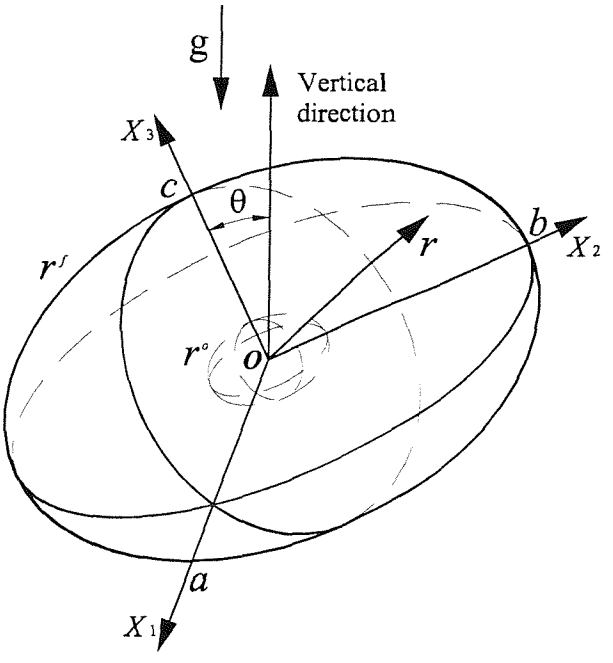

Figure 4.8: Three-dimensional radial flows in anisotropic media.

where β_i^g represents the directional cosine of the negative gravity direction. The flow rate caused by the gravity is a constant vector,

$$\boldsymbol{q}^g = -\frac{1}{\mu}(k^{(1)}\beta_1^g \boldsymbol{n}^{(1)} + k^{(2)}\beta_2^g \boldsymbol{n}^{(2)} + k^{(3)}\beta_3^g \boldsymbol{n}^{(3)}), \tag{4.103}$$

at every points in the media. This constant flow causes the wet volume of the media to move a distance $\boldsymbol{q}^g t/\varepsilon$.

The equation satisfied by the radial flow pressure p takes the form,

$$k^{(1)}\frac{\partial^2 p}{\partial x_1^2} + k^{(2)}\frac{\partial^2 p}{\partial x_2^2} + k^{(3)}\frac{\partial^2 p}{\partial x_3^2} = 0 \tag{4.104}$$

An application of the following coordinate transformation,

$$\overline{x}_i = \frac{x_i}{\sqrt{k^{(i)}}}, \tag{4.105}$$

transform equation (4.87) to a standard Laplace's equation,

$$\frac{\partial^2 p}{\partial \overline{x}_1^2} + \frac{\partial^2 p}{\partial \overline{x}_2^2} + \frac{\partial^2 p}{\partial \overline{x}_3^2} = 0, \tag{4.106}$$

which describes a quasi-isotropic system. Under a spherical polar coordinate system, a quasi-isotropic radial flow in anisotropic media can be defined as follows

$$\begin{aligned} &\frac{1}{\overline{r}^2}\frac{d}{d\overline{r}}(\overline{r}^2\frac{dp}{d\overline{r}}) = 0, \\ &p = p^0, \qquad \overline{r} = \overline{r}^0, \\ &p = p^f, \qquad \overline{r} = \overline{r}^f, \end{aligned} \tag{4.107}$$

where

$$\begin{aligned} \overline{r} &= \sqrt{\overline{x}_j\overline{x}_j}, \\ \overline{r}^f &= \sqrt{\overline{x}_j^f\overline{x}_j^f}, \\ \overline{r}^0 &= \sqrt{\overline{x}_j^0\overline{x}_j^0}. \end{aligned} \tag{4.108}$$

A comparison between equations (4.91-95) and (4.107) can give the solution of equations (4.107) as,

$$p(\overline{r}) = -\frac{\overline{r}^0\overline{r}^f(p^f - p^0)}{\overline{r}(\overline{r}^f - \overline{r}^0)} + \frac{p^f\overline{r}^f - p^0\overline{r}^0}{\overline{r}^f - \overline{r}^0}. \tag{4.109}$$

The flow rates q_i under this principal axis system can be obtained by using equations (4.1) and (3.37) as well as the transformation rule for tensor described in section 3.2, that is,

$$\begin{aligned} q_i &= -\frac{k^{(i)}}{\mu}\frac{\partial p}{\partial x_i} \\ &= -\frac{k^{(i)}}{\mu}\frac{\partial p}{\partial \overline{r}}\frac{\partial \overline{r}}{\partial \overline{x}_j}\frac{\partial \overline{x}_j}{\partial x_i}, \end{aligned} \tag{4.110}$$

From equations (4.105) and (4.108), it follows that

$$\begin{aligned} \frac{\partial \overline{r}}{\partial \overline{x}_j} &= \frac{\overline{x}_j}{\overline{r}} = \beta_{\overline{r}j}, \\ \frac{\partial \overline{x}_j}{\partial x_i} &= \delta_{ij}/\sqrt{k^{(i)}}, \end{aligned} \tag{4.111}$$

which are substituted into equation (4.110) to obtain,

$$\begin{aligned} \overline{q}_i &= \frac{q_i}{\sqrt{k^{(i)}}} \\ &= -\frac{1}{\mu}\frac{\partial p}{\partial \overline{r}}\beta_{\overline{r}i}, \end{aligned} \tag{4.112}$$

and,

$$\begin{aligned}\overline{q}_{\overline{r}} &= \beta_{\overline{r}i}\overline{q}_i \\ &= -\frac{1}{\mu}\frac{\partial p}{\partial \overline{r}}\beta_{\overline{r}i}\beta_{\overline{r}i} \\ &= -\frac{1}{\mu}\frac{\partial p}{\partial \overline{r}}, \end{aligned} \tag{4.113}$$

where $\beta_{\overline{r}i}\beta_{\overline{r}i} = 1$ has been introduced. From equations (4.109) and (4.113),

$$\overline{q}_{\overline{r}}(\overline{r}^f) = -\frac{\overline{k}^r}{\mu}\frac{\overline{r}^0(p^f - p^0)}{\overline{r}^f(\overline{r}^f - \overline{r}^0)}, \tag{4.114}$$

$$\varepsilon\frac{d\overline{r}^f}{dt} = -\frac{\overline{k}^r}{\mu}\frac{\overline{r}^0(p^f - p^0)}{\overline{r}^f(\overline{r}^f - \overline{r}^0)}, \tag{4.115}$$

$$\overline{k}^r = -\frac{\mu\varepsilon(\frac{1}{3}\overline{r}^{f3} - \frac{1}{2}\overline{r}^0\overline{r}^{f2} + \frac{1}{6}\overline{r}^{03})}{\overline{r}^0\int_0^t(p^f - p^0)dt} = 1. \tag{4.116}$$

From equations (4.105) and (4.108), it is obtained the following two ellipsoid equations,

$$\frac{x_1^{f2}}{k^{(1)}\overline{r}^{f2}} + \frac{x_2^{f2}}{k^{(2)}\overline{r}^{f2}} + \frac{x_3^{f2}}{k^{(3)}\overline{r}^{f2}} = 1, \tag{4.117}$$

and,

$$\frac{x_1^{02}}{k^{(1)}\overline{r}^{02}} + \frac{x_2^{02}}{k^{(2)}\overline{r}^{02}} + \frac{x_3^{02}}{k^{(3)}\overline{r}^{02}} = 1, \tag{4.118}$$

which describe the flow front and the inlet flow boundary, respectively.

4.3 Injection velocity is given

In this section some analytical solutions for the case in which the injection velocity $q_i^0(t)$ is given are developed.

4.3.1 One-dimensional channel flows in isotropic and anisotropic media

As shown in Figure 4.1, one-dimensional flow with the injection velocity q^0 at the injection end is considered. If S denotes the section area of a flow channel, the injection volume rate $Q = q^0 S$.

The flow along a horizontal direction x_1

(i) *x_1 is a principal direction*

It is assumed that the x_1 direction is a principal direction of the porous medium. The governing equations for this flow are as follows,

$$q_1 = -\frac{k_{11}}{\mu} p_{,1}, \tag{4.119}$$

$$\frac{dq_1}{dx_1} = 0, \tag{4.120}$$

$$q_1 = q^0, \qquad x_1 = x^0, \tag{4.121}$$

$$p = p^f, \qquad x_1 = x^f, \tag{4.122}$$

where q^0 and p^f represent the injection velocity at resin injection end $x_1 = x^0$ and the resin injection pressure on the flow front $x_1 = x^f$. In general, q^0 and p^f are time functions. The solution of this problem is,

$$q_1 = q^0, \tag{4.123}$$

$$p = p^f - \frac{\mu}{k_{11}} q^0 (x_1 - x^f). \tag{4.124}$$

From this solution it follows that,

$$p^0 = p^f - \frac{\mu}{k_{11}} q^0 (x^0 - x^f), \tag{4.125}$$

and

$$k_{11} = \frac{\mu q^0 (x^f - x^0)}{p^0 - p^f}. \tag{4.126}$$

(ii) *x_1 is an arbitrary direction*

In this case, as the direction x_1 is an arbitrary direction, the pressure gradient component $p_{,1}$ will produce flows on the section perpendicular to the x_1 axis. The governing equations of this problem are equations (4.20) and (4.120)-(4.122). The solutions of the problem are,

$$q_1 = q^0, \tag{4.127}$$

$$p = p^f - \frac{\mu}{\tilde{k}_{11}} q^0 (x - x^f), \tag{4.128}$$

$$\tilde{k}_{11} = \frac{\mu q^0 (x^f - x^0)}{p^0 - p^f}. \tag{4.129}$$

The flow along a vertical direction x_3

As shown in Figure 4.2, for the flow along a vertical direction x_3, the gravitational effect have to be considered. By using the similar mathematical method used in the study of the flow along a horizontal direction x_1 described above, to obtain the following results.

(i) *x_3 is a principal direction*

In this case, the pressure gradient component $p_{,3} + \rho g$ will not produce any flow on the section perpendicular to the x_3 axis, and hence the following governing equations of the problem,

$$q_3 = -\frac{k_{33}}{\mu}(p_{,3} + \rho g), \tag{4.130}$$

$$\frac{dq_3}{dx_3} = 0, \tag{4.131}$$

$$q_3 = q^0, \qquad x_3 = x^0, \tag{4.132}$$

$$p = p^f, \qquad x_3 = x^f. \tag{4.133}$$

The solution of this problem is,

$$q_3 = q^0, \tag{4.134}$$

$$p = p^f - (\frac{\mu q^0}{k_{33}} + \rho g)(x_3 - x^f). \tag{4.135}$$

From this solution it follows that,

$$p^0 = p^f - (\frac{\mu q^0}{k_{33}} + \rho g)(x^0 - x^f), \tag{4.136}$$

which gives that,

$$k_{33} = \frac{\mu q^0}{\frac{p^0 - p^f}{x^f - x^0} - \rho g}. \tag{4.137}$$

(ii) x_3 *is an arbitrary direction*

As the direction x_3 is an arbitrary direction, the pressure gradient component $p_{,3} + \rho g$ will produce flows on the section perpendicular to the x_3 axis. The equation (4.130) is replaced by,

$$q_3 = -\frac{1}{\mu}\tilde{k}_{33}(p_{,3} + \rho g), \tag{4.138}$$

and the solution of the problem is given by equations (4.135) - (4.138) associated with k_{33} replacing $\tilde{k}_{33}$. Hence the effective permeability is,

$$\tilde{k}_{33} = \frac{\mu q^0}{\frac{p^0 - p^f}{x^f - x^0} - \rho g}. \tag{4.139}$$

4.3.2 Two-dimensional radial flows in isotropic and anisotropic media

Radial flow of isotropic media in a horizontal plane

The governing equations for a radial flow in isotropic media are as follows,

$$q_r = -\frac{k^r}{\mu}\frac{dp}{dr}, \tag{4.140}$$

$$\frac{1}{r}\frac{d}{dr}(r\frac{dp}{dr}) = 0, \tag{4.141}$$

$$q_r = q^0, \qquad r = r^0, \tag{4.142}$$

$$p = p^f, \qquad r = r^f, \tag{4.143}$$

where the injection rate q^0 can be replaced by the volume injection rate Q by using equation $Q = 2\pi r^0 q^0 h$, h is the thickness of a two-dimensional radial flow layer.

The solution of these governing equations are,

$$p = p^f + \frac{r^0 q^0 \mu}{k^r} \ln \frac{r^f}{r}, \qquad q_r = q^0 r^0 / r, \tag{4.144}$$

from which it is obtained,

$$p^0 = p^f + \frac{r^0 q^0 \mu}{k^r} \ln \frac{r^f}{r^0}, \tag{4.145}$$

$$k^r = \frac{r^0 q^0 \mu}{p^0 - p^f} \ln \frac{r^f}{r^0} = \frac{Q\mu}{2\pi h(p^0 - p^f)} \ln \frac{r^f}{r^0}, \tag{4.146}$$

where h and $Q = 2\pi r^0 h q^0$ represent the thickness of the medium and the volume flow rate, respectively. This equation is same as Chan's equation (1993).

Radial flow of isotropic media in a vertical plane

The flow rate caused by gravity is,

$$q_2^g = -\frac{k}{\mu}\rho g \tag{4.147}$$

which corresponds a volume flow rate through a closed curve,

$$Q = \int_S -\frac{k}{\mu}\rho g \nu_2 dS = 0, \tag{4.148}$$

where ν_2 represents the unit vector along the outer normal to the curve S. From the equation (4.148), it follows that the volume injection rate Q for a two-dimensional radial flow through isotropic media is independent of the gravitation effect. The gravitational effect for flows through isotropic media during time period t produce a translation distance d_g of the wetted area along the gravity direction, i.e $d_g = \frac{k^r}{\varepsilon\mu}\rho g t$. The equations of radial flows relate to the moving system are same as equations (4.140) - (4.146).

Radial flow of anisotropic media in a horizontal plane

The governing equations of this problem are,

$$\overline{q}_r = -\frac{1}{\mu}\frac{\partial p}{\partial \overline{r}}, \tag{4.149}$$

$$\frac{1}{\overline{r}}\frac{d}{d\overline{r}}(\overline{r}\frac{dp}{d\overline{r}}) = 0, \tag{4.150}$$

$$\overline{q}_r = \overline{q}^0, \qquad \overline{r} = \overline{r}^0, \tag{4.151}$$

$$p = p^f, \qquad \overline{r} = \overline{r}^f, \tag{4.152}$$

where $\overline{q}_r$ and $\overline{r}$ are defined by equations (4.69) and (4.74), respectively. A comparison between equations (4.140-4.143) and (4.149-4.152) can give the solution of equations (4.149-4.152) as,

$$p = p^f + \frac{\overline{r}^0 \overline{q}^0 \mu}{k^{\overline{r}}} \ln \frac{\overline{r}^f}{\overline{r}}, \qquad \overline{q}_r = \overline{q}^0 \frac{\overline{r}^0}{\overline{r}}, \tag{4.153}$$

from which it is obtained that,

$$p^0 = p^f + \frac{\overline{r}^0 \overline{q}^0 \mu}{k^{\overline{r}}} \ln \frac{\overline{r}^f}{\overline{r}^0}, \tag{4.154}$$

$$k^{\overline{r}} = \frac{\overline{r}^0 \overline{q}^0 \mu}{p^0 - p^f} \ln \frac{\overline{r}^f}{\overline{r}^0} = 1. \tag{4.155}$$

As it has known that equations (4.149-4.152) describe a quasi-isotropic radial flow, the flow rate $\overline{q}^0$ at every point on the injection boundary $\overline{r} = \overline{r}^0$ has the same value. For example, along the two principal directions,

$$\frac{q_1^0}{\sqrt{k^{(1)}}} = \overline{q}^0 = \frac{q_2^0}{\sqrt{k^{(2)}}}. \tag{4.156}$$

Therefore, if the injection rate at a point on the injection boundary, such as q_1^0 or q_2^0, is a constant, the $\overline{q}^0$ will be the same constant. This injection rate $\overline{q}^0$ can be replaced by the quasi-volume injection rate,

$$\overline{Q} = 2\pi \overline{r}^0 \overline{q}^0 h = 2\pi \frac{x_1^0}{k^{(1)}} q_1^0 h = 2\pi \frac{x_2^0}{k^{(2)}} q_2^0 h. \tag{4.157}$$

The real volume flow rate Q is defined as (see, for example, Chick et al 1996),

$$\frac{Q}{h\varepsilon} = \pi \frac{d}{dt}(x_1^f x_2^f), \tag{4.158}$$

which can further be rewritten as,

$$\begin{aligned} \frac{Q}{h\varepsilon} &= \sqrt{k^{(1)}k^{(2)}}\pi \frac{d}{dt}(\overline{x}_1^f \overline{x}_2^f) \\ &= \sqrt{k^{(1)}k^{(2)}} \frac{d}{dt}(\pi \overline{r}^{f\,2}) \\ &= \sqrt{k^{(1)}k^{(2)}} \frac{\overline{Q}}{h\varepsilon}, \end{aligned} \tag{4.159}$$

which gives the relation,

$$Q = \sqrt{k^{(1)}k^{(2)}}\overline{Q}. \tag{4.160}$$

Radial flow of anisotropic media in a vertical plane

The flow vector caused by the gravitational force is a constant vector,

$$\boldsymbol{q}^g = -\frac{k^{(1)}}{\mu}\rho g\beta_1^g \boldsymbol{n}^{(1)} - \frac{k^{(2)}}{\mu}\rho g\beta_2^g \boldsymbol{n}^{(2)}, \tag{4.161}$$

which corresponds to a volume flow rate,

$$Q^g = \int_S q_i^g \nu_i dS. \tag{4.162}$$

The gravitation effect cause a translation displacement $\boldsymbol{q}^g t/\varepsilon$ of the wetted volume in the porous media along the direction of $\boldsymbol{q}^g$.

4.3.3 Three-dimensional radial flows in isotropic and anisotropic media

Radial flows in isotropic media

For a three-dimensional flow, the gravitational effect has to be considered. The solution of this problem can be obtained by a flow caused by gravity and a radial flow related to the moving system. The flow rate caused by gravity is

$$\boldsymbol{q}^g = -\frac{k^{(3)}}{\mu}\rho g \boldsymbol{n}^{(3)}, \tag{4.163}$$

which corresponds to a volume flow rate,

$$Q^g = \int_V -\frac{k^r}{\mu}\rho g \nu_3 dV. \tag{4.164}$$

From this result it can be concluded that the volume injection rate Q for a three-dimensional radial flow through isotropic media is independent of the gravitation effect. The gravitational effect for flows through isotropic media during time period t produce a translation distance $\frac{k^r}{\varepsilon\mu}\rho g t$ of the wetted area along the gravitation direction. The radial flow relative to the moving system is defined by the following equations,

$$q_r = -\frac{k^r}{\mu}\frac{\partial p}{\partial r}, \tag{4.165}$$

$$\frac{1}{r^2}\frac{d}{dr}(r^2\frac{dp}{dr}) = 0, \tag{4.166}$$

$$q_r = q^0, \qquad r = r^0, \tag{4.167}$$

$$p = p^f, \qquad r = r^f. \tag{4.168}$$

Integrating these governing equations, the follow are obtained,

$$q_r(r) = q^0\frac{r^{0^2}}{r^2}, \tag{4.169}$$

$$p(r) = p^f + \frac{q^0\mu r^{0^2}}{k^r}(\frac{1}{r} - \frac{1}{r^f}), \tag{4.170}$$

$$p^0 = p^f + \frac{q^0\mu r^{0^2}}{k^r}(\frac{1}{r^0} - \frac{1}{r^f}), \tag{4.171}$$

$$k^r = \frac{q^0\mu r^0(r^f - r^0)}{r^f(p^0 - p^f)}. \tag{4.172}$$

The injection flow rate q^0 in these equations given above can be replaced by the volume flow rate Q,

$$Q = \int_S q_r(r^0)dS = \int_S q^0 dS = 4\pi r^{0^2}q^0, \tag{4.173}$$

in which S denotes the surface of the injection boundary.

Radial flows in anisotropic media

Using the principal axis system and the coordinate transformation relationship described in equations (4.105) - (4.107) and equation (4.113), to obtain the following governing equations describing a quasi-isotropic system,

$$\overline{q}_r = -\frac{1}{\mu}(\frac{\partial p}{\partial \overline{r}} + \rho g\frac{r}{\overline{r}}\cos\gamma), \tag{4.174}$$

$$\frac{1}{\overline{r}^2}\frac{d}{d\overline{r}}(\overline{r}^2\frac{dp}{d\overline{r}}) = 0, \tag{4.175}$$

$$\overline{q}_r = \overline{q}^0 + \overline{q}^g_r, \qquad \overline{r} = \overline{r}^0, \tag{4.176}$$

$$p = p^f, \qquad \overline{r} = \overline{r}^f, \tag{4.177}$$

where $\overline{q}^g_r = -\frac{1}{\mu}\rho g\frac{r}{\overline{r}}\cos\gamma$ represents the flow rate caused by the gravitational effect. The solution of these equations are,

$$\overline{q}_r(\overline{r}) = \overline{q}^0\frac{\overline{r}^{0^2}}{\overline{r}^2} - \frac{\overline{k}^r}{\mu}\rho g\frac{r}{\overline{r}}\cos\gamma, \tag{4.178}$$

$$p(\overline{r}) = p^f + \frac{\overline{q}^0 \mu \overline{r}^{0\,2}}{\overline{k}^r}(\frac{1}{\overline{r}} - \frac{1}{\overline{r}^f}), \tag{4.179}$$

$$p^0 = p^f + \frac{\overline{q}^0 \mu \overline{r}^{0\,2}}{\overline{k}^r}(\frac{1}{\overline{r}^0} - \frac{1}{\overline{r}^f}), \tag{4.180}$$

$$\overline{k}^r = \frac{\overline{q}^0 \mu \overline{r}^0 (\overline{r}^f - \overline{r}^0)}{\overline{r}^f (p^0 - p^f)} = 1. \tag{4.181}$$

The volume injection rate produced by the gravitation effect vanishes which can be demonstrated as follows. From equation (4.110), the flow rate caused by the gravitation effect is,

$$q_i^g = -\frac{k^{(i)}}{\mu}\rho g \beta_i^g, \tag{4.182}$$

from which the volume rate through the close injection boundary S can be calculated as,

$$\begin{aligned} Q^g &= \int_S q_i^g \nu_i dS, \\ &= \int_V q_{i,i}^g dV = 0, \end{aligned} \tag{4.183}$$

Based on this consideration, the quasi-volume injection rate is,

$$\begin{aligned} \overline{Q} &= 4\pi \overline{r}^{0\,2} \overline{q}^0 \\ &= 4\pi \frac{x_1^{0\,2}}{(k^{(1)})^{3/2}} q_1^0 \\ &= 4\pi \frac{x_2^{0\,2}}{(k^{(2)})^{3/2}} q_2^0 \\ &= 4\pi \frac{x_3^{0\,2}}{(k^{(3)})^{3/2}} q_3^0. \end{aligned} \tag{4.184}$$

The relation between this quasi-volume injection rate $\overline{Q}$ and the real volume injection rate Q can be obtained as,

$$Q = \frac{4}{3}\pi \frac{d}{dt}(x_1^f x_2^f x_3^f) = \frac{4}{3}\pi \sqrt{k^{(1)}k^{(2)}k^{(3)}} \frac{d}{dt}(\overline{x}_1^f \overline{x}_2^f \overline{x}_3^f) = \sqrt{k^{(1)}k^{(2)}k^{(3)}}\overline{Q}. \tag{4.185}$$

For the general cases of anisotropic media, the gravitation force produce the three flow components along three principal directions. The flow vector caused by the gravitation is, a constant vector

$$\boldsymbol{q}^g = -\frac{k^{(1)}}{\mu}\rho g \beta_1^g \boldsymbol{n}^{(1)} - \frac{k^{(2)}}{\mu}\rho g \beta_2^g \boldsymbol{n}^{(2)} - \frac{k^{(3)}}{\mu}\rho g \beta_3^g \boldsymbol{n}^{(3)}. \tag{4.186}$$

The gravitation effect causes a translation displacement d_g of the wetted volume in the medium along the direction of $\boldsymbol{q}^g$.

Chapter 5

Identification methods of permeability

The main purpose is to identify the permeability of a prescribed porous medium which consists of fibre reinforcement materials in RTM. A prescribed porous medium means that both the fibre reinforcement material and its preform have been fixed and will not change during the process to identify its permeability by experiment method. In order to describe identification methods of permeability in RTM, as shown in Figure 5.1 three reference coordinate systems are defined as follows:

Spatial reference coordinate system: This is a Cartesian coordinate system $O - x_1x_2x_3$ fixed in the porous medium and it can be chosen in any convenience manner. It is assumed that the coordinate axis x_3 is upward. Therefore, the gravitation force takes the negative direction of the coordinate axis x_3. Under this reference system, the permeability tensor of a porous medium is represented by k_{ij}, which as an entity can be represented by equation (3.1), where $\boldsymbol{e}_i$, $(i = 1, 2, 3)$ are the three base vectors of the coordinate system $O - x_1x_2x_3$. For a prescribed porous medium, the entity permeability tensor $\boldsymbol{k}$ in equation (3.1) does not change under different reference systems, although its components k_{ij} for different systems change.

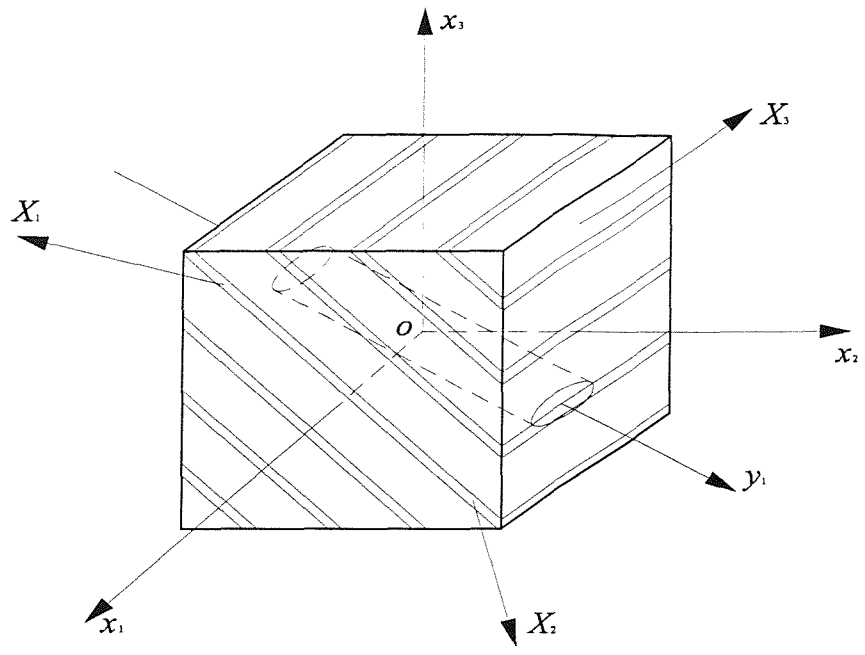

Figure 5.1: Three coordinate systems.

Material coordinate system: It is a Cartesian coordinate system $O - X_1X_2X_3$ constructed by the three principal direction $\boldsymbol{n}^{(1)}$, $\boldsymbol{n}^{(2)}$ and $\boldsymbol{n}^{(3)}$ described in sections 3.2. Under this coordinate system, the permeability tensor of a porous medium takes its simplest form presented in equation (3.30). For a prescribed porous medium, its principal directions $\boldsymbol{n}^{(r)}$ and the corresponding principal permeability $k^{(r)}$, $r = 1, 2, 3$ are unchangeable. Therefore, the position of this material coordinate system is not changeable relative to the material body. If the principal directions $\boldsymbol{n}^{(r)}$ and the corresponding principal permeability $k^{(r)}$ of the porous medium are obtained, hence all the information of the permeability of the porous medium is known. The main task of the permeability identification is to determine the principal directions and corresponding principal permeabilities of a porous medium.

Measurement coordinate system: This coordinate system is another Cartesian system $O - y_1y_2y_3$ which is used to describe an measurement direction in per-

meability experiments. For example, in a one-dimensional flow measurement, the $O - y_1$ direction represents the flow measurement direction, which may or not be one of the directions $\boldsymbol{e}_i$, $(i = 1, 2, 3)$ of the spatial coordinate axes x_i and the principal directions $\boldsymbol{n}^{(r)}$, $r = 1, 2, 3$ of the material coordinate system $O - X_1X_2X_3$.

5.1 One-dimensional channel flow methods

The permeability identification methods by means of one-dimensional channel flows are based on the analytical solutions described in section 4.2.1. The fundamental idea is to cut out a strip along a direction in the porous medium and fill this strip into a tube to construct a one-dimensional flow channel flow as shown in Figure 4.1 or 4.2. The permeability coefficient in the flow tube direction can be calculated by measuring the inlet flow pressure $p^0(t)$, the flow front pressure $p^f(t)$ and the position x^f of the flow front.

5.1.1 Isotropic media

For an isotropic medium, any direction in it is its principal direction to which the corresponding permeability coefficient is a real number k. Therefore, a test material strip can be cut out along any direction of this isotopic medium to construct a one-dimensional flow channel for experiment. The permeability parameter k can be directly given by the coefficient k_{11} in equation (4.19). It is convenience to choose the flow front pressure p^f as the atmosphere pressure, that is $p^f = 1.013 \times 10^5 Pa$, and the permeability parameter k is given by,

$$k = \frac{\varepsilon \mu {x^f}^2}{2P}, \tag{5.1}$$

where,

$$P = \int_0^{t^f} p^0(t)dt = \sum_{I=1}^{n} \left(p^0_{(t_I)} + p^0_{(t_{I-1})}\right) \frac{t^f - t^0}{2N}, \tag{5.2}$$

which is called the *injection pressure impulse*. This injection pressure impulse P can be obtained by the shaded area as shown in Figure 5.2.

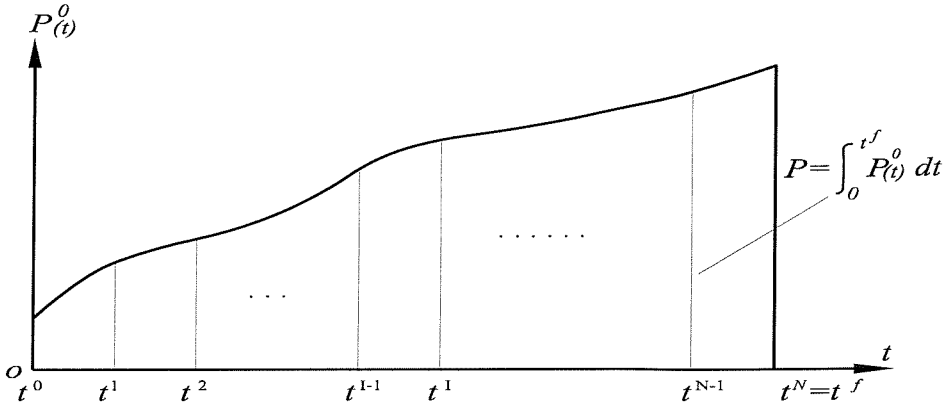

Figure 5.2: The resin injection pressure impulse P.

5.1.2 Anisotropic media

Case 1: Three principal directions prescribed

As demonstrated in section 3.2, a pressure gradient along a principal direction does not cause any flows in the plane perpendicular to this principal direction. Because of this, the one-dimensional flow in the channel along a principal direction of anisotropic media is same as the one-dimensional flow described in section 5.1.1 for isotropic media. The equation (5.1) can directly give the principal permeability in this principal direction. Therefore, if the three principal directions are known, the three corresponding principal permeability coefficients can be obtained by three separated one-dimensional flow measurements which are designed along the three prescribed principal directions, respectively. In fact, because the three principal directions are orthogonal each other as described in section 3.2.2, if two of them are known, the third one can be determined by their orthogonality.

In engineering production, the three principal directions of some materials can be determined according to the preform type of fibre reinforcement. For example, a transversely anisotropic medium is a typical example, for which the longitudinal direction of is a principal direction and the plane perpendicular to its longitudinal direction is an isotropic plane in which any direction is its principal direction, see

section 3.2.3. For these transversely anisotropic media, only two one-dimensional flow experiments are needed to identify their permeabilities.

Case 2: One principal direction prescribed

For this known principal direction, a one-dimensional flow measurement along this direction can be used to obtain its principal permeability. The plane perpendicular to this principal direction is a principal plane which is shown in Figure 5.3. In this figure, $O - X_1X_2$ represents the principal axes of this principal plane, their directions and the corresponding permeabilities are unknown, which are determined by experiments. The coordinate systems $O - y_1y_2$ and $O - y_1'y_2'$ are two measurement systems, where the angle θ represents the angle between the axes OX_1 and Oy_1 to be determined. Therefore, for a chosen measurement reference system $O - y_1y_2$, if θ can be determined, the principal axes $O - X_1X_2$ can be determined. Now to demonstrate that three effective permeabilities measured by the three separated one-dimensional flow experiments along the directions y_1, y_2 and y_1' can determine the principal permeabilities $k^{(1)}$, $k^{(2)}$ and the angle θ.

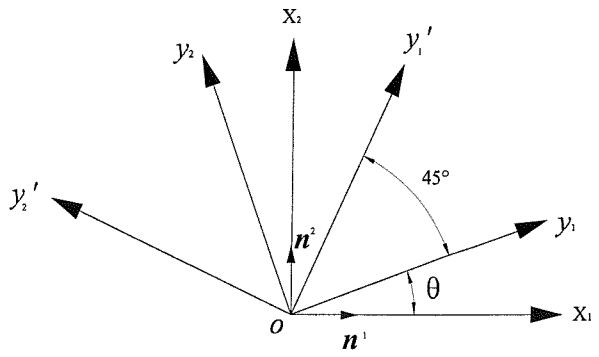

Figure 5.3: The reference coordinate systems for three one-dimensional flow measurements in a principal plane of the permeability tensor.

Using the transformation relations given in equation (3.8), to obtain the two

Using the transformation relations given in equation (3.8), to obtain the two dimensional permeability tensor k_{ij} under the system $O - y_1y_2$ as,

$$\begin{bmatrix} k_{11} & k_{12} \\ k_{21} & k_{22} \end{bmatrix} = \begin{bmatrix} \cos\theta & \sin\theta \\ -\sin\theta & \cos\theta \end{bmatrix} \begin{bmatrix} k^{(1)} & 0 \\ 0 & k^{(2)} \end{bmatrix} \begin{bmatrix} \cos\theta & -\sin\theta \\ \sin\theta & \cos\theta \end{bmatrix}. \tag{5.3}$$

This equation gives,

$$k_{11} = \frac{k^{(1)} + k^{(2)}}{2} + \frac{k^{(1)} - k^{(2)}}{2}\cos 2\theta, \tag{5.4}$$

$$k_{22} = \frac{k^{(1)} + k^{(2)}}{2} - \frac{k^{(1)} - k^{(2)}}{2}\cos 2\theta. \tag{5.5}$$

From equations (3.52) and (3.53), the effective permeabilities along y_1 and y_2 directions are,

$$\tilde{k}_{11} = \frac{I_2}{k_{22}}, \tag{5.6}$$

$$\tilde{k}_{22} = \frac{I_2}{k_{11}}, \tag{5.7}$$

where I_2 takes the form,

$$I_2 = k^{(1)}k^{(2)}. \tag{5.8}$$

Replacing θ by $\theta + 45°$ into equation (5.5), to obtain the permeability coefficient k'_{22} under the measurement system $O - y'_1y'_2$ as,

$$k'_{22} = \frac{k^{(1)} + k^{(2)}}{2} + \frac{k^{(1)} - k^{(2)}}{2}\sin 2\theta, \tag{5.9}$$

which by using equation (5.6) gives the effective permeability along Oy'_1 direction as,

$$\tilde{k}'_{11} = \frac{I_2}{k'_{22}}. \tag{5.10}$$

From equations (5.4) - (5.10),

$$\tan 2\theta = -\frac{A}{B} + \frac{A^2 - B^2}{\tilde{k}'_{11}B}, \tag{5.11}$$

$$k^{(1)} = \tilde{k}_{11}\frac{A - B}{A - B/\cos 2\theta}, \tag{5.12}$$

$$k^{(2)} = \tilde{k}_{22}\frac{A + B}{A + B/\cos 2\theta}. \tag{5.13}$$

Where $A = \dfrac{\tilde{k}_{11} + \tilde{k}_{22}}{2}$ and $B = \dfrac{\tilde{k}_{11} - \tilde{k}_{22}}{2}$.

Case 3: No principal direction prescribed

This is a three-dimensional general case and the three principal directions and the corresponding principal permeability coefficient need to be determined by one-dimensional flow method. As shown in Figure 5.4, $O - X_1X_2X_3$ and $O - y_1y_2y_3$ are the principal coordinate system and a measurement coordinate system. The relative position between these two systems can be determined by three Euler angles θ_1, θ_2 and θ_3. A rotation angle θ_1 of the coordinate system $O - X_1X_2X_3$ about the axis $O - X_3$ produces the coordinate system $O - 12X_3$ which makes a rotation of angle θ_2 about its axis $O - 1$ gives a coordinate system $O - 12'y_3$. Furthermore, a rotation of angle θ_3 about the axis $O - y_3$ produces the measurement system $O - y_1y_2y_3$. These three rotations give the following three transformation matrices,

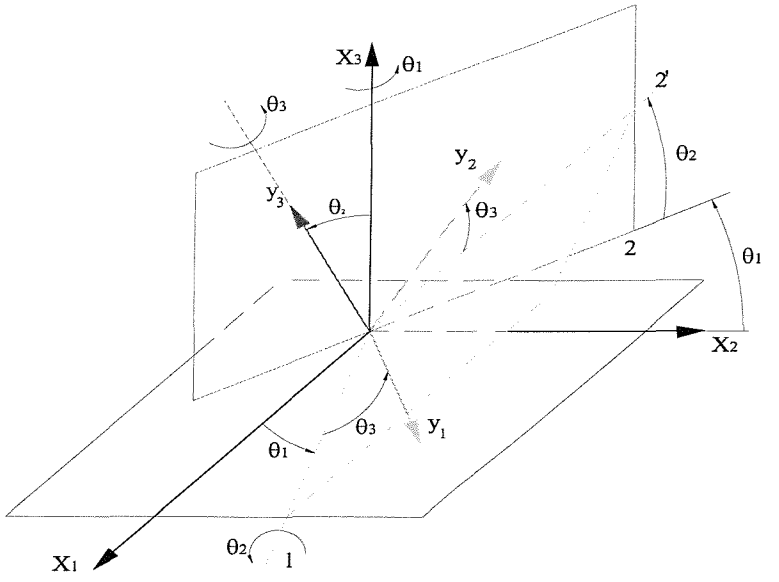

Figure 5.4: Three Euler angles θ_1, θ_2 and θ_3.

$$\text{Rotation } \theta_1: \quad \boldsymbol{\beta}_1 = \begin{bmatrix} \cos\theta_1 & \sin\theta_1 & 0 \\ -\sin\theta_1 & \cos\theta_1 & 0 \\ 0 & 0 & 1 \end{bmatrix}, \tag{5.14}$$

$$\text{Rotation } \theta_2: \quad \boldsymbol{\beta}_2 = \begin{bmatrix} 1 & 0 & 0 \\ 0 & \cos\theta_2 & \sin\theta_2 \\ 0 & -\sin\theta_2 & \cos\theta_2 \end{bmatrix}, \tag{5.15}$$

$$\text{Rotation } \theta_3: \quad \boldsymbol{\beta}_3 = \begin{bmatrix} \cos\theta_3 & \sin\theta_3 & 0 \\ -\sin\theta_3 & \cos\theta_3 & 0 \\ 0 & 0 & 1 \end{bmatrix}. \tag{5.16}$$

From these three transformation matrices, the transformation matrix can be obtained $\boldsymbol{\beta}$ between the coordinate systems $O - X_1X_2X_3$ and $O - y_1y_2y_3$

$$\boldsymbol{\beta} = \boldsymbol{\beta}_3\boldsymbol{\beta}_2\boldsymbol{\beta}_1, \tag{5.17}$$

Therefore, the following transformation relationships between the permeability tensor $\boldsymbol{k}$ under the measurement coordinate system $O - y_1y_2y_3$ and the three principal permeability coefficients $k^{(1)}$, $k^{(2)}$ and $k^{(3)}$ under the principal coordinate system $O - X_1X_2X_3$, i.e.

$$\boldsymbol{k} = \boldsymbol{\beta} \begin{bmatrix} k^{(1)} & & \\ & k^{(2)} & \\ & & k^{(3)} \end{bmatrix} \boldsymbol{\beta}^T \tag{5.18}$$

and

$$\begin{bmatrix} k^{(1)} & & \\ & k^{(2)} & \\ & & k^{(3)} \end{bmatrix} = \boldsymbol{\beta}^T \boldsymbol{k} \boldsymbol{\beta}. \tag{5.19}$$

According to the one-dimensional effective permeability theorem described in equations (3.45-3.47), the effective permeability along the measurement coordinate axes Oy_1, Oy_2 and Oy_3 respectively take the forms

$$\tilde{k}_{11} = \frac{I_3}{\begin{vmatrix} k_{22} & k_{23} \\ k_{32} & k_{33} \end{vmatrix}}, \tag{5.20}$$

$$\tilde{k}_{22} = \frac{I_3}{\begin{vmatrix} k_{11} & k_{13} \\ k_{31} & k_{33} \end{vmatrix}}, \tag{5.21}$$

$$\tilde{k}_{33} = \frac{I_3}{\begin{vmatrix} k_{11} & k_{12} \\ k_{21} & k_{22} \end{vmatrix}}. \tag{5.22}$$

To represent the six permeability coefficients k_{ij} by the effective permeability

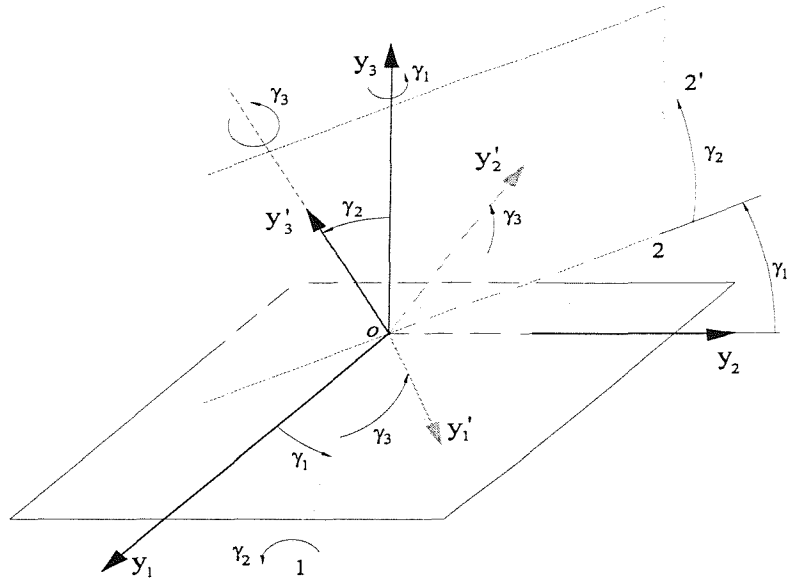

Figure 5.5: Three Euler angles γ_1, γ_2 and γ_3.

measured, three equations (5.20-22) are not sufficient. Now other three measurements are required. As shown in Figure 5.5, the other three measurement directions Oy_1', Oy_2' and Oy_3' are determined by choosing other three Euler's angles $\gamma_1 = 45°$, $\gamma_2 = 45°$ and $\gamma_3 = 45°$ relative to the system $O - y_1y_2y_3$. Obviously, the transformation matrix between these two measurement systems $O - y_1y_2y_3$ and $O - y_1'y_2'y_3'$ can be obtained by equation (5.17) with $\theta_1 = \theta_2 = \theta_3 = 45°$, i.e.

$$\boldsymbol{\beta}' = \frac{1}{2}\begin{bmatrix} \frac{2-\sqrt{2}}{2} & \frac{2+\sqrt{2}}{2} & 1 \\ \frac{-2-\sqrt{2}}{2} & \frac{-2+\sqrt{2}}{2} & 1 \\ 1 & -1 & \sqrt{2} \end{bmatrix}. \tag{5.23}$$

Using this transformation matrix, to obtain the permeability tensor $\boldsymbol{k}'$ under the system $O - y_1'y_2'y_3'$ as follows,

$$\boldsymbol{k}' = \boldsymbol{\beta}'\boldsymbol{k}\boldsymbol{\beta}'^T. \tag{5.24}$$

similarly, according to the one-dimensional effective permeability invariant theorem described in equations (3.45-3.47), the effective permeability along the measurement coordinate axes Oy'_1, Oy'_2 and Oy'_3 respectively take the form,

$$\tilde{k}'_{11} = \frac{I_3}{\begin{vmatrix} k'_{22} & k'_{23} \\ k'_{32} & k'_{33} \end{vmatrix}}, \tag{5.25}$$

$$\tilde{k}'_{22} = \frac{I_3}{\begin{vmatrix} k'_{11} & k'_{13} \\ k'_{31} & k'_{33} \end{vmatrix}}, \tag{5.26}$$

$$\tilde{k}'_{33} = \frac{I_3}{\begin{vmatrix} k'_{11} & k'_{12} \\ k'_{21} & k'_{22} \end{vmatrix}}. \tag{5.27}$$

Now, there are six equations (5.20-22) and (5.25-27) to determine the permeability tensor $\boldsymbol{k}$ with six components by the six known effective permeabilities measured. Using the one-dimensional effective permeability invariant theorem described in equation (3.51), to obtain that,

$$\frac{1}{\tilde{k}_{11}} + \frac{1}{\tilde{k}_{22}} + \frac{1}{\tilde{k}_{33}} = \frac{1}{\tilde{k}'_{11}} + \frac{1}{\tilde{k}'_{22}} + \frac{1}{\tilde{k}'_{33}}, \tag{5.28}$$

From equation (5.28), it can be concluded that the six equations (5.20-22) and (5.25-27) are not independent of each other. Therefore, the six measurement directions chosen in an experiment should not form more than one three-axis-orthogonal system to keep the independence of effective permeability measurement. After the permeability tensor $\boldsymbol{k}$ is determined, the principal permeability and its principal directions can be obtained by equation (5.19) or by solving the related eigenvalue problem described in section 3.2.1.

5.2 Two-dimensional radial flow methods

Applications of the solutions described in sections 4.2.2 provide a permeability identification method by radial flow measurements. All of these solutions are

generalised solutions in which the injection pressure p^0 does not be required to be controlled as a constant pressure which is difficult in practical experiments.

5.2.1 Isotropic media

In a horizontal plane

As shown in Figure 4.3, for a two-dimensional radial flow, the front of the flow is a circle about the injection centre. The permeability coefficient k^r can be determined by equation (4.56). During an experiment based on this solution, the resin injection radius r^0 can be given and the pressure on the front of the flow p^f can be chosen as the atmosphere pressure. Recording the injection pressure time history from the beginning time 0 to the final time t and the radius r^f of the flow front at time t, the permeability coefficient k^r can be calculated by equation (4.56).

In a vertical plane

In this problem, the flow front is also a circle but the centre of this circle has a translation (see in Figure 4.4). By using a moving coordinate system, the permeability coefficient k^r now can also be determined by equation (4.56). The gravitational effect for flow through isotropic media during time period t produces a translation distance along the g-direction, which can be obtained as:

$$d_g = \frac{k^r}{\mu\varepsilon}\rho g t. \tag{5.29}$$

5.2.2 Anisotropic media

In a horizontal plane

For anisotropic media, through a coordinate transformation described in equations (4.63) and (4.64) or equation (4.105), a quasi-isotropic radial flow for a two-dimensional case can be obtained. This quasi-isotropic radial flow provides an approach to identify the permeability tensor in an anisotropic medium. As

demonstrated in section 4.2.2 and shown in Figure 4.5, the flow front of a two-dimensional radial flow in an anisotropic medium is an ellipse described by equation (4.80). The inlet boundary should be another ellipse described by equation (4.81). Under the transformation described in equations (4.63) and (4.64), these two ellipses are transformed to the two circles. The front flow circle and the inlet flow circle have their radii $\overline{r}^f$ and $\overline{r}^0$, respectively. For all points (x_1^f, x_2^f) on the flow front ellipse, there is the same radius $\overline{r}^f$. For all points (x_1^0, x_2^0) on the inlet flow ellipse, there is also a same radius $\overline{r}^0$. By the experiment to obtain a figure as shown in Figure 4.5, from which the directions of the two principal axes and their semiaxes a and b can be determined. By using equations (4.80), the following formula are derived

$$k^{(1)}\overline{r}^{f\,2} = a^2, \tag{5.30}$$

$$k^{(2)}\overline{r}^{f\,2} = b^2. \tag{5.31}$$

From equations (4.63)-(4.64), for an arbitrary point (x_1^0, x_2^0) on the inlet boundary, equation (4.79) can be represented as

$$\overline{r}^{0\,2} = \frac{x_1^{0\,2}}{k^{(1)}} + \frac{x_2^{0\,2}}{k^{(2)}} \tag{5.32}$$

Substituting $k^{(1)}$ and $k^{(2)}$ obtained from equations (5.30) and (5.31) into equation (5.32), to obtain that,

$$\overline{r}^{0\,2} = \overline{r}^{f\,2}\left(\frac{x_1^{0\,2}}{a^2} + \frac{x_2^{0\,2}}{b^2}\right) \tag{5.33}$$

or,

$$\overline{r}^{0\,2} = B\overline{r}^{f\,2}, \tag{5.34}$$

where,

$$B = \frac{x_1^{0\,2}}{a^2} + \frac{x_2^{0\,2}}{b^2}. \tag{5.35}$$

Substituting $\overline{r}^{0\,2}$ in equation (5.35) into equation (4.77), to obtain

$$\overline{r}^{f\,2}(\ln B - B + 1)\frac{\mu\varepsilon}{4P} = 1, \tag{5.36}$$

where,

$$P = \int_0^t (p^f - p^0)dt, \tag{5.37}$$

therefore,

$$\overline{r}^{f^2} = \frac{4P}{\mu\varepsilon(\ln B - B + 1)}. \tag{5.38}$$

A substitution of this equation into equations (5.30) and (5.31) gives the two principal permeability coefficients as,

$$k^{(1)} = \frac{a^2}{\overline{r}^{f^2}} = \frac{a^2\mu\varepsilon(\ln B - B + 1)}{4P} \tag{5.39}$$

$$k^{(2)} = \frac{b^2}{\overline{r}^{f^2}} = \frac{b^2\mu\varepsilon(\ln B - B + 1)}{4P}. \tag{5.40}$$

It is noted that the inlet boundary ellipse is not known before the experiment is finished. Therefore the exact inlet boundary shape required by the solutions given in section 5.2.2 can not been determined before experiments. In practical measurements, a small circle with its radius r^0 is chosen as the real inlet boundary. A point $(x_1^0 = r^0/\sqrt{2}, x_2^0 = r^0/\sqrt{2})$ on this circle is used to calculate the constant B in equation (5.34), which represents that an ellipse passing through the point $(x_1^0 = r^0/\sqrt{2}, x_2^0 = r^0/\sqrt{2})$ and very near to the real inlet circle is imagined as an idealised inlet ellipse boundary required by equation (4.81), as shown in Figure 5.6. Since the inlet circle area is very small compared with all experiment area, this approximation can be accepted.

In a vertical plane

As same as in the isotropic case, an application of the moving coordinate system gives a convenience to measure the permeability, so the equations described in the above to determine the permeability of an anisotropic media in a horizontal plane are also valid. The two principal permeability can be obtained by using equations (5.39) and (5.40).

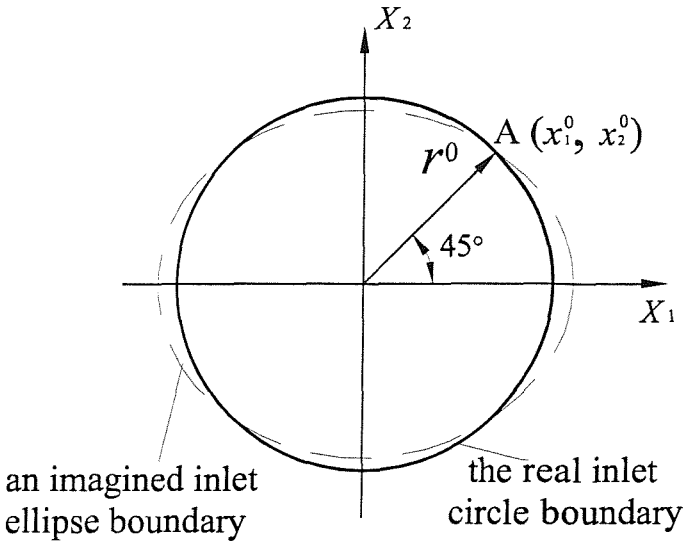

Figure 5.6: An imagined inlet ellipse boundary.

The translation distance $\boldsymbol{d}_g$ caused by the gravitational effect can be obtained as,

$$\begin{aligned} \boldsymbol{d}_g &= \frac{\boldsymbol{q}^g t}{\varepsilon}, \\ &= -\frac{k^{(1)}}{\mu\varepsilon}\rho g t \beta_1^g \boldsymbol{n}^{(1)} - \frac{k^{(2)}}{\mu\varepsilon}\rho g t \beta_2^g \boldsymbol{n}^{(2)}, \end{aligned} \tag{5.41}$$

where $\boldsymbol{q}^g$ was given in equation (4.84).

For a special case in which the gravity direction has the same direction as one of principal permeability direction. For example, as shown in Figure 5.7, assume the direction of $k^{(2)}$ is the vertical direction, then $\beta_1^g = \cos\frac{\pi}{2} = 0$ and $\beta_2^g = \cos 0° = 1$. Now the equation (4.84) can be reduced to,

$$q_2^g = -\frac{k^{(2)}}{\mu}\rho g, \tag{5.42}$$

and,

$$d_g = \frac{k^{(2)}}{\mu\varepsilon}\rho g t, \tag{5.43}$$

where d_g is along the g-direction.

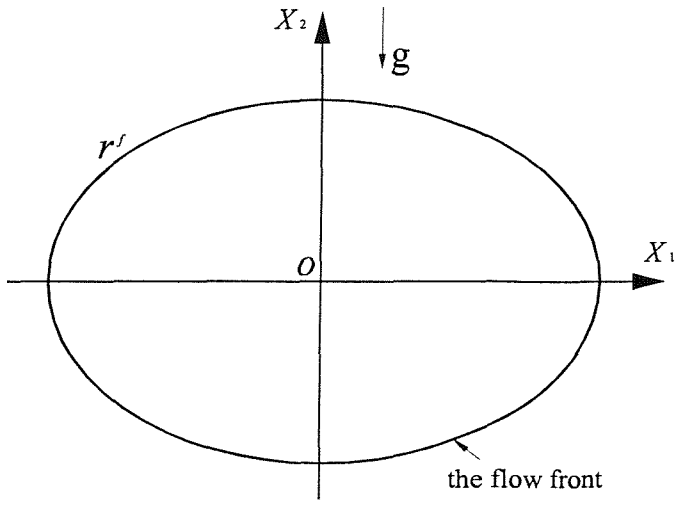

Figure 5.7: A radial flow in a vertical plane $O - X_1X_2$.

5.3 Three-dimensional radial flow methods

5.3.1 Isotropic media

For a three-dimensional radial flow as shown in Figure 4.7, the flow front, which if the effect of the gravity is neglected, is a sphere about the centre of the injection centre. The permeability coefficient k^r given by equation (4.101). Also, in this case, the effect of the gravity will cause a translation of the wet volume along the gravitational direction, which can be given by,

$$d_g = \frac{k^r}{\mu\varepsilon}\rho g t. \tag{5.44}$$

5.3.2 Anisotropic media

The solutions of radial flows in a three-dimensional anisotropic media are described in section 4.2.3. As shown in Figure 4.8, the flow front of a three-dimensional radial flow in an anisotropic medium is an ellipsoid described by equation (4.117). The inlet boundary should be another ellipsoid described by equation (4.118). Under the transformation described in equation (4.105), these two ellipsoids are transformed to two spheres. The front flow sphere and the inlet

flow sphere have radii $\overline{r}^f$ and $\overline{r}^0$, respectively. For all points (x_1^f, x_2^f, x_3^f) on the flow front ellipsoid, there is the same radius $\overline{r}^f$. For all points (x_1^0, x_2^0, x_3^0) on the inlet flow ellipsoid, there is also the same radius $\overline{r}^0$. From the experiments it is possible obtain a figure as shown in Figure 4.8, from which the directions of the three principal axes and their semiaxes a, b and c can be determined. By using equation (4.117), it is obtained,

$$k^{(1)}\overline{r}^{f\,2} = a^2, \tag{5.45}$$

$$k^{(2)}\overline{r}^{f\,2} = b^2, \tag{5.46}$$

$$k^{(3)}\overline{r}^{f\,2} = c^2. \tag{5.47}$$

From equations (4.105)-(4.105), for an arbitrary point (x_1^0, x_2^0, x_3^0) on the inlet boundary, equation (4.108) can be represented as,

$$\overline{r}^{0\,2} = \frac{x_1^{0\,2}}{k^{(1)}} + \frac{x_2^{0\,2}}{k^{(2)}} + \frac{x_3^{0\,2}}{k^{(3)}} \tag{5.48}$$

Substituting $k^{(1)}$, $k^{(2)}$ and $k^{(3)}$ obtained from equations (5.45), (5.46) and (5.47) into equation (5.48), to obtain,

$$\overline{r}^{0\,2} = \overline{r}^{f\,2}\left(\frac{x_1^{0\,2}}{a^2} + \frac{x_2^{0\,2}}{b^2} + \frac{x_3^{0\,2}}{c^2}\right) \tag{5.49}$$

or,

$$\overline{r}^{0\,2} = B\overline{r}^{f\,2}, \tag{5.50}$$

where,

$$B = \frac{x_1^{0\,2}}{a^2} + \frac{x_2^{0\,2}}{b^2} + \frac{x_3^{0\,2}}{c^2}. \tag{5.51}$$

Substituting $\overline{r}^{0\,2}$ in equation (5.50) into equation (4.116), to obtain

$$\mu\varepsilon\left(\frac{1}{3} - \frac{\sqrt{B}}{2} + \frac{B^{3/2}}{6}\right)\overline{r}^{f\,2} + \sqrt{B}\int_0^t (p^f - p^0)dt = 0. \tag{5.52}$$

From this equation, $\overline{r}^f$ can be obtained and then the three principal permeabilities can be obtained by using equations (5.45)-(5.47). Also, the gravitational effect causes a translation displacement $\boldsymbol{d}_g$ of the wetted volume in the medium along

the direction of $\boldsymbol{q}^g$ and it can be obtained as follows,

$$\begin{aligned} \boldsymbol{d}_g &= \frac{\boldsymbol{q}^g t}{\varepsilon} \\ &= -\frac{k^{(1)}}{\mu\varepsilon}\rho g\beta_1^g \boldsymbol{n}^{(1)} - \frac{k^{(2)}}{\mu\varepsilon}\rho g\beta_2^g \boldsymbol{n}^{(2)} - \frac{k^{(3)}}{\mu\varepsilon}\rho g\beta_3^g \boldsymbol{n}^{(3)}. \end{aligned} \tag{5.53}$$

Chapter 6

Identification examples

6.1 Aim of experiments

The aim of the experiments is to demonstrate if the theory, developed in the Chapters 5, for the variable injection pressure tests and the effect of gravity in permeability measurement are valid and then to provide a generalized permeability identification method. The permeability can be calculated from the flow front positions and inlet pressures measured at various time steps of the experiment.

6.2 Experiment setup

6.2.1 Facility

The RTM Facility, the result of a Master Engineering group design project by Boyde, Clothier and Inglis (1995), is used in the experiments in this thesis. This Facility is suitable for both of radial and channel flow tests. The main test rig of this facility, as shown in Figure 6.1 (Weitzenböck 1999a, 1999b), has an aluminum work surface with a supporting steel structure and maximum working section of 1400 $\times$ 500 mm. The deformation of this tests rig can be neglected (see Appendix F). This plate can be arranged on a horizontal or vertical plane. The constant and variable inlet pressure experiments are all run on a horizontal plane and the

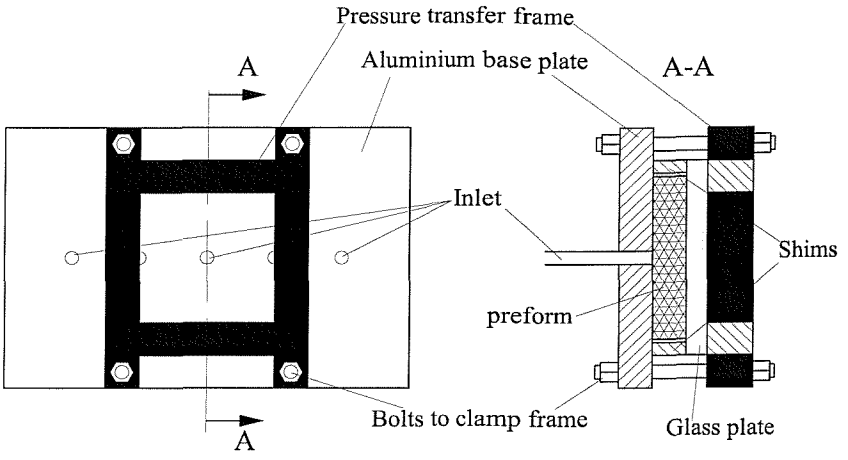

Figure 6.1: The main test rig to be used in this thesis.

experiments of gravitational effect are carried out on a vertical plane. There are five possible injection ports in the plate. The radius of these five ports are all 5.25 mm. The test in this thesis are all radial flow. For radial flow experiments, a glass top plate of 400 × 400 × 25 mm is used. A pressure transfer frame made of steel box sections is used to compress the fibre stack by using four M16 bolts. The shims are used to measure the thickness of the mould cavity and the thickness of each shim is $1.16mm$. Figure 6.2 provides a schematic diagram of the experimental setup. The compressed air used in this system comes from the

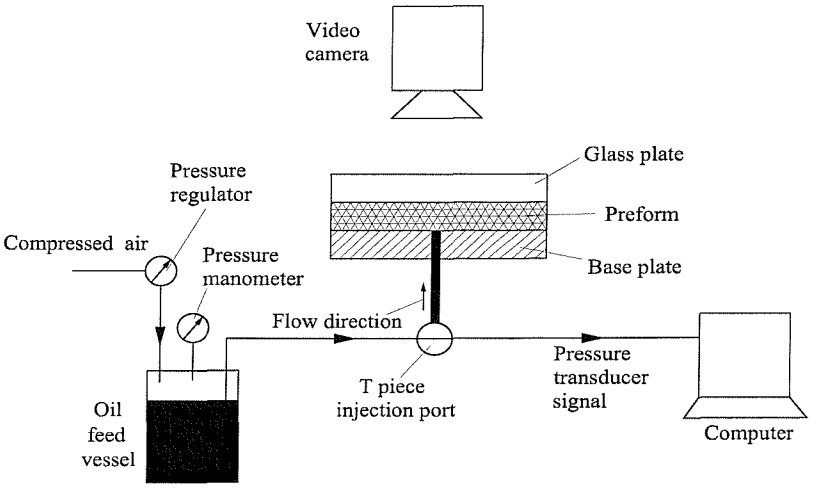

Figure 6.2: Schematic diagram of equipment setup.

air line in the lab, which can supply the compressed air of the pressure up to 10^6 Pascal. When the compressed air enters into the oil feed vessels, the test fluid is driven into the preform. A pressure transducer is mounted at the inlet port which is located at the centre of the bottom plate. The signal from the pressure transducer is recorded as a function of mould filling time in a computer. When the fluid flows into the mould, the flow front shows as a circle for isotropic or a ellipse for anisotropic preform. The images of the flow process is recorded by a video recording system and stored initially on video cassette. After an experiment has been finished, the images of the flow process are digitised and stored in a computer for further analysis to calculate the permeabilities measured.

6.2.2 Materials used and lay-up procedures

Three groups of experiments have been performed. They are constant inlet pressure experiments, variable inlet pressure experiments and experiments of gravitational effect. Four kinds of glass fabrics are used in these experiments, these glass fabrics are a continuous filament mat (U750-450) and the twill fabric RC 600 both from Vetrotex, the twill fabric WRE580T from SP Systems and a quasi-unidirectional non crimp fabric E-LPb 567 from Tech Textiles. The details of these glass fabrics have listed in Table 6.1, in which, N, W_f, H, and ρ_f represent the number of fibre layers, the mass per square meter of fibre mat, the thickness of the cavity and the density of the fibre material, respectively. The set up II of U 750-450, in which $v_f = 45.5\%$, is only for comparison with Weitzenböck's results (1996). By using the fabric reference coordinate system as shown in Figure 6.3, the orientation of the fibres in the fabric is distinguished in an attempt to keep the lay-up procedure as uniform as possible. These fibre pieces have a size of 350×350 (mm) which are cut out of a roll. For all experiments, the lay-up form represents the fibre pieces are laid up in an arrangement keeping the 0° direction of each layer, as shown in Figure 6.3, along a same direction on the experiment table. The flow front along these two direction, the axes X_1 and X_2, is measured during the tests. The corresponding fibre volume fraction (v_f) used

Table 6.1: Experiment arrangements.

Set up	Material	Property	N	W_f (g/m^2)	H (mm)	ρ_f $(\times 10^6 g/m^3)$	v_f (%)
I	U 750-450	Random	3	450	2.32	2.56	22.7
II			6		2.32		45.5
III			6		4.64		22.7
I	RC 600 WRE580T	Twill Weave (2×2)	5	600	2.32	2.56	50.4
II			6		2.32		60.6
III			6	580	2.32		58.6
I	E-LPb 567	Quasi-unidirectional	4	660	2.32	2.56	44.5
II			5		2.32		55.6
III			8		4.64		44.5

in the experiments is calculated by using the following formula,

$$v_f = \frac{NW_f}{H\rho_f}. \tag{6.1}$$

All the tests were radial flow tests. For all experiments, the Shell Vitrea M100 oil is used, the viscosity of this test fluid is $0.3515Pa * s$ at $15 - 18°C$ and the density is $0.878 \times 10^3 kg/m^3$.

6.3 Results

6.3.1 Introduction

In this section the results from constant inlet pressure experiments, variable inlet pressure experiments and experiments of gravitational effect are reported.

6.3.2 Constant inlet pressure experiments

An as lower as possibly pressure is used in these part of experiments, as it is easy to keep the pressure as constant at the inlet gate. Equations (2.20), (5.39),

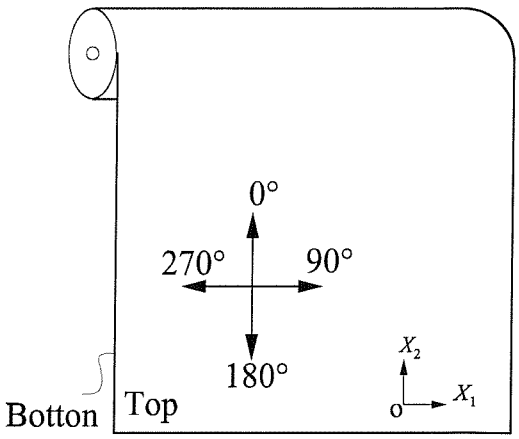

Figure 6.3: The fabric reference coordinate system.

(5.40) or (7.3) and (7.4) are used in these part of experiments. The main aim of these experiments in the constant inlet pressure is to proffer some results for a comparison.

A. Experiments on U750-450

U750-450 is a nominated isotropic material, the flow front should be a circle in radial flow tests. Six times experiments are done to reduce the random error. Equation (2.20) is used to calculate the permeabilities. Figures C.1 and C.2 show the injection pressures measured at the injection gate of the six radial flow tests on the continuous filament mat (U750-450) from Vetrotex. From this two figures, it is seen that the injection pressures for each experiment can be considered as constant. The permeability of this continuous filament mat with constant inlet pressure are summarised in Table 6.2. In this table X_1 and X_2 are two diameters of the flow front and t is time of flow process. Figure D.1 gives the images of the flow front during the experiment Cr5. A circle flow front is observed. As shown in Table B.1, the ratio $\frac{X_1}{X_2} \approx 1.00$ and $k^{(1)} \approx k^{(2)}$, which is independent on the time, but determined by the material characteristics.

Table 6.2: Results of U750-450 in constant inlet pressure experiments with $v_f = 22.7\%$, $N = 3$ and $H = 2.32mm$.

Run	Results of experiments				Results of calculation	
No.	X_1 (mm)	X_2 (mm)	t (s)	p^0 (bar)	$k^{(1)}$ $(\times 10^{-12})$ (m^2)	$k^{(2)}$ $(\times 10^{-12})$ (m^2)
Cr1	245	244	62.28	1.596	1488.63	1474.23
Cr2	282	280	135.58	1.420	1367.50	1344.74
Cr3	290	288	127.63	1.477	1360.17	1338.18
Cr4	267	265	85.03	1.539	1481.30	1455.19
Cr5	254	247	85.52	1.471	1502.67	1406.24
Cr6	243.5	242	91.94	1.427	1399.29	1378.88

B. Experiments on RC 600

RC 600 is a twill woven fabric, and an ellipse flow front has be observed in radial flow experiments. It is easier to obtain the principal permeabilities as the directions of warp and weft of RC 600 are two principal directions. Again, six experiments and a lower inlet pressure used in these tests. Equations (5.39) and (5.40), with the simplified P (equation 7.2), are used to calculate the permeabilities. Figures C.3 and C.4 show the injection pressures measured at the injection gate of the six radial flow tests on the twill fabric RC 600 from Vetrotex. Also a constant injection pressure has been used for each experiment. The permeabilities of the twill fabric RC 600 measured in the experiments with constant inlet pressure are shown in Table 6.3. Figure D.2 shows the images of the advancing flow front at the several time instants in the experiment Ct6. The flow fronts are ellipses. As shown in Table B.9, the ratio $\frac{X_1}{X_2} \approx 1.58$ and $\frac{k^{(1)}}{k^{(2)}} \approx 2.49$, which is also independent on the time, but determined by the material characteristics.

Table 6.3: Results of RC 600 in constant inlet pressure experiments with $v_f = 50.4\%$, $N = 5$ and $H = 2.32mm$.

Run	Results of experiments				Results of calculation	
	X_1	X_2	t	p^0	$k^{(1)}$ $(\times 10^{-12})$	$k^{(2)}$ $(\times 10^{-12})$
No.	(mm)	(mm)	(s)	(bar)	(m^2)	(m^2)
Ct1	122	76	156.08	1.653	54.18	21.02
Ct2	124.5	80.5	232.22	1.516	49.55	20.71
Ct3	137.5	88.5	258.74	1.529	55.86	23.14
Ct4	124.5	85	267.36	1.510	44.53	20.76
Ct5	148	106	277.86	1.775	44.10	22.62
Ct6	134.5	90.5	260.51	1.586	48.03	21.75

C. Experiments on E-LPb 567

E-LPb 567 is a unidirectional fabric, where the majority of fibres run in one direction only and this direction is one of the principal directions. The details of the experiments are described above, with lower injection pressure, six tests again used in this case and also equations (5.39) and (5.40) are used in these tests. Figures C.5 and C.6 show the injection pressures measured at the injection gate of the six radial flow tests on the quasi-unidirectional non-crimp fabric E-LPb 567. The injection pressures are constant in every experiment. The permeability of the quasi-unidirectional non crimp fabric E-LPb 567 are given in Table 6.4. The images of the flow front of experiment Cu2 are given in Figure D.3, again an elliptical flow front is observed.

Table 6.4: Results of E-LPb 567 in constant inlet pressure experiments with $v_f = 44.5\%$, $N = 4$ and $H = 2.32mm$.

Run	Results of experiments				Results of calculation	
No.	X_1 (mm)	X_2 (mm)	t (s)	p^0 (bar)	$k^{(1)}$ $(\times 10^{-12})$ (m^2)	$k^{(2)}$ $(\times 10^{-12})$ (m^2)
Cu1	86.5	192.5	97.22	1.544	66.20	327.86
Cu2	88	198	113.37	1.504	64.26	325.31
Cu3	83	184	69.86	1.692	64.95	319.18
Cu4	89	194	80.41	1.737	63.01	299.41
Cu5	83.5	183	63.60	1.793	62.98	302.50
Cu6	86	176.5	82.72	1.584	70.81	298.24

6.3.3 Variable inlet pressure experiments

When a higher injection pressure is used in the experiments, it was found that the recorded inlet pressure is not a constant, it is variable with respect to time. In these tests, the compressed air with the nominal pressure of $2.5 - 3.5bar$ is used, but as can be seen from these figures C.7-C.18, the maximum inlet pressure are all lower than the nominated pressure. This is because: 1) there is a loss of pressure between oil feed vessel and injection port (see in Figure 6.2); 2) the pressure at source is lower than nominal pressure which may be caused by some unknown random factors; 3) the pressure manometer and the pressure regulator are not precise enough to control the pressure which have been designed. However, this nominated pressure value does not affect our experiment results, since the pressure recorded by a pressure transducer at the injection port are correct. The inlet pressure increases when the time goes, as shown in Figures C.7-C.18. Therefore, to calculate the permeabilities under the variable inlet pressure condition, equations (2.20), (7.3) and (7.4) are are not valid,, the new equations (4.56), (5.39) and (5.40) which developed in Chapters 4 and 5 should be used. An Example of calculate the permeabilities by using these equations is given in Appendix E.

A. Experiments on U750-450

A higher injection pressure is used in these tests. Three kinds of set up are used. As shown in Figures C.7, C.8, C.9 and C.10, variable inlet pressures are measured at the injection gate of these radial flow tests on the random fabric U750-450. Equation (4.56) is used to calculate the permeabilities. The permeabilities of the U750-450 with different set up and variable inlet pressures are listed in Tables 6.5, 6.6 and 6.7. Figure D.4 gives the images of experiment Vr5.

Table 6.5: Results of U750-450 in variable inlet pressure experiments with v_f = 22.7%, $N = 3$ and $H = 2.32mm$.

Run	Results of experiments				Results of calculation	
	X_1	X_2	t	p^0	$k^{(1)}$ $(\times 10^{-12})$	$k^{(2)}$ $(\times 10^{-12})$
No.	(mm)	(mm)	(s)	(bar)	(m^2)	(m^2)
Vr1	265	258	36.94	2.026 – 2.318	1500.52	1408.36
Vr2	299	288	44.32	2.084 – 2.436	1434.09	1410.91
Vr3	282	280	51.60	1.909 – 2.143	1433.25	1409.39
Vr4	293	291	53.72	1.909 – 2.143	1531.47	1506.98
Vr5	260	258	38.24	1.879 – 2.172	1574.03	1545.49
Vr6	255	250	36.28	1.996 – 2.172	1518.20	1448.53

Table 6.6: Results of U750-450 in variable inlet pressure experiments with v_f = 45.5%, $N = 6$ and $H = 2.32mm$.

Run	Results of experiments				Results of calculation	
	X_1	X_2	t	p^0	$k^{(1)}$ $(\times 10^{-12})$	$k^{(2)}$ $(\times 10^{-12})$
No.	(mm)	(mm)	(s)	(bar)	(m^2)	(m^2)
Vra1	110	108.5	62.96	1.205 – 1.322	349.33	337.38
Vra2	106	104	54.32	1.234 – 1.410	334.69	318.83
Vra3	114.5	112	53.28	1.293 – 1.410	340.96	322.47

Table 6.7: Results of U750-450 in variable inlet pressure experiments with $v_f = 22.7\%$, $N = 6$ and $H = 4.64mm$.

Run	Results of experiments				Results of calculation	
	X_1	X_2	t	p^0	$k^{(1)}$ $(\times 10^{-12})$	$k^{(2)}$ $(\times 10^{-12})$
No.	(mm)	(mm)	(s)	(bar)	(m^2)	(m^2)
Vrb1	117	115.5	21.84	1.234 – 1.293	1527.84	1478.96
Vrb2	137.5	135.5	30.88	1.264 – 1.351	1535.64	1480.82
Vrb3	107.5	106	27.84	1.146 – 1.264	1503.33	1450.56

B. Experiments on twill weave fabric

A higher injection pressure is used in this section. Two kinds of twill weave fibre were used in this part of experiments. Figures C.11, C.12, C.13 and C.14 show the injection pressures measured at the injection gate of these experiments on the twill fabric RC 600 and WRE580T. Equations (5.39) and (5.40) are used and the permeabilities of these tests are shown in Tables 6.8, 6.9 and 6.10. Figure D.5 shows the images of test Vt1 and Figure D.6 shows the images of test Vtb3.

Table 6.8: Results of RC 600 in variable inlet pressure experiments with $v_f = 50.4\%$, $N = 5$ and $H = 2.32mm$.

Run	Results of experiments				Results of calculation	
	X_1	X_2	t	p^0	$k^{(1)}$ $(\times 10^{-12})$	$k^{(2)}$ $(\times 10^{-12})$
No.	(mm)	(mm)	(s)	(bar)	(m^2)	(m^2)
Vt1	163.5	110	206.14	1.732 – 2.348	50.54	22.88
Vt2	155	103	178.45	1.762 – 2.290	51.86	22.90
Vt3	149.5	101	177.79	1.762 – 2.172	52.06	23.76
Vt4	163	113.5	174.33	1.967 – 2.641	49.65	24.07
Vt5	194	132	247.33	1.937 – 2.495	52.62	26.55
Vt6	160.5	114	222.45	1.615 – 2.231	53.19	24.81

Table 6.9: Results of RC 600 in variable inlet pressure experiments with v_f = 60.6%, $N = 6$ and $H = 2.32mm$.

Run	Results of experiments				Results of calculation	
	X_1	X_2	t	p^0	$k^{(1)}$ $(\times 10^{-12})$	$k^{(2)}$ $(\times 10^{-12})$
No.	(mm)	(mm)	(s)	(bar)	(m^2)	(m^2)
Vta1	142	108	150.28	2.436 – 3.198	24.48	14.16
Vta2	152.5	115.5	174.66	2.377 – 3.374	24.33	13.95
Vta3	160	123.5	164.61	3.100 – 3.550	23.58	14.05

Table 6.10: Results of WRE580T in variable inlet pressure experiments with $v_f = 58.6\%$, $N = 6$ and $H = 2.32mm$.

Run	Results of experiments				Results of calculation	
	X_1	X_2	t	p^0	$k^{(1)}$ $(\times 10^{-12})$	$k^{(2)}$ $(\times 10^{-12})$
No.	(mm)	(mm)	(s)	(bar)	(m^2)	(m^2)
Vtb1	142	145.5	124.73	1.996 – 2.348	53.72	56.40
Vtb2	131	140	106.45	1.967 – 2.290	53.62	61.24
Vtb3	168	180	127.72	2.524 – 3.286	48.39	55.55

C. Experiments on E-LPb 567

As described in the above sections, a higher injection pressure is used in the experiments. This time a unidirectional fabric is used during the tests. Figures C.15, C.16, C.17 and C.18 show the variable injection pressures measured at the injection gate in the radial flow tests. The permeabilities of the quasi-unidirectional non crimp fabric E-LPb 567 with different set up, which can be calculated by equations (5.39) and (5.40), are given in Tables 6.11, 6.12 and 6.13. Figure D.7 gives the images of experiment Vu5.

Table 6.11: Results of E-LPb 567 in variable inlet pressure experiments with $v_f = 44.5\%$, $N = 4$ and $H = 2.32mm$.

Run	Results of experiments				Results of calculation	
No.	X_1 (mm)	X_2 (mm)	t (s)	p^0 (bar)	$k^{(1)}$ $(\times 10^{-12})$ (m^2)	$k^{(2)}$ $(\times 10^{-12})$ (m^2)
Vu1	76	154	60.48	1.381 – 1.703	75.09	308.31
Vu2	98	217	86.67	1.469 – 2.231	64.32	315.36
Vu3	85	183.5	51.74	1.645 – 2.172	70.83	330.12
Vu4	100.5	227	61.30	1.967 – 2.377	67.90	346.37
Vu5	121	260.5	106.44	1.820 – 2.113	73.38	340.12
Vu6	120	252	93.75	1.820 – 2.318	72.38	319.22

Table 6.12: Results of E-LPb 567 in variable inlet pressure experiments with $v_f = 55.6\%$, $N = 5$ and $H = 2.32mm$.

Run	Results of experiments				Results of calculation	
No.	X_1 (mm)	X_2 (mm)	t (s)	p^0 (bar)	$k^{(1)}$ $(\times 10^{-12})$ (m^2)	$k^{(2)}$ $(\times 10^{-12})$ (m^2)
Vua1	65.5	145.5	119.46	1.205 – 1.703	24.47	120.75
Vua2	83	177	112.05	1.586 – 2.084	25.89	117.73
Vua3	92.5	212	125.40	1.674 – 2.318	25.76	135.31

Table 6.13: Results of E-LPb 567 in variable inlet pressure experiments with $v_f = 44.5\%$, $N = 8$ and $H = 4.64mm$.

Run	Results of experiments				Results of calculation	
No.	X_1 (mm)	X_2 (mm)	t (s)	p^0 (bar)	$k^{(1)}$ $(\times 10^{-12})$ (m^2)	$k^{(2)}$ $(\times 10^{-12})$ (m^2)
Vub1	86.5	184.5	42.52	1.996 – 2.260	72.64	330.49
Vub2	108.5	230	48.19	2.641 – 2.905	69.91	314.16
Vub3	101	218.5	42.52	2.553 – 2.817	70.61	330.46

6.3.4 Experiments on gravitational effects

As it is well know that for a two-dimensional flow experiment, the test plane can always be chosen in a horizontal plane in which the gravitational effect can be neglected. However, for a three-dimensional flow experiment, the gravitational effect along the vertical direction has to be considered. Although in Darcy's original experiment, the gravitational effect was considered, but this effect is nearly always neglected in modern references. From a practical viewpoint, during the production process of a big composite structure, such as, build a ship hull, some parts of the total structure have to be located in the vertical direction. Therefore, the gravitational effect can not be avoided. In these experiments, the radial flow happens on a vertical plane and the injection pressures are also as low as possible to make the gravitational effect more obvious. It has been theoretically derived that the effect of the gravitation on two- or three-dimensional radial flows is to produce a translation of the wetted domain of the medium. This translation is along the flow vector direction caused by the gravitation, which is not same as the direction of the gravity for general anisotropic cases. To avoid the effect of the gravity on permeability identification measurements, a moving coordinate system fixed at the centre of the wetted area is presented, which provides a convenience in experiments. Therefore, equations (4.56), (5.39) and (5.40) can also be used to calculate the permeabilities of isotropic or anisotropic materials, respectively. The translation distance caused by the gravitational effect on isotropic media can be obtained by equation (5.29) and equation (5.41) is used for anisotropic media. As one of principal direction of anisotropic materials is arranged along the gravity direction in this part of experiments, the translation distance can be obtained by using equation (5.43).

A. Experiments on U750-450

In these experiments, the radial flow is on a vertical plane and the injection pressures are chosen as low as possible to want to make the gravitational effect more obvious. Figures C.19, C.20, C.21 and C.22 give the inlet pressure measured

at the injection gate of these radial flow tests on the vertical plane for U750-450. Equations (4.56) and (5.29) are used to calculated the permeabilities and translation distances, respectively. The permeabilities of this continuous filament mat and translation distance d_g (measured and calculated) are summarised in Tables 6.14, 6.15 and 6.16. Figure D.8 shows the images of the tests Gr3.

Table 6.14: Results of U750-450 in vertical plane with $v_f = 22.7\%$, $N = 3$ and $H = 2.32mm$.

Run	Results of experiments					Results of calculation		
	X_1	X_2	d_g	t	p^0	$k^{(1)}$ $(\times 10^{-12})$	$k^{(2)}$ $(\times 10^{-12})$	d_g
No.	(mm)	(mm)	(mm)	(s)	(bar)	(m^2)	(m^2)	(mm)
Gr1	198.5	194	2.1	45.65	1.476	1544.13	1461.09	2.11
Gr2	140.5	136.5	3.7	85.13	1.124	1487.86	1385.11	3.74
Gr3	192.5	190	4.8	105.62	1.206	1491.64	1445.29	4.84
Gr4	160	155	2.3	54.22	1.256	1470.58	1360.50	2.34
Gr5	159	157	2.6	58.83	1.239	1430.72	1387.03	2.59
Gr6	160	159	2.5	59.15	1.251	1383.88	1352.44	2.54

Table 6.15: Results of U750-450 in vertical plane with $v_f = 45.5\%$, $N = 6$ and $H = 2.32mm$.

Run	Results of experiments					Results of calculation		
	X_1	X_2	d_g	t	p^0	$k^{(1)}$ $(\times 10^{-12})$	$k^{(2)}$ $(\times 10^{-12})$	d_g
No.	(mm)	(mm)	(mm)	(s)	(bar)	(m^2)	(m^2)	(mm)
Gra1	189.5	187	1.7	119.29	1.529	334.52	323.95	1.74
Gra2	214	211.5	2.0	139.86	1.605	333.21	323.96	2.04
Gra3	201	199.5	2.6	174.65	1.413	339.74	333.67	2.62

Table 6.16: Results of U750-450 in vertical plane with $v_f = 22.7\%$, $N = 6$ and $H = 4.64mm$.

Run	Results of experiments					Results of calculation		
No.	X_1 (mm)	X_2 (mm)	d_g (mm)	t (s)	p^0 (bar)	$k^{(1)}$ ($\times 10^{-12}$) (m^2)	$k^{(2)}$ ($\times 10^{-12}$) (m^2)	d_g (mm)
Grb1	250	246.5	3.6	76.13	1.498	1535.56	1485.00	3.58
Grb2	206	202.5	2.6	54.54	1.439	1537.06	1478.03	2.56
Grb3	251.5	249	3.0	62.78	1.613	1526.71	1490.93	2.97

B. Experiments on twill weave fabric

In this part of experiments, one of principal directions with a bigger permeability value, is arranged in the vertical direction. Also a lower injection pressure is used for each experiment. Figures C.23 and C.24 show the inlet pressure of the six radial flow tests on the twill fabric RC 600 and Figure C.25 shows the inlet pressure of the tests on WRE580T. The experimental results, which can be calculated by equation (5.39), (5.40) and (5.41) or (5.43), are listed in Tables 6.17 and 6.18. Figure D.9 shows the images of the tests Gt2.

Table 6.17: Results of RC 600 in vertical plane with $v_f = 50.4\%$, $N = 5$ and $H = 2.32mm$.

Run	Results of experiments					Results of calculation		
	X_1	X_2	d_g	t	p^0	$k^{(1)}$ $(\times 10^{-12})$	$k^{(2)}$ $(\times 10^{-12})$	d_g
No.	(mm)	(mm)	(mm)	(s)	(bar)	(m^2)	(m^2)	(mm)
Gt1	116	75	0.7	262.82	1.379	50.08	20.94	0.65
Gt2	120	76	0.7	260.02	1.412	50.34	20.19	0.65
Gt3	126	79.5	0.4	167.41	1.716	50.28	20.02	0.42
Gt4	104	66.5	0.4	142.20	1.528	49.21	20.12	0.35
Gt5	130	82	0.8	302.86	1.437	49.89	19.85	0.75
Gt6	138	89	0.6	253.40	1.642	47.26	19.66	0.59

Table 6.18: Results of WRE580T in vertical plane with $v_f = 58.6\%$, $N = 6$ and $H = 2.32mm$.

Run	Results of experiments					Results of calculation		
No.	X_1 (mm)	X_2 (mm)	d_g (mm)	t (s)	p^0 (bar)	$k^{(1)}$ ($\times 10^{-12}$) (m^2)	$k^{(2)}$ ($\times 10^{-12}$) (m^2)	d_g (mm)
Gtb1	189.5	190.5	0.7	259.09	2.282	47.63	48.13	0.74
Gtb2	184.5	187.5	1.2	316.54	1.750	63.06	65.13	1.22
Gtb3	199.5	200	1.6	516.06	1.671	52.17	52.43	1.60

C. Experiments on E-LPb 567

The X_2 direction of this material (one of principal directions) is arranged in the vertical direction and a lower injection pressure is used for each experiment. Figures C.26, C.27, C.28 and C.29 show the inlet pressures measured at the injection gate in the radial flow tests on the E-LPb 567. Equation (5.39), (5.40) and (5.41) or (5.43) are used in these tests. The results are given in Tables 6.19, 6.20 and 6.21. Figure D.10 shows the images of the tests Gu3.

Table 6.19: Results of E-LPb 567 in vertical plane with $v_f = 44.5\%$, $N = 4$ and $H = 2.32mm$.

Run	Results of experiments					Results of calculation		
No.	X_1 (mm)	X_2 (mm)	d_g (mm)	t (s)	p^0 (bar)	$k^{(1)}$ $(\times 10^{-12})$ (m^2)	$k^{(2)}$ $(\times 10^{-12})$ (m^2)	d_g (mm)
Gu1	101	220	2.3	162.80	1.472	67.40	319.77	2.29
Gu2	99	217	3.3	249.80	1.324	61.71	296.48	3.26
Gu3	85	186	4.2	300.22	1.178	66.07	316.38	4.18
Gu4	80	155	1.7	144.34	1.277	72.45	271.97	1.73
Gu5	100.5	223	2.6	193.28	1.422	63.01	310.27	2.64
Gu6	96	202	2.2	159.18	1.407	70.62	312.67	2.19

Table 6.20: Results of E-LPb 567 in vertical plane with $v_f = 55.6\%$, $N = 5$ and $H = 2.32mm$.

Run	Results of experiments					Results of calculation		
	X_1	X_2	d_g	t	p^0	$k^{(1)}$ $(\times 10^{-12})$	$k^{(2)}$ $(\times 10^{-12})$	d_g
No.	(mm)	(mm)	(mm)	(s)	(bar)	(m^2)	(m^2)	(mm)
Gua1	99	219.5	1.5	210.92	1.731	25.27	124.20	1.45
Gua2	119.5	260	2.2	315.71	1.737	26.63	126.07	2.20
Gua3	125.5	278.5	2.8	417.38	1.681	24.65	121.41	2.80

Table 6.21: Results of E-LPb 567 in vertical plane with $v_f = 44.5\%$, $N = 8$ and $H = 4.64mm$.

Run	Results of experiments					Results of calculation		
	X_1	X_2	d_g	t	p^0	$k^{(1)}$ $(\times 10^{-12})$	$k^{(2)}$ $(\times 10^{-12})$	d_g
No.	(mm)	(mm)	(mm)	(s)	(bar)	(m^2)	(m^2)	(mm)
Gub1	132.5	281	2.9	207.78	1.683	70.22	315.81	2.90
Gub2	130	271.5	2.6	188.51	1.700	71.97	313.89	2.61
Gub3	94.5	201	1.8	126.05	1.483	71.59	323.90	1.80

Chapter 7

Discussion of results

7.1 Introduction

The aim of this chapter is to discuss the significance of the results developed in previous Chapters. This discussion will include the following aspects:

- The permeability identification with variable pressure.
- The gravitational effect on permeability identification.
- Suggest a guideline for practical implementation of the developed methods.

7.2 The permeability identification with variable pressure

7.2.1 Genesis

In practical experiments or production processes, it is, sometimes, very difficult to keep a constant inlet pressure.

Figure 7.1 represents a inlet pressure recorded during the constant pressure test Cu5 and the variable pressure experiment Vua1. The quasi-unidirectional non-crimp fabric E-LPb 567 is used in both of tests. This figure demonstrates that it

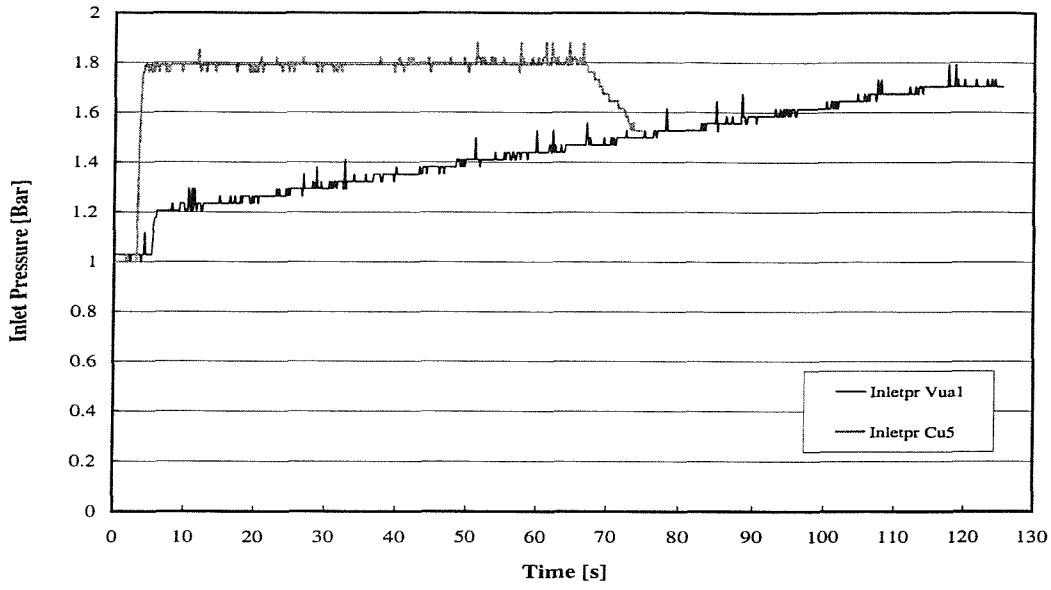

Figure 7.1: The inlet pressure recorded in experiments Cu5 and Vua1.

is hard to keep a constant pressure at the injection port. Although a lower pressure used in the experiments, two different pressure histories are recorded, one is constant pressure and another is variable pressure. As also shown in Figures C.7, C.8, C.9, C.10, C.11, C.12 , C.13, C.14, C.15, C.16, C.17 and C.18, the inlet pressure are often variable with respect to time t. It is noticeable from this that where the injection pressure can not be controlled accurately there is a need to allow for the pressure variations in estimation of permeabilities. In most practical cases it is not known that if the inlet pressure can be kept as a constant, therefore the variable inlet pressure formulations and the corresponding experiment methods are required. Even in the case of which the recorded time history of the inlet pressure demonstrates that it is a constant, the variable pressure formulation can still obtain the same results without adding more calculation task.

By using the variable pressure formulation, it is no longer necessary to adopt or design a particular method to keep a constant inlet pressure but only to record the real time history of the inlet pressure and to calculate the permeabilities. This provides a convenience in practical applications. Therefore the variable inlet pressure formulations are very useful for permeability identification.

7.2.2 Theoretical results

The variable pressure formulations for permeability identification developed in this thesis are generalized formulations which include the traditional constant pressure formulation as a special case.

This main point is valid for all of the formulations developed for two-dimensional and three-dimensional cases described in Chapter 5. For example, for the two-dimensional case, equation (4.56) is given in this thesis to calculate the permeability of an isotropic fabric by using experiments with variable inlet pressure. If the pressure is constant, this equation degenerates to equation (2.20) which is the well known traditional formulation for constant inlet pressure tests and it is

$$k = -[r^{f\,2}(2\ln\frac{r^f}{r^0} - 1) + r^{0\,2}]\frac{\varepsilon\mu}{4(p^f - p^0)t}. \tag{7.1}$$

This equation is widely used in great number of references, for example, Adams et al. 1986, 1987,1988, 1991a and 1991b, Weitzenböck 1996, 1999a and 1999b. For anisotropic materials, equations (5.39) and (5.40) are derived in this research to calculate the permeabilities by using experiments with variable inlet pressures. Again, if the pressure is constant, the integral P in these two equations, represented by equation (5.37), degenerates to

$$P = (p^f - p^0)t, \tag{7.2}$$

and therefore equations (5.39) and (5.40) degenerate to,

$$k^{(1)} = \frac{a^2}{\overline{r}^{f\,2}} = \frac{a^2\mu\varepsilon(\ln B - B + 1)}{4(p^f - p^0)t} \tag{7.3}$$

$$k^{(2)} = \frac{b^2}{\overline{r}^{f\,2}} = \frac{b^2\mu\varepsilon(\ln B - B + 1)}{4(p^f - p^0)t}, \tag{7.4}$$

which are the traditional formulations for constant inlet pressure tests, and used in modern references, for example, Chan et al 1991 and 1993, Weitzenböck 1996.

7.2.3 Experimental method

A practical experiment method for two-dimensional case corresponding to the developed formulations for variable inlet pressure tests is well designed as described in Chapter 6. This method has been conducted by using the RTM test facilities in the Transport Systems Research Laboratory of the School of Engineering Sciences, the University of Southampton. The results obtained by the generalized new method has been validated and its implementation in practice is applicable.

For the proposed experiment process with variable inlet pressures, only two measurements of the flow front along the two directions are needed. The flow fronts along these two directions, two principal directions of the anisotropic fabric, correspond to the maximum and the minimum diameters of the recorded flow figures, respectively, which can be found by observing the recorded flow front figures as listed in Figures D.1 - D.10. Hence it is not necessary to know the principal directions of a material before the experiments.

7.2.4 Validation of the approach

To validate the new theory and the corresponding experimental approach, the following two kinds of comparison experiments are designed and conducted.

Comparison between the results of variable pressure tests and constant pressure tests

The experiments with constant inlet pressure and the corresponding comparative experiments with variable inlet pressure are conducted in this research as shown in Chapter 6. For these experiments with the constant inlet pressure, an as lower as possible pressure is used to easily keep the pressure as an constant at

the inlet gate. The equations (2.20), (7.3) and (7.4) for constant pressure cases are used to calculate the permeabilities. The details of the recorded flow front figures and the results are given by Figures D.1, D.2 D.3 and Tables 6.2, 6.3 and 6.4, respectively. For the comparative experiments of the same materials as the corresponding constant pressure tests, when a higher injection pressure is used, it was found that the recorded inlet pressure is not a constant, it is variable with respect to time, as shown in Figures C.7 - C.18. Therefore, to calculate the permeabilities under variable inlet pressure condition, equations (2.20), (7.3) and (7.4) are are not valid, and the new equations (4.56), (5.39) and (5.40) which developed in Chapters 4 and 5 should be used. The results are listed in the section 6.4.3.

Table 7.1: The averaged permeability of each kind of experiment in set up I ($\times 10^{-12}\ m^2$) and differences.

Fibre	Set up	Constant inlet pressure		Variable inlet pressure		Difference %	
		$k^{(1)}$	$k^{(2)}$	$k^{(1)}$	$k^{(2)}$		
U750-450	I	1433.26	1399.58	1498.59	1454.94	4.56	3.96
RC 600	I	49.38	21.67	51.61	25.27	4.61	11.51
E-LPb 567	I	65.37	312.08	70.65	326.58	8.08	4.65

The averaged results obtained in the experiments set up I are listed in Table 7.1. If it is assumed that the results obtained by the experiments with constant inlet pressure are 'idealized results', the differences in results obtained in the experiments with variable inlet pressure are also listed in Table 7.1.

Comparison with literature

As it is described in Chapter 3, the permeability is a constant of the material, it does not depend on the methods to be used to measure it. Therefore, for a

same fabric and same fibre volume fraction the measured permeabilities reported in the literature are comparable.

Table 7.2: The results for random mat U750-450 reported in the references and the results(*) obtained in this thesis ($\times 10^{-10} m^2$).

Investigators	Range of permeability		v_f
	$k^{(1)}$	$k^{(2)}$	(%)
Greve (1990)	9-14		20-25
Chick (1996)	6-20	5-21	20-25
Rudd (1996)	10-20		20-25
Weitzenböck (1996)	15.94	15.62	22.7
Rudd (1997)	5-30		20-25
Constant pressure*	14.33	14.00	22.7
Variable pressure*	14.99	14.55	22.7

Table 7.2 and Table 7.3 provides comparisons of the permeability obtained in this thesis with some experiment results reported in the references. Table 7.4 is for the continuous filament mat (U750-450) and Table 7.5 is for the twill fabric RC 600 and the quasi-unidirectional non crimp fabric E-LPb 567. A good agreement is observed between our results and the one reported by Weitzenböck (1996). Also, from these reported results, it can be found that there exists an obvious difference between the permeability values for these fabric measured by different authors. In Consideration of these practical cases in the field of permeability identification, the 11.51% difference in Table 7.1 is acceptable from a point of view of engineering applications. Therefore, it can be concluded form Table 7.1 that there is a good agreement in the results obtained by using the new methods developed in this thesis compared with the results obtained by the traditional method of constant inlet pressure. These experiments demonstrate that:

Table 7.3: Published results for twill and quasi-unidirectional non-crimp fabric the results(*) obtained in this thesis ($\times 10^{-10} m^2$).

Investigators	RC 600			E-LPb 567		
	$k^{(1)}$	$k^{(2)}$	$v_f(\%)$	$k^{(1)}$	$k^{(2)}$	$v_f(\%)$
Fell (1996)	61.9	15.2	50.5	/	/	/
Gebart (1996)	/	/	/	39.2-80.6	222.7-590.9	40-50
Rudd (1997)	/	/	/	30.1-85.3	200.4-550.5	40-50
Weitzenböck (1996)	50.5	24.5	50.4	74.18	304.5	44.3
Constant pressure*	49.38	21.67	50.4	65.37	312.08	44.3
Variable pressure*	51.61	25.27	50.4	70.65	326.58	44.3

- The mathematical analysis and the new formulations developed in this thesis are correct. These formulations provide the theoretical basis of the new generalized method to identify permeabilities by using variable inlet pressure.

- The implementation of the new method with variable inlet pressure is applicable by using the RTM facilities of permeability identification in the Transport Systems Research Laboratory of the School of Engineering Sciences.

- The results obtained by the generalized new methods has been validated.

7.3 Gravitational effect on permeability identification

7.3.1 Genesis

As it is well known that for the permeability identification experiments in two-dimensional case, it can always choose a horizontal plane as the experimental

plane, then the gravitational effect does not need to be considered. However, for a three-dimensional flow experiment or the production process of a big composite structure, such as, build a ship hull, in which some parts of the total structure have to be located in the vertical direction, there exists the gravitational effect in the vertical direction. This effect has to be considered and need to be avoided during permeability identification experiments. Although in Darcy's original experiment, the gravitational effect was considered, but this effect is nearly always neglected in modern references, for example, Gauvin et al 1986 and 1996, Fracchia et al 1989, Bruschke et al 1990, Kim et al 1991, Gebart et al 1991, 1992 and 1996 and Perry et al 1992 in channel flow tests and Adams et al. 1986, 1987,1988, 1991a and 1991b, Chan et al 1991, 1993, Chick 1996, Gauvin 1996, Gebart et al 1996, Rudd 1995, Weitzenböck 1996, 1999a and 1999b in radial flow tests.

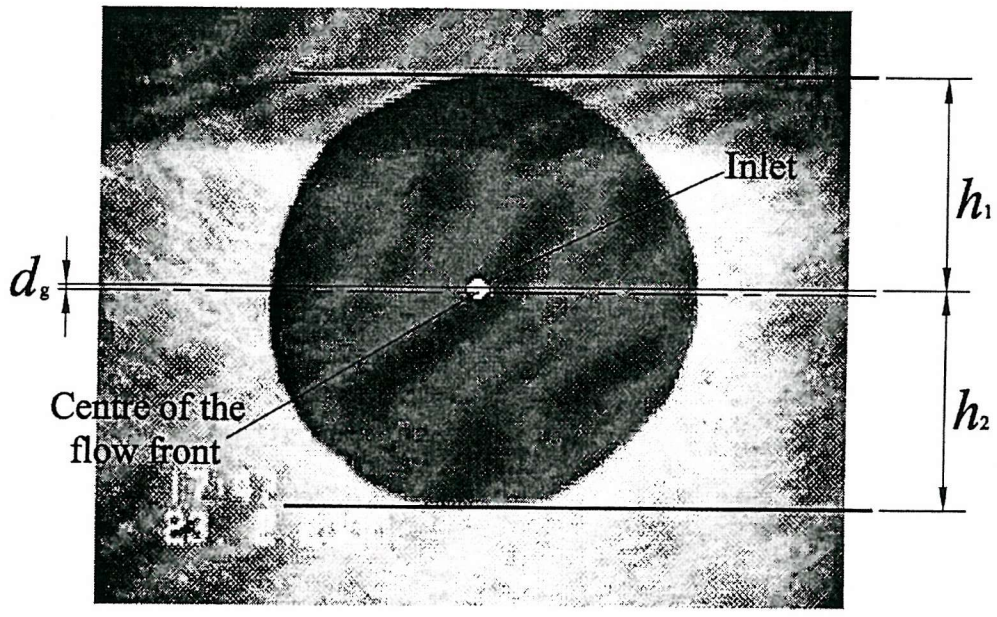

Figure 7.2: The flow front recorded in the experiments Gr3 at 105.62 s.

Figure 7.2 shows the flow front recorded in the test Gr3 that is a radial flow

happening on a vertical plane. In this figure, h_1 is the distance from the centre of inlet to the top of flow front and h_2 is the distance from the centre of inlet to the bottom of flow front. The d_g is the translation distance, in the other words, d_g is distance from the centre of inlet to the centre of wetted domain of the fabric and it can be obtained by the following equation

$$d_g = \frac{h_2 - h_1}{2}, \tag{7.5}$$

in the experiment.

If the gravitational effect is not considered in the experiments, the permeabilities measured for the three kind fabric along the vertical direction are list in Tables 7.4, 7.5 and 7.6. In these tables h_1 and h_2 are two distances as shown in Figure 7.2, k_1 and k_2 are two permeabilities calculated by using h_1 and h_2, respectively. As can be seen from these tables, the differences between the results measured by using the developed method to avoid the gravitational effect and the results affected by the gravitation can be upto -12.56% or 13.51%. Therefore, the gravitational effect should be considered for a three-dimensional flow case or a two-dimensional flow which happens on the vertical plane.

Table 7.4: Differences of U 750-450.

Set	h_1	h_2	k_1	k_2	k^r	Difference	
Up	mm	mm	$10^{-12}\ m^2$	$10^{-12}\ m^2$	$10^{-12}\ m^2$	h_1 %	h_2 %
Gr1	97.2	101.4	1466.55	1623.94	1544.13	-5.02	5.17
Gr2	66.6	74.0	1301.00	1688.86	1487.86	-12.56	13.51
Gr3	91.5	101.1	1318.08	1677.23	1491.64	-11.64	12.44
Gr4	77.7	82.3	1369.13	1576.08	1470.58	-6.90	7.17
Gr5	75.9	81.1	1276.97	1502.19	1430.72	-10.75	5.00
Gr6	77.8	82.8	1280.64	1491.61	1383.88	-7.46	7.78

Table 7.5: Differences of RC 600.

Set Up	h_1 mm	h_2 mm	k_1 $10^{-12}\ m^2$	k_2 $10^{-12}\ m^2$	$k^{(1)}$ $10^{-12}\ m^2$	Difference h_1 %	Difference h_2 %
Gt1	57.3	58.7	48.88	51.30	50.08	-2.40	2.44
Gt2	59.3	60.7	49.17	51.52	50.34	-2.32	2.34
Gt3	62.6	63.4	49.65	50.92	50.28	-1.25	1.27
Gt4	51.6	52.4	48.46	49.97	49.21	-1.52	1.54
Gt5	64.2	65.8	48.67	51.13	49.89	-2.45	2.49
Gt6	68.4	69.6	46.44	48.08	47.26	-1.74	1.74

Table 7.6: Differences of E-LPb 567.

Set Up	h_1 mm	h_2 mm	k_1 $10^{-12}\ m^2$	k_2 $10^{-12}\ m^2$	$k^{(2)}$ $10^{-12}\ m^2$	Difference h_1 %	Difference h_2 %
Gu1	107.7	112.3	306.54	333.28	319.77	-4.14	4.22
Gu2	105.2	111.8	278.72	314.78	296.48	-5.99	6.17
Gu3	88.8	97.2	288.45	345.60	316.38	-8.83	9.24
Gu4	75.8	79.2	260.17	284.03	271.97	-4.34	4.43
Gu5	108.9	114.1	295.97	324.91	310.27	-4.61	4.72
Gu6	98.8	103.2	299.20	326.44	312.67	-4.31	4.40

7.3.2 Theoretical results and experiment method to avoid the gravitational effect

The effect of the gravitation on two- or three-dimensional radial flows is to produce a translation of the wetted domain of the medium. This translation is along the flow vector direction caused by the gravitation, which is not same as the direction of the gravity for general anisotropic cases as demonstrated in Section 4.2.2.

The translation distance caused by the gravitational effect on isotropic media satisfies equation (5.29), i.e.

$$d_g = \frac{k^r}{\mu\varepsilon}\rho g t, \tag{7.6}$$

and equation (5.41) is used for anisotropic media. As one of principal directions of anisotropic materials with bigger permeability value is arranged along the gravity direction in the experiments, the translation distance satisfies equation (5.43), i.e.

$$d_g = \frac{k^{(2)}}{\mu\varepsilon}\rho g t. \tag{7.7}$$

As can be seen from these two equations, the translation displacement of the centre of the wetted area is in proportion to permeability of fabric and the injection time.

To avoid the effect of the gravity on permeability identification, a moving coordinate system fixed at the centre of the wetted area is used to measure the flow front, that is to measure the flow front relative to the centre of the wetted domain. This method provides a convenience to avoid the gravitational effect in experiments. Through this method, the equations obtained in the case with no gravitational effect can still be used in the case considering the gravitational effect. For example, equations (4.56), (5.39) and (5.40) can be used to calculate the permeabilities of isotropic or anisotropic materials, respectively.

7.3.3 Experimental results

To demonstrate the theoretical results of the developed method to avoid the gravitational effect, a two-dimensional radial flow which happens on the vertical plane is well designed as described in Chapter 6. This method has also been conducted by using the RTM facilities. The results obtained by this new method has been validated and its implementation in practice is applicable.

In these experiments, the aluminium base plate (see Figure 6.1) is arranged on the vertical plane and the radial flow happens on this plane. The injection pressures

are chosen as low as possible to make the gravitational effect more obvious. By using the method to avoid the gravitational effect, the measurements are conducted and equations (4.56), (5.39) and (5.40) are used to calculate the permeabilities. The calculated results are listed in section 6.4.4. The main averaged permeabilities of experiments set up I and the difference in results between the constant inlet pressure experiments and the experiments of gravitational effect are listed in Table 7.7. It is observed from this table that there is a good agreement in the results, obtained by using the method developed in this thesis to avoid the gravitational effect, compared with the results obtained by the experiments in the horizontal plane using the traditional method of constant inlet pressure. It is demonstrated that the mathematical analysis and the experiment method to avoid the gravitational effects in permeability identification are valid.

Table 7.7: The averaged permeability of each kind of experiment in set up I ($\times 10^{-12}\ m^2$) and differences.

Fibre	Set up	Constant inlet pressure		Gravitational effect		Difference	
		$k^{(1)}$	$k^{(2)}$	$k^{(1)}$	$k^{(2)}$	%	
U750-450	I	1433.26	1399.58	1468.14	1398.58	2.43	-0.07
RC 600	I	49.38	21.67	49.12	19.97	-0.51	-9.23
E-LPb 567	I	65.37	312.08	66.88	304.59	2.31	-2.41

The translation distances, measured and calculated by using equations (7.6) and (7.7) of experiments set up I, are listed in Table 7.8. In this table, d_g^* represents the translation distance which measured during the experiments.

As can be seen in Table 7.8, there is a good agreement between the results of the translation distance measured and calculated.

Table 7.8: The translation distance of experiments set up I (mm).

Run No.	U 750-450			
	t (s)	k^r ($\times 10^{-12}$ m^2)	d_g	d_g^*
Gr1	45.65	1544.13	2.11	2.1
Gr2	90.13	1487.86	3.74	3.7
Gr3	105.62	1491.64	4.84	4.8
Gr4	54.22	1470.58	2.34	2.3
Gr5	58.83	1430.72	2.59	2.6
Gr6	59.15	1383.88	2.54	2.5
Run No.	RC 600			
	t (s)	$k^{(1)}$ ($\times 10^{-12}$ m^2)	d_g	d_g^*
Gt1	262.82	50.08	0.65	0.7
Gt2	260.02	50.34	0.65	0.7
Gt3	167.41	50.28	0.42	0.4
Gt4	142.20	49.21	0.35	0.4
Gt5	302.86	49.89	0.75	0.8
Gt6	253.40	47.26	0.59	0.6
Run No.	E-LPb 567			
	t (s)	$k^{(2)}$ ($\times 10^{-12}$ m^2)	d_g	d_g^*
Gu1	162.80	319.77	2.29	2.3
Gu2	249.80	296.48	3.26	3.3
Gu3	300.22	316.38	4.18	4.2
Gu4	144.34	271.97	1.73	1.7
Gu5	193.28	310.27	2.64	2.6
Gu6	159.18	312.67	2.19	2.2

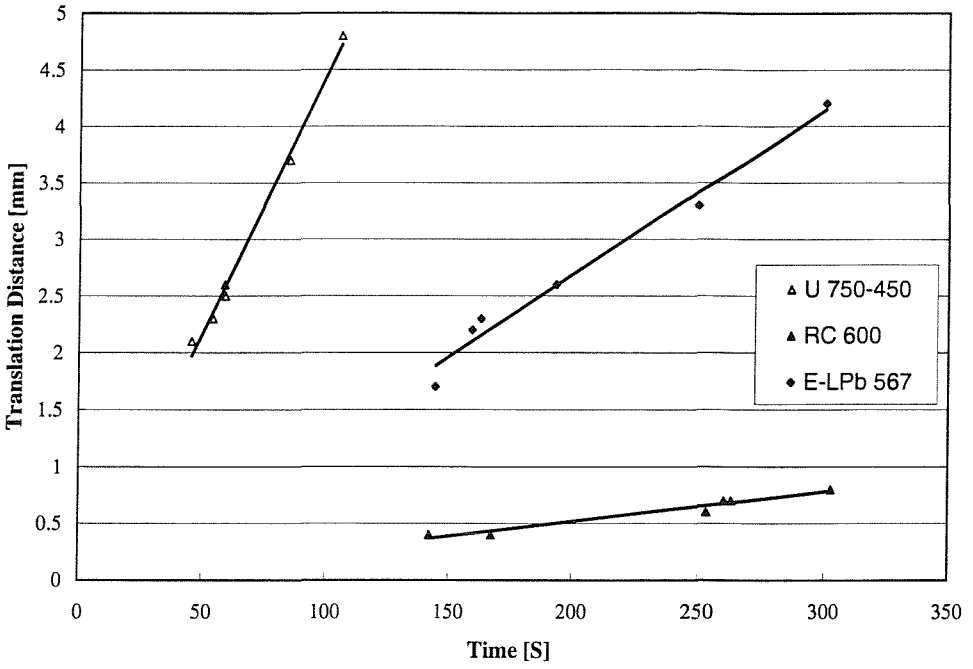

Figure 7.3: The relation between the translation distance and time.

Figure 7.3 shows the relation between the translation distance and flow time for three kinds of fabric in experiments set up I. As can be seen the translation displacement of the centre of the wetted area is in proportion to the injection time. These results demonstrate that the theoretical formulations (7.6) and (7.7) are valid.

7.4 A suggestion guideline

In base of the discussions given above, the following guideline for practical implementation of the scheme in an industrial context is suggested.

- Because in most practical cases it is not known that if the inlet pressure can be kept as a constant, the variable inlet pressure formulations and the corresponding experiment methods are recommended. Even in the case of which the recorded time history of the inlet pressure demonstrates that the

inlet pressure is a constant, the variable pressure formulation can provide the same results without adding more calculation task.

If from the previous experience, the inlet pressure is definitely a constant, the constant pressure formulation can be used.

- For all experiments or practical production in two-dimensional cases, it is suggested to choose the horizontal plane as the test plane . In this experiment arrangement, the gravitational effect is automatically avoided.

- For any experiment in three-dimensional cases or any production process of a big composite structure in which some parts of the total structure have to be located in the vertical direction, the gravitational effect needs to be considered. The method developed in this thesis provides a very simple way to avoid the gravitational effect. The only thing is to consider the translation of the centre of the wetted fibre area and do all of same calculations as in the case without the gravitational effect.

- The translation distance of the centre of the wetted area is proportional to the flow time. Therefore, for a long time flow process in experiments, it is better to use the method given in the thesis to avoid the gravitational effect. If the flow time is very short, the gravitational effect will not cause significant error.

Chapter 8

Conclusions and Recommendations

8.1 Conclusions

The fundamental research areas concerning RTM are categorized into three main topics: permeability identification, flow analysis and injection pressure predication. The permeability identification is a base of these three research topics and is theoretically and experimentally investigated in this thesis. The main contributions are summarised as follows:

1) Under the generalized boundary conditions in which the inlet pressures or the inlet flow rates are considered as time functions, several analytical solutions for both channel flows and radial flows in two- and three-dimensional cases through isotropic or anisotropic fibre preform are developed. These analytical solutions present a theoretical basis of permeability identification by using variable inlet pressures or variable inlet flow rates. Based on these results, the inlet pressure or inlet flow rate during a permeability identification experiment are no longer to be controlled as a constant, which may be difficult in practical RTM production processes. By measuring the real variable time histories of the inlet pressures or inlet flow rates and the flow front positions in an experiment, the principal

permeabilities can be calculated by means of the theoretical solutions presented in this thesis.

2) Following the original contribution developed by Darcy (1856), the gravitational effect on permeability identification experiments is investigated, which is not considered in current references. This proposed research topic is based on the fact that in practical RTM production processes some parts have to be located in the vertical direction along which the gravitational effect acts. It has been theoretically derived that the effect of the gravitation on two- or three-dimensional radial flows is to produce a translation of the wetted domain of the medium. This translation is along the flow vector direction caused by the gravitation, which is not same as the direction of the gravity for general anisotropic cases.

To avoid the effect of the gravity on permeability identification measurements, a moving coordinate system fixed at the centre of the wetted area is presented, which provides a convenience in experiments.

3) By using the facility of permeability measurement in the Transport Systems Research Laboratory, the School of Engineering Sciences, University of Southampton, eighty seven practical identification experiments in two-dimensional radial flows through isotropic and anisotropic materials have been done. The results measured in the cases of variable inlet pressure and the gravitational effect are compared with the results in the constant inlet pressure experiment obtained by this research and the other published research papers. The errors are in the region acceptable to the permeability measurement area. The experiments demonstrate that the analytical solutions are valid and the corresponding permeability identification methods are applicable and attractive.

8.2 Further research considerations

1) Although some theoretical solutions for three-dimensional cases are presented in this thesis, practical permeability identification experiments have not been done. The materials used in three-dimensional experiments should have a three-dimensional fibre preform characteristics. The three kinds of fabric used in the two-dimensional experiments given in this thesis are not suitable to three-dimensional experiments. The reason is that the fabric sheets of all materials are very thin and the direction normal to the fabric sheet plane is one principal direction of the permeability tensor of a thick fabric preform constructed by a lot of these thin fabric sheets. As a result of this, a generalized three-dimensional material can not be obtained during this research period, and therefore the corresponding three-dimensional experiments can not be done.

2) Two characteristics of the generalized permeability tensor for anisotropic materials are obtained in the thesis. These results may be used to check the independence of the measurement directions in three-dimensional experiment. A further research for this consideration needs to be done.

3) The techniques to measure the flow front in three-dimensional experiments are needed. The method presented in this thesis is difficult to be used in three-dimensional experiment, as the flow front in a three-dimensional body constructed by fibre materials is not observed. If thermistor sensors are used to measure the flow front, these thermistor sensors have to be arranged into the experiment preform while to construct this preform before doing experiment. For a practical three-dimensional material, it is very difficult to put the thermistor sensors into it without cutting the material.

4) The date has potential to provide validation of the effect of gravity on commercial flow simulation software.

Appendix A

The summation convention, the Kronecker delta and the permutation symbol

A system of three linear equations in three unknowns can be written as

$$\begin{aligned} a_{11}x_1 + a_{12}x_2 + a_{13}x_3 &= b_1 \\ a_{21}x_1 + a_{22}x_2 + a_{23}x_3 &= b_2 \\ a_{31}x_1 + a_{32}x_2 + a_{33}x_3 &= b_3 \end{aligned} \tag{A.1}$$

or its matrix form

$$\begin{bmatrix} a_{11} & a_{12} & a_{12} \\ a_{21} & a_{22} & a_{23} \\ a_{31} & a_{32} & a_{33} \end{bmatrix} \begin{bmatrix} x_1 \\ x_2 \\ x_3 \end{bmatrix} = \begin{bmatrix} b_1 \\ b_2 \\ b_3 \end{bmatrix}, \tag{A.2}$$

where $x_j (j = 1, 2, 3)$ are the unknowns, a_{ij} and b_i $(i = 1, 2, 3)$ are known constants. This equation can also be written as

$$\sum_{j=1}^{3} a_{ij}x_j = b_i, \tag{A.3}$$

where the symbol $\sum_{j=1}^{3}$ denotes summation over the repeated subscript j. The final notational simplification consists of omitting the summation symbol in equa-

tion (A.3), which is now written in the form

$$a_{ij}x_j = b_i. \tag{A.4}$$

It is noted that the index i appears only once in each term of equation (A.4). It is called the free index. The index j is repeated, and this repetition implies summation with respect to j in equation (A.4). The index j in equation (A.4) is called the summation index.

General rules of the summation convention can be stated as follows. When an index (subscript) is repeated in an expression of the form A_iB_i, C_{jj} or $\frac{\partial f_k}{\partial x_k} \equiv f_{k,k}$, it is called a summation index and the expression is a sum of three terms that can be obtained by summing over the range $(1, 2, 3)$. Consequently,

$$\begin{aligned} A_iB_i &\equiv A_1B_1 + A_2B_2 + A_3B_3, \\ C_{jj} &\equiv C_{11} + C_{22} + C_{33}, \\ \frac{\partial f_k}{\partial x_k} &\equiv \frac{\partial f_1}{\partial x_1} + \frac{\partial f_2}{\partial x_2} + \frac{\partial f_3}{\partial x_3} \\ &\equiv f_{k,k} \equiv f_{1,1} + f_{2,2} + f_{3,3}. \end{aligned} \tag{A.5}$$

It is also noted that in the case of a repeated subscript, the actual symbol used is immaterial. For example,

$$\begin{aligned} A_iB_i &\equiv A_jB_j \equiv A_kB_k, \\ C_{jj} &\equiv C_{kk} \equiv C_{ii}, \\ f_{i,i} &\equiv f_{k,k} \equiv f_{j,j}, \end{aligned} \tag{A.6}$$

and so on. In this thesis, only small english letters in subscripts are considered as tensor indices which obey this summation convention.

The Kronecker delta δ_{ij} and the permutation symbol e_{ijk} are the two notational devices that enhance the convenience of the repeated subscript summation convention described above. They are defined by

$$\delta_{ij} = \begin{cases} 1 & \text{if } i = j \\ 0 & \text{if } i \neq j \end{cases} \tag{A.7}$$

and

$$e_{ijk} = \begin{cases} 1 & \text{for } ijk = 123, 231, 312 \\ -1 & \text{for } ijk = 132, 321, 213 \\ 0 & \text{for } ijk = \text{others} \end{cases}, \tag{A.8}$$

respectively. From these definitions, we can say that δ_{ij} is symmetric with respect to its indices i and j, and e_{ijk} is skew-symmetric with respect to an interchange of any two of its subscripts. It can be checked that the following formulations are valid, i.e.

$$\begin{aligned} \delta_{ij}A_i &= A_j, \\ \delta_{ij}\delta_{jk} &= \delta_{ik}, \\ e_{ijk} &= \begin{vmatrix} \delta_{i1} & \delta_{i2} & \delta_{i3} \\ \delta_{j1} & \delta_{j2} & \delta_{j3} \\ \delta_{k1} & \delta_{k2} & \delta_{k3} \end{vmatrix}, \\ e_{ijk}e_{pqr} &= \begin{vmatrix} \delta_{ip} & \delta_{iq} & \delta_{ir} \\ \delta_{jp} & \delta_{jq} & \delta_{jr} \\ \delta_{kp} & \delta_{kq} & \delta_{kr} \end{vmatrix}, \\ e_{ijk}e_{irs} &= \delta_{jr}\delta_{ks} - \delta_{js}\delta_{kr}. \end{aligned} \tag{A.9}$$

Consider the determinant

$$a \equiv |a_{ij}| \equiv \begin{vmatrix} a_{11} & a_{12} & a_{13} \\ a_{21} & a_{22} & a_{23} \\ a_{31} & a_{32} & a_{33} \end{vmatrix}, \tag{A.10}$$

The notations developed here enables us to write equation (A.10) in the forms

$$\begin{aligned} a &= e_{ijk}a_{1i}a_{2j}a_{3k} = e_{ijk}a_{i1}a_{j2}a_{k3}, \\ a &= \frac{1}{6}e_{ijk}e_{pqr}a_{ip}a_{jq}a_{kr}. \end{aligned} \tag{A.11}$$

Appendix B

The results of permeability experiments

The results of all the permeability experiments carried out in the Transport Systems Research Laboratory of the University of Southampton are listed in the following. The flow front is measured along the the X_1 and X_2 axis (denoted 90° and 0° respectively, see Figure 6.3). For all experiments, the Shell Vitrea M100 oil is used, the viscosity of this test fluid is 3.515 poise at $15 - 18°C$ and the density is $0.878 \times 10^3 kg/m^3$. The inlet radius is $5.25mm$.

B.1 Results of constant inlet pressure tests

The following tables show the flow front position at a given time step.

B.1.1 Experiments of U750-450

Set up I

In these experiments, the fibre volume fraction $v_f = 22.7\%$, the thickness of the cavity $H = 2.32mm$ and the number of fibre layers $N = 3$.

Table B.1: Experiment Cr1 [mm]

Time [s]	X_1	X_2	X_1/X_2	$k^{(1)}$ $(\times 10^{-12})$	$k^{(2)}$ $(\times 10^{-12})$
5.00	88.50	93.93	0.94	1495.39	1683.70
10.00	117.64	122.57	0.96	1548.14	1680.35
15.00	140.31	144.34	0.97	1602.04	1695.27
20.00	154.34	161.52	0.96	1519.63	1664.15
25.00	171.61	175.27	0.98	1575.47	1643.33
30.00	184.56	187.87	0.98	1566.47	1623.12
35.00	196.43	201.62	0.97	1560.86	1644.38
40.00	209.38	210.78	0.99	1592.42	1613.78
45.00	219.10	221.09	0.99	1578.09	1606.88
50.00	229.89	231.40	0.99	1593.15	1614.14
55.00	238.52	238.27	1.00	1581.27	1577.95
62.28	245.00	244.00	1.00	1488.63	1474.23

Table B.2: Experiment Cr2 [mm]

Time [s]	X_1	X_2
5.00	71.53	70.69
10.00	94.92	94.26
15.00	111.42	109.50
20.00	123.80	124.75
25.00	137.56	137.23
30.00	148.57	146.93
35.00	158.20	156.63
40.00	169.20	167.72
45.00	177.45	176.04
50.00	184.33	184.36
55.00	192.59	191.29
60.00	200.84	198.22
65.00	206.34	205.15
70.00	214.60	212.08
75.00	220.10	219.01
80.00	225.60	224.55
85.00	233.85	230.10
90.00	239.36	237.03
95.00	244.86	241.19
100.00	247.61	246.73
105.00	254.49	253.66
110.00	258.61	259.21
115.00	262.74	261.98
120.00	268.24	267.52
125.00	273.75	273.07
130.00	277.87	277.23
135.58	282.00	280.00

Table B.3: Experiment Cr3 [mm]

Time [s]	X_1	X_2
5.00	75.40	73.81
10.00	100.05	98.41
15.00	117.45	114.33
20.00	130.50	130.25
25.00	145.00	143.28
30.00	156.60	153.41
35.00	166.75	163.54
40.00	178.35	175.12
45.00	187.05	183.80
50.00	194.30	192.48
55.00	203.00	199.72
60.00	211.70	206.95
65.00	217.50	214.19
70.00	226.20	221.43
75.00	232.00	228.66
80.00	237.80	234.45
85.00	246.50	240.24
90.00	252.30	247.48
95.00	258.10	251.82
100.00	261.00	257.61
105.00	268.25	264.84
110.00	272.60	270.63
115.00	276.95	273.53
120.00	282.75	279.32
125.00	288.55	285.11
127.63	290.00	288.00

Table B.4: Experiment Cr4 [mm]

Time [s]	X_1	X_2
5.00	79.48	79.50
10.00	105.56	106.00
15.00	126.67	124.93
20.00	144.06	142.60
25.00	160.20	156.48
30.00	172.62	169.10
35.00	185.04	181.71
40.00	196.21	190.55
45.00	207.39	201.90
50.00	214.84	212.00
55.00	224.78	219.57
60.00	232.23	227.14
65.00	238.44	237.24
70.00	245.89	242.29
75.00	252.10	252.38
80.00	260.79	258.69
85.03	267.00	265.00

Table B.5: Experiment Cr5 [mm]

Time [s]	X_1	X_2
5.00	75.16	74.49
10.00	101.08	100.63
15.00	117.93	117.62
20.00	134.78	133.30
25.00	146.44	147.68
30.00	158.10	158.13
35.00	171.06	171.20
40.00	181.43	179.04
45.00	191.80	188.19
50.00	199.57	196.03
55.00	208.64	203.87
60.00	217.71	211.71
65.00	225.49	218.25
70.00	231.97	227.40
75.00	241.04	233.93
80.00	247.52	239.16
85.52	254.00	247.00

Table B.6: Experiment Cr6 [mm]

Time [s]	X_1	X_2
5.00	71.91	70.42
10.00	97.15	97.31
15.00	113.55	113.96
20.00	127.43	128.04
25.00	141.31	139.57
30.00	152.66	152.37
35.00	162.75	161.33
40.00	172.85	170.30
45.00	181.68	180.54
50.00	189.25	188.22
55.00	198.08	195.90
60.00	204.39	203.59
65.00	211.96	209.99
70.00	219.53	217.67
75.00	224.58	222.79
80.00	232.15	227.92
85.00	238.45	235.60
91.94	243.50	242.00

B.1.2 Experiments of RC 600

Set up I

In these experiments, the fibre volume fraction $v_f = 50.4\%$, the thickness of the cavity $H = 2.32mm$ and the number of fibre layers $N = 5$.

Table B.7: Experiment Ct1 [mm]

Time [s]	X_1	X_2
10.00	39.84	20.82
20.00	57.27	29.15
30.00	63.49	33.32
40.00	68.47	38.52
50.00	74.69	42.68
60.00	82.16	45.81
70.00	87.14	48.93
80.00	92.12	54.14
90.00	95.86	56.22
100.00	99.59	60.38
110.00	104.57	66.63
120.00	107.06	68.71
130.00	114.53	70.79
140.00	117.02	74.96
150.00	120.76	74.96
156.08	122.00	76.00

Table B.8: Experiment Ct2 [mm]

Time [s]	X_1	X_2
10.00	41.23	24.83
20.00	52.77	32.35
30.00	58.54	36.86
40.00	65.96	39.87
50.00	73.38	45.14
60.00	79.15	47.40
70.00	84.10	50.41
80.00	86.57	52.66
90.00	89.87	54.92
100.00	92.34	57.18
110.00	94.82	59.43
120.00	98.94	60.94
130.00	101.41	62.44
140.00	104.71	64.70
150.00	108.01	66.21
160.00	109.66	67.71
170.00	111.31	70.72
180.00	112.96	72.22
190.00	116.25	73.73
200.00	117.90	74.48
210.00	119.55	76.74
220.00	121.20	78.24
232.20	124.50	80.50

Table B.9: Experiment Ct3 [mm]

Time [s]	X_1	X_2	X_1/X_2	$k^{(1)}$ ($\times 10^{-12}$)	$k^{(2)}$ ($\times 10^{-12}$)
10.00	45.23	26.64	1.70	58.84	20.41
20.00	59.70	32.65	1.83	66.52	19.90
30.00	65.13	39.52	1.65	62.07	22.85
40.00	69.65	44.68	1.56	58.49	24.07
50.00	74.18	47.26	1.57	55.68	22.60
60.00	81.41	53.27	1.53	60.94	26.09
70.00	91.37	54.99	1.66	68.51	24.82
80.00	93.17	56.71	1.64	63.58	23.55
90.00	94.98	59.29	1.60	60.28	23.49
100.00	97.70	61.00	1.60	58.53	22.82
110.00	100.41	64.44	1.56	57.98	23.88
120.00	104.93	66.16	1.59	59.24	23.55
130.00	107.65	67.02	1.61	58.16	22.54
140.00	108.55	68.74	1.58	55.63	22.31
150.00	109.46	71.32	1.53	53.75	22.82
160.00	112.12	73.03	1.54	53.64	22.76
170.00	116.69	73.89	1.58	55.35	22.19
180.00	122.12	75.61	1.62	58.27	22.34
190.00	123.93	78.19	1.58	57.80	23.01
200.00	124.84	80.77	1.55	56.54	23.67
210.00	126.64	82.49	1.54	56.02	23.77
220.00	128.45	84.20	1.53	55.60	23.89
230.00	130.26	95.92	1.36	57.54	31.20
240.00	133.88	86.78	1.54	56.41	23.70
250.00	136.60	87.64	1.56	56.78	23.37
258.74	137.50	88.50	1.55	55.86	23.14

Table B.10: Experiment Ct4 [mm]

Time [s]	X_1	X_2
10.00	39.40	27.26
20.00	36.25	32.08
30.00	55.95	37.69
40.00	63.04	42.50
50.00	66.98	44.91
60.00	72.49	48.11
70.00	78.01	52.12
80.00	80.37	53.73
90.00	85.10	56.13
100.00	89.04	58.54
110.00	89.83	61.75
120.00	91.41	62.55
130.00	92.98	64.15
140.00	96.92	65.75
150.00	99.28	67.36
160.00	102.44	68.96
170.00	104.01	70.57
180.00	107.16	72.17
190.00	109.53	73.77
200.00	111.89	75.38
210.00	113.47	76.18
220.00	115.04	76.98
230.00	116.62	77.78
240.00	118.20	79.39
250.00	120.56	82.59
260.00	121.35	83.40
267.36	124.50	85.00

Table B.11: Experiment Ct5 [mm]

Time [s]	X_1	X_2
10.00	37.60	26.13
20.00	45.60	32.85
30.00	58.40	39.56
40.00	64.00	44.04
50.00	69.60	49.27
60.00	74.40	55.24
70.00	80.80	59.72
80.00	86.40	65.69
90.00	88.00	68.68
100.00	91.20	71.66
110.00	94.40	74.65
120.00	96.80	76.89
130.00	102.40	78.38
140.00	105.60	80.62
150.00	109.60	82.11
160.00	113.60	85.85
170.00	116.00	88.08
180.00	119.20	89.58
190.00	122.40	91.07
200.00	126.40	93.31
210.00	129.60	94.06
220.00	131.20	95.55
230.00	136.00	97.04
240.00	139.20	99.28
250.00	142.40	101.52
260.00	144.80	103.01
277.86	148.00	106.00

Table B.12: Experiment Ct6 [mm]

Time [s]	X_1	X_2
10.00	29.21	24.61
20.00	47.65	32.55
30.00	53.80	38.90
40.00	59.95	40.49
50.00	67.63	46.04
60.00	72.25	48.43
70.00	77.63	51.60
80.00	83.77	53.19
90.00	87.62	58.75
100.00	90.69	61.92
110.00	92.23	63.51
120.00	95.30	64.30
130.00	99.15	65.89
140.00	103.76	68.27
150.00	105.29	69.86
160.00	109.91	70.65
170.00	111.44	72.24
180.00	115.29	74.62
190.00	117.59	78.59
200.00	119.90	79.39
210.00	122.20	80.97
220.00	124.51	82.56
230.00	126.81	83.36
240.00	130.66	85.74
250.00	132.96	88.91
260.51	134.50	90.50

B.1.3 Experiments of E-LPb 567

Set up I

In these experiments, the fibre volume fraction $v_f = 44.5\%$, the thickness of the cavity $H = 2.32mm$ and the number of fibre layers $N = 4$.

Table B.13: Experiment Cu1 [mm]

Time [s]	X_1	X_2
5.00	30.89	62.21
10.00	40.60	84.06
15.00	46.78	97.51
20.00	52.08	105.08
25.00	53.84	112.64
30.00	55.61	118.53
35.00	61.79	131.14
40.00	63.55	137.86
45.00	66.20	145.43
50.00	69.73	150.47
55.00	71.49	152.99
60.00	72.38	157.19
65.00	75.03	163.08
70.00	76.79	165.60
75.00	78.56	169.80
80.00	80.32	174.85
85.00	82.97	178.21
90.00	84.73	182.41
97.22	86.50	192.50

Table B.14: Experiment Cu2 [mm]

Time [s]	X_1	X_2
5.00	29.33	65.38
10.00	36.67	82.19
15.00	44.00	107.41
20.00	48.89	112.08
25.00	52.96	116.75
30.00	54.59	122.35
35.00	57.85	128.89
40.00	60.30	133.56
45.00	62.74	141.96
50.00	64.37	145.70
55.00	66.81	149.43
60.00	70.07	155.04
65.00	71.70	163.44
70.00	73.33	166.25
75.00	75.78	169.98
80.00	77.41	174.65
85.00	78.22	179.32
90.00	81.48	183.06
95.00	83.11	187.73
100.00	83.93	190.53
105.00	85.56	193.33
110.00	87.19	196.13
113.37	88.00	198.00

Table B.15: Experiment Cu3 [mm]

Time [s]	X_1	X_2
5.00	30.11	58.85
10.00	40.69	84.54
15.00	47.20	99.46
20.00	52.89	111.89
25.00	55.33	118.52
30.00	59.40	130.13
35.00	62.66	138.41
40.00	65.10	146.70
45.00	70.79	153.33
50.00	72.42	159.96
55.00	74.86	164.94
60.00	78.93	171.57
65.00	80.56	179.86
69.86	83.00	184.00

Table B.16: Experiment Cu4 [mm]

Time [s]	X_1	X_2
5.00	34.71	67.72
10.00	44.50	87.85
15.00	49.84	100.66
20.00	56.07	112.56
25.00	58.74	124.45
30.00	63.19	132.69
35.00	65.86	140.92
40.00	69.42	147.33
45.00	72.98	154.65
50.00	75.65	161.06
55.00	79.21	169.29
60.00	80.99	172.95
65.00	83.66	181.19
70.00	85.44	183.93
75.00	88.11	189.42
80.41	89.00	194.00

Table B.17: Experiment Cu5 [mm]

Time [s]	X_1	X_2
5	35.59	64.81
10	43.12	83.88
15	48.59	99.89
20	56.12	114.38
25	58.86	123.53
30	63.65	132.68
35	67.07	144.88
40	70.5	154.02
45	71.86	160.12
50	75.97	168.51
55	77.34	175.38
60	82.82	179.95
63.6	83.5	183

Table B.18: Experiment Cu6 [mm]

Time [s]	X_1	X_2
5	33.81	63.76
10	42.63	78.53
15	48.51	96.41
20	52.92	104.97
25	56.6	115.07
30	61.01	118.96
35	64.68	128.29
40	66.15	132.96
45	70.56	138.4
50	72.77	142.29
55	74.97	149.29
60	77.18	152.4
65	79.38	158.62
70	82.32	163.28
75	84.53	167.17
80	85.26	174.94
82.72	86	176.5

B.2 Results of variable inlet pressure tests

The following tables show the flow front position and inlet pressure at a given time step.

B.2.1 Experiments of U750-450

Set up I

In these experiments, the fibre volume fraction $v_f = 22.7\%$, the thickness of the cavity $H = 2.32mm$ and the number of fibre layers $N = 3$.

Table B.19: Experiment Vr1 [mm]

Time [s]	X_1	X_2	$p^0(Bar)$
5.00	113.57	109.71	2.084
10.00	153.87	148.29	2.113
15.00	181.96	174.81	2.113
20.00	205.16	200.13	2.231
25.00	228.36	220.63	2.260
30.00	246.68	239.92	2.290
36.94	265.00	258.00	2.318

Table B.20: Experiment Vr2 [mm]

Time [s]	X_1	X_2	$p^0(Bar)$
5.00	115.60	109.66	2.143
10.00	155.61	149.54	2.172
15.00	183.40	177.23	2.231
20.00	210.08	201.60	2.260
25.00	230.09	220.43	2.290
30.00	252.32	239.26	2.348
35.00	267.88	256.98	2.377
40.00	284.55	271.38	2.407
44.32	299.00	288.00	2.436

Table B.21: Experiment Vr3 [mm]

Time [s]	X_1	X_2	$p^0(Bar)$
5.00	105.49	101.72	1.937
10.00	137.87	136.33	1.967
15.00	169.20	167.79	1.996
20.00	188.00	187.72	2.026
25.00	209.93	207.64	2.026
30.00	227.69	225.47	2.055
35.00	243.36	239.10	2.084
40.00	256.93	254.83	2.084
45.00	268.42	264.27	2.113
51.60	282.00	280.00	2.143

Table B.22: Experiment Vr4 [mm]

Time [s]	X_1	X_2	$p^0(Bar)$
5.00	109.29	107.39	1.909
10.00	145.34	144.35	1.937
15.00	172.08	170.90	1.967
20.00	196.50	194.00	1.996
25.00	216.26	213.63	2.026
30.00	236.03	233.26	2.055
35.00	251.14	248.27	2.084
40.00	265.10	262.13	2.113
45.00	281.37	279.45	2.143
50.00	291.84	288.69	2.143
53.72	293.00	291.00	2.143

Table B.23: Experiment Vr5 [mm]

Time [s]	X_1	X_2	$p^0(Bar)$
5.00	107.32	108.63	1.937
10.00	147.15	149.37	1.967
15.00	177.02	178.79	1.996
20.00	200.26	202.55	2.055
25.00	222.38	224.05	2.113
30.00	242.30	242.16	2.143
35.00	257.79	258.00	2.172
38.24	260.00	258.00	2.172

Table B.24: Experiment Vr6 [mm]

Time [s]	X_1	X_2	$p^0(Bar)$
5.00	110.00	105.91	1.996
10.00	147.50	145.32	2.026
15.00	177.50	173.65	2.055
20.00	200.00	195.81	2.084
25.00	220.00	215.52	2.113
30.00	238.75	233.99	2.143
36.28	255.00	250.00	2.172

Set up II

In these experiments, the fibre volume fraction $v_f = 45.5\%$, the thickness of the cavity $H = 2.32mm$ and the number of fibre layers $N = 6$.

Table B.25: Experiment Vra1 [mm]

Time [s]	X_1	X_2	$p^0(Bar)$
10.00	50.13	48.22	1.205
15.00	60.35	57.87	1.234
20.00	67.65	65.58	1.234
25.00	73.98	71.85	1.234
30.00	80.31	78.12	1.264
35.00	85.66	83.91	1.264
40.00	90.04	88.25	1.293
45.00	95.40	93.07	1.293
50.00	99.29	97.41	1.293
62.96	110.00	108.50	1.322

Table B.26: Experiment Vra2 [mm]

Time [s]	X_1	X_2	$p^0(Bar)$
5.00	37.99	37.69	1.234
10.00	51.12	50.09	1.234
15.00	60.50	60.11	1.264
20.00	67.54	66.79	1.264
25.00	75.51	74.42	1.264
30.00	81.14	81.10	1.293
35.00	86.77	86.83	1.293
40.00	92.40	92.07	1.322
45.00	97.56	97.32	1.322
50.00	102.25	101.14	1.410
54.32	106.00	104.00	1.410

Table B.27: Experiment Vra3 [mm]

Time [s]	X_1	X_2	$p^0(Bar)$
5.00	41.26	40.54	1.293
10.00	55.70	53.72	1.293
15.00	66.02	63.86	1.322
20.00	74.79	72.47	1.322
25.00	81.49	80.07	1.351
30.00	88.71	86.66	1.351
35.00	95.42	93.25	1.351
40.00	101.61	99.33	1.381
45.00	106.76	104.40	1.381
50.00	111.41	108.96	1.410
53.28	114.50	112.00	1.410

Set up III

In these experiments, the fibre volume fraction $v_f = 22.7\%$, the thickness of the cavity $H = 4.64mm$ and the number of fibre layers $N = 6$.

Table B.28: Experiment Vrb1 [mm]

Time [s]	X_1	X_2	$p^0(Bar)$
2.50	63.33	61.24	1.234
5.00	75.14	73.06	1.264
7.50	84.80	83.80	1.264
10.00	92.85	91.33	1.264
12.50	99.83	99.38	1.293
15.00	107.34	106.37	1.293
17.50	113.24	111.74	1.293
21.84	117.00	115.50	1.293

Table B.29: Experiment Vrb2 [mm]

Time [s]	X_1	X_2	$p^0(Bar)$
5.00	62.77	61.21	1.264
10.00	85.49	83.80	1.293
15.00	102.23	100.44	1.293
20.00	114.78	113.51	1.293
25.00	126.74	125.40	1.322
30.00	136.30	134.91	1.322
30.88	137.50	135.50	1.351

Table B.30: Experiment Vrb3 [mm]

Time [s]	X_1	X_2	$p^0(Bar)$
5.00	51.99	51.25	1.175
10.00	69.61	69.21	1.175
15.00	82.83	81.91	1.175
20.00	94.28	92.86	1.205
25.00	103.09	101.62	1.205
27.84	107.50	106.00	1.264

B.2.2 Experiments of twill weave fabrics

Set up I

RC 600 was used in these experiments, the fibre volume fraction $v_f = 50.4\%$, the thickness of the cavity $H = 2.32mm$ and the number of fibre layers $N = 5$.

Table B.31: Experiment Vt1 [mm]

Time [s]	X_1	X_2	$p^0(Bar)$
20.00	68.47	45.56	1.850
30.00	77.66	52.22	1.879
40.00	85.84	60.00	1.937
50.00	94.01	64.44	1.967
60.00	101.17	68.89	2.026
70.00	107.30	74.44	2.055
80.00	112.41	77.78	2.084
90.00	118.54	81.11	2.143
100.00	124.67	84.44	2.172
110.00	127.73	88.89	2.201
120.00	132.84	91.11	2.231
130.00	136.93	93.33	2.260
140.00	141.02	95.56	2.290
150.00	144.08	100.00	2.318
160.00	148.17	102.22	2.318
170.00	154.30	104.44	2.348
180.00	157.37	106.67	2.348
190.00	160.43	107.78	2.348
206.14	163.50	110.00	2.348

Table B.32: Experiment Vt2 [mm]

Time [s]	X_1	X_2	$p^0(Bar)$
10.00	52.34	40.63	1.791
20.00	65.42	49.14	1.879
30.00	76.49	54.81	1.937
40.00	85.55	60.48	1.996
50.00	95.62	66.15	2.055
60.00	100.65	69.93	2.084
70.00	105.68	72.76	2.113
80.00	112.73	76.54	2.143
90.00	119.77	80.32	2.172
100.00	122.79	83.16	2.201
110.00	127.82	85.05	2.201
120.00	132.86	87.88	2.231
130.00	135.88	91.66	2.231
140.00	141.92	94.50	2.260
150.00	144.94	98.28	2.260
160.00	149.97	100.17	2.290
170.00	152.99	101.11	2.290
178.45	155.00	103.00	2.290

Table B.33: Experiment Vt3 [mm]

Time [s]	X_1	X_2	$p^0(Bar)$
10.00	48.30	34.79	1.791
20.00	64.40	42.64	1.850
30.00	71.30	48.26	1.879
40.00	80.50	53.87	1.909
50.00	89.70	58.36	1.937
60.00	95.45	61.72	1.967
70.00	103.50	67.33	1.996
80.00	112.70	72.94	2.026
90.00	118.45	75.19	2.055
100.00	121.90	77.43	2.084
110.00	125.35	80.80	2.113
120.00	132.25	85.29	2.113
130.00	135.70	87.53	2.143
140.00	132.25	85.29	2.143
150.00	141.45	92.02	2.172
160.00	143.75	93.14	2.172
170.00	147.20	109.98	2.172
177.79	149.50	101.00	2.172

Table B.34: Experiment Vt4 [mm]

Time [s]	X_1	X_2	$p^0(Bar)$
10.00	58.65	40.93	2.055
20.00	73.31	52.10	2.113
30.00	87.11	58.61	2.172
40.00	95.73	63.26	2.231
50.00	105.22	71.64	2.260
60.00	108.67	75.36	2.318
70.00	115.57	79.08	2.348
80.00	121.60	84.66	2.377
90.00	126.78	90.24	2.407
100.00	132.81	91.17	2.436
110.00	136.26	95.82	2.465
120.00	139.71	97.68	2.495
130.00	145.75	93.03	2.524
140.00	150.06	105.13	2.524
150.00	154.38	106.99	2.553
160.00	158.69	110.71	2.582
170.00	162.14	112.57	2.641
174.33	163.00	113.50	2.641

Table B.35: Experiment Vt5 [mm]

Time [s]	X_1	X_2	$p^0(Bar)$
10.00	69.84	49.87	1.996
20.00	89.24	60.62	2.084
30.00	100.88	67.47	2.172
40.00	109.61	73.33	2.231
50.00	117.37	77.24	2.290
60.00	127.07	82.13	2.318
70.00	131.92	86.04	2.348
80.00	134.83	89.96	2.407
90.00	141.62	92.89	2.407
100.00	146.47	96.80	2.436
110.00	151.32	99.73	2.436
120.00	156.17	103.64	2.436
130.00	161.02	106.58	2.436
140.00	163.93	108.53	2.465
150.00	166.84	111.47	2.465
160.00	170.72	113.42	2.465
170.00	172.66	116.36	2.465
180.00	177.51	118.31	2.465
190.00	180.42	121.24	2.465
200.00	182.36	123.20	2.465
210.00	185.27	125.16	2.495
220.00	188.18	126.13	2.495
230.00	190.12	128.09	2.495
240.00	193.03	131.02	2.495
247.33	194.00	132.00	2.495

Table B.36: Experiment Vt6 [mm]

Time [s]	X_1	X_2	$p^0(Bar)$
10.00	56.86	44.53	1.645
20.00	68.79	51.66	1.703
30.00	81.63	57.89	1.732
40.00	88.05	63.23	1.791
50.00	98.13	68.58	1.820
60.00	106.39	72.14	1.879
70.00	109.14	75.70	1.909
80.00	114.64	79.27	1.937
90.00	118.31	81.94	1.967
100.00	124.73	86.39	1.996
110.00	127.48	88.17	2.026
120.00	129.32	90.84	2.055
130.00	133.90	93.52	2.055
140.00	138.49	97.97	2.084
150.00	142.16	99.75	2.113
160.00	143.99	101.53	2.113
170.00	146.74	104.20	2.143
180.00	147.66	106.88	2.172
190.00	149.49	108.66	2.172
200.00	152.25	110.44	2.201
210.00	157.75	112.22	2.201
220.00	159.58	113.11	2.231
222.45	160.50	114.00	2.231

Set up II

Also RC 600 was used in this part of experiments, the fibre volume fraction $v_f = 60.6\%$, the thickness of the cavity $H = 2.32mm$ and the number of fibre layers $N = 6$.

Table B.37: Experiment Vta1 [mm]

Time [s]	X_1	X_2	$p^0(Bar)$
10.00	45.02	33.88	2.465
20.00	60.03	49.76	2.524
30.00	73.89	56.12	2.612
40.00	79.66	64.59	2.671
50.00	87.74	70.94	2.723
60.00	95.82	76.24	2.788
70.00	98.13	82.59	2.846
80.00	103.90	85.76	2.905
90.00	110.83	90.00	2.963
100.00	116.60	95.29	2.993
110.00	123.53	98.47	3.052
120.00	130.46	101.65	3.110
130.00	135.07	103.76	3.139
140.00	138.54	105.88	3.198
150.28	142.00	108.00	3.198

Table B.38: Experiment Vta2 [mm]

Time [s]	X_1	X_2	$p^0(Bar)$
10.00	47.29	38.15	2.436
20.00	60.81	50.86	2.495
30.00	74.32	59.34	2.553
40.00	83.97	65.70	2.641
50.00	94.59	72.06	2.700
60.00	102.31	78.41	2.758
70.00	109.07	81.59	2.846
80.00	115.82	84.77	2.905
90.00	119.68	91.13	2.963
100.00	124.51	93.25	3.022
110.00	129.34	96.43	3.081
120.00	136.09	100.67	3.139
130.00	138.02	104.90	3.198
140.00	143.81	109.14	3.257
150.00	145.74	110.20	3.286
160.00	148.64	112.32	3.315
174.66	152.50	115.50	3.374

Table B.39: Experiment Vta3 [mm]

Time [s]	X_1	X_2	$p^0(Bar)$
10.00	49.16	41.17	3.169
20.00	72.29	52.21	3.198
30.00	83.86	64.26	3.227
40.00	92.53	72.29	3.286
50.00	102.17	79.32	3.315
60.00	109.88	86.35	3.344
70.00	115.66	89.36	3.374
80.00	122.41	94.38	3.403
90.00	129.16	97.39	3.433
100.00	133.01	101.41	3.462
110.00	135.90	105.43	3.491
120.00	139.76	109.44	3.491
130.00	145.54	113.46	3.520
140.00	151.33	116.47	3.520
150.00	156.14	118.48	3.550
160.00	159.04	121.49	3.550
164.61	160.00	123.50	3.550

Set up III

In these experiments,the twill weave fabrics WRE580T was used. The fibre volume fraction $v_f = 58.6\%$, the thickness of the cavity $H = 2.32mm$ and the number of fibre layers $N = 6$.

Table B.40: Experiment Vtb1 [mm]

Time [s]	X_1	X_2	$p^0(Bar)$
10.00	62.87	63.53	1.996
20.00	74.79	76.85	2.026
30.00	87.80	88.12	2.084
40.00	97.56	98.37	2.113
50.00	107.31	107.59	2.143
60.00	113.82	114.76	2.172
70.00	118.15	120.91	2.201
80.00	124.66	125.01	2.231
90.00	128.99	130.13	2.260
100.00	132.24	134.23	2.290
110.00	136.58	139.35	2.318
120.00	139.83	143.45	2.348
124.73	142.00	145.50	2.348

Table B.41: Experiment Vtb2 [mm]

Time [s]	X_1	X_2	$p^0(Bar)$
10.00	55.99	59.86	1.996
20.00	73.95	79.17	2.055
30.00	82.40	94.62	2.084
40.00	90.85	100.41	2.113
50.00	100.36	111.03	2.143
60.00	105.65	118.76	2.172
70.00	114.10	123.59	2.201
80.00	118.32	128.41	2.231
90.00	124.66	132.28	2.260
100.00	128.89	137.10	2.290
106.45	131.00	140.00	2.290

Table B.42: Experiment Vtb3 [mm]

Time [s]	X_1	X_2	$p^0(Bar)$
10.00	81.14	81.22	2.582
20.00	99.43	99.88	2.641
30.00	110.86	113.05	2.729
40.00	117.71	122.93	2.788
50.00	129.14	132.80	2.846
60.00	137.14	140.49	2.934
70.00	140.57	149.27	2.993
80.00	144.00	154.76	3.052
90.00	148.57	160.24	3.081
100.00	154.29	164.63	3.169
110.00	160.00	170.12	3.198
120.00	164.57	175.61	3.257
127.72	168.00	180.00	3.286

B.2.3 Experiments of E-LPb 567

Set up I

In these experiments, the fibre volume fraction $v_f = 44.5\%$, the thickness of the cavity $H = 2.32mm$ and the number of fibre layers $N = 4$.

Table B.43: Experiment Vu1 [mm]

Time [s]	X_1	X_2	$p^0(Bar)$
5.00	33.63	63.34	1.410
10.00	41.03	80.10	1.439
15.00	47.08	92.52	1.467
20.00	52.46	103.70	1.498
25.00	55.82	111.15	1.527
30.00	59.86	121.71	1.556
35.00	62.55	127.92	1.586
40.00	66.58	133.51	1.615
45.00	67.93	139.72	1.644
50.00	71.29	145.93	1.674
55.00	73.98	150.27	1.703
60.48	76.00	154.00	1.703

Table B.44: Experiment Vu2 [mm]

Time [s]	X_1	X_2	$p^0(Bar)$
5.00	33.30	77.24	1.527
10.00	40.91	97.47	1.557
15.00	46.62	113.10	1.586
20.00	53.28	125.05	1.645
25.00	58.99	135.17	1.703
30.00	63.75	147.12	1.732
35.00	66.60	156.31	1.791
40.00	71.36	163.67	1.850
45.00	74.21	171.03	1.909
50.00	77.07	178.38	1.937
55.00	79.92	184.82	1.996
60.00	82.78	193.09	2.026
65.00	86.58	197.69	2.084
70.00	88.49	201.37	2.143
75.00	90.39	207.81	2.172
80.00	95.15	214.24	2.201
86.67	98.00	217.00	2.231

Table B.45: Experiment Vu3 [mm]

Time [s]	X_1	X_2	$p^0(Bar)$
5.00	39.17	79.46	1.674
10.00	48.33	99.94	1.762
15.00	55.00	113.87	1.791
20.00	60.00	126.16	1.850
25.00	64.17	136.81	1.879
30.00	70.00	147.46	1.937
35.00	72.50	158.92	1.996
40.00	76.67	167.12	2.055
45.00	80.00	173.67	2.143
51.74	85.00	183.50	2.172

Table B.46: Experiment Vu4 [mm]

Time [s]	X_1	X_2	$p^0(Bar)$
5.00	39.03	94.49	2.026
10.00	50.74	116.22	2.055
15.00	58.54	132.51	2.113
20.00	65.37	147.71	2.143
25.00	72.20	158.57	2.172
30.00	74.16	169.44	2.231
35.00	80.99	179.21	2.260
40.00	84.89	190.07	2.290
45.00	88.79	196.59	2.318
50.00	92.69	204.19	2.348
55.00	95.62	213.97	2.377
61.30	100.50	227.00	2.377

Table B.47: Experiment Vu5 [mm]

Time [s]	X_1	X_2	$p^0(Bar)$
5.00	41.14	74.96	1.850
10.00	50.82	98.30	1.879
15.00	59.29	115.50	1.909
20.00	60.50	130.25	1.937
25.00	70.18	146.22	1.967
30.00	73.81	153.60	1.967
35.00	78.65	164.66	1.996
40.00	82.28	175.71	1.996
45.00	87.12	183.09	2.026
50.00	89.54	189.23	2.055
55.00	91.96	196.60	2.055
60.00	96.80	203.98	2.084
65.00	99.22	212.58	2.084
70.00	101.64	219.95	2.084
75.00	104.06	224.87	2.084
80.00	107.69	232.24	2.084
85.00	108.90	237.15	2.113
90.00	112.53	244.53	2.113
95.00	117.37	248.21	2.113
100.00	118.58	254.36	2.113
106.44	121.00	260.50	2.113

Table B.48: Experiment Vu6 [mm]

Time [s]	X_1	X_2	$p^0(Bar)$
5.00	43.02	82.05	1.967
10.00	53.21	107.83	1.996
15.00	61.13	123.07	2.026
20.00	67.92	139.48	2.055
25.00	72.45	154.72	2.084
30.00	76.98	161.75	2.113
35.00	81.51	169.95	2.113
40.00	86.04	184.02	2.143
45.00	89.43	193.40	2.172
50.00	92.83	200.43	2.172
55.00	97.36	205.12	2.201
60.00	101.89	210.98	2.231
65.00	104.15	219.18	2.260
70.00	106.42	228.56	2.260
75.00	108.68	234.42	2.290
80.00	112.08	240.28	2.290
85.00	116.60	243.80	2.318
90.00	117.74	248.48	2.318
93.75	120.00	252.00	2.318

Set up II

In this part of experiments, the fibre volume fraction $v_f = 55.6\%$, the thickness of the cavity $H = 2.32mm$ and the number of fibre layers $N = 5$.

Table B.49: Experiment Vua1 [mm]

Time [s]	X_1	X_2	$p^0(Bar)$
10.00	25.28	55.09	1.234
20.00	32.18	71.85	1.293
30.00	36.77	83.23	1.322
40.00	41.37	92.81	1.381
50.00	44.82	103.59	1.410
60.00	48.26	110.77	1.469
70.00	51.71	117.96	1.498
80.00	54.58	124.54	1.556
90.00	56.31	131.73	1.615
100.00	58.61	135.92	1.645
110.00	61.48	141.31	1.703
119.46	65.50	145.50	1.703

Table B.50: Experiment Vua2 [mm]

Time [s]	X_1	X_2	$p^0(Bar)$
10.00	33.67	68.14	1.615
20.00	45.42	87.72	1.674
30.00	51.68	103.38	1.703
40.00	55.59	117.48	1.762
50.00	61.08	128.44	1.820
60.00	64.21	135.49	1.879
70.00	68.12	147.24	1.937
80.00	71.25	154.29	1.967
90.00	75.95	161.34	2.026
100.00	79.08	167.60	2.084
112.05	83.00	177.00	2.084

Table B.51: Experiment Vua3 [mm]

Time [s]	X_1	X_2	$p^0(Bar)$
10.00	34.29	78.45	1.703
20.00	45.45	104.60	1.762
30.00	53.43	120.48	1.820
40.00	58.21	137.29	1.879
50.00	63.79	149.43	1.937
60.00	70.17	157.83	1.996
70.00	73.36	170.91	2.055
80.00	76.55	180.25	2.113
90.00	80.54	189.59	2.172
100.00	84.53	197.06	2.231
110.00	87.72	203.59	2.290
120.00	90.91	209.20	2.318
125.40	92.50	212.00	2.318

Set up III

In these experiments,the twill weave fabrics WRE580T was used. The fibre volume fraction $v_f = 44.5\%$, the thickness of the cavity $H = 4.64mm$ and the number of fibre layers $N = 8$.

Table B.52: Experiment Vub1 [mm]

Time [s]	X_1	X_2	$p^0(Bar)$
5.00	42.45	87.15	1.996
10.00	52.86	107.56	2.026
15.00	60.07	125.62	2.055
20.00	67.28	137.39	2.084
25.00	72.08	150.74	2.113
30.00	75.29	160.16	2.172
35.00	80.89	173.51	2.201
40.00	84.90	182.14	2.231
42.52	86.50	184.50	2.260

Table B.53: Experiment Vub2 [mm]

Time [s]	X_1	X_2	$p^0(Bar)$
5.00	48.44	101.20	2.671
10.00	61.03	126.96	2.700
15.00	70.72	150.88	2.729
20.00	77.50	165.60	2.758
25.00	83.31	179.40	2.788
30.00	90.09	194.12	2.817
35.00	95.91	202.40	2.846
40.00	98.81	210.68	2.876
45.00	105.59	223.56	2.905
48.19	108.50	230.00	2.905

Table B.54: Experiment Vub3 [mm]

Time [s]	X_1	X_2	$p^0(Bar)$
5.00	45.69	104.21	2.582
10.00	58.52	131.10	2.612
15.00	66.53	149.59	2.641
20.00	76.15	166.40	2.671
25.00	80.16	179.84	2.700
30.00	88.17	189.93	2.729
35.00	92.98	199.17	2.788
40.00	96.19	215.14	2.817
42.52	101.00	218.50	2.817

B.3 Results of tests of gravitational effect

The tables below show the flow front and displacement position at a given time step. The displacement d_g is measured along the vertical direction. All experiments in this section are carried out in the vertical plane.

B.3.1 Experiments of U750-450

Set up I

In these experiments, the fibre volume fraction $v_f = 22.7\%$, the thickness of the cavity $H = 2.32mm$ and the number of fibre layers $N = 3$.

Table B.55: Experiment Gr1 [mm]

Time [s]	X_1	X_2	d_g
5.00	76.93	76.08	0.20
10.00	104.47	103.66	0.45
15.00	125.37	124.58	0.71
20.00	142.46	141.70	0.98
25.00	158.61	155.96	1.24
30.00	172.86	169.27	1.52
35.00	185.20	181.64	1.80
40.00	194.70	190.20	2.02
45.65	198.50	194.00	2.11

Table B.56: Experiment Gr2 [mm]

Time [s]	X_1	X_2	d_g
5.00	44.56	44.44	0.19
10.00	57.56	57.77	0.40
15.00	68.70	67.30	0.60
20.00	77.99	76.82	0.86
25.00	86.03	84.44	1.10
30.00	93.46	90.79	1.33
35.00	99.65	97.77	1.61
40.00	103.98	102.85	1.83
45.00	108.93	106.66	2.01
50.00	113.89	110.47	2.20
55.00	118.84	115.55	2.46
60.00	122.55	119.99	2.71
65.00	126.26	123.80	2.93
70.00	130.60	126.98	3.12
75.00	134.31	130.79	3.36
80.00	137.40	133.96	3.57
85.13	140.50	136.50	3.74

Table B.57: Experiment Gr3 [mm]

Time [s]	X_1	X_2	d_g
5.00	52.50	49.95	0.15
10.00	72.92	70.52	0.39
15.00	87.50	83.25	0.61
20.00	94.31	93.04	0.82
25.00	105.00	102.83	1.06
30.00	113.75	112.63	1.33
35.00	124.44	122.42	1.64
40.00	129.31	127.32	1.81
45.00	135.14	133.20	2.03
50.00	141.94	139.07	2.26
55.00	148.75	146.91	2.58
60.00	153.61	152.78	2.85
65.00	159.44	158.66	3.12
70.00	164.31	162.58	3.31
75.00	169.17	167.47	3.56
80.00	173.06	171.39	3.77
85.00	177.92	176.29	4.04
90.00	182.78	180.21	4.26
95.00	186.67	184.12	4.49
100.00	190.56	187.06	4.66
105.62	192.50	190.00	4.84

Table B.58: Experiment Gr4 [mm]

Time [s]	X_1	X_2	d_g
5.00	60.95	57.44	0.18
10.00	82.12	77.11	0.40
15.00	97.35	92.06	0.63
20.00	108.36	103.86	0.86
25.00	119.36	113.30	1.07
30.00	128.68	123.53	1.33
35.00	136.30	130.61	1.53
40.00	144.76	138.48	1.77
45.00	150.69	144.77	1.98
50.00	157.46	151.07	2.20
54.22	160.00	155.00	2.34

Table B.59: Experiment Gr5 [mm]

Time [s]	X_1	X_2	d_g
5.00	49.88	50.30	0.13
10.00	67.03	67.07	0.29
15.00	81.84	81.55	0.49
20.00	93.53	92.98	0.69
25.00	103.66	102.89	0.90
30.00	113.01	112.03	1.12
35.00	122.37	120.42	1.34
40.00	130.16	128.04	1.56
45.00	137.18	134.90	1.78
50.00	144.97	142.52	2.04
55.00	151.21	149.38	2.29
58.83	159.00	157.00	2.59

Table B.60: Experiment Gr6 [mm]

Time [s]	X_1	X_2	d_g
5.00	56.65	57.18	0.18
10.00	77.32	77.54	0.41
15.00	91.87	92.42	0.65
20.00	103.35	104.17	0.88
25.00	114.07	113.57	1.10
30.00	123.25	122.97	1.34
35.00	130.14	130.02	1.54
40.00	138.57	138.63	1.81
45.00	145.46	144.12	1.99
50.00	150.81	151.17	2.24
55.00	156.94	156.65	2.45
59.15	160.00	159.00	2.54

Set up II

In these experiments, the fibre volume fraction $v_f = 45.5\%$, the thickness of the cavity $H = 2.32mm$ and the number of fibre layers $N = 6$.

Table B.61: Experiment Gra1 [mm]

Time [s]	X_1	X_2	d_g
10.00	69.03	67.83	0.15
20.00	89.59	87.13	0.29
30.00	105.44	104.86	0.44
40.00	118.23	117.97	0.58
50.00	130.86	129.33	0.73
60.00	138.12	138.07	0.87
70.00	149.92	147.68	1.02
80.00	158.34	157.29	1.17
90.00	166.76	163.41	1.31
100.00	175.18	172.14	1.46
110.00	181.92	178.26	1.60
119.29	189.50	187.00	1.74

Table B.62: Experiment Gra2 [mm]

Time [s]	X_1	X_2	d_g
10.00	70.62	70.15	0.15
20.00	94.16	92.46	0.29
30.00	111.28	109.47	0.44
40.00	125.19	121.16	0.58
50.00	138.03	134.98	0.73
60.00	148.73	145.61	0.87
70.00	158.36	156.23	1.02
80.00	169.06	165.80	1.17
90.00	177.62	174.30	1.31
100.00	186.18	181.74	1.46
110.00	192.60	189.18	1.60
120.00	200.09	196.62	1.75
130.00	206.51	204.06	1.89
139.86	214.00	211.50	2.04

Table B.63: Experiment Gra3 [mm]

Time [s]	X_1	X_2	d_g
10.00	62.14	61.23	0.15
20.00	81.97	81.57	0.30
30.00	96.13	94.81	0.45
40.00	108.75	108.64	0.60
50.00	118.46	117.53	0.75
60.00	130.12	128.39	0.90
70.00	137.88	137.28	1.05
80.00	144.68	144.19	1.20
90.00	153.42	151.11	1.35
100.00	159.25	157.03	1.50
110.00	166.04	164.93	1.65
120.00	171.87	170.86	1.80
130.00	177.70	174.81	1.95
140.00	182.55	179.75	2.10
150.00	187.41	185.67	2.25
160.00	192.26	190.61	2.40
170.00	198.09	195.55	2.55
174.65	201.00	199.50	2.62

Set up III

In these experiments, the fibre volume fraction $v_f = 22.7\%$, the thickness of the cavity $H = 4.64mm$ and the number of fibre layers $N = 6$.

Table B.64: Experiment Grb1 [mm]

Time [s]	X_1	X_2	d_g
10.00	103.38	102.98	0.47
20.00	140.24	139.23	0.94
30.00	165.61	164.33	1.41
40.00	188.82	186.24	1.88
50.00	205.70	204.87	2.35
60.00	224.68	223.49	2.82
70.00	241.56	238.83	3.30
76.13	250.00	246.50	3.58

Table B.65: Experiment Grb2 [mm]

Time [s]	X_1	X_2	d_g
10.00	101.13	100.29	0.47
20.00	133.90	133.73	0.94
30.00	160.12	159.52	1.41
40.00	179.78	179.58	1.87
50.00	196.64	194.86	2.34
54.54	206.00	202.50	2.56

Table B.66: Experiment Grb3 [mm]

Time [s]	X_1	X_2	d_g
10.00	114.42	113.39	0.47
20.00	155.20	154.31	0.95
30.00	183.53	180.03	1.42
40.00	207.32	204.58	1.89
50.00	226.58	225.62	2.36
60.00	245.84	244.32	2.84
62.78	251.50	249.00	2.97

B.3.2 Experiments of twill weave

Set up I

In these experiments, The RC 600 was used and the fibre volume fraction $v_f = 50.4\%$, the thickness of the cavity $H = 2.32mm$ and the number of fibre layers $N = 5$.

Table B.67: Experiment Gt1 [mm]

Time [s]	X_1	X_2	d_g
10	18.81	11.93	0.00
30	47.03	25.57	0.04
50	59.57	32.39	0.09
70	68.97	39.20	0.15
90	76.81	40.91	0.19
110	81.51	47.73	0.24
130	86.22	52.84	0.29
150	94.05	54.55	0.35
170	98.76	57.95	0.41
190	101.89	61.36	0.45
210	111.30	64.77	0.56
230	112.86	68.18	0.59
262.82	116.00	75.00	0.65

Table B.68: Experiment Gt2 [mm]

Time [s]	X_1	X_2	d_g
20	33.19	27.64	0.02
40	53.62	37.31	0.07
60	62.55	41.45	0.11
80	68.94	45.60	0.15
100	75.32	51.13	0.19
120	84.26	53.89	0.25
140	88.09	60.80	0.30
160	95.74	64.95	0.37
180	103.40	67.71	0.44
200	108.51	69.09	0.50
220	113.62	71.85	0.56
240	116.17	74.62	0.60
260.02	120.00	76.00	0.65

Table B.69: Experiment Gt3 [mm]

Time [s]	X_1	X_2	d_g
10	42.00	24.63	0.02
20	59.29	32.47	0.05
30	66.71	43.67	0.08
40	71.65	49.27	0.10
50	79.06	51.51	0.12
60	86.47	52.63	0.15
70	88.94	57.11	0.17
80	95.12	61.58	0.20
90	101.29	63.82	0.23
100	107.47	64.94	0.27
110	113.65	67.18	0.31
120	116.12	71.66	0.33
130	121.06	72.78	0.37
140	123.53	76.14	0.39
150	124.76	78.38	0.40
167.41	126.00	79.50	0.42

Table B.70: Experiment Gt4 [mm]

Time [s]	X_1	X_2	d_g
20	43.09	29.71	0.03
30	52.00	32.54	0.05
40	65.37	39.62	0.09
50	69.83	43.86	0.12
60	77.26	49.52	0.15
70	80.23	50.94	0.17
80	86.17	53.77	0.21
90	89.14	56.60	0.23
100	92.11	58.01	0.25
110	98.06	62.26	0.29
120	101.03	65.09	0.32
142.2	104.00	66.50	0.35

Table B.71: Experiment Gt5 [mm]

Time [s]	X_1	X_2	d_g
20	42.87	25.81	0.03
40	59.47	37.96	0.09
60	67.77	45.56	0.13
80	71.91	48.59	0.16
100	81.60	51.63	0.22
120	89.89	57.70	0.29
140	96.81	60.74	0.34
160	103.72	65.30	0.41
180	106.49	66.81	0.44
200	110.64	69.85	0.49
220	116.17	72.89	0.56
240	117.55	74.41	0.58
260	124.47	77.44	0.66
280	128.62	78.96	0.72
302.86	130.00	82.00	0.75

Table B.72: Experiment Gt6 [mm]

Time [s]	X_1	X_2	d_g
20	60.62	31.79	0.05
40	69.64	41.96	0.09
60	83.83	47.04	0.15
80	90.28	55.94	0.19
100	96.73	62.30	0.23
120	105.76	67.39	0.30
140	112.21	71.20	0.34
160	116.07	73.74	0.38
180	123.81	76.29	0.44
200	127.68	78.83	0.48
220	130.26	83.91	0.51
240	135.42	87.73	0.56
253.4	138.00	89.00	0.59

Set up III

The twill weave fabric WRE580T was used in these experiments. The fibre volume fraction $v_f = 58.6\%$, the thickness of the cavity $H = 2.32mm$ and the number of fibre layers $N = 6$.

Table B.73: Experiment Gtb1 [mm]

Time [s]	X_1	X_2	d_g
20.00	61.18	61.55	0.06
40.00	82.07	83.53	0.11
60.00	92.51	95.25	0.17
80.00	110.42	112.83	0.23
100.00	122.35	124.56	0.28
120.00	134.29	136.28	0.34
140.00	146.23	146.54	0.40
160.00	149.21	152.40	0.46
180.00	156.67	158.26	0.51
200.00	164.13	167.05	0.57
220.00	170.10	172.92	0.63
240.00	182.04	183.17	0.68
259.09	189.50	190.50	0.74

Table B.74: Experiment Gtb2 [mm]

Time [s]	X_1	X_2	d_g
30.00	65.12	66.81	0.12
60.00	88.99	92.67	0.23
90.00	108.53	112.07	0.35
120.00	119.38	122.84	0.46
150.00	132.41	135.78	0.58
180.00	138.92	144.40	0.69
210.00	149.77	155.17	0.81
240.00	156.28	161.64	0.93
270.00	164.96	172.41	1.04
300.00	173.65	181.03	1.16
316.54	184.50	187.50	1.22

Table B.75: Experiment Gtb3 [mm]

Time [s]	X_1	X_2	d_g
50.00	64.04	64.20	0.16
100.00	98.52	101.23	0.31
150.00	105.91	108.64	0.47
200.00	135.46	135.80	0.62
250.00	147.78	150.62	0.78
300.00	162.56	165.43	0.93
350.00	172.41	175.31	1.09
400.00	179.80	182.72	1.24
450.00	192.11	195.06	1.40
500.00	197.04	197.53	1.55
516.06	199.50	200.00	1.60

B.3.3 Experiments of E-LPb 567

Set up I

In these experiments, the fibre volume fraction $v_f = 44.5\%$, the thickness of the cavity $H = 2.32mm$ and the number of fibre layers $N = 4$.

Table B.76: Experiment Gu1 [mm]

Time [s]	X_1	X_2	d_g
5.00	23.76	59.23	0.05
15.00	39.61	88.85	0.20
25.00	47.53	101.54	0.31
35.00	53.47	118.46	0.46
45.00	59.41	129.04	0.58
55.00	65.35	139.62	0.72
65.00	69.31	145.96	0.82
75.00	75.25	158.65	1.02
85.00	79.22	167.12	1.16
95.00	81.20	173.46	1.27
105.00	83.18	181.92	1.42
115.00	87.14	188.27	1.55
125.00	91.10	194.62	1.70
135.00	93.08	200.96	1.83
145.00	95.06	207.31	1.97
155.00	99.02	213.65	2.14
162.80	101.00	220.00	2.29

Table B.77: Experiment Gu2 [mm]

Time [s]	X_1	X_2	d_g
10.00	33.70	63.82	0.13
30.00	48.45	97.86	0.42
50.00	56.87	117.01	0.68
70.00	63.19	131.90	0.93
90.00	69.51	148.92	1.26
110.00	73.72	159.56	1.50
130.00	77.94	170.20	1.77
150.00	82.15	178.71	2.00
170.00	86.36	187.22	2.26
190.00	90.57	197.85	2.59
210.00	92.68	206.36	2.85
230.00	96.89	214.87	3.16
249.80	99.00	217.00	3.26

Table B.78: Experiment Gu3 [mm]

Time [s]	X_1	X_2	d_g
20.00	30.22	63.94	0.22
40.00	37.78	83.31	0.48
60.00	43.44	96.88	0.73
80.00	49.11	106.56	0.97
100.00	54.78	122.06	1.38
120.00	58.56	129.81	1.63
140.00	60.44	135.62	1.82
160.00	64.22	145.31	2.18
180.00	68.00	149.19	2.37
200.00	71.78	158.88	2.78
220.00	73.67	164.69	3.03
240.00	75.56	170.50	3.30
260.00	79.33	178.25	3.70
280.00	83.11	184.06	4.05
300.22	85.00	186.00	4.18

Table B.79: Experiment Gu4 [mm]

Time [s]	X_1	X_2	d_g
10.00	30.94	57.55	0.11
20.00	38.49	72.13	0.22
30.00	43.77	77.50	0.28
40.00	49.06	92.08	0.44
50.00	52.83	103.59	0.59
60.00	56.60	112.03	0.73
70.00	61.13	118.17	0.85
80.00	64.15	124.31	0.97
90.00	67.17	128.91	1.08
100.00	69.43	137.35	1.25
110.00	72.45	141.96	1.37
120.00	73.96	148.09	1.51
130.00	77.74	152.70	1.65
144.34	80.00	155.00	1.73

Table B.80: Experiment Gu5 [mm]

Time [s]	X_1	X_2	d_g
5.00	25.58	61.82	0.07
15.00	43.85	92.73	0.27
30.00	52.99	117.02	0.50
45.00	60.30	132.48	0.70
60.00	67.61	143.51	0.88
75.00	71.26	156.76	1.08
90.00	74.92	167.80	1.28
105.00	78.57	174.43	1.42
120.00	84.05	187.67	1.71
135.00	87.71	196.51	1.91
150.00	91.36	205.34	2.13
165.00	95.02	209.75	2.27
180.00	98.67	216.38	2.46
193.28	100.50	223.00	2.64

Table B.81: Experiment Gu6 [mm]

Time [s]	X_1	X_2	d_g
10.00	38.81	68.02	0.13
20.00	44.94	88.63	0.26
30.00	51.06	103.06	0.39
40.00	57.19	117.49	0.55
50.00	63.32	123.67	0.64
60.00	67.40	133.98	0.79
70.00	71.49	144.29	0.95
80.00	75.57	152.53	1.09
90.00	77.62	158.71	1.20
100.00	81.70	164.90	1.33
110.00	83.74	171.08	1.46
120.00	87.83	177.26	1.60
130.00	89.87	183.45	1.74
140.00	91.91	191.69	1.93
150.00	93.96	197.88	2.08
159.18	96.00	202.00	2.19

Set up II

In these experiments, the fibre volume fraction $v_f = 44.5\%$, the thickness of the cavity $H = 2.32mm$ and the number of fibre layers $N = 4$.

Table B.82: Experiment Gua1 [mm]

Time [s]	X_1	X_2	d_g
20.00	44.79	91.57	0.14
40.00	55.39	114.46	0.27
60.00	62.46	134.66	0.41
80.00	69.54	152.17	0.55
100.00	76.61	165.63	0.69
120.00	81.32	175.06	0.82
140.00	84.86	187.18	0.96
160.00	88.39	196.61	1.10
180.00	94.29	208.73	1.23
200.00	96.64	215.46	1.37
210.92	99.00	219.50	1.45

Table B.83: Experiment Gua2 [mm]

Time [s]	X_1	X_2	d_g
30.00	50.46	109.94	0.21
60.00	65.06	142.63	0.42
90.00	75.68	163.43	0.63
120.00	82.32	182.74	0.83
150.00	90.29	202.06	1.04
180.00	96.93	209.49	1.25
210.00	102.24	221.37	1.46
240.00	107.55	233.26	1.67
270.00	112.86	243.66	1.88
300.00	116.84	257.03	2.09
315.71	119.50	260.00	2.20

Table B.84: Experiment Gua3 [mm]

Time [s]	X_1	X_2	d_g
40.00	51.61	175.67	0.27
80.00	65.68	224.94	0.54
120.00	78.58	276.36	0.80
160.00	85.62	306.35	1.07
200.00	93.83	334.20	1.34
240.00	100.87	351.34	1.61
280.00	106.73	379.19	1.88
320.00	112.60	402.75	2.14
360.00	117.29	419.89	2.41
400.00	121.98	265.65	2.68
417.38	125.50	278.50	2.80

Set up III

In these experiments, the fibre volume fraction $v_f = 44.5\%$, the thickness of the cavity $H = 2.32mm$ and the number of fibre layers $N = 4$.

Table B.85: Experiment Gub1 [mm]

Time [s]	X_1	X_2	d_g
20.00	56.59	107.76	0.28
40.00	73.15	141.86	0.56
60.00	84.19	171.87	0.84
80.00	93.85	190.97	1.12
100.00	100.76	210.07	1.39
120.00	109.04	229.17	1.67
140.00	114.56	244.17	1.95
160.00	122.84	253.72	2.23
180.00	125.60	266.00	2.51
200.00	131.12	278.27	2.79
207.78	132.50	281.00	2.90

Table B.86: Experiment Gub2 [mm]

Time [s]	X_1	X_2	d_g
20.00	54.52	112.20	0.28
40.00	69.89	148.22	0.55
60.00	81.08	167.61	0.83
80.00	90.86	191.16	1.11
100.00	97.85	210.55	1.39
120.00	107.63	223.02	1.66
140.00	114.62	235.48	1.94
160.00	121.61	250.72	2.22
180.00	127.20	267.34	2.49
188.51	130.00	271.50	2.61

Table B.87: Experiment Gub3 [mm]

Time [s]	X_1	X_2	d_g
20.00	48.81	97.84	0.29
40.00	61.27	131.87	0.57
60.00	69.58	158.46	0.86
80.00	81.00	171.22	1.14
100.00	87.23	183.98	1.43
120.00	92.42	196.75	1.72
126.05	94.50	201.00	1.80

Appendix C

The inlet pressure in the experiments

The following figures show the inlet pressure of time history during the experiments of permeability identification.

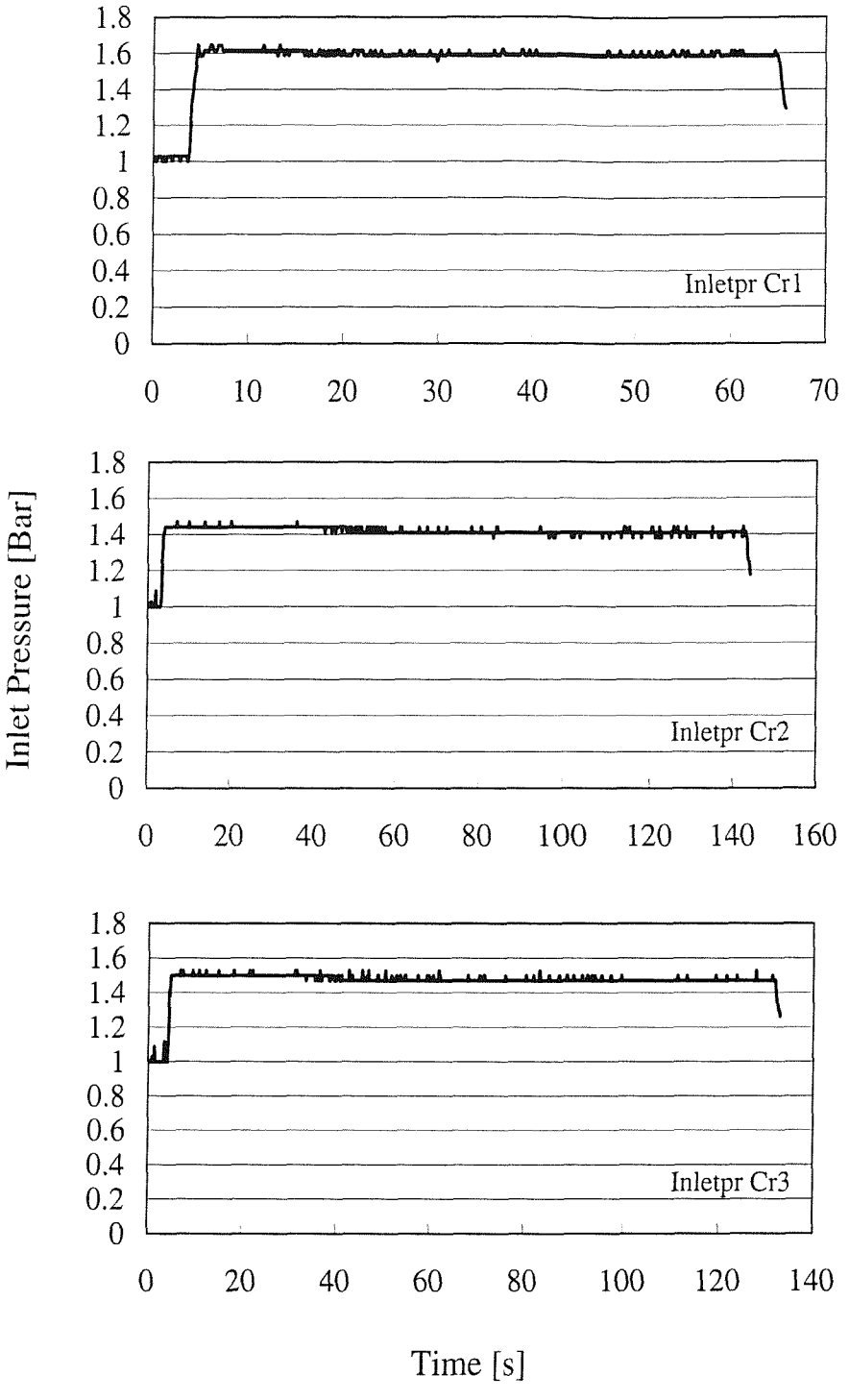

Figure C.1: Inlet pressures in constant pressure experiments of U750-450 in set up I (a).

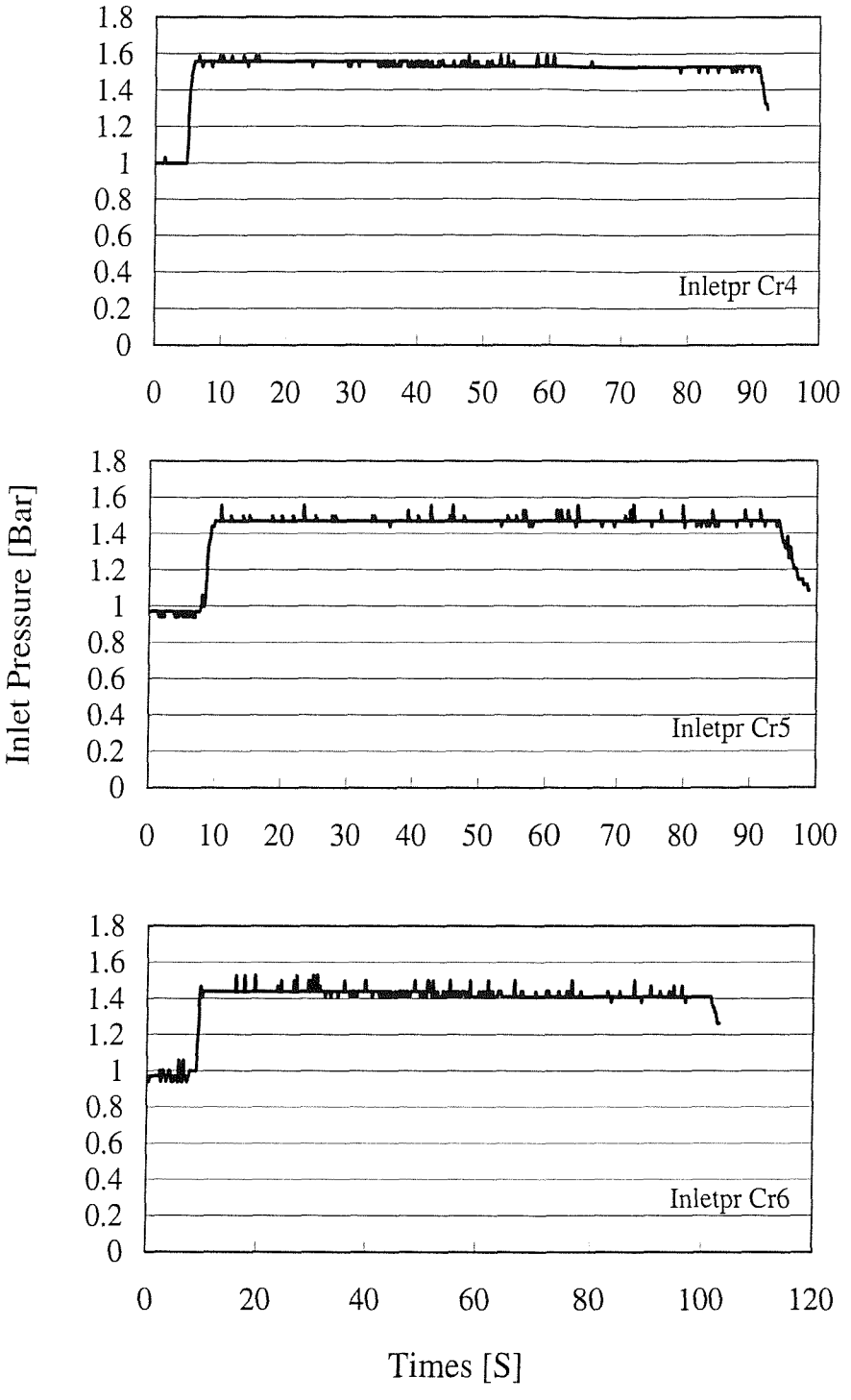

Figure C.2: Inlet pressures in constant pressure experiments of U750-450 in set up I (b).

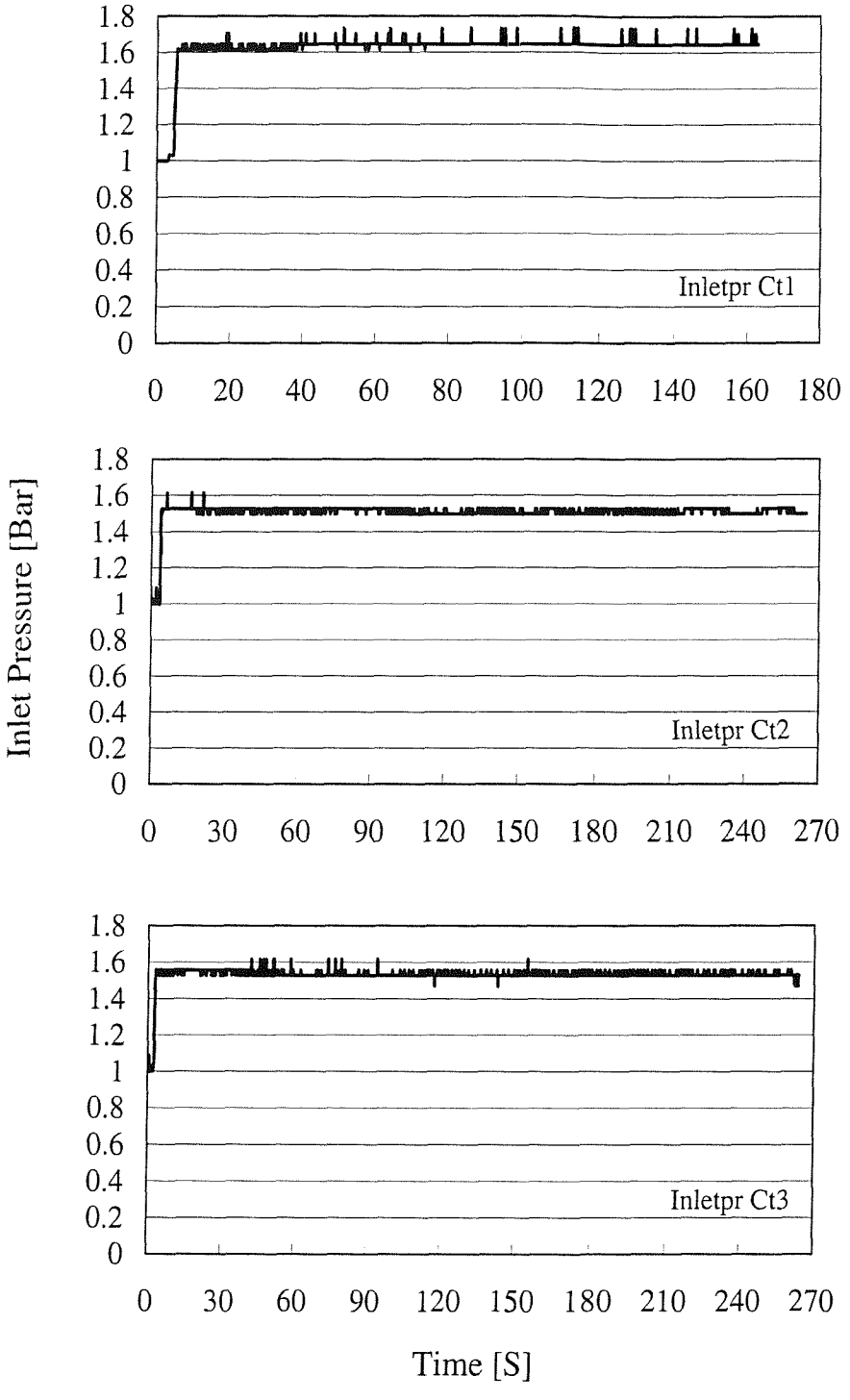

Figure C.3: Inlet pressures in constant pressure experiments of RC 600 in set up I (a).

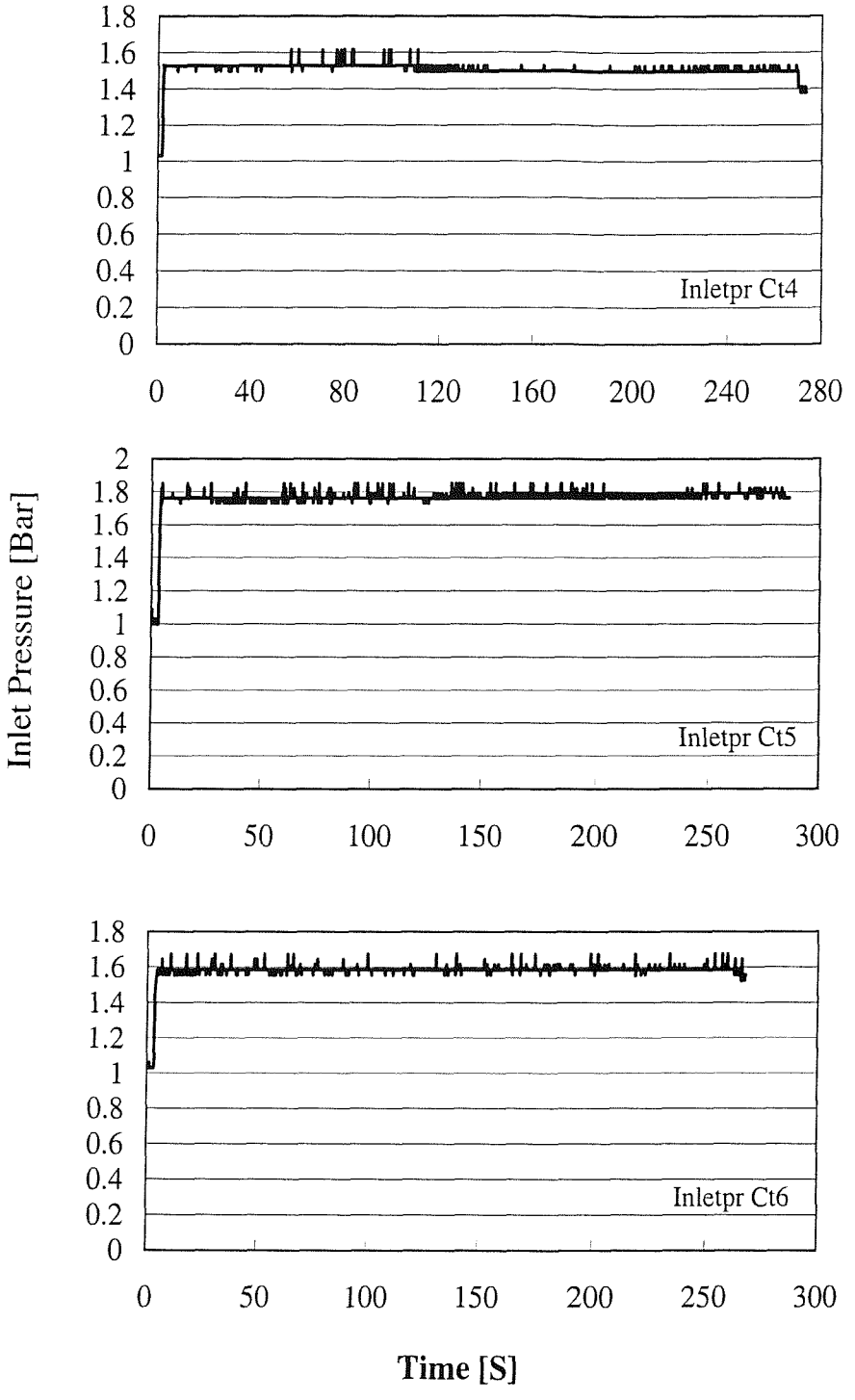

Figure C.4: Inlet pressures in constant pressure experiments of RC 600 in set up I (b).

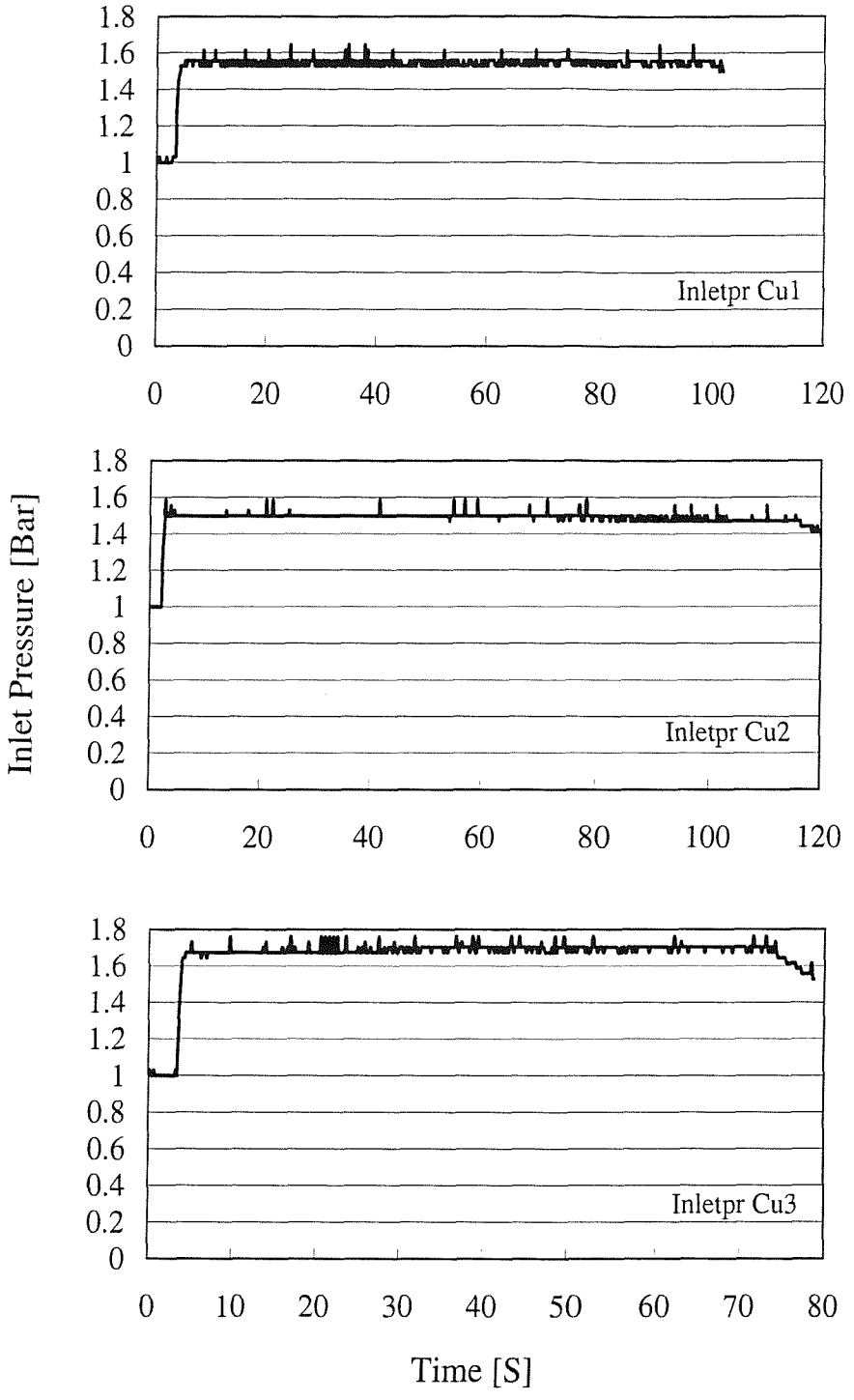

Figure C.5: Inlet pressures in constant pressure experiments of E-LPb 567 in set up I (a).

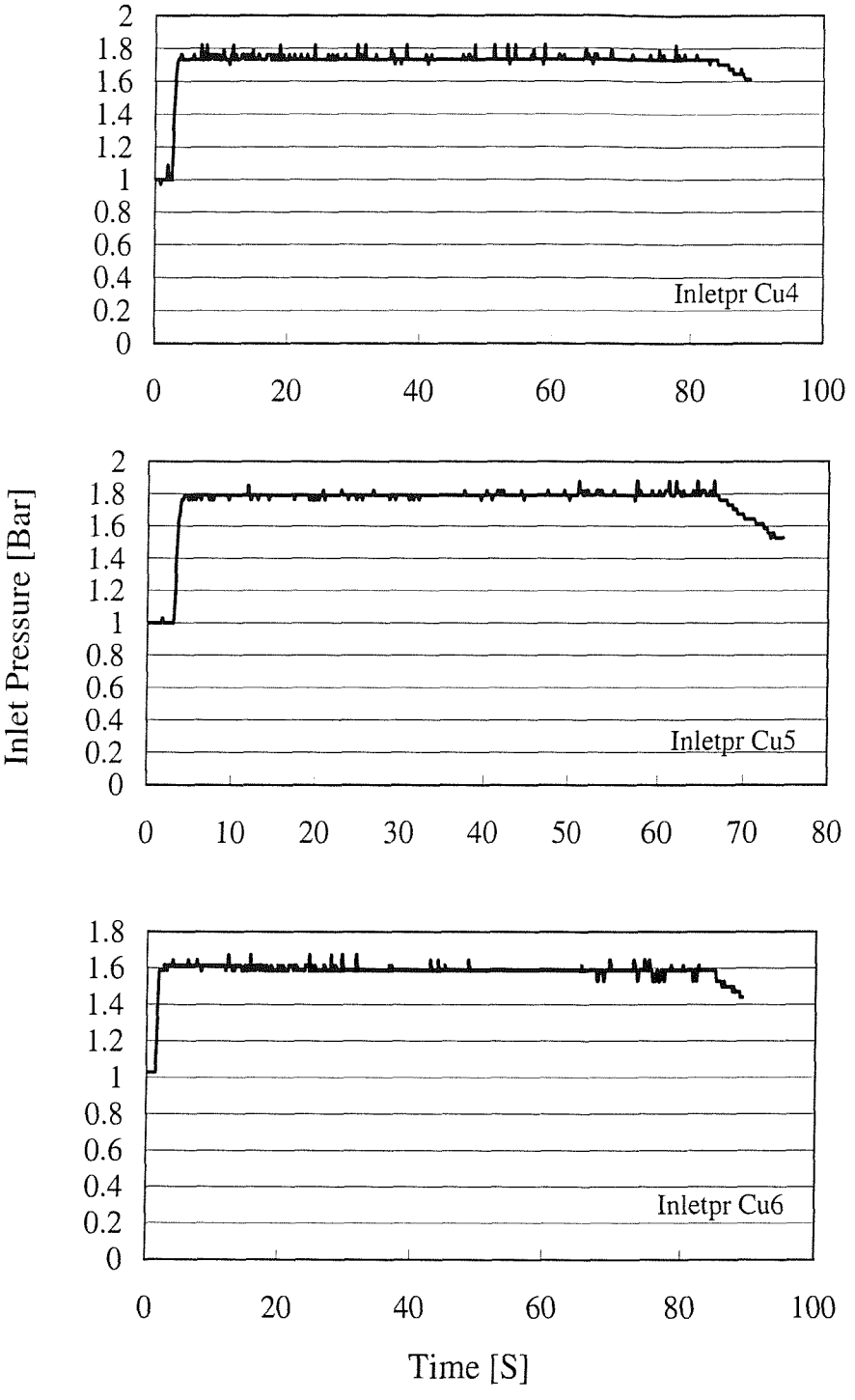

Figure C.6: Inlet pressures in constant pressure experiments of E-LPb 567 in set up I (b).

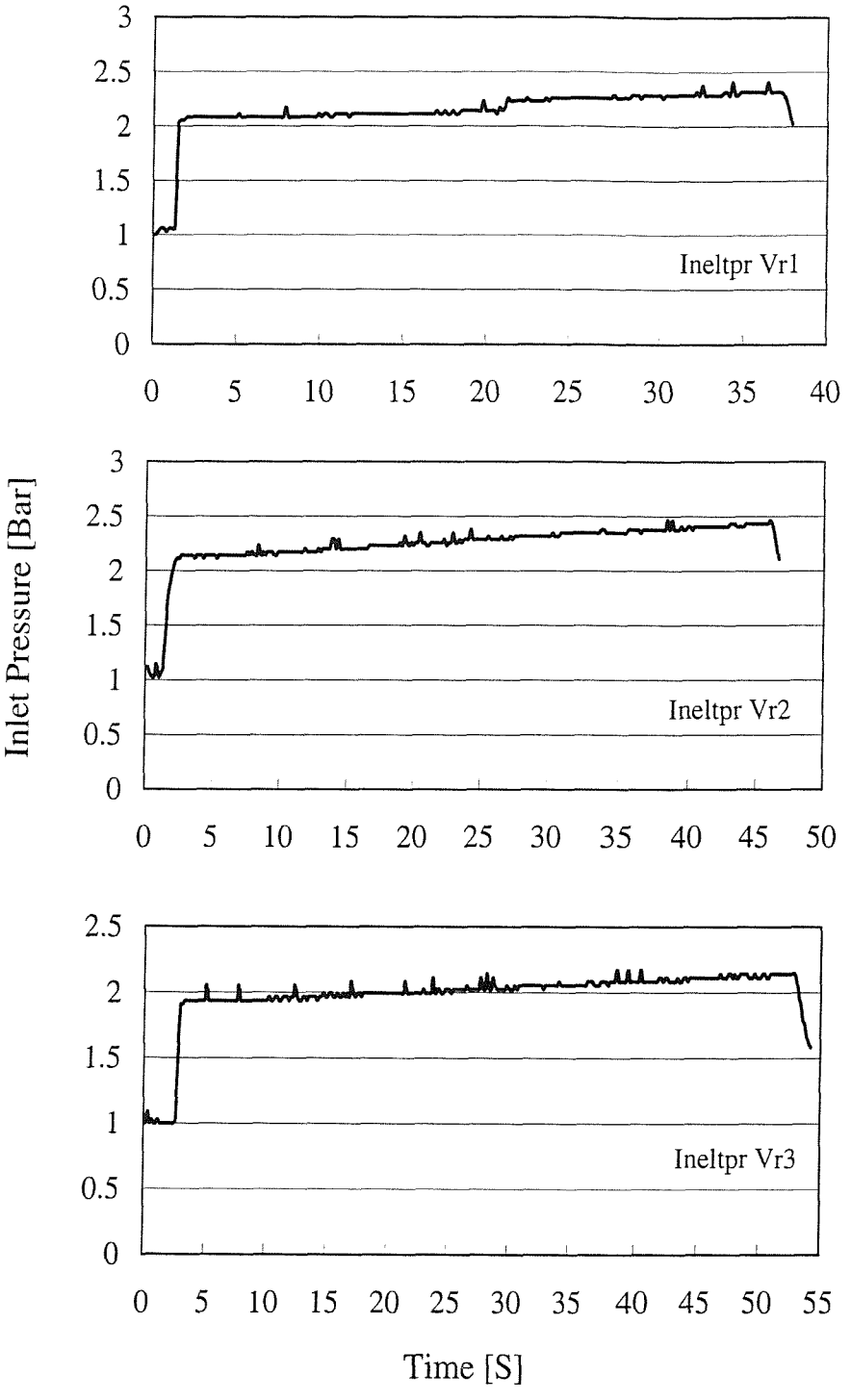

Figure C.7: Inlet pressures in variable pressure experiments of U750-450 in set up I (a).

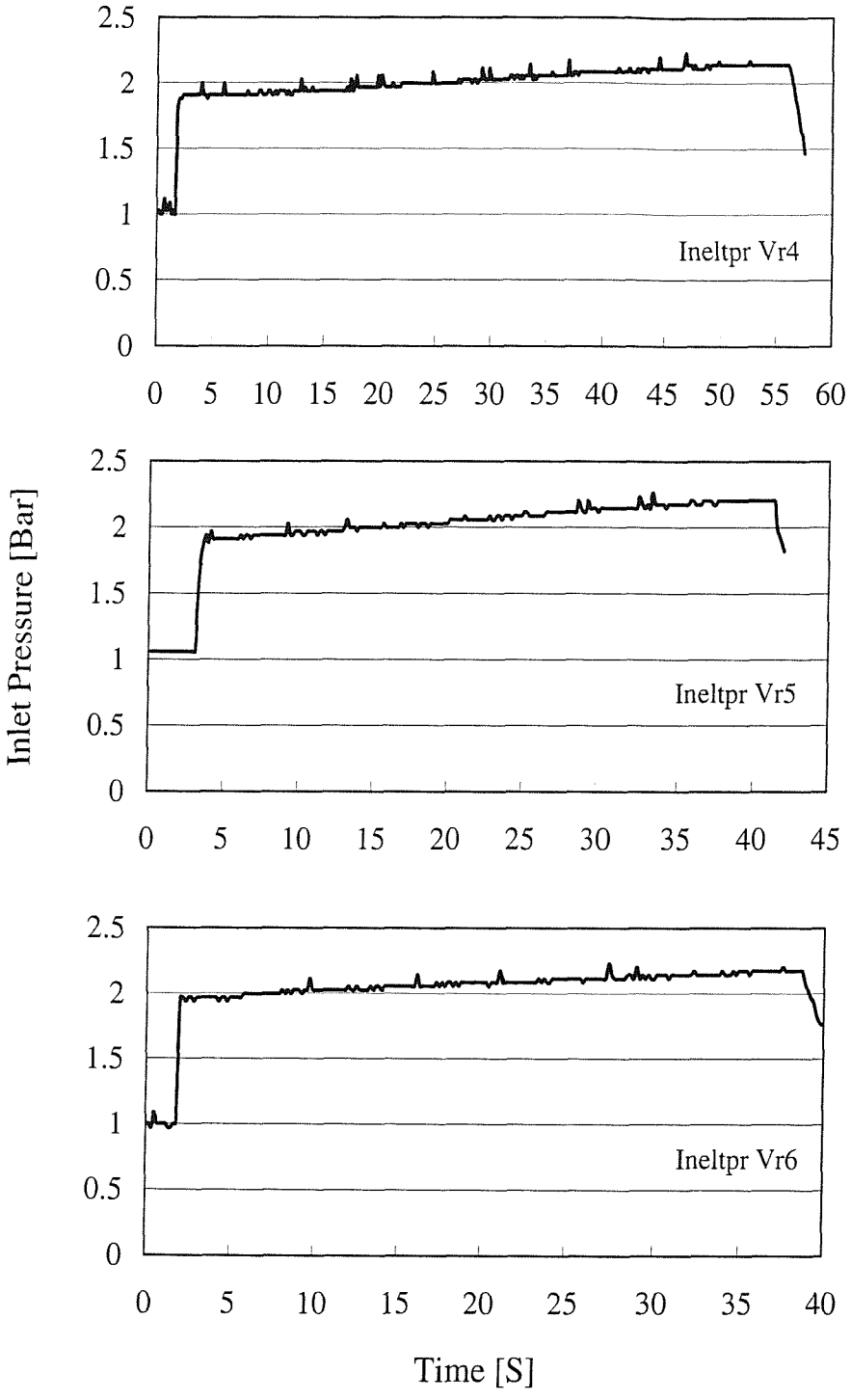

Figure C.8: Inlet pressures in variable pressure experiments of U750-450 in set up I (b).

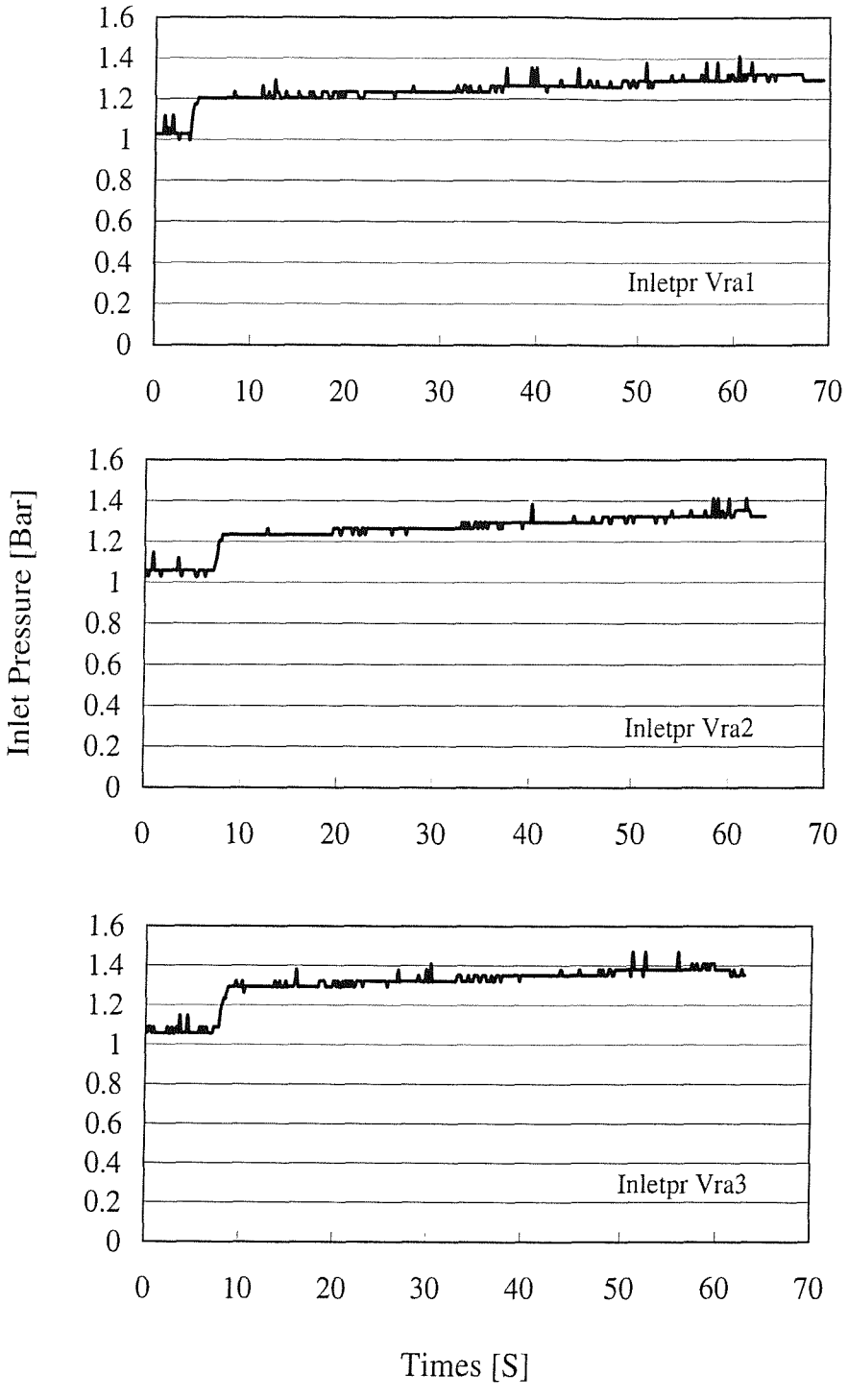

Figure C.9: Inlet pressures in variable pressure experiments of U750-450 in set up II.

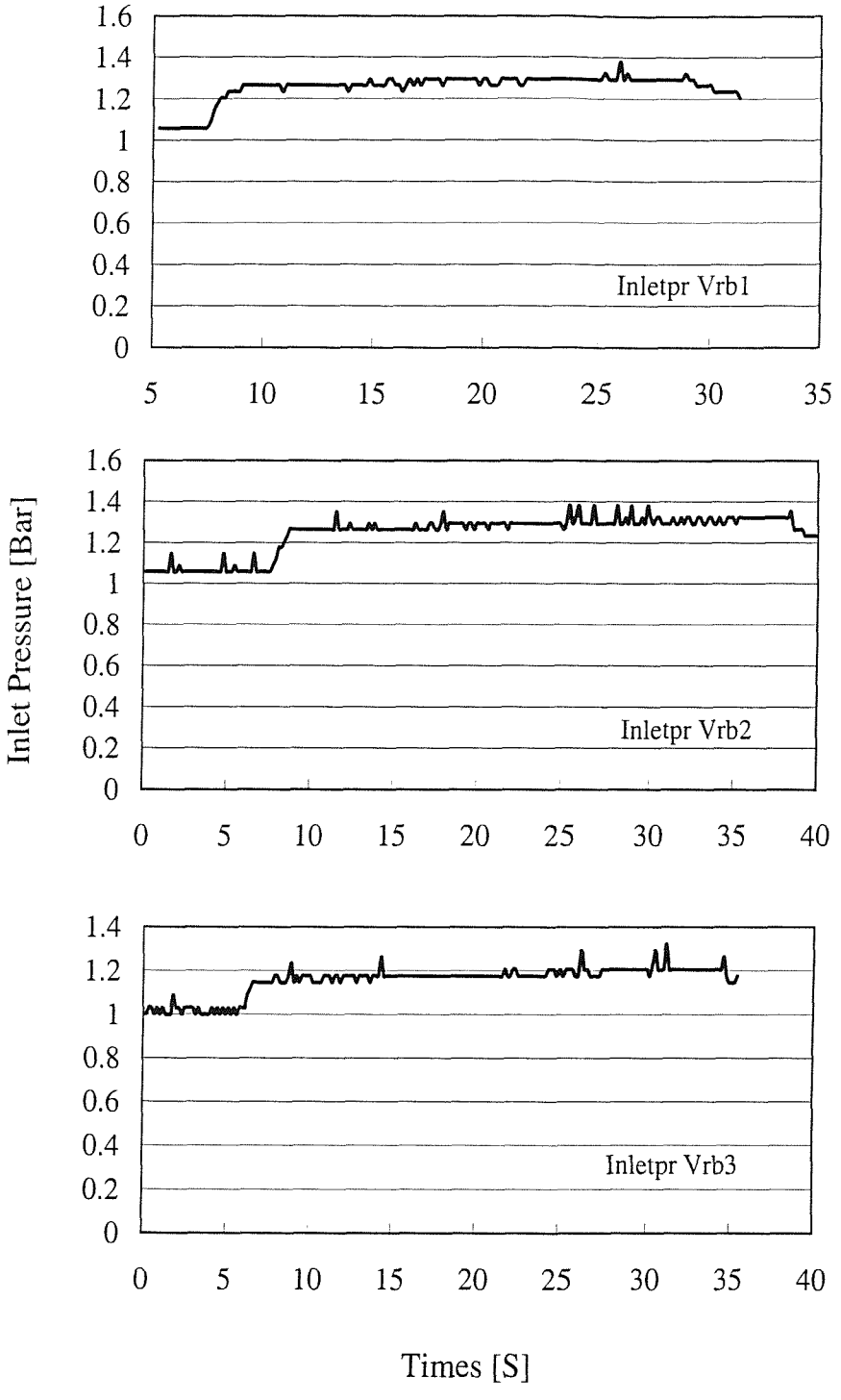

Figure C.10: Inlet pressures in variable pressure experiments of U750-450 in set up III.

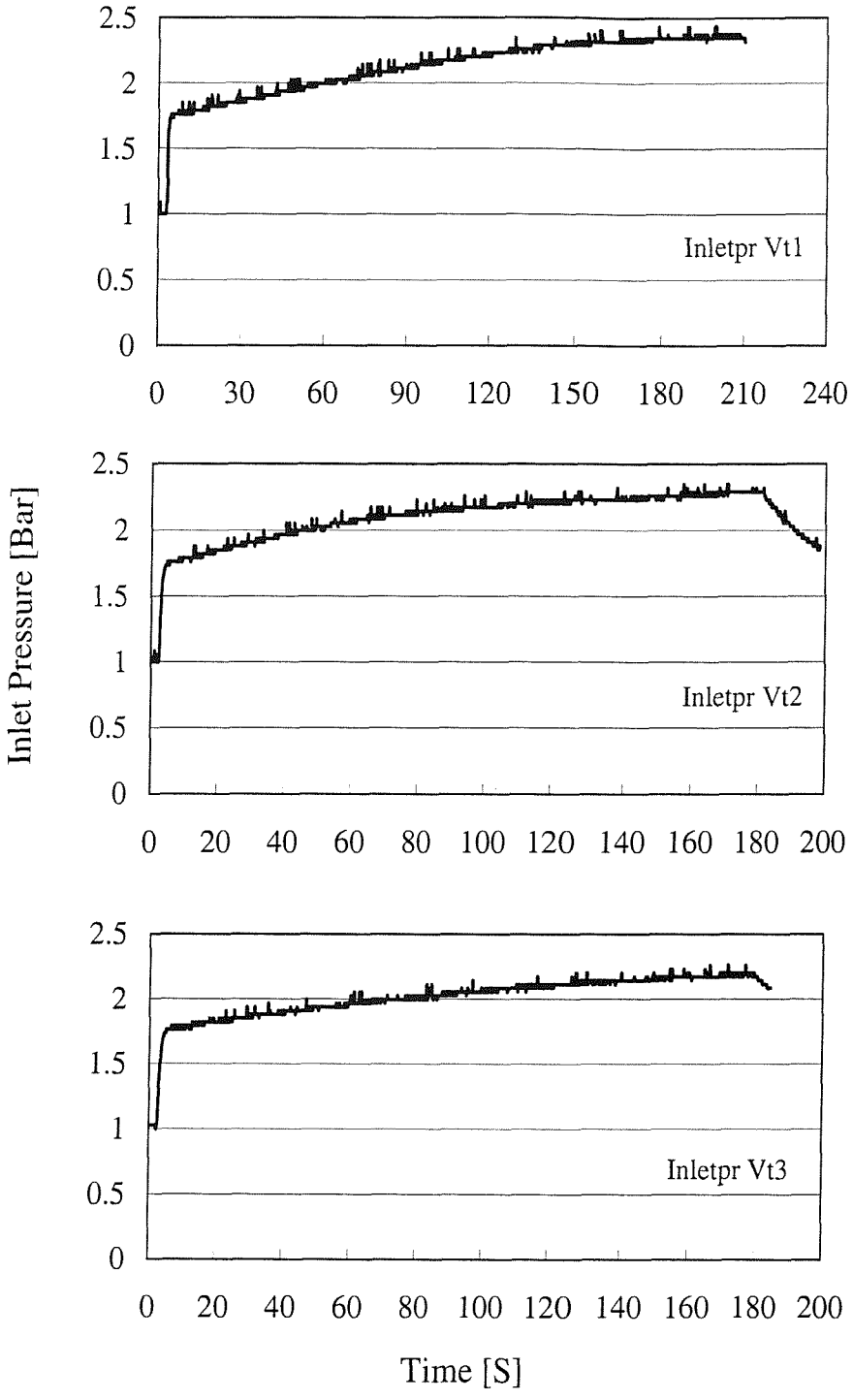

Figure C.11: Inlet pressures in variable pressure experiments of RC 600 in set up I (a).

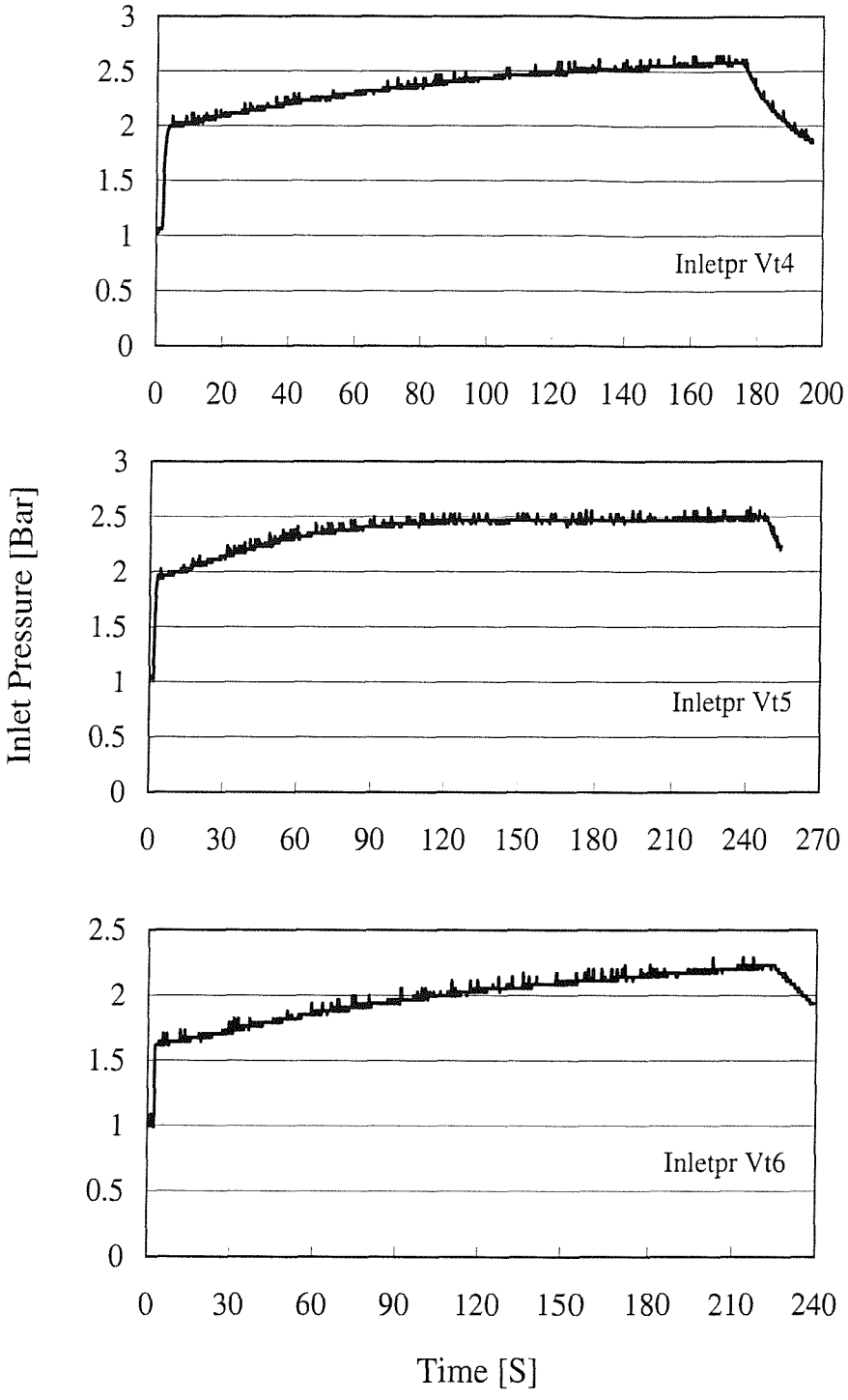

Figure C.12: Inlet pressures in variable pressure experiments of RC 600 in set up I (b).

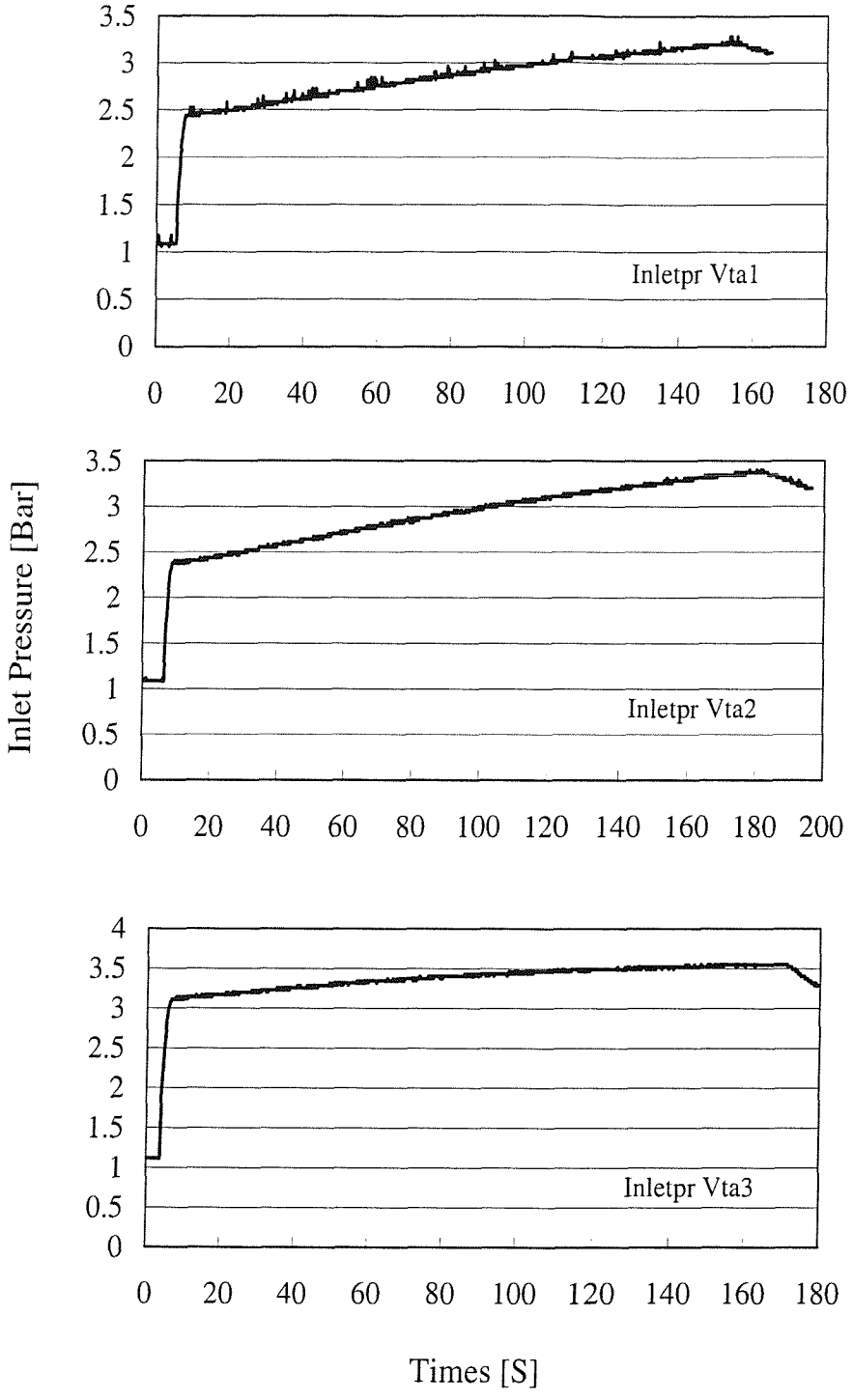

Figure C.13: Inlet pressures in variable pressure experiments of RC 600 in set up II.

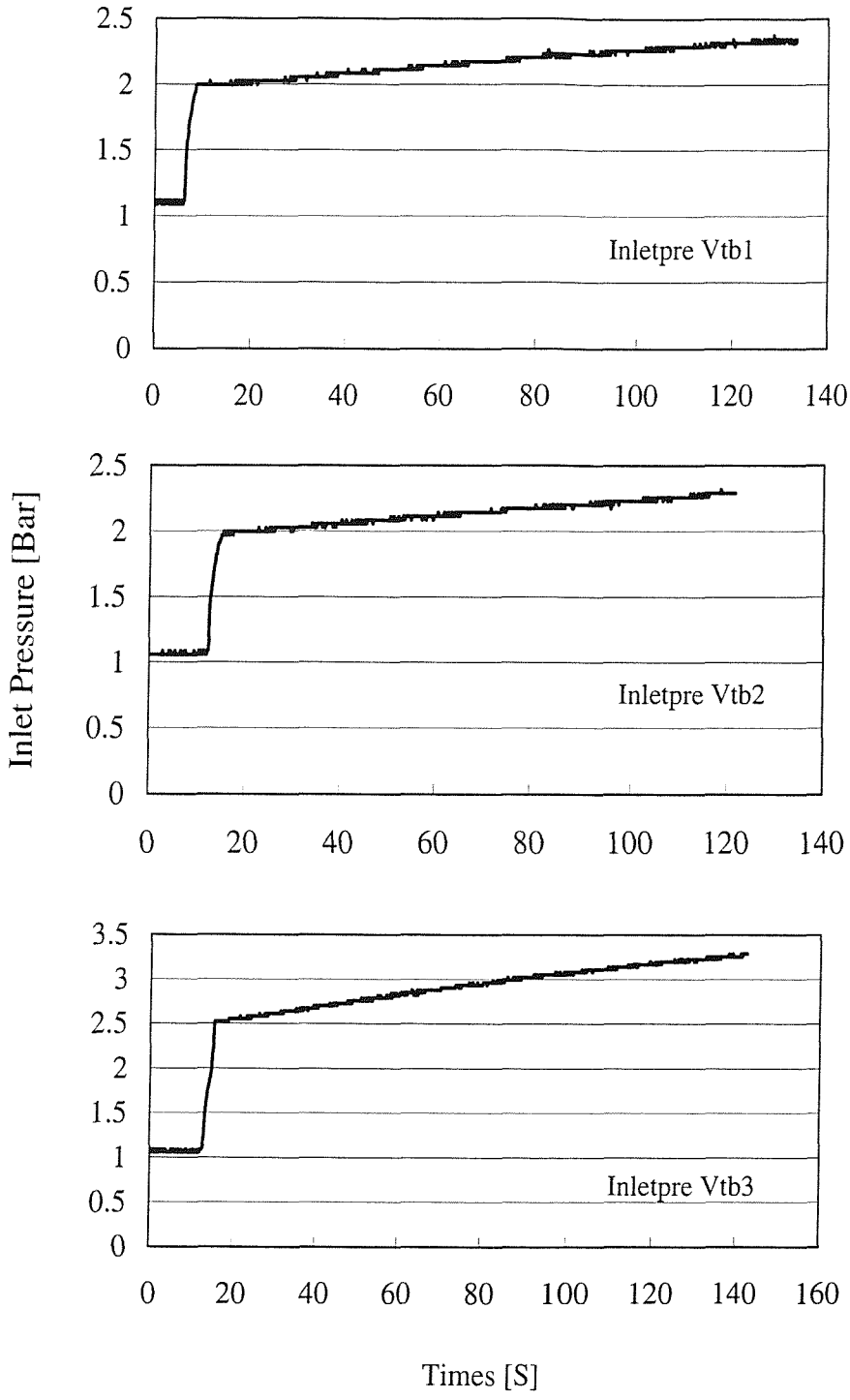

Figure C.14: Inlet pressures in variable pressure experiments of WRE580T in set up III.

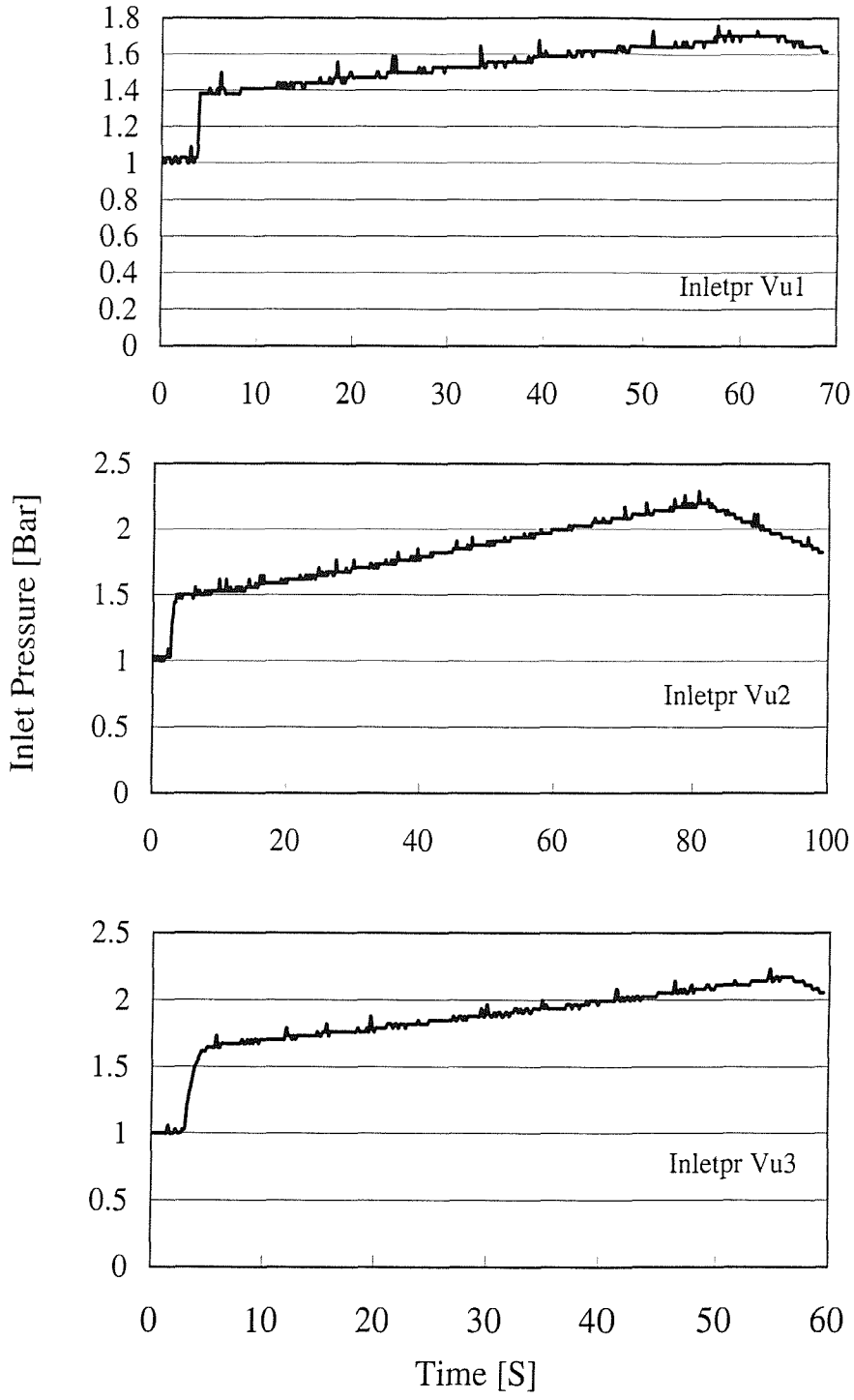

Figure C.15: Inlet pressures in variable pressure experiments of E-LPb 567 in set up I (a).

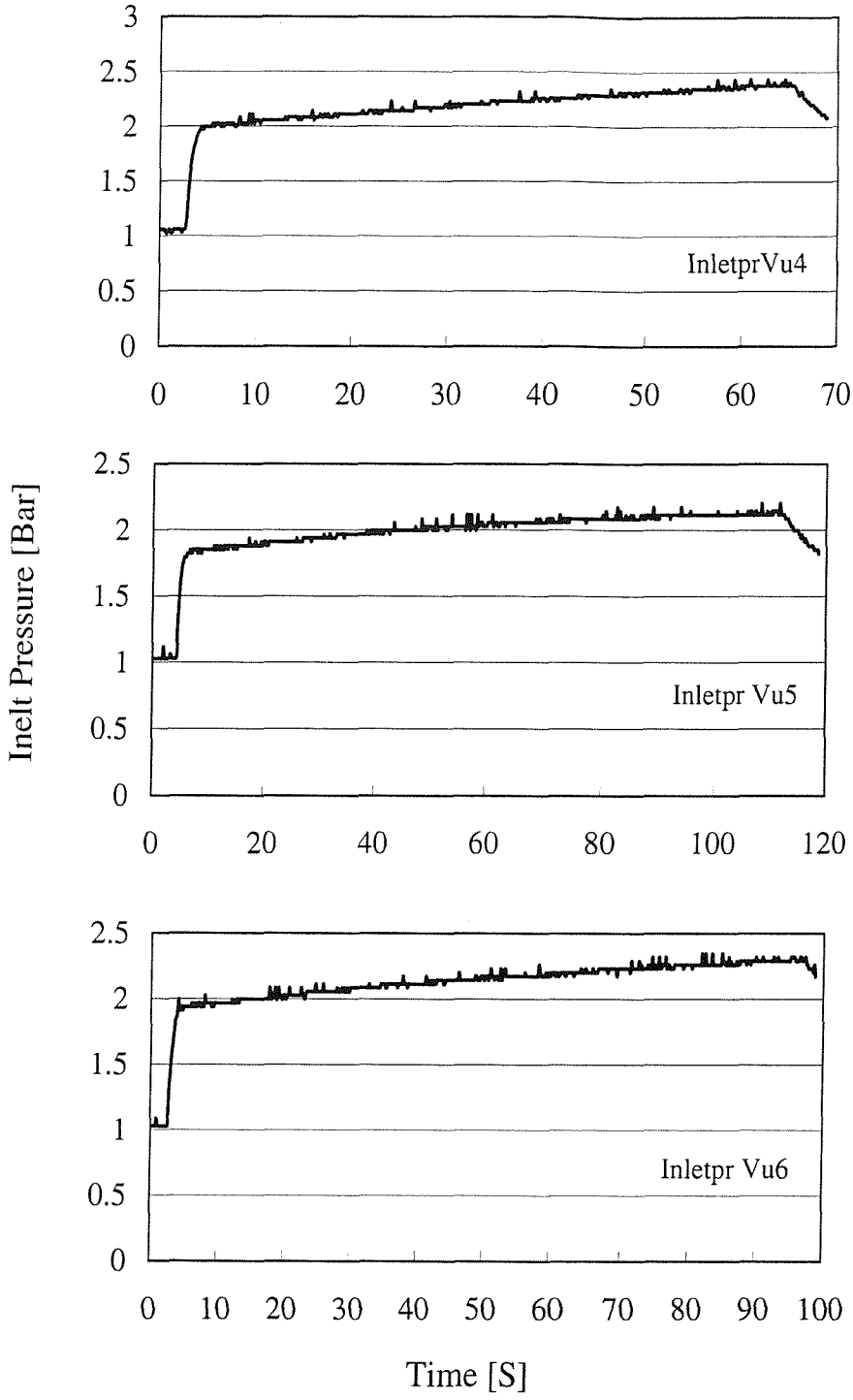

Figure C.16: Inlet pressures in variable pressure experiments of E-LPb 567 in set up I (b).

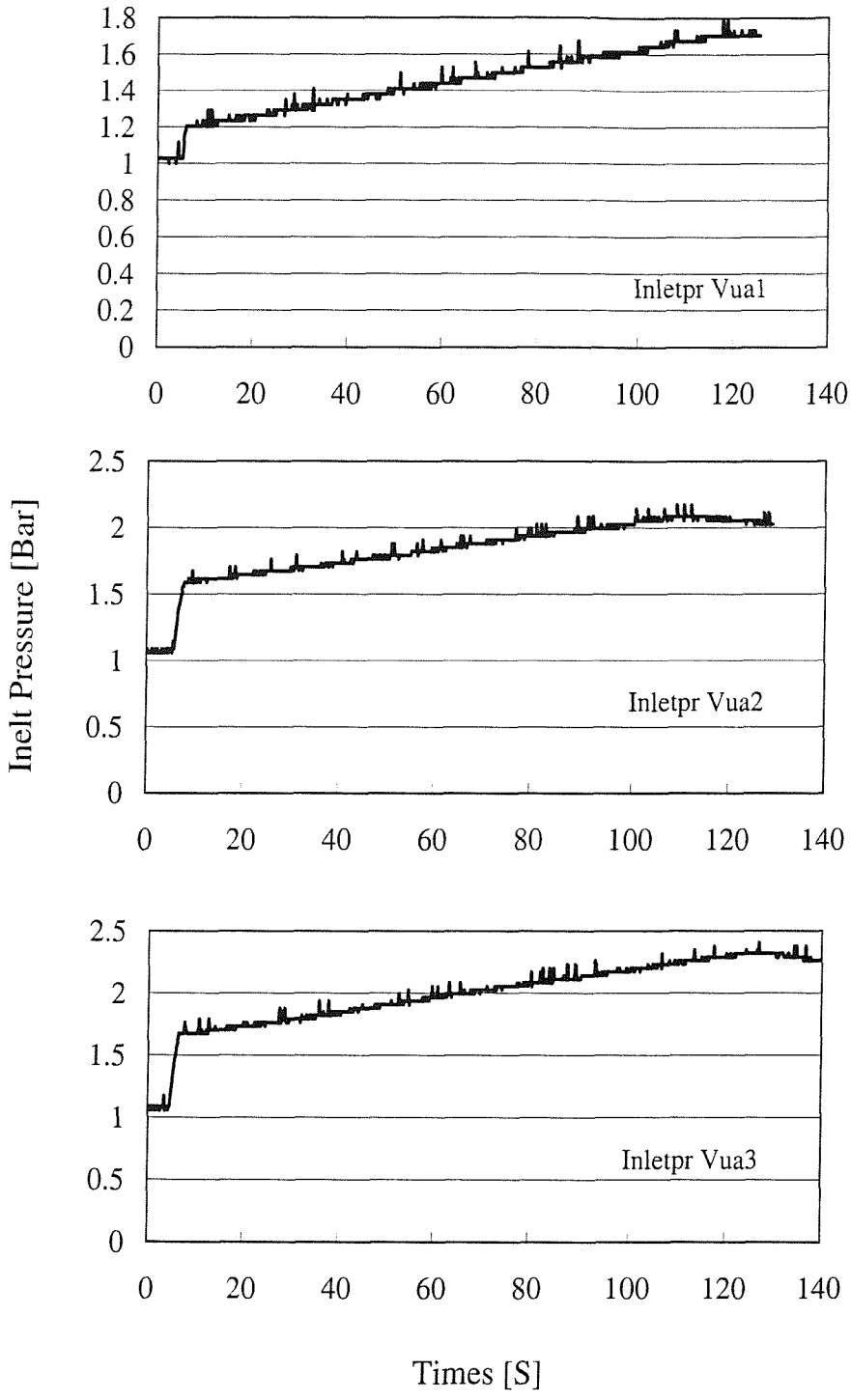

Figure C.17: Inlet pressures in variable pressure experiments of E-LPb 567 in set up II.

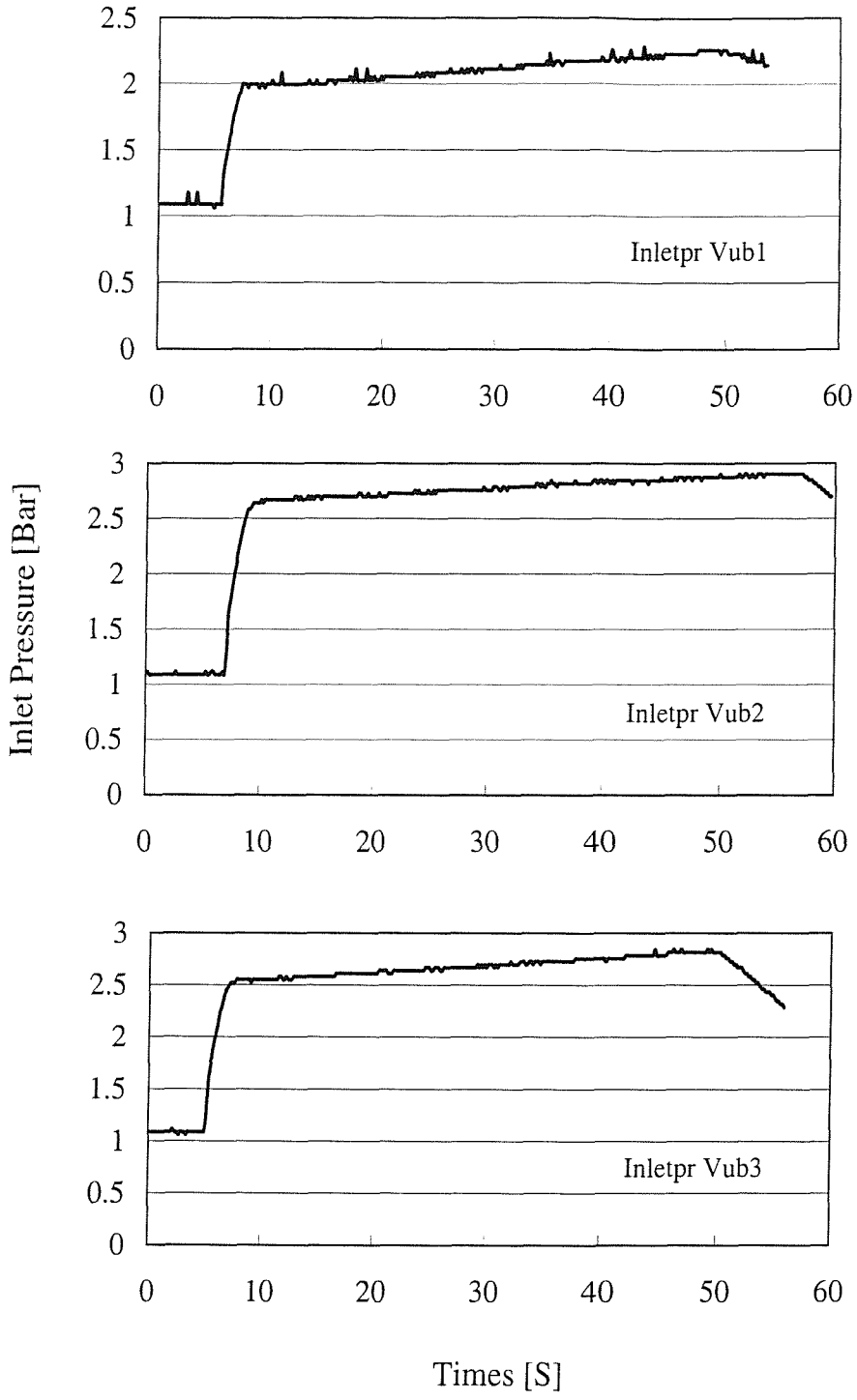

Figure C.18: Inlet pressures in variable pressure experiments of E-LPb 567 in set up III.

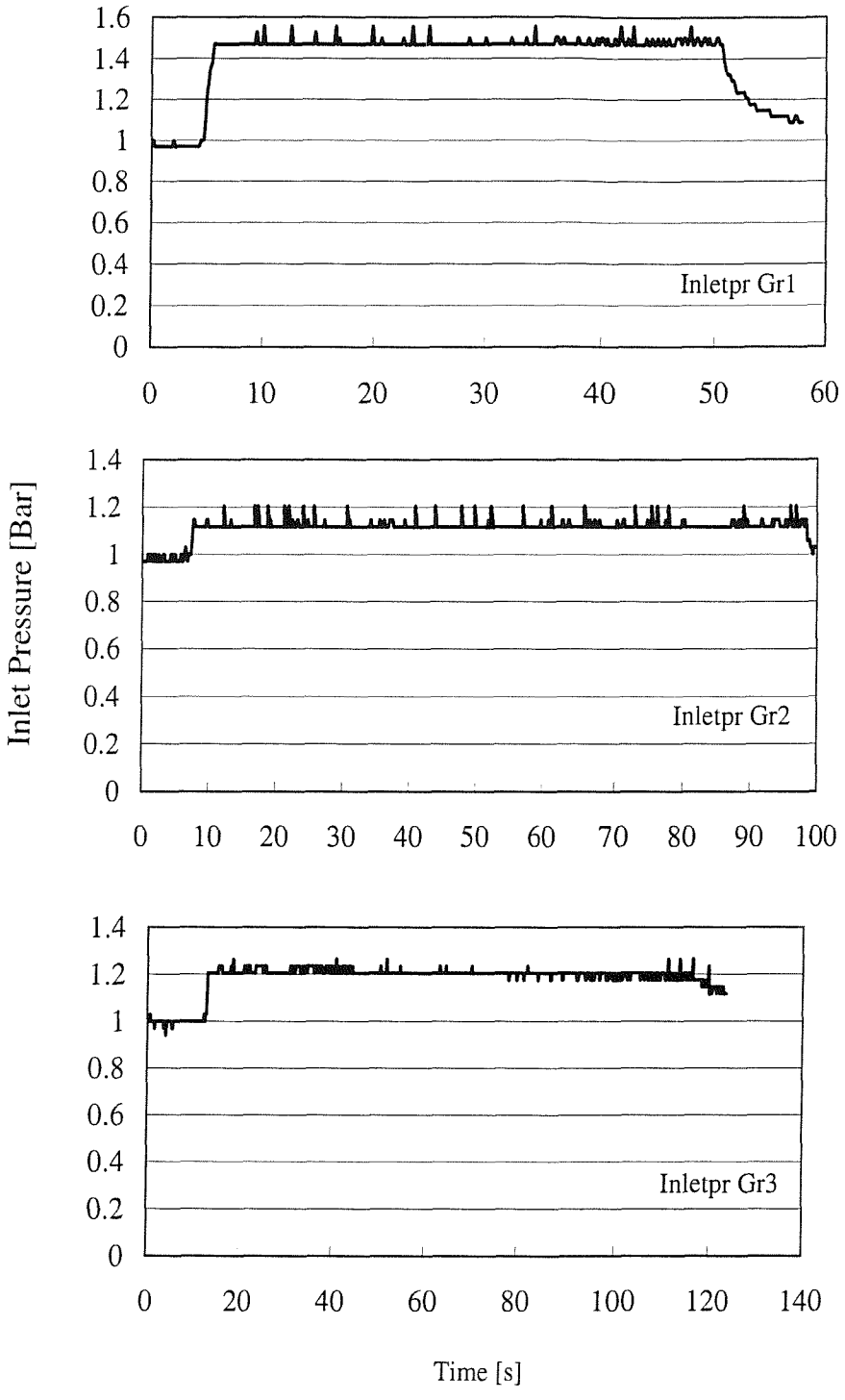

Figure C.19: Inlet pressures in vertical plane experiments of U750-450 in set up I (a).

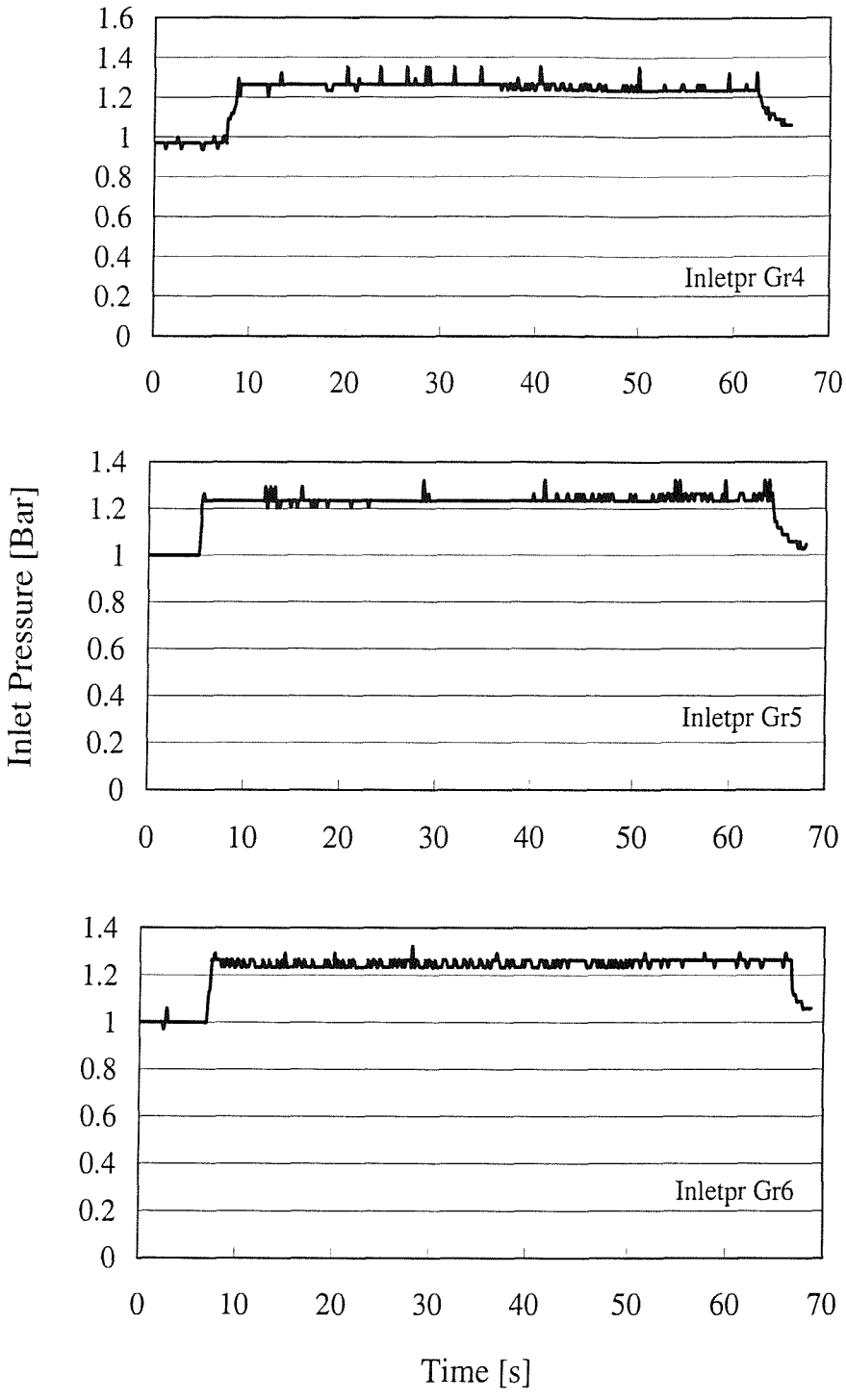

Figure C.20: Inlet pressures in vertical plane experiments of U750-450 in set up I (b).

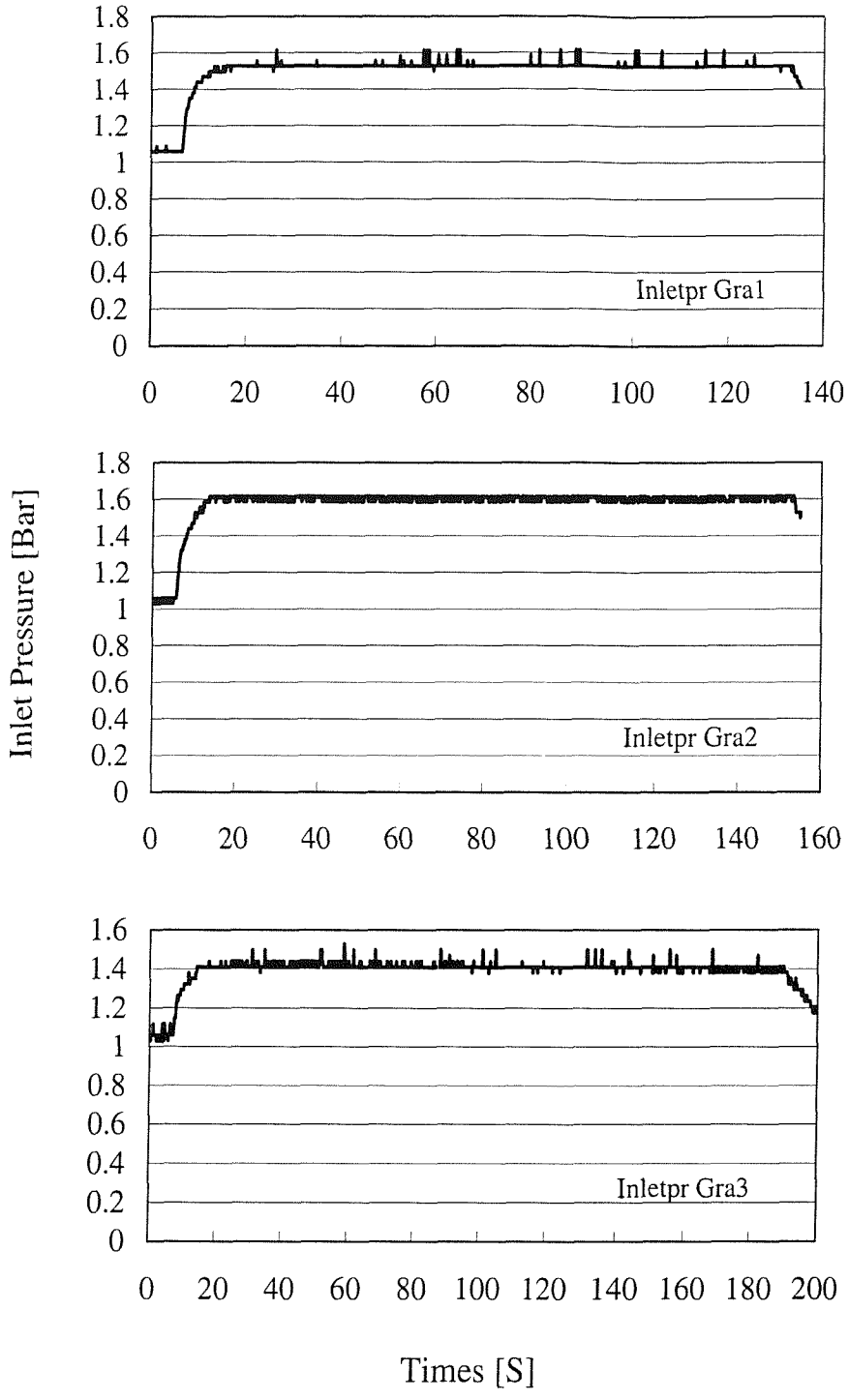

Figure C.21: Inlet pressures in vertical plane experiments of U750-450 in set up II.

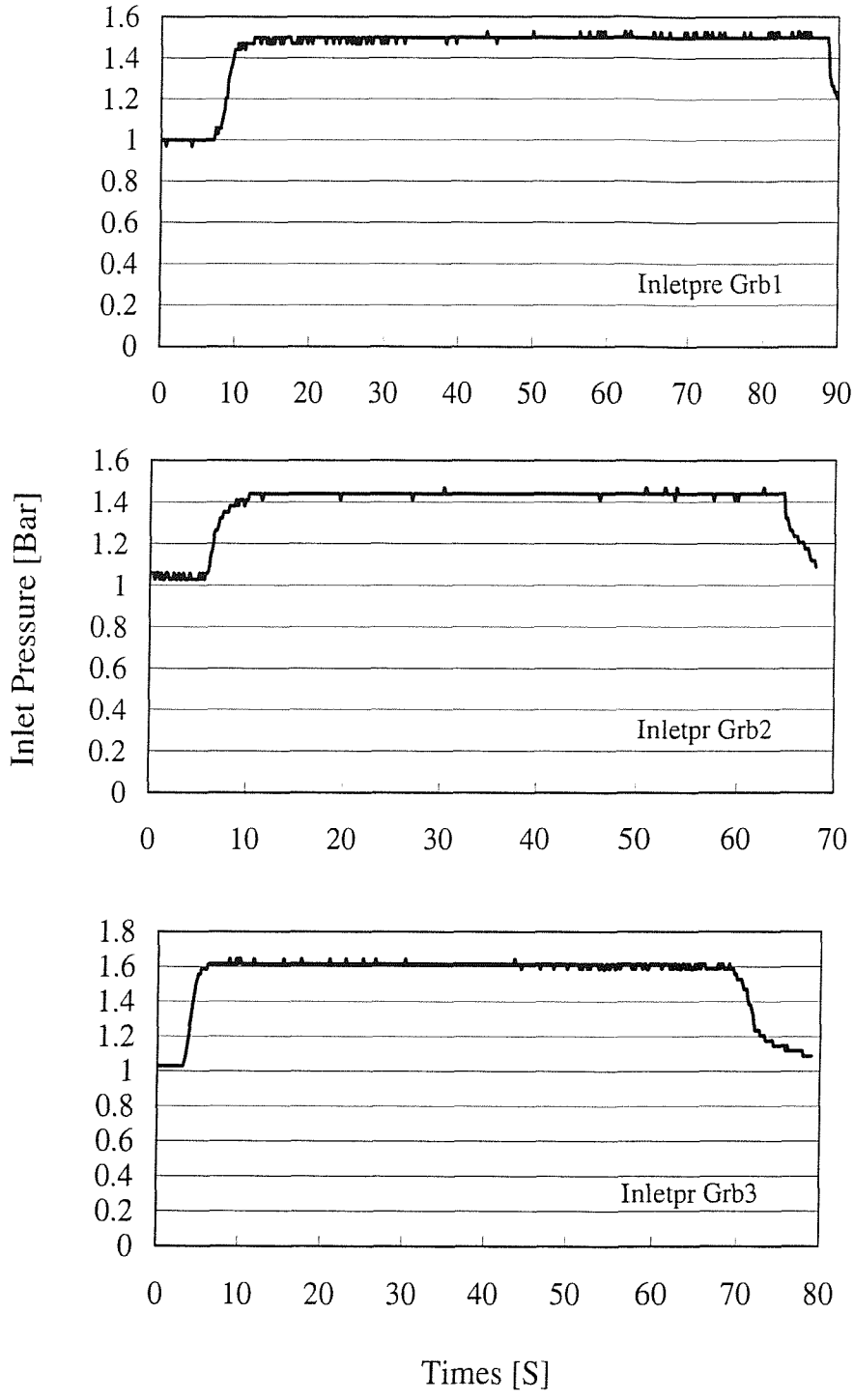

Figure C.22: Inlet pressures in vertical plane experiments of U750-450 in set up III.

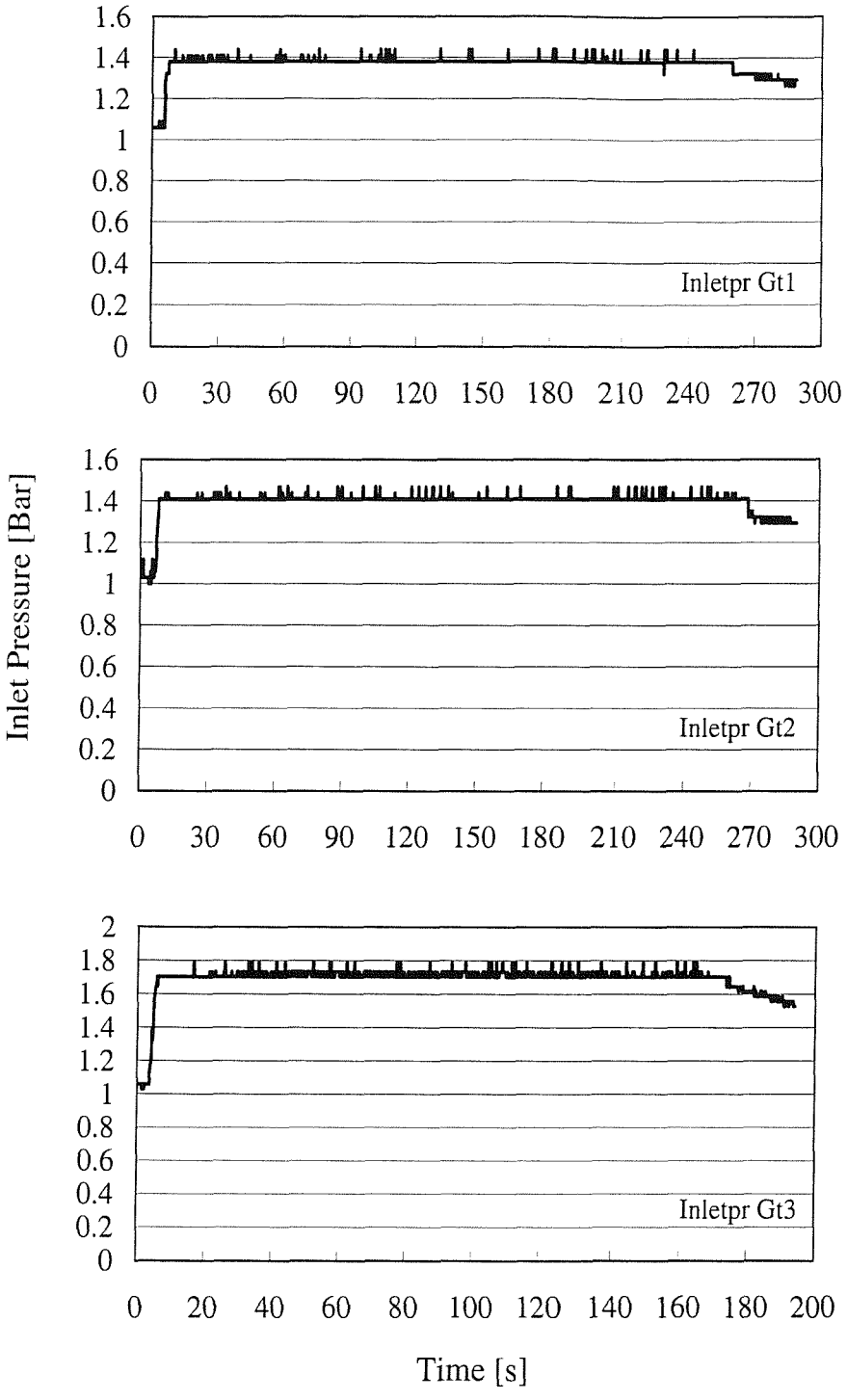

Figure C.23: Inlet pressures in vertical plane experiments of RC 600 in set up I (a).

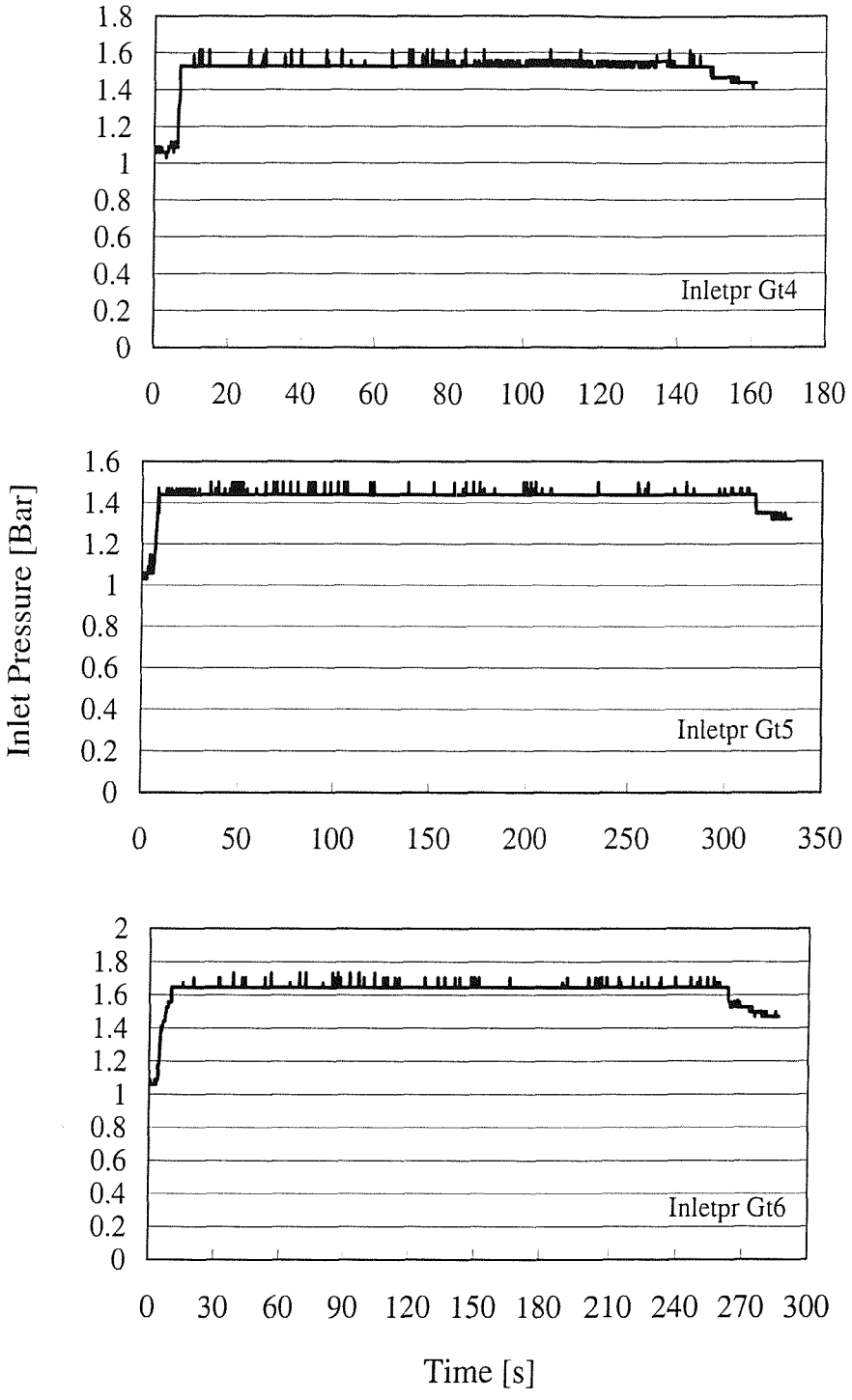

Figure C.24: Inlet pressures in vertical plane experiments of RC 600 in set up I (b).

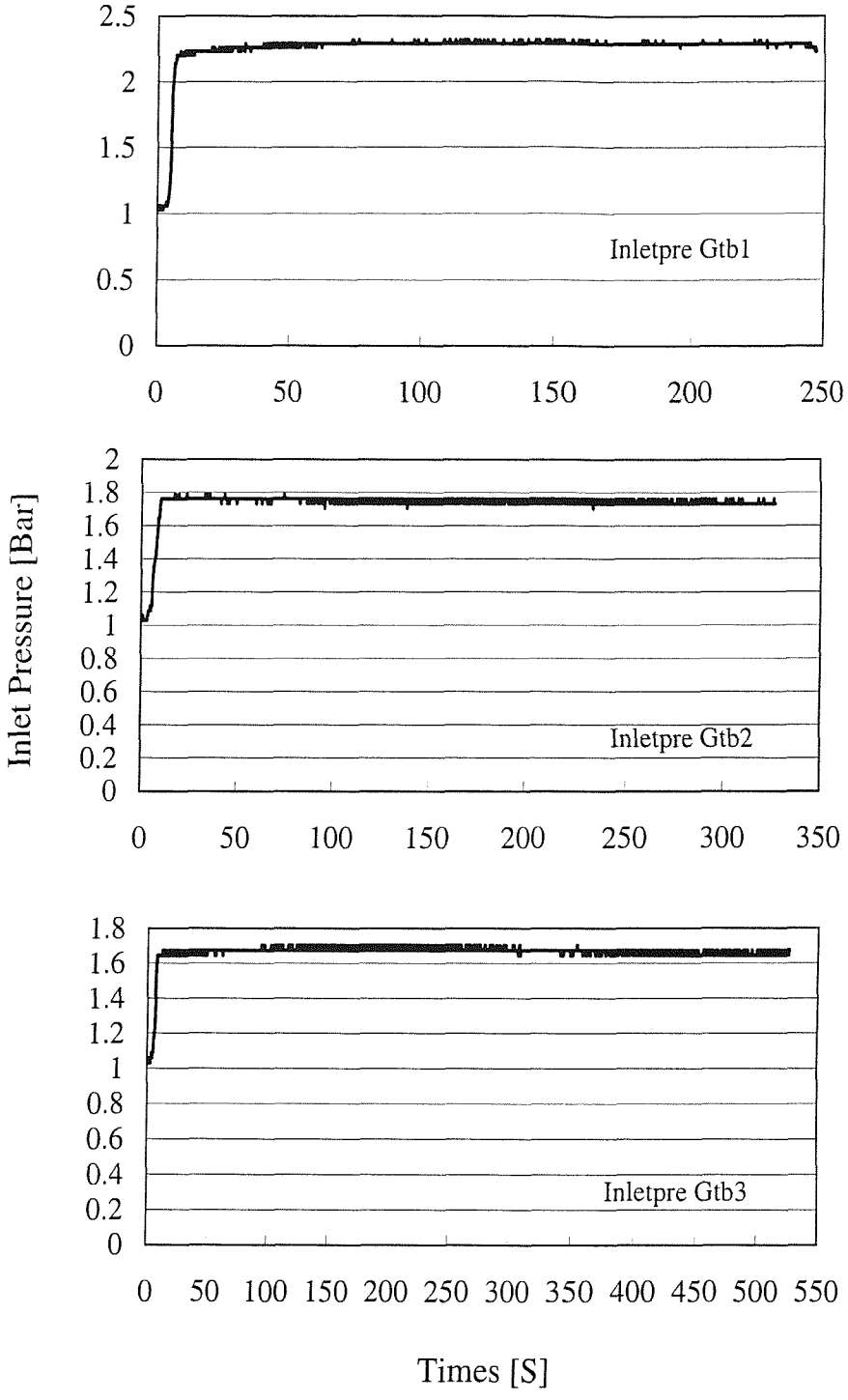

Figure C.25: Inlet pressures in vertical plane experiments of WRE580T in set up III.

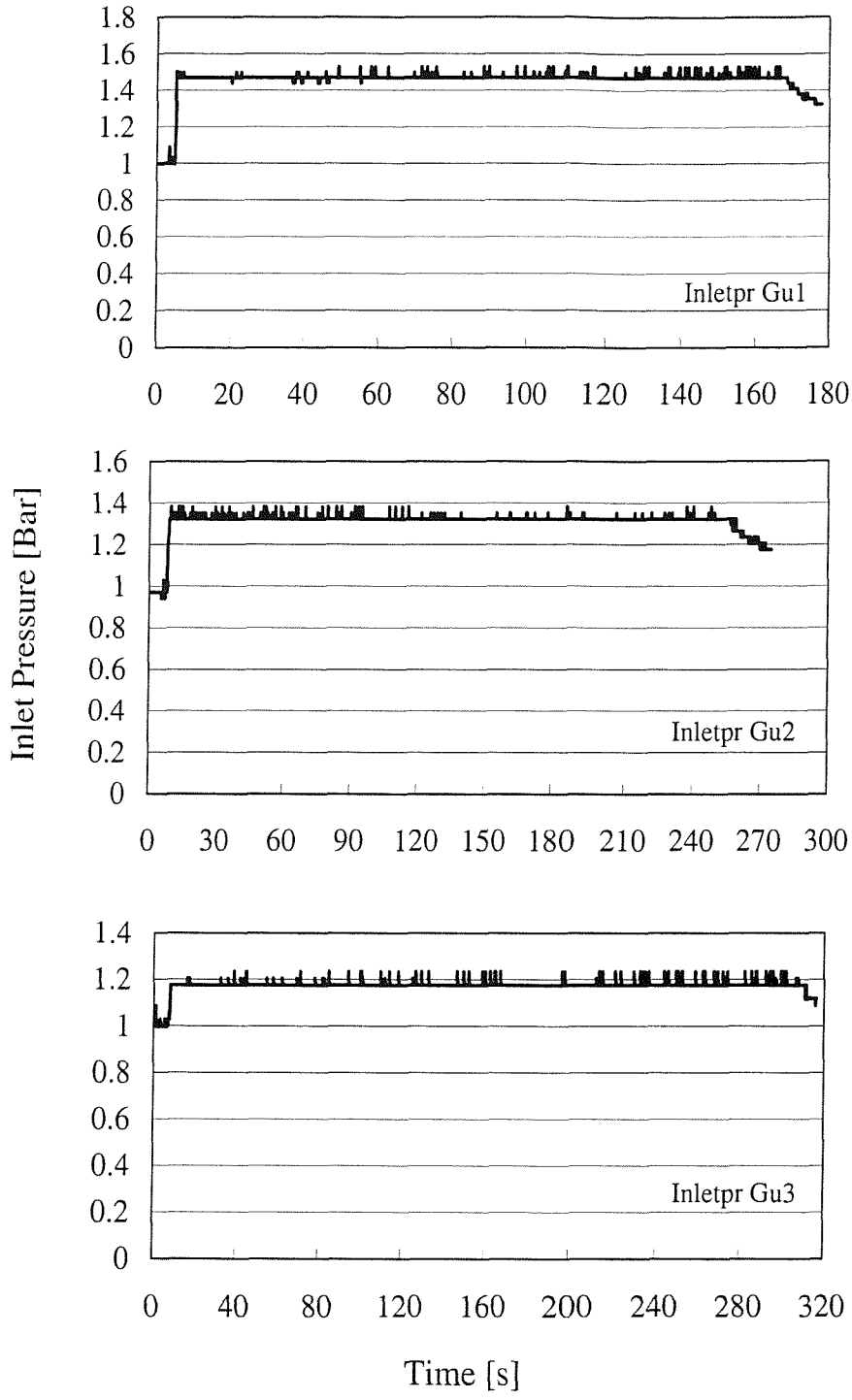

Figure C.26: Inlet pressures in vertical plane experiments of E-LPb 567 in set up I (a).

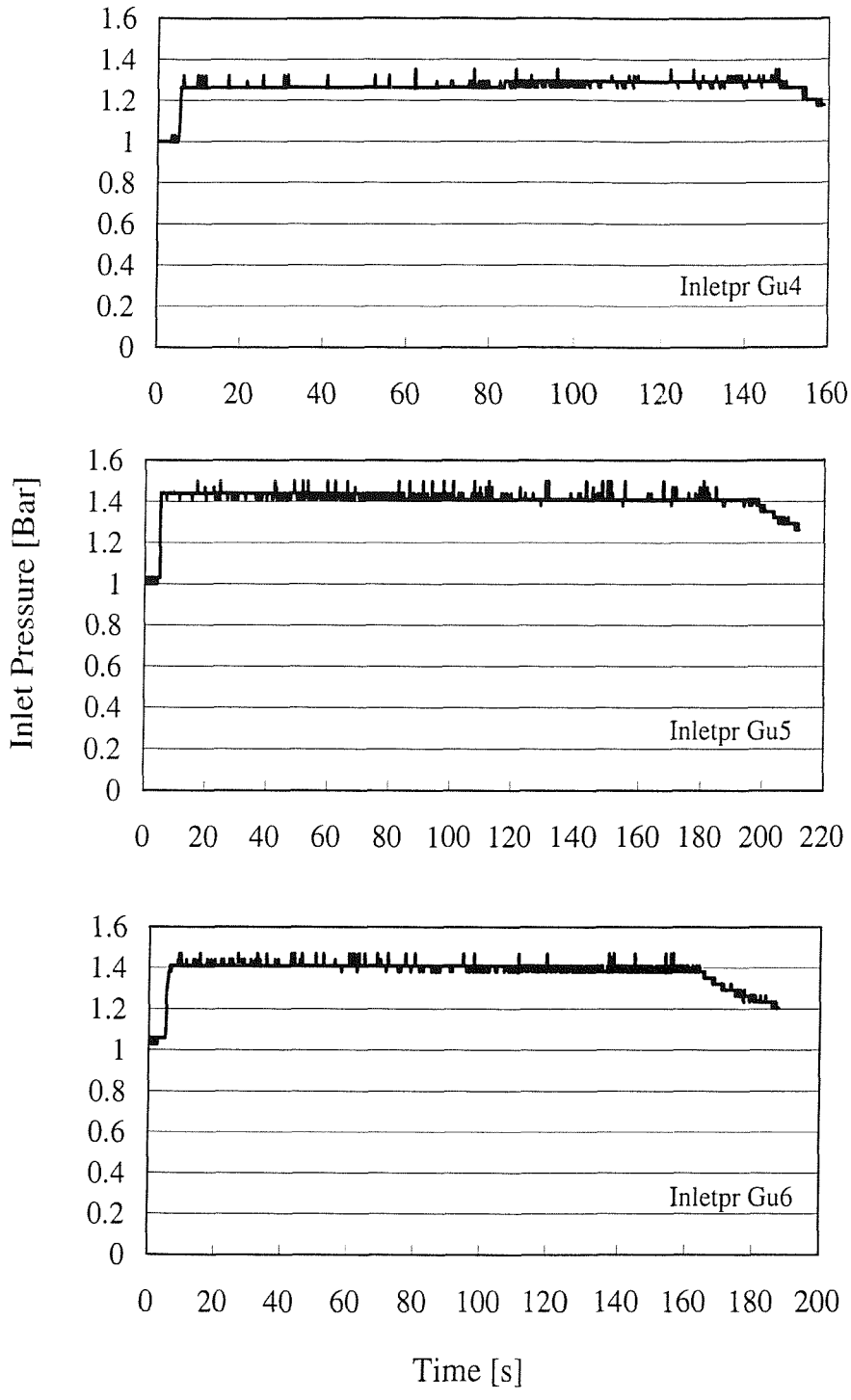

Figure C.27: Inlet pressures in vertical plane experiments of E-LPb 567 in set up I (b).

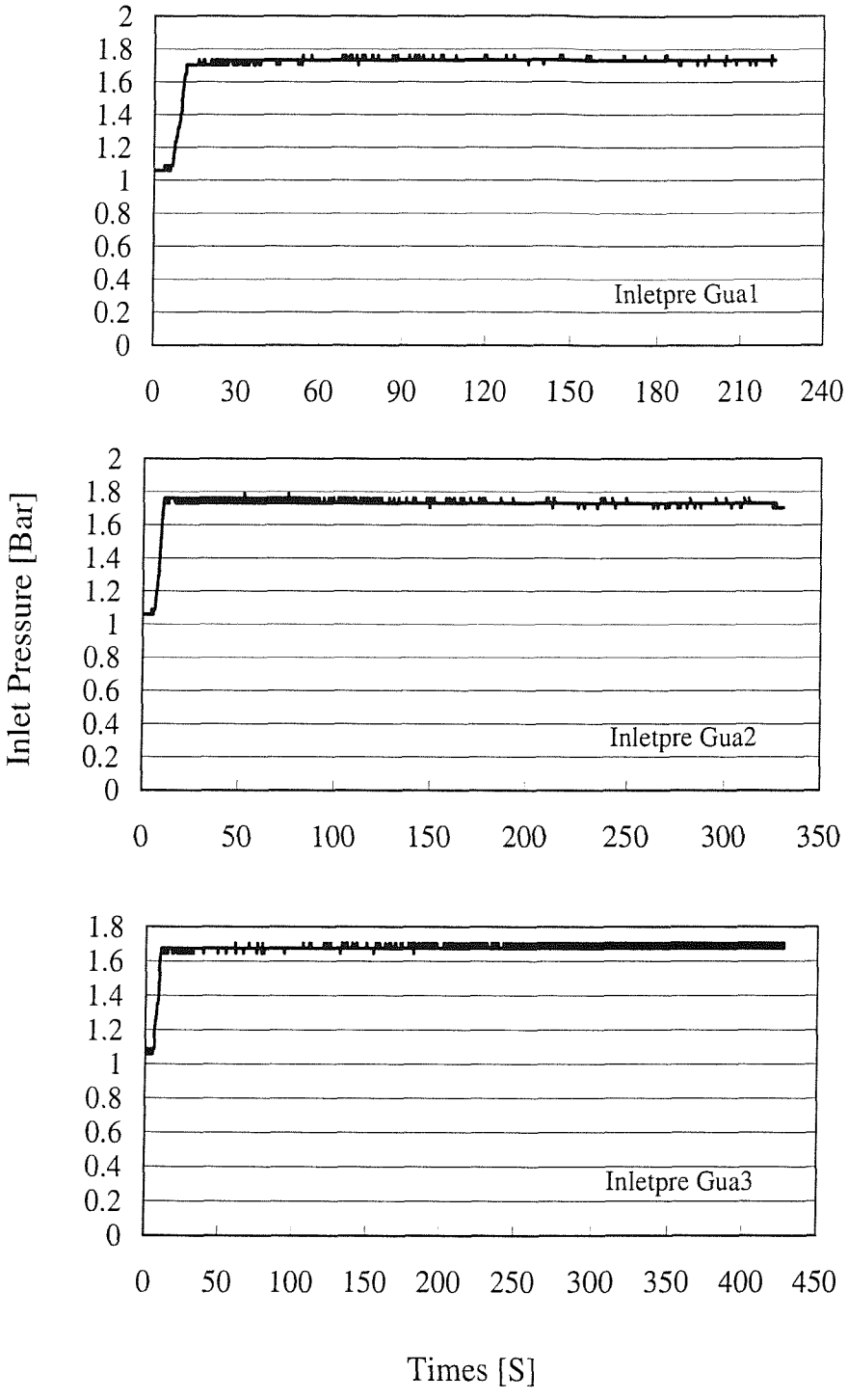

Figure C.28: Inlet pressures in vertical plane experiments of E-LPb 567 in set up II.

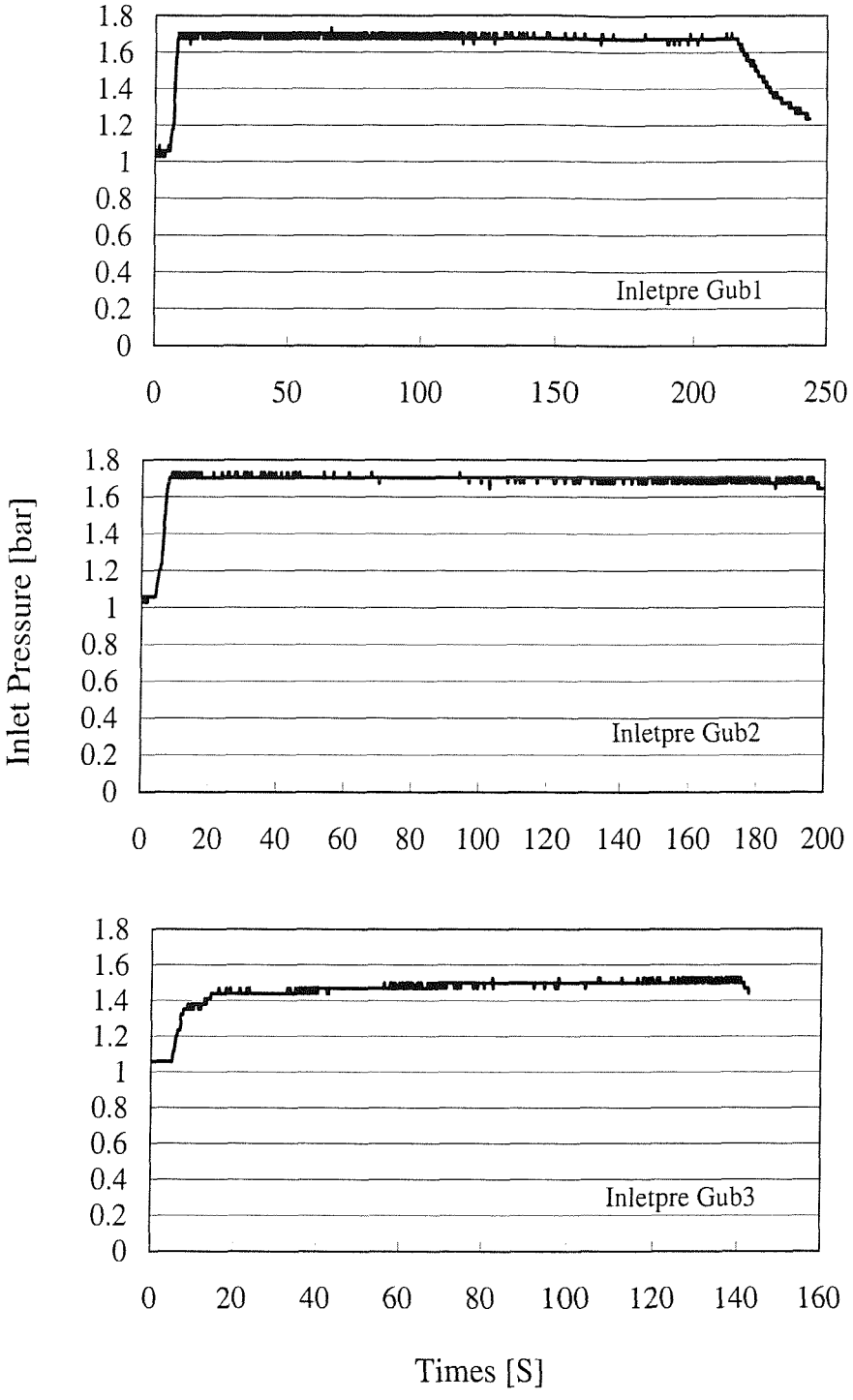

Figure C.29: Inlet pressures in vertical plane experiments of E-LPb 567 in set up III.

Appendix D

The flow front in the experiments

In this chapter, the image of the advancing flow front at several time instants recorded in some experiments are given.

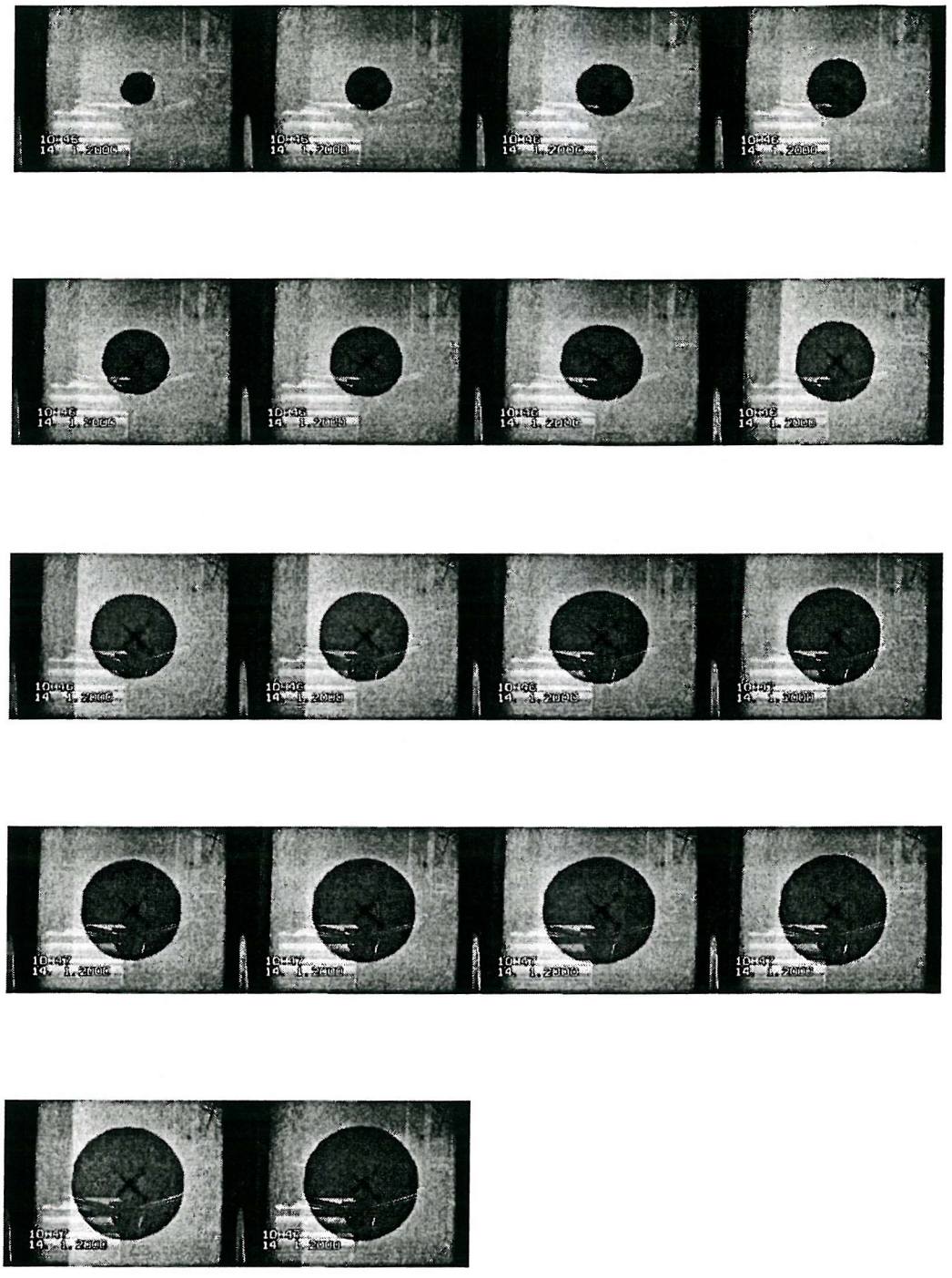

Figure D.1: Images of the advancing flow front at several time instants recorded in the experiment Cr5.

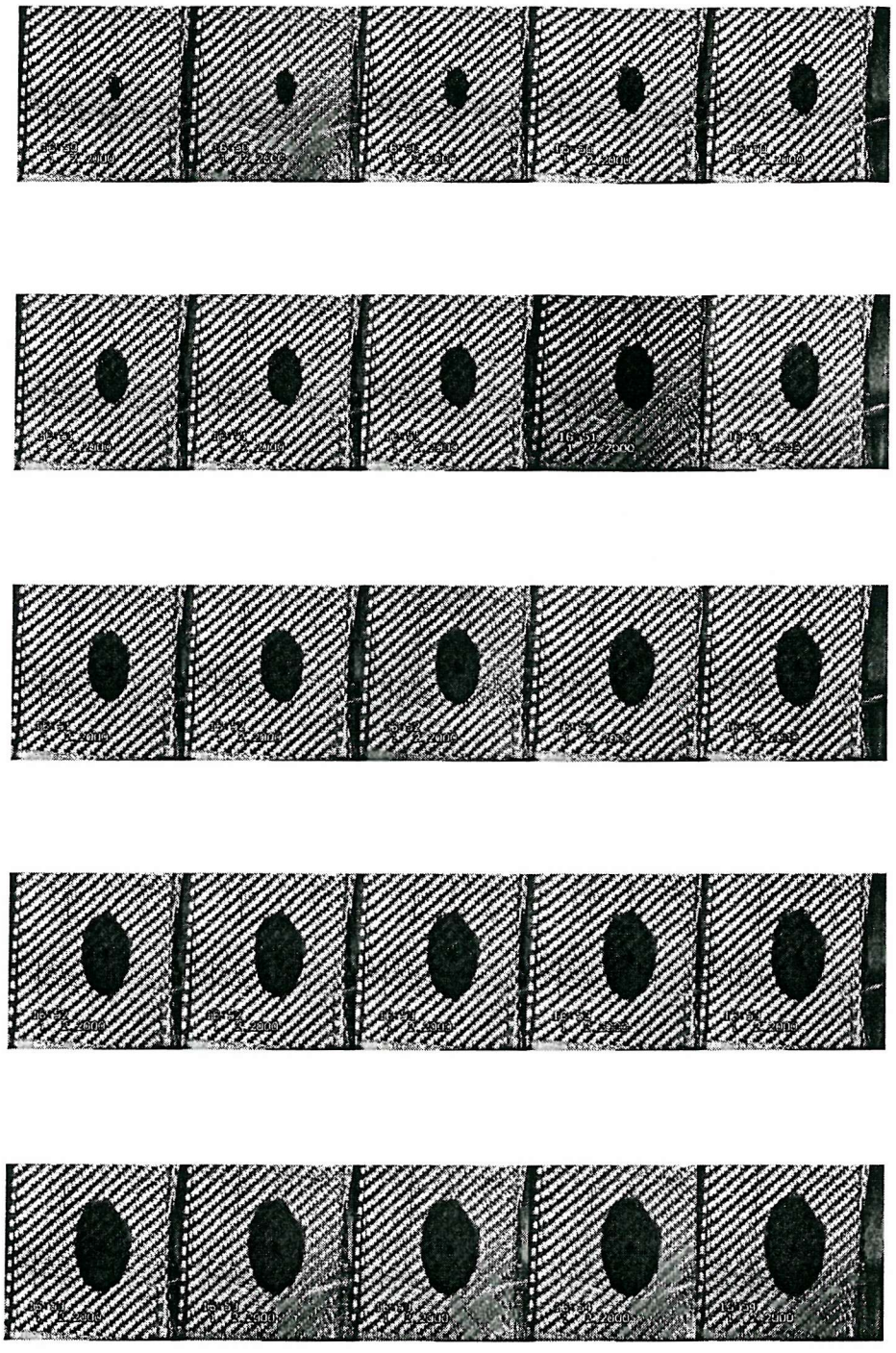

Figure D.2: Images of the advancing flow front at several time instants recorded in the experiment Ct6.

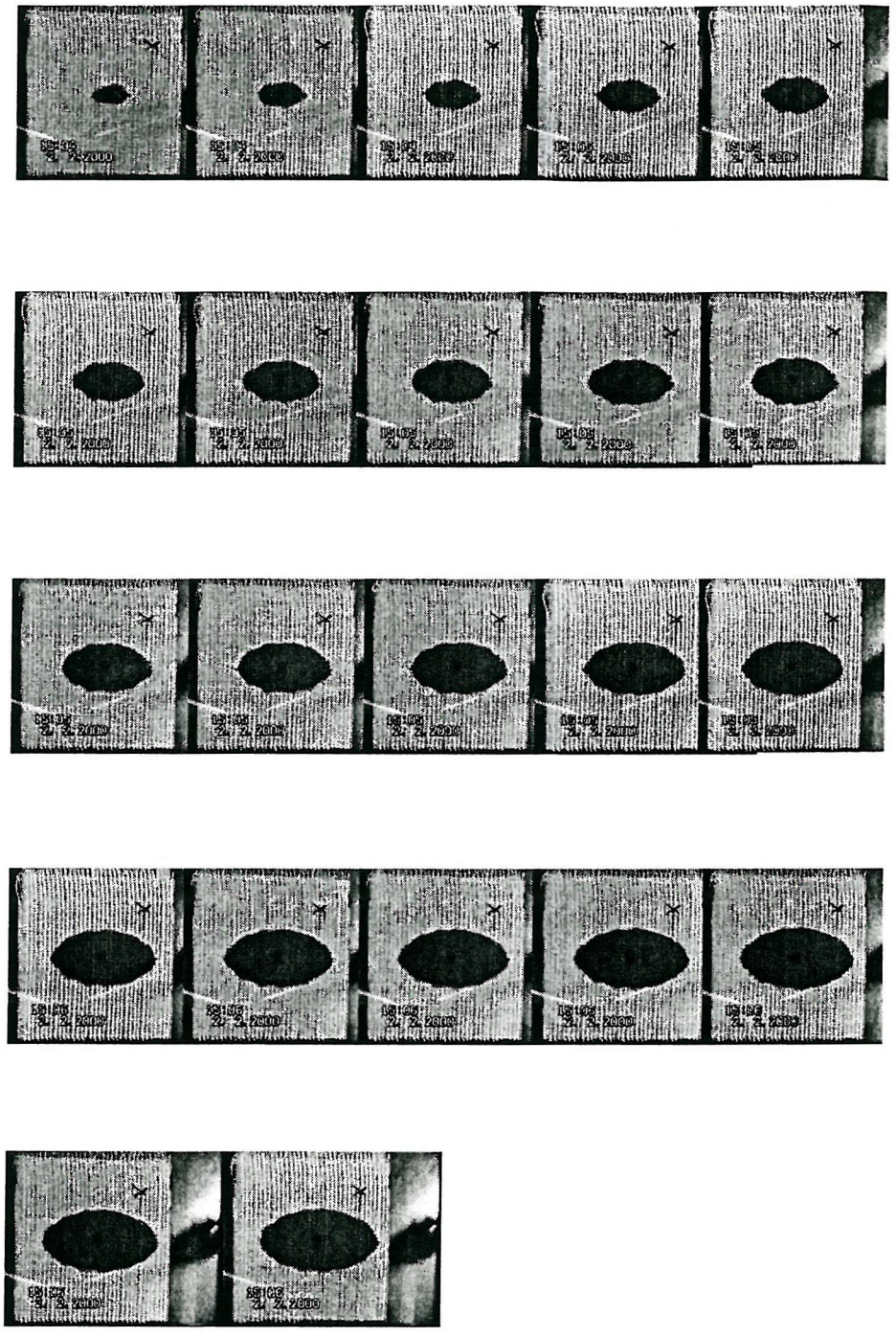

Figure D.3: Images of the advancing flow front at several time instants recorded in the experiment Cu2.

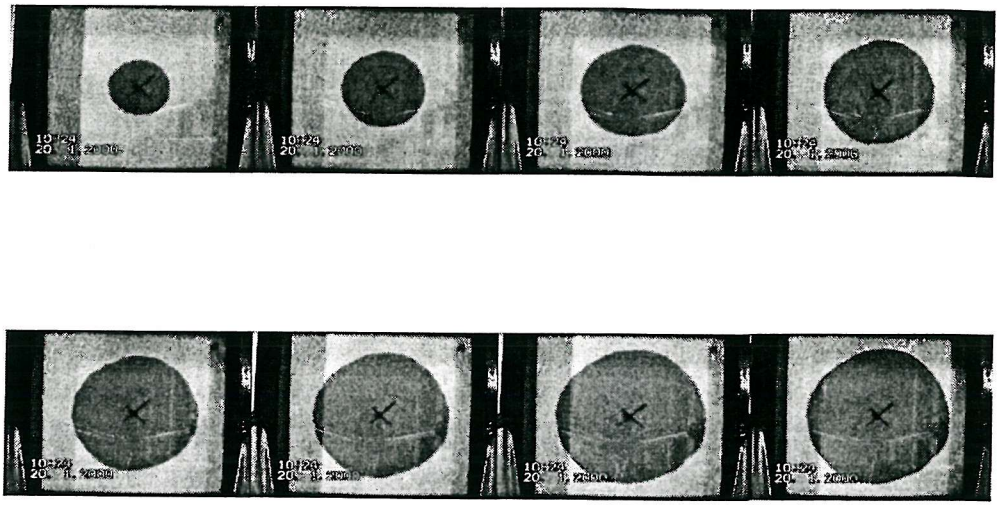

Figure D.4: Images of the advancing flow front at several time instants recorded in the experiment Vr5.

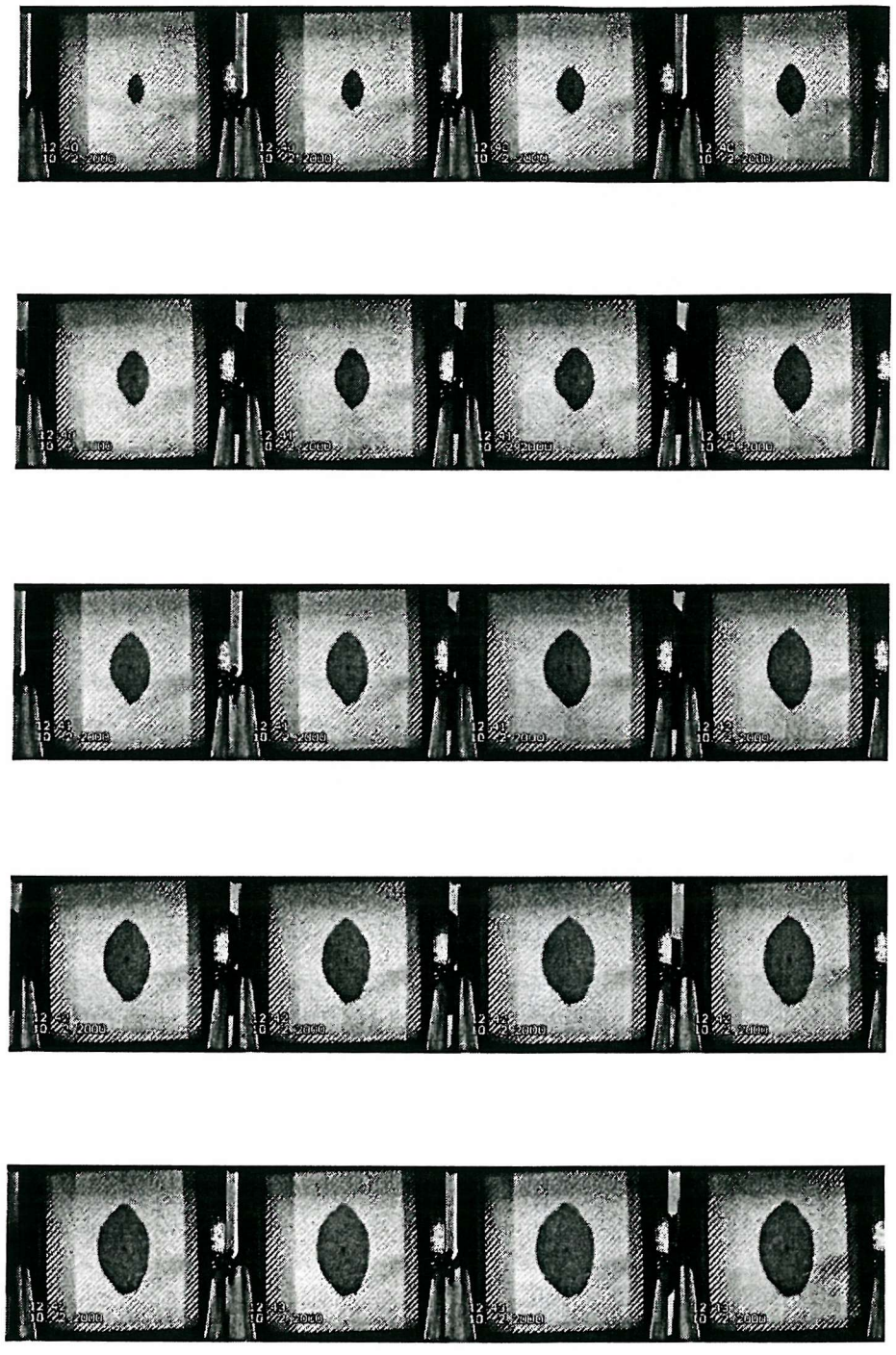

Figure D.5: Images of the advancing flow front at several time instants recorded in the experiment Vt1.

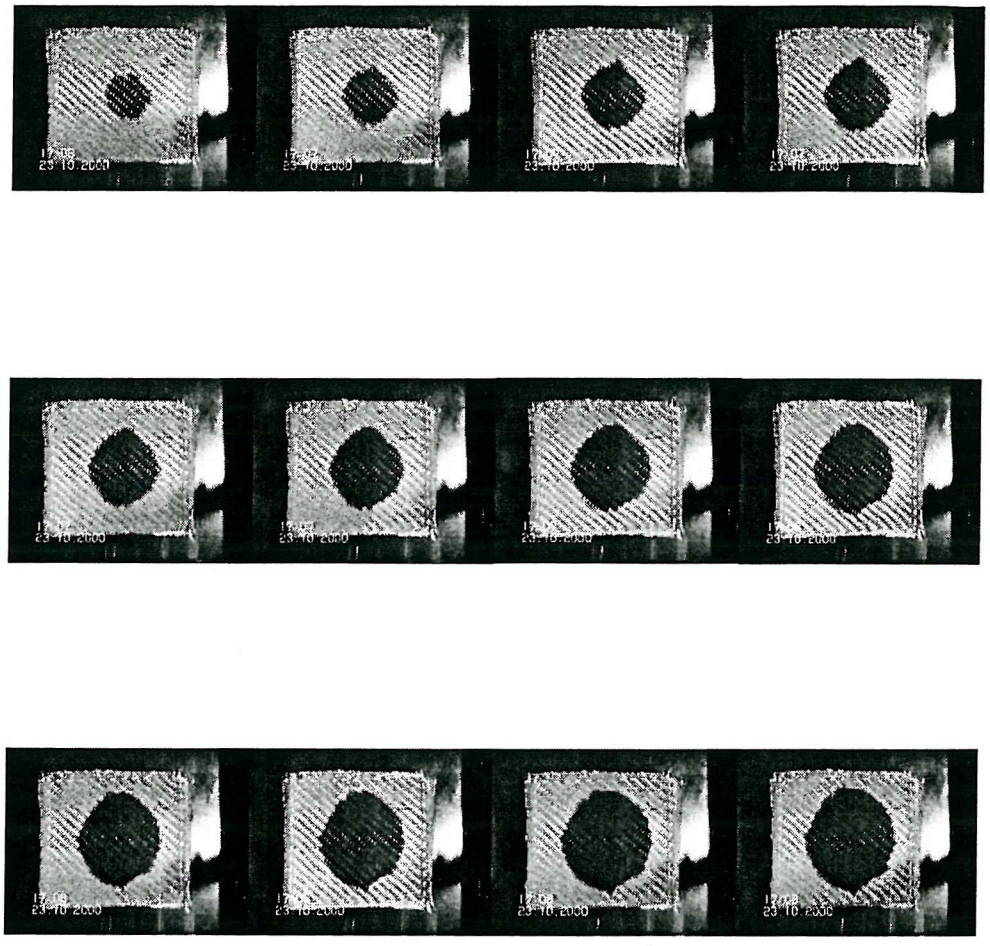

Figure D.6: Images of the advancing flow front at several time instants recorded in the experiment Vtb3.

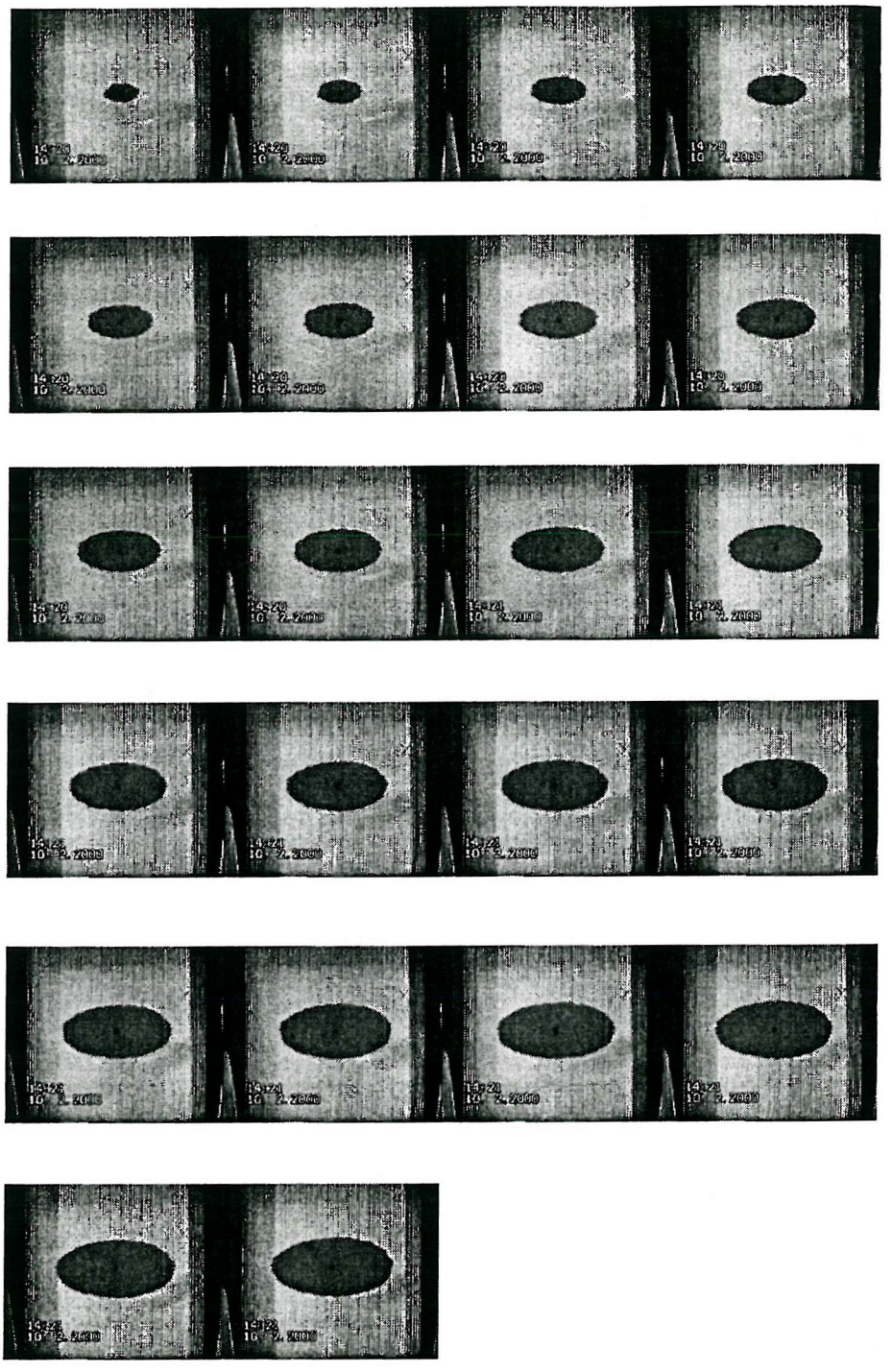

Figure D.7: Images of the advancing flow front at several time instants recorded in the experiment Vu5.

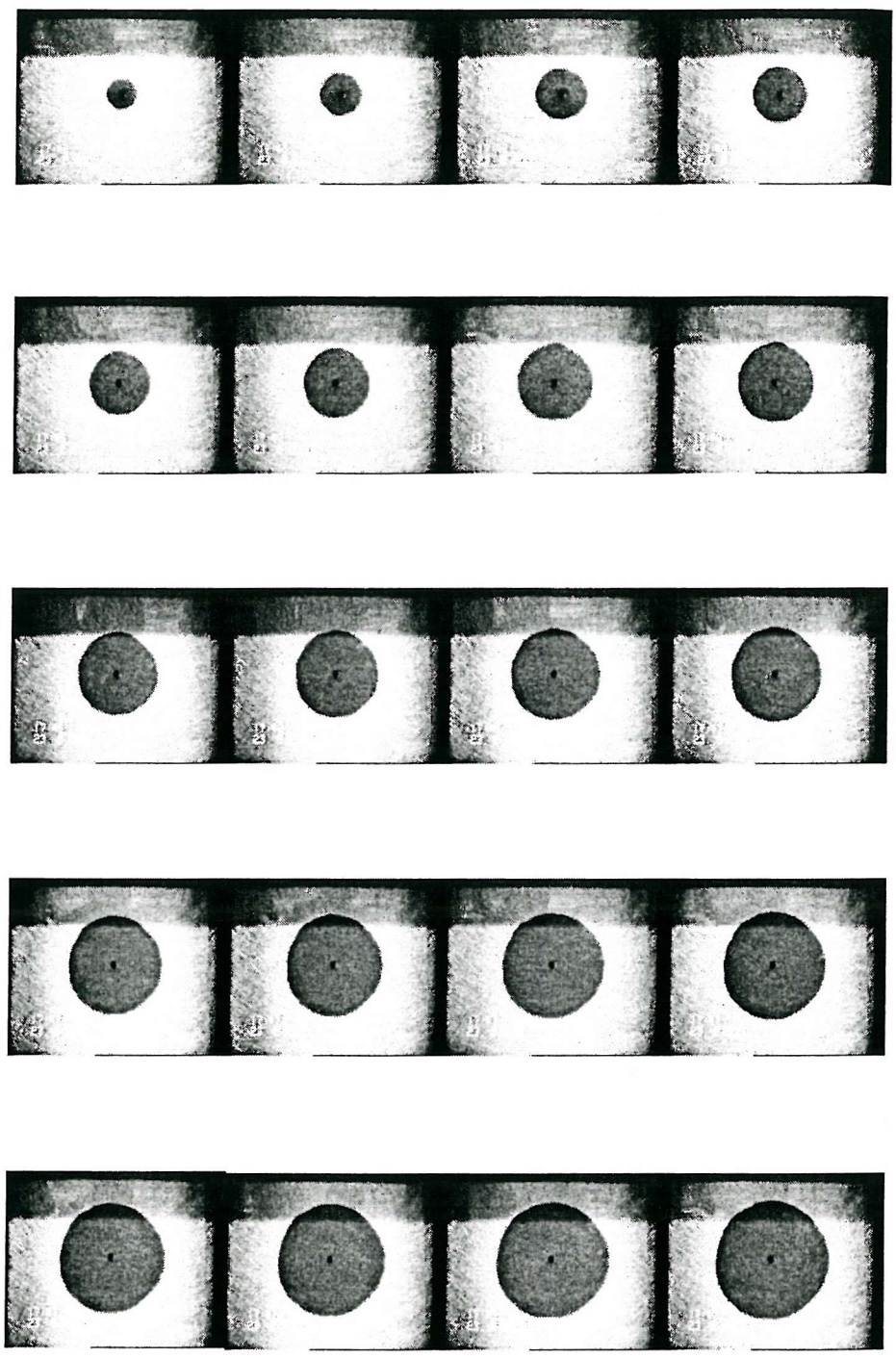

Figure D.8: Images of the advancing flow front at several time instants recorded in the experiment Gr3.

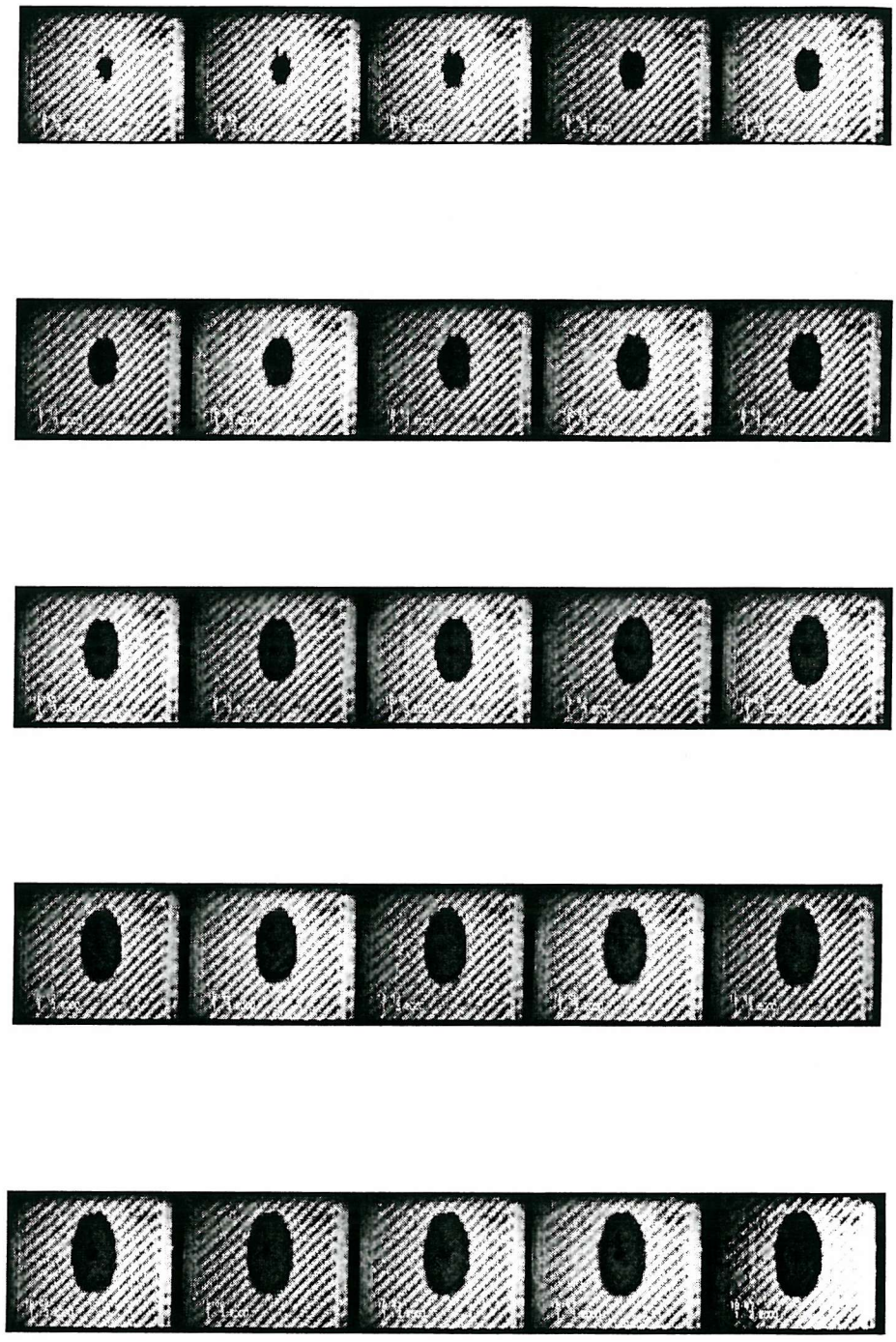

Figure D.9: Images of the advancing flow front at several time instants recorded in the experiment Gt2.

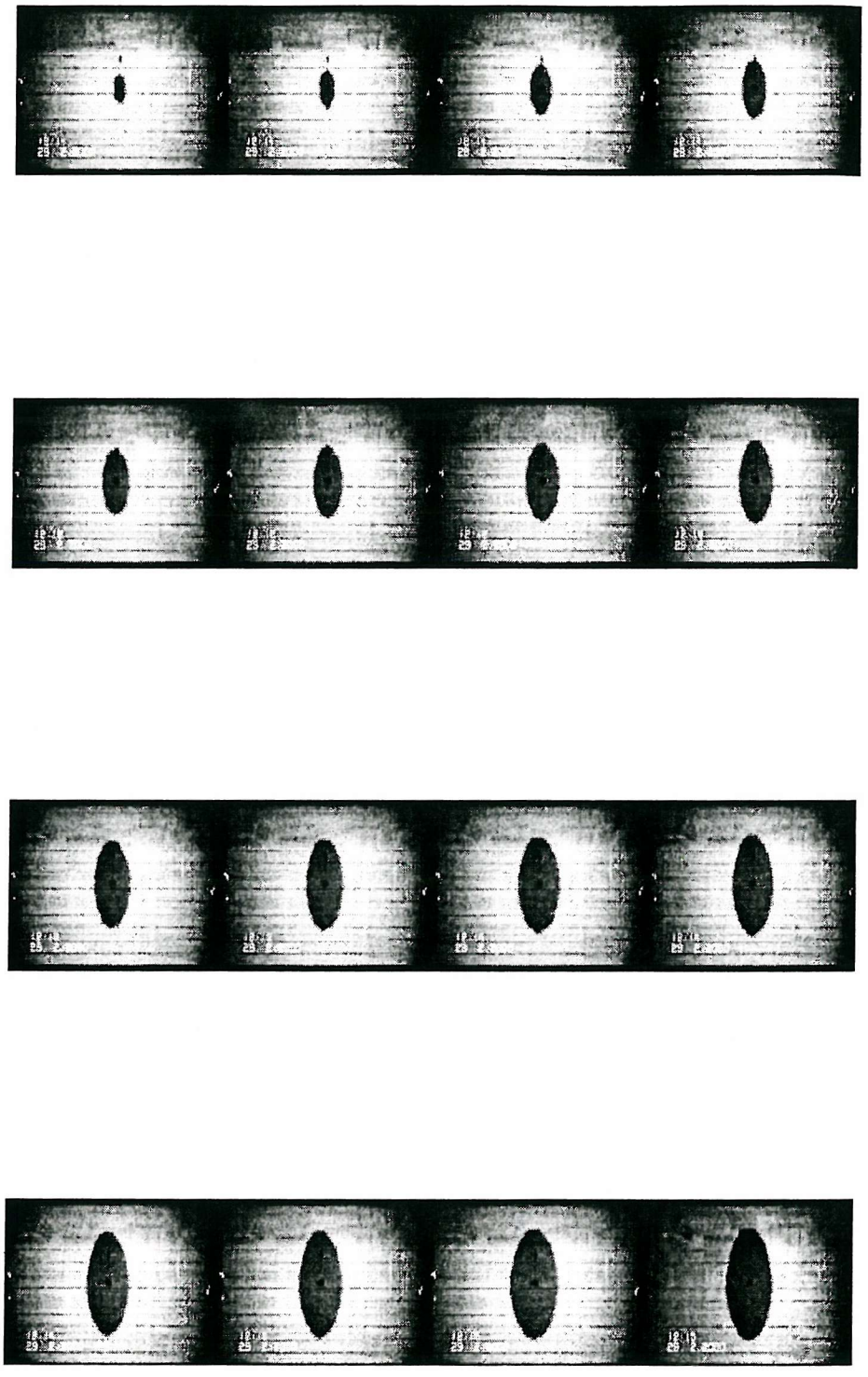

Figure D.10: Images of the advancing flow front at several time instants recorded in the experiment Gu3.

Appendix E

An example of calculate the permeabilities

An example using the formulae described in Chapter 4 and 5 to calculate the permeabilities is given in this Chapter.

E.1 Variable inlet pressure experiments

For experiment Vr1 (see Table 6.5), the random mat U 750-450 with set up I is used in this experiments (see Table 6.1). It is a two-dimensional radial flow in isotropic media with a variable inlet pressure. Therefore, in order to calculate the permeabilities using the results in this experimental measurement, equation (4.56) should be used. The calculations are as follows. From equation (6.1), it is obtained,

$$\begin{aligned} v_f &= \frac{NW_f}{H\rho_f} \\ &= \frac{3 \times 450}{2.32 \times 10^{-3} \times 2.56 \times 10^6} \\ &= 22.7\%, \end{aligned} \tag{E.1}$$

from which it follows that,

$$\varepsilon = 1 - v_f = 77.3\%. \tag{E.2}$$

The X_1 and X_2 listed in Table B.19, are the positions of flow front along the two axes X_1 and X_2 (see Figure 6.3). At time $t = 36.94s$, the measurement distances are,

$$\begin{aligned} X_1 &= 265.00mm, \\ X_2 &= 258.00mm, \end{aligned} \tag{E.3}$$

and, the radius are,

$$r_1^f = \frac{X_1}{2} = 132.50mm, \tag{E.4}$$

$$r_2^f = \frac{X_2}{2} = 129.00mm. \tag{E.5}$$

Also, the pressure measured at $t = 36.94s$ is,

$$p^0 = 2.318Bar, \tag{E.6}$$

and at $t = 0s$,

$$p^0 = 2.026Bar. \tag{E.7}$$

The pressure p^f on the flow front is the atmospheric pressure, i.e.

$$p^f = 1.013Bar. \tag{E.8}$$

Integral P represented by equation (5.37) is calculated

$$P = \int_0^t (p^f - p^0)dt = 80.233. \tag{E.9}$$

The radius of inlet gate is $r^0 = 5.25mm$ and the viscosity of test fluid is $\mu = 3.515poise$. Substituting all these values into equation (4.56) gives,

$$k^{(1)} = 1500.52 \times 10^{12}m^2, \tag{E.10}$$

$$k^{(2)} = 1408.36 \times 10^{12}m^2, \tag{E.11}$$

in which, $k^{(1)}$ is the permeability along the axis X_1 and $k^{(2)}$ is the in along the axis X_2.

Appendix F

Deformation of test rig

The relative displacement between the glass top and the metal bed of the mould was measured. The Random fabric U 750-450 with set up III in Table 6.1 is used in this test. The experiment set up is shown in Figure F.1. The inlet pressure is given in Figure F.2. There are no observable deflection in either the two dial indicators during the experimental process. From this observation, it is concluded that the glass top and the metal bed of the mould can be assumed as rigid.

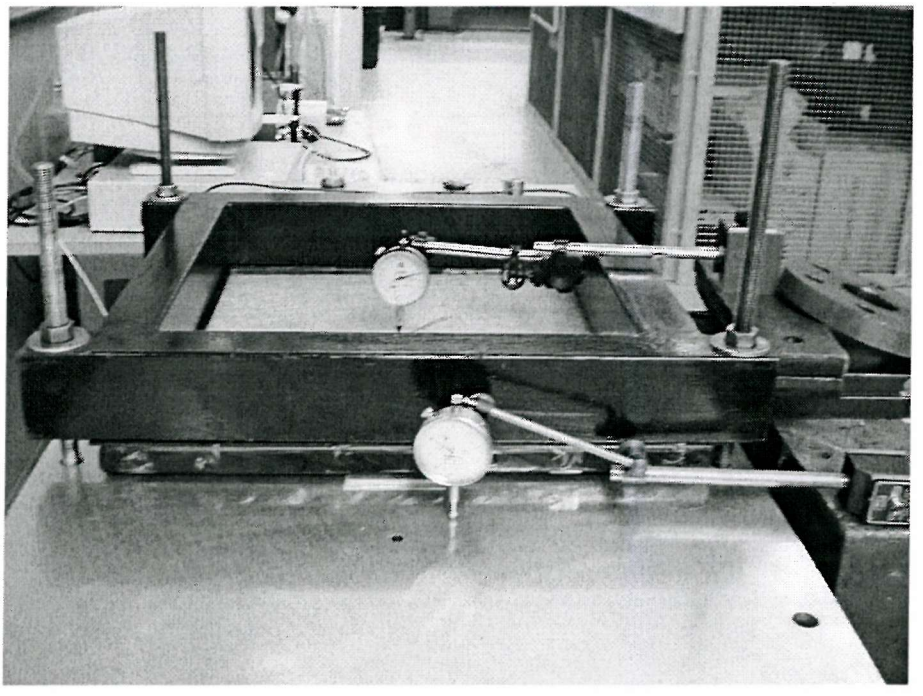

Figure F.1: Coordinate rotations.

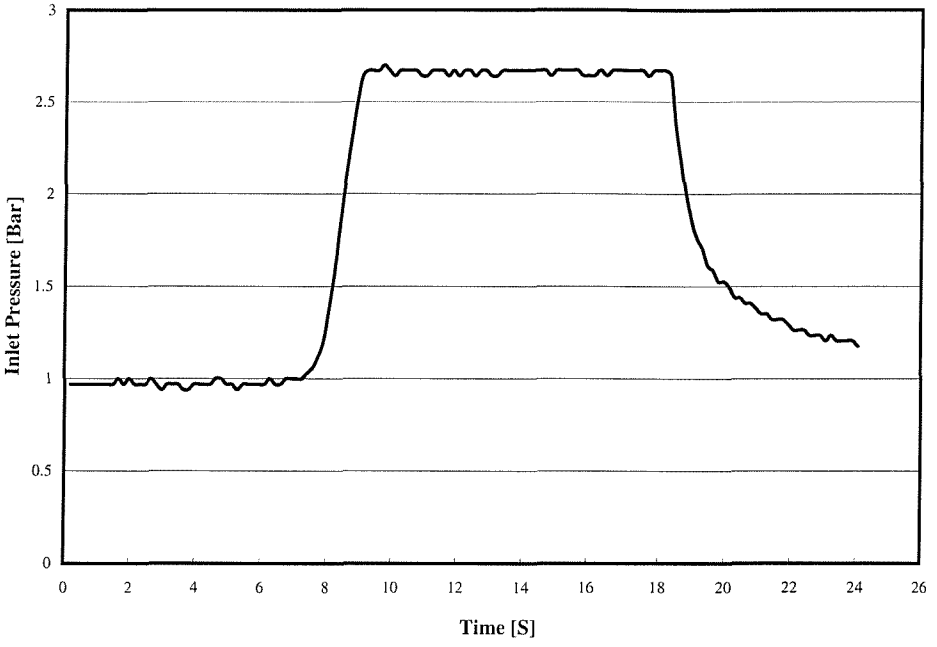

Figure F.2: Inlet pressure.

References

Aboudi, J., (1989), Micromechanical Analysis of Composites by the Method of Cells, *Appl. Mech. Rev.,* Vol. 42 (7), 193-221.

Aboudi, J., (1991), *Mechanics of Composite Materials: a Unified Micromechanical Approach,* Elsevier, Amsterdam.

Aboudi, J., (1996), Micromechanical Analysis of Composites by the Method of Cells - Update, *Appl. Mech. Rev.,* Vol. 48 (10), Part 2, S83-S91.

Adams, A. A. and Roberts, J. H., (1985), A General Outline of the Main Characteristics and Prime Uses of a Vacuum Injection Moulding System, *Hands Off GRP II Conf., Plastics and Rubber Institute,* May PP. 5/1-5/3.

Adams, K. L., Miller, B. and Rebenfeld, L., (1986), Forced In-Plane Flow of an Epoxy-Resin in Fibrous Networks, *Polymer Engineering and Science,* Vol. 26, No. 20, pp. 1434-1441.

Adams, K. L. and Rebenfeld,l., (1987), Inplane Flow of Fluids in Fabrics-Structure Flow Characterization, *Textiles Research Journal,* Vol. 57, No. 11, pp. 647-654.

Adams, K. L., Russel, W. B., and Rebenfeld, L., (1988), Radial Penetration of a Viscous-Liquid into a Planar Anisotropic Porous Medium, *International Journal of Multiphase Flow,* Vol. 14, No. 2, pp. 203-215.

Adams, K. L. and Rebenfeld, L., (1991a), Permeability Characteristics of Multilayer Fiber Reinforcements 1. Experimental Observations, *Polymer Composites,* Vol. 12, No. 3, pp. 179-185.

Adams, K. L. and Rebenfeld, L., (1991b), Permeability Characteristics of Multilayer Fiber Reinforcements 2. Theoretical Model, *Polymer Composites,* Vol. 12, No. 3, pp. 186-190.

Advani,S. G. and Bruschke, M. V., (1994), Resin Transfer Moulding phenomena in Polymeric Composites, in *Flow & Rheology in Polymer Composites Manufacturing,* chapter 12, Elsevier, Amsterdam, pp. 465-515.

Ahn, S. H., Lee W. I. and Springer, G. S., (1995), Measurement of the Three-Dimensional Permeability of Fiber Preforms Using Embedded Fiber Optic Sensors, *Journal of Composites materials,* Vol. 29, No. 6, pp. 714-733.

Allen, R., Best, P. F. and Short, D., (1982), Vacuum Injection Moulding of High Volume Fraction Fibre Composites, *13th Reinforced Plastics Conference,* BPF RPG, Brighton, November, Paper 49, pp. 207-209.

Bear, J., (1972), *Dynamics of Fluids in Porous Media,* New York: Marcel Dekker.

Beers, Y., (1972), *Introduction to the Theory of Error,* Addison-Wesley Publishing Company, INC.

Boyde, P., Clothier, B. and Inglis, A., (1995), *Design Fabrication and Commissioning of a Resin Transfer Moulding Facility,* Master of Engineering Group Design Project Report, Faculty of Engineering And Applied Science, University of Southampton, May.

Brittles, L., (1994), New Developments in RTM, *19th International BPF Composites Congress,* BPF, Birmingham, 22-23 November, PP. 11-26.

Bruschke, M. and Advani, S. G., (1990), A Finite Element/Control Volume Approach to Mold Filling in Anisotropic Porous Media, *Polymer Composites,* Vol, 11, pp. 398-405.

Cai, S. W., (1987), *Mechanics of Composite Structures,* (In Chinese), People's Communication Publication, Beijing.

Calado, V. M. A. and Advani, S. G., (1996), Effective Permeability of Multi-Layer Preforms in Resin Transfer Molding, *Composites Science and Technology,* Vol. 56, pp. 519-531.

Chan, A. W. and Hwang, S. T., (1991), Anisotropic In-Plane Permeability Of Fabric Media, *Polymer Engineering and Science,* August, Vol. 31, No. 16, pp. 1233-1239.

Chan, A. W. Larive, D. E. and Morgan. R. J, (1993), Anisotropic Permeability of Fiber Preforms: Constant Flow Rate Measurement, *Journal of Composite Materials,* Vol. 27, No. 10, pp. 996-1008.

Chibani, M., (1990), PhD thesis, Ecole Polytechnique de Montreal.

Chick, J. P., Rudd, C. D. Van Leeuwen, P. A. and Frenay. T. I., (1996), Material Characterization for Flow Modeling in Structural reaction Injection Molding, *Polymer Composites,* Vol.17, No.1, pp. 124-145.

Ciba-Geigy, Publication, Vacuum Injection Process-Ciba Geigy Aileron publication No. 28626/d,f,e 880. 729/40(Printed Switzerland).

Darcy, H., (1856), *Les Fontaine publiques de la ville de Dijon,* Paris: Dalmont.

De Wiest, R. J. M., (1969), *Flow Through Porous Media,* New York: Academic.

Diallo, M. L., Gauvin, R. and Trochu, F., (1995), Experimental Analysis of Flow Through Multi-Layer Fiber Reinforcements in Liquid Composite Molding, *4th International Conferee on Automated Composites (ICAC'95),* Nottingham, 6-7 September, pp. 201-210.

Douglas, J. F., Gasiorek, J. K. and Swaffield, J. A., (1995), *Fluid Mechanics,* 3rd Edition, Longman Singapore publishers (Pte) Ltd.

Fell, A. W. and Summerscales, J., (1996), Advanced Composites Manufacturing Centre, School of Manufacturing and Mechanical Engineering, University of Plymouth, *Personal communication.*

Ferland, P., Guittard, D. and Trochu, F., (1996), Concurrent Methods for Permeability Measurement in Resin Transfer Molding, *Polymer Composites,* Vol.17, No.1, pp. 149-158.

Foley, M. f., (1991), Techno-Economic Automated Composite Manufacturing Techniques, *SAMPE Quarterly,* January, pp. 61-68.

Fracchia, C. A., Castro, J. and Tucker, C. L., (1989), in *4th Tech. Conf. pf the Amer. Soc. for Composites,* 157, Technomic Publishing Co., Lancaster, Pa.

Fracchia, C. A., PhD thesis, (1990), University of Illinois at Urbana-Champaign.

Fung, Y. C., (1977), *A first course in Continuum mechanics,* Second Edition, Prentice-hall, INC., Englewood Cliffs, New Jersey.

Garg, S. K., Svalbonas, V. and Gurtman, G. A., (1973), *Analysis of Structural Composite Materials,* Marcel Dekker, Inc., New York.

Gauvin, R. and Chibani, M., (1986), The Modelling of Mold Filling in Resin Transfer Molding, *International Polymer Processing,* Vol. 1, pp. 42-46.

Gauvin, R. and Chibani, M., (1990), Analysis of Composite Molding with Woven and Non-Woven Reinforcements, *45th Annual Conference,* Reinforced Plastics/Composites Institute, The Society of the Plastics Industry, Washington D. C., February 12-15 Session 9-f.

Gauvin, R., Kerachni, A. and Fisa, B., (1994), Variation of Mat Surface Density and its Effects on Permeability Evaluation for RTM Molding, *Journal of Reinforced Plastics and Composites,* Vol. 13, pp. 371-383.

Gauvin, R., Trochu, F. and Diallo, L., (1996), Permeability Measurement and Flow Simulation Through Fiber Reinforcement, *Polymer Composites,* Vol. 17, No.1, pp. 34 - 42.

Gebart, B. R., Gudmunndson, P., Strömbeck, L. A. and Lundermo, C. Y., (1991), Analysis of the Permeability in RTM Reinforcements, *Proceedings of the 8th International Conference on Composite Materials (ICCM-8),* Honolulu, July 15-19, Session 15-E.

Gebart, B. R., (1992), Permeability of Unidirectional Reinforcements for RTM, *Journal of Composites materials,* Vol. 26 No. 8, pp. 1100-1133.

Gebart, B. R. and Lidström, P., (1996), Measurement of In-Plane Permeability of Anisotropic Fiber Reinforcements, *Polymer Composites,* Vol. 17, No. 1, pp. 43-51.

Gotch, T. M., (1978), Improved Production Process for Manufacture of GRP on British Rail, *11th Reinforced Plastics Conference,* BPF RPG, Brighton, November, Paper 4, pp. 33-39.

Gotch, T. M., (1980), Developments and Potential of Vacuum Impregnation Techniques for GRP Manufacture, *12th Reinforced Plastics Conference,* BPF RPG, Brighton, November, Paper 7, pp. 25-31.

Gotch, T. M., (1985), Low Investment Alternatives to Hand Lay GRP Production, *Hands Off GRP II Conf., Plastics and Rubber Institute,* May PP. 1/1-1/11.

Greenkorn, R. A., (1983), *Flow Phenomena in Porous Media,* New York: American Elsevier Publishing Company.

Greve, B. N. and Soh, S. K., (1990), In Proc. SAE Int. Congress Exposition on "Polymer Composites for Structural Automotive Applications", November, Society of Automotive Engineers, pp. 101-113.

Group Lotus Car Ltd., (1972), Vacuum Moulding Patent, *GB Patent, No. 1432333,* 30 March.

Gutowski, T. G. Morigaki, T. and Zhong, C., (1987), The Consolidation of Laminate Composites, *Composite Materials,* 21(2), 172-188.

Hammami, A., Gauvin, R. and Trochu, F., (1998), Modeling the Edge Effect in Liquid Composites Molding *Composites Part A – Applied Science and Manufacturing,* Vol.29, No.5-6, pp. 603-609.

Hammami, A., Gauvin, R., Trochu, F., Touret, O. and Ferland,P., (1998), Analysis of the Edge Effect on Flow Patterns in Liquid Composites Molding, *Applied Composites Materials,* Vol.5, No.3, pp. 161-173.

Hayward, J. S. and Harris, B., (1989), Processing Factors Affecting the Quality of Resin Transfer Moulded Composites, *Plastics & Rubber Processing & Applications,* 11(4), 191-198.

Hayward, J. S. and Harris, B., (1990), The Effect of Vacuum Assistance in Resin Transfer Moulding, *Composites Manufacturing,* 1(3), 161-166.

Hazebrook, P., Rainbow, H. and Matthews, C. S., (1958), Trans. AIME 213, 250.

Hirt, D.E., Adams, K. L., Prudhomme, R. K. and Rebenfeld, L., (1987), In-plane Radial Fluid Flow Characterization of Fibrous Material, *Journal of Thermal Insulation,* Vol. 1, pp. 153-172.

Horner, D. R., (1951), Proc. Third World petrol. Congr. 2. 504.

Kendall, K.N., Rudd, C.D., Owen, M.J. and Middleton, V, (1992), Characterisation of the Resin Transfer Moulding Process, *Composites Manufacturing,* Vol. 3, No. 4, pp. 235-249.

Kim, Y. R., Mccarthy, S. p., Fanucci, J. P., Nolet, S. C. and Koppernaes, C., (1991), Resin Flow through Fiber Reinforcements during Composite Processing, *Proceeding: 22th International SAMPE Technical Conference,* November 6-8, pp. 709-723.

Le Comte, A., (1982), Method and Apparatus for Producing a Thin Walled Article of Synthetic Resin, in Particular a Large Sized Vehicle, *US Patent No. 4359437,* 16 November.

Longman Illustrated Science Dictionary, (ISBN 0 582 556457), Longman York Press.

Luce, T., Advani, S. G., Howard, G. and Parnas, R., (1995), Permeability Characterization: Part 2: Flow behavior in Multiple-Layer Preforms, *Polymer Composites,* Vol.16, pp. 447-458.

Marco Method, (1950), *US Patent No. 2495640,* 24 January.

Martin, G. Q. and Son, J. s., (1986), in Advanced Composites: The Latest Developments, 149, Dearbon, Mrch.

Matthews, F. L. and Rawlings, R. D., (1994), *Composite Materials: Engineering and Science,* Chapman & Hall, London.

Miller, C. C., Dyes, A. B. and Hutchinson, C. A., (1950), Trans. AIME, 189, 91.

Noor, A. K., Burton, W. S. and Bert, C. W., (1996), Computational Models for Sandwich Panels and Shells, *Appl. Mech. Rev.,* Vol. 49 (3), 155-199.

Nutting, P. G., (1930), *Bull. Amer. Ass. Petrol. Geol.,* 14, 1337.

Parnas, R. and Salem, A. J., (1993), A Comparison of the Unidirectional and Radial In-Plane Flow of Fluids Through Woven Composite Reinforcements, *Polymer Composites,* Vol. 14, No. 5, pp. 383-394.

Parnas, R. S., Luce, T., Advani, S. G. and Howard, G., (1995), Permeability Characterization: Part 1: A Proposed Standard Reference Material, *Polymer Composites,* Vol. 16, No. 6, pp. 430-446.

Perry, M. J., Wang, J. T., MA, Y. AND LEE, L. J.,(1992) In *International SAMPE Technical Conference,* T421, October.

Ranganattan, S., Phelan. F. and Advani, S. G., (1996), A Generalized Model for the Transverse Permeability of Unidirectional Fibrous Media, *Polymer Composites,* Vol.17, pp. 222-230.

Resimann, H. and Pawlik, P. S., (1980), *Elasticity Theory and Applications,* New York: John Wiley & Sons.

Rudd,C. D., Middleton, V., Owen, M. J., Long, A. C. and McGeehin, P., (1994), Modelling the Processing and Performance of Preforms for Liquid Moulding Processing, *Composites Manufacturing,* Vol. 5, No. 3, pp. 177-185.

Rudd,C. D., Long, A. C., McGeehin, P. and Smith, P., (1996a), In-Plane Permeability Determination for Simulation of Liquid Composite Moulding of Complex Shapes, *Polymer Composites,* Vol. 17, No. 1, pp. 52-59.

Rudd,C. D., Bulmer, L. J., Morris, D. J. and Kendall, K. N., (1996b), Compaction and In-Plane Permeability Characteristics of Quasi-Unidirectional and Continuous Random Reinforcements, *Materials Science and Technology* Vol. 12, pp. 436-444.

Rudd,C. D., Long, A. C., Kendall, K. N. and Mangin, C. G. E., (1997), *Liquid Moulding Technologies,* Woodhead Publishing Ltd, Cambridge England.

Scheidegger, A. E., (1960), *The Physics of Flow Through Porous Media,* Revised Edition, University of Toronto Press.

Scheidegger, A. E., (1963a), Hydrodynamics in Porous Media, *Encyclopedia of Physics,* by S. Flugge, Vol. VIII/Z, Fluid dynamics II, 625-662.

Scheidegger, A. E., (1963b), *The Physics of Flow Through Porous Media,* London: Oxford University Press.

Schwartz, M. M., (1992), *Composite Materials Handbook,* 2nd edition, McGraw-Hill, Inc., London.

Senibi, S., Klang, E. C., Sadler, R. L. and Avva, V. S., (1993), Resin Transfer Moulding (RTM), : Experiments with Vacuum Assisted Methods, *Proceedings of Ninth International Conference on Composite Materials* (ICCM/9), Vol III, pp 529-544.

Shackelford, J. F., (1988), *Introduction to Materials Science for Engineers,* 2st edition, Macmillan Publishing Company, New York.

Smith, C. S., (1990), *Design of Marine Structures in Composite Materials,* Elsevier Science Publishing Ltd, ISBN 1-85166-416-5.

Simacek, P. and Advani, S. G., (1996), Permeability Model for a Woven Fabric, *Polymer Composites,* Vol. 17, pp. 887-899.

Summerscales, J., (1993), A Model for the Effect of Fibre Clustering on the Flow Rate in Resin Transfer Moulding, *Composites Manufacturing,* 4(1), 27-31.

Thirion, J. M., Girardy, H. and Waldvogel, U., (1988), New Developments for Producing High-Performance Composite Components by the RTM Process, *Composites (Paris),* 28(3), 81-84.

Trevino, L., Rupel, K., Young, W. B., Liou, M. J. and James Lee L., (1991), Analysis of Resin Injection Moulding on Molds with Preplaced Fiber Mats. I: Permeability and Compressibility Measurement, *Polymer Composites,* Vol. 12, No. 1, pp. 20-29.

Trochu, F., Horareau, C., Gauvin, R. and Vincent, M., (1993), Experimental Analysis and Computer Simulation of the Resin Transfer Molding Through Multilayer Fiber Reinforcement, In *Proceedings of the 9th International Conference on Composite Materials (ICCM-9),* Madrid, 12-16 July, Vol III, pp. 481-488.

Watts, A. A., (1980), *Commercial opportunities for advanced Composites,* American Society for Testing and Materials, Philadelphia.

Weitzenböck, J. R., Shenoi, R. A. and Wilson, P. A., (1995), Flow Front Measurement in RTM, *4th International Conference on Automated Composites (ICAC'95),* Nottingham, 6-7 September, Vol. 2, pp. 307-314.

Weitzenböck, J. R., (1996), PhD. thesis, Flow Characterization in Resin Transfer Moulding, University of Southampton.

Weitzenböck, J. R., Shenoi, R. A. and Wilson, P. A., (1998), Measurement of Three-Dimensional Permeability, *Composites Part A,* 29A, pp. 159-169.

Weitzenböck, J. R., Shenoi, R. A. and Wilson, P. A., (1999a), Radial Flow Permeability Measurement. Part A: Theory, *Composites Part A,* Vol. 30, No.6, pp. 781-796.

Weitzenböck, J. R., Shenoi, R. A. and Wilson, P. A., (1999b), Radial Flow Permeability Measurement. Part B: Application, *Composites Part A,* Vol. 30, No. 6, pp. 797-813.

Weitzenböck, J. R., Shenoi, R. A. and Wilson, P. A., (1999c), Measurement of Principal Permeability with the Channel Flow Experiment, *Polymer Composites,* Vol. 20, No. 2, pp. 321 - 335.

Woerdeman, D. L., Phelan, F. R. and Parnas, R. S., (1995), Interpretation of 3-D Permeability Measurements for RTM Modeling, *Polymer Composites,* Vol. 16, No. 6, pp.470-480.

Williams, C., Summerscales, J. and Grove, S., (1996), Resin Infusion under flexible tooling (RIFT), : a Review, *Composites,* Part A, 27A, 517-524.